

Università degli Studi di Milano-Bicocca
Dipartimento di Biotecnologie e Bioscienze
Dottorato di ricerca in Biologia e Biotecnologie
XXXII Ciclo



**A CASE STUDY ON COMBUSTION-DERIVED PARTICLES:
EVALUATION OF THE BIOLOGICAL EFFECTS
ON HUMAN PULMONARY CELL LINES**

Sara Marchetti
Matr. 725747

Tutor: Prof. Anita Colombo

Anno Accademico 2018-2019



SCUOLA DI DOTTORATO
UNIVERSITÀ DEGLI STUDI DI MILANO-BICOCCA

Department of Biotechnologies and Biosciences
Doctorate Course in Biology and Biotechnologies - Cycle XXXII
Curriculum in BIOLOGICAL – ENVIRONMENTAL INTERACTIONS

A CASE STUDY ON COMBUSTION-DERIVED PARTICLES: EVALUATION OF THE BIOLOGICAL EFFECTS ON HUMAN PULMONARY CELL LINES

Sara Marchetti

Matr. 725747

Tutor: Prof. Anita Colombo

Co-Tutor: Prof. Paride Mantecca

Coordinator: Prof. Paola Branduardi

ACADEMIC YEAR 2018/2019

*To Professor Marina Camatini
In memoriam*

SUMMARY	1
INTRODUCTION	7
1. AIRBORNE POLLUTION	9
1.1. <i>PM physico-chemical characteristics</i>	9
1.1.1. Size	9
1.1.2. Chemical composition	10
1.1.3. Particle deposition and lung defense mechanisms	11
1.2. <i>PM sources</i>	13
2. COMBUSTION-DERIVED PARTICLES: CASE OF STUDY	14
2.1. <i>Biomass-derived particles</i>	14
2.1.1. Biomass-particles: physico-chemical properties	14
2.1.2. Health effects	16
2.2. <i>Diesel exhaust particles</i>	16
3. IMPACTS OF AIR POLLUTION ON HEALTH	18
4. IN VITRO SYSTEMS	18
5. IN VITRO TOXICOLOGICAL STUDIES	21
6. PERSPECTIVES	25
REFERENCES	26

CHAPTER 1: IN VITRO LUNG TOXICITY OF INDOOR PM₁₀ FROM A STOVE FUELED WITH DIFFERENT BIOMASSES

ABSTRACT	37
KEYWORDS	37
ABBREVIATIONS	38
1. INTRODUCTION	39
2. MATERIALS AND METHODS	40
2.1. <i>Particles sampling</i>	40
2.2. <i>Particles characterization</i>	41
2.2.1. Polycyclic aromatic hydrocarbons (PAHs)	41
2.2.2. Elements	42
2.3. <i>Particles extraction for biological investigations</i>	42
2.4. <i>Morphological characterization of extracted particles</i>	43
2.5. <i>Cell culture and exposure</i>	43
2.6. <i>Cell viability</i>	44
2.7. <i>Pro-inflammatory cytokines release</i>	44
2.8. <i>Protein extraction and immunoblotting</i>	45
2.9. <i>DNA damage analysis</i>	45
2.10. <i>Cell cycle analysis</i>	46
2.11. <i>Treatment with metal chelator</i>	46
2.12. <i>Statistical analysis</i>	46
3. RESULTS	47
3.1. <i>Biomass PM₁₀ chemico-physical characterization</i>	47
3.2. <i>Biomass PM₁₀ biological effects</i>	49
3.2.1. Cell viability	49

3.2.2. Synthesis and release of pro-inflammatory cytokines	50
3.2.3. Antioxidant response	51
3.2.4. Xenobiotic metabolism activation	52
3.2.5. DNA damage	53
3.2.6 Cell cycle analysis	54
4. DISCUSSION	55
5. CONCLUSIONS	59
ACKNOWLEDGMENTS	60
FUNDING	60
CONFLICTS OF INTEREST	60
APPENDIX A. SUPPLEMENTARY DATA	61
REFERENCES	64
CHAPTER 2: COMBUSTION-DERIVED PARTICLES FROM BIOMASS SOURCES DIFFERENTLY PROMOTE EPITHELIAL TO MESENCHYMAL TRANSITION ON A549 CELLS	71
ABSTRACT	73
KEYWORDS	73
1. INTRODUCTION	74
2. MATERIALS AND METHODS	75
2.1. CDPs sampling and extraction	75
2.2. Cell culture	76
2.3. Cell viability	76
2.4. ELISA	76
2.5. BPDE DNA bulky adducts detection	77
2.6. Protein expression analysis	77
2.7. Immunofluorescence microscopy	78
2.8. Migration and invasion assays	78
2.9. Statistical analysis	79
3. RESULTS	79
4. DISCUSSION	84
SUPPLEMENTARY DATA	89
REFERENCES	91
CHAPTER 3: BIOLOGICAL EFFECTS OF COMBUSTION-DERIVED PARTICLES FROM DIFFERENT SOURCES ON HUMAN BRONCHIAL EPITHELIAL CELLS	97
1. INTRODUCTION	99
2. MATERIALS AND METHODS	100
2.1. Biomass particles: sampling and extraction for biological experiments	100
2.2. Chemical analysis (ongoing)	101
2.3. Cell culture: maintenance and treatments	101
2.4. Cytotoxicity assay	101
2.5. Cell migration	102
2.6. Gene expression	102
2.7. Measurement of cytokine IL-1 β release	102
2.8. COMET analysis	103

2.9. <i>Flow cytometry</i>	103
2.10. <i>Statistical analysis</i>	103
3. RESULTS	104
4. DISCUSSION	110
5. CONCLUSIONS	113
ACKNOWLEDGEMENTS	113
SUPPLEMENTARY DATA	114
REFERENCES	117
CHAPTER 4: THE ROLE OF IL-6 RELEASED FROM PULMONARY EPITHELIAL CELLS IN	
DIESEL UFP-INDUCED ENDOTHELIAL ACTIVATION	121
ABSTRACT	123
KEYWORDS	123
1. INTRODUCTION	124
2. MATERIALS AND METHODS	125
2.1. <i>Preparation of diesel particles</i>	125
2.2. <i>Cells culture and exposure</i>	125
2.3. <i>ROS formation</i>	126
2.4. <i>RNA extraction and QPCR</i>	126
2.5. <i>Western blotting</i>	127
2.6. <i>Protein arrays</i>	127
2.7. <i>ELISA</i>	128
2.8. <i>Inhibitory studies</i>	128
2.9. <i>Statistical analyses</i>	128
3. RESULTS	129
3.1. <i>Effects on epithelial cells</i>	129
3.2. <i>Effects on endothelial cells</i>	132
3.3. <i>Mechanisms of endothelial activation</i>	133
4. DISCUSSION	135
ACKNOWLEDGMENTS	138
REFERENCES	139
CONCLUSIONS AND FUTURE PERSPECTIVES	143
REFERENCES	150
APPENDIX	155

Summary

Airborne pollution is a significant environmental and health hazard and largely contributes to increased morbidity and mortality as well as respiratory and cardiovascular diseases. Moreover, it has been classified as carcinogenic to humans (Group 1).

Studies on air quality and their consequent health effects are mostly performed on particles collected in urban area, where anthropogenic sources such as diesel exhaust and biomass-derived particles largely contribute to air pollution. In recent years, experimental and epidemiological studies have validated the emerging importance of traffic-related and biomass burning-derived particles as chief contributors to the adverse health effects due to airborne pollution exposure. However, our knowledge on the biological responses triggered by particles emitted from different sources with variable physico-chemical properties is still poor, as well as the comprehension of their modes of action.

In the present work the cytotoxic, genotoxic and pro-carcinogenic properties of particles collected during combustion of different biomass and diesel sources (CDPs) have been investigated:

- biomass particles collected from the emission of a heating system operating with pellet, charcoal or wood respectively;
- diesel exhaust ultrafine particles (DEP) directly sampled from a Euro IV vehicle run over a chassis dynamometer.

In the first part of the work, attention was given to biomass-derived particles. Several studies described the potential toxicological effects of particles emitted from biomass burning reporting different responses on the biological endpoints investigated on *in vitro* and *in vivo* systems. Dissimilarities in the results are linked to the use of different type of particles, which vary a lot in composition. Particle physico-chemical properties indeed are strongly influenced by type of fuel, combustion conditions and combustion appliances used.

In the present study, the various toxicological properties of particles collected during the combustion of different fuels under identical conditions in the same stove (commonly used) were investigated. Two different cell lines were used: A549 alveolar epithelial cells (Chapters 1 and 2) and HBEC-3KT bronchial epithelial cells (Chapter 3).

In Chapter 1 several toxicity outcomes observed after acute exposure to biomass particles have been described. PM₁₀ particles collected from combustion of pellet, charcoal and wood were first morphologically and chemically characterized. Then, A549 cells were exposed for 24 h to 5 µg/cm² PM. Numerous biological endpoints were evaluated: cell viability, inflammatory response, antioxidant and xenobiotic metabolism activity, DNA damage and cell cycle regulation. Results showed that charcoal and wood mainly induced the xenobiotic response enzymes activation and cell apoptosis. Pellet particles instead, displayed a different toxicological mechanism, inducing a mild inflammatory response, DNA damage, cell cycle arrest

in G1 phase and cell death by necrosis. Such a difference in the toxicological profiles was likely dependent on the different amount of PAHs and metals. Pellet indeed, has a higher amount of metals with respect to charcoal and wood that instead resulted to be enriched in PAHs. With regards to metals, the highest concentration of zinc (Zn) was observed in pellet. Literature data have demonstrated that high concentrations of Zn in PM correspond to higher particle toxic properties. Considering this, cell cycle analysis was performed also after exposure to particles pre-incubated with the chelating agent TPEN. Results obtained show that by administering TPEN, the genotoxic effects were rescued.

In Chapter 2 the adverse chronic health effects after a prolonged exposure to biomass particles have been reported. The purpose of the study was to investigate the mechanisms by which biomass particles exert their pro-carcinogenic properties. Attention was given to the epithelial-to-mesenchymal transition (EMT) process, which represents a crucial step in lung cancer progression involving several morphological and phenotypical changes. Time course and dose response evaluation on cell viability and pro-inflammatory response reveal a significant release of IL-8 after 72 h of exposure to 2,5 $\mu\text{g}/\text{cm}^2$. The augmented release of the cytokine has been reported to support EMT and tumor microenvironment remodeling. EMT process activation was then investigated, by evaluating the expression of typical EMT markers on A549 cells. Results showed a reduction in the epithelial marker E-cadherin and a parallel increase in the mesenchymal marker N-cadherin after exposure to charcoal and wood mainly. Increased motility and invasiveness were also found, confirming that PAHs more than metals may be effective in the process activation.

Finally, in Chapter 3 the role possibly played by biomass particles in different processes associated to *in vitro* lung carcinogenesis has been investigated using human bronchial HBEC-3KT epithelial cells. HBEC-3KT cells have been indeed described as a good model for mechanistic studies regarding genotoxic and pro-carcinogenic effects. To further characterize and compare the relative role of the particle core versus particle-adsorbed compounds in the lung epithelial cells response, the organic fractions and the remaining washed particles were also tested. HBEC3-KT were exposed to 2.5 $\mu\text{g}/\text{cm}^2$ of whole PMs, organic extracts and washed particles. The endpoints measured include cell viability, migration, expression of various genes involved in numerous PM-activated processes, inflammatory response, DNA damage and cell cycle alterations. Experiments with HBEC3-KT showed that biomass particles differentially modulate cell viability, proliferation and cell migration as well as genes linked to xenobiotic metabolism, inflammation and EMT response. Also in this case, genotoxic effects were reported mainly after exposure to pellet, which induced DNA damage and de-regulation of the cell cycle. Most interestingly, the study suggest that specific attached particle components could be responsible for the diverse effects observed following

exposure to pellet and wood PM; whereas with regard to charcoal, the PM as such seems more toxic. However, the role played by the different chemical compounds in the different toxicity outcomes observed needs to be further explored.

In the second part of the work (Chapter 4), the biological effects induced by diesel combustion particles (DEP) has been described focusing on their health hazard at both respiratory and vascular levels. We also explored the mechanisms leading to cardiovascular effects induced by DEP, which is characterized by a high amount of PAHs.

The release of mediators from exposed lung cells has been reported in literature to contribute to the endothelial activation. Thus, we set up a conditioned media *in vitro* model to investigate the role of epithelial-released mediators in the endothelial cells activation. Lung epithelial cells (BEAS-2B) were exposed for 20 h (dose 5 $\mu\text{g}/\text{cm}^2$) to diesel UFP and the supernatants used to treat endothelial cells (HPMEC-ST1.6R) for 24 h. The biological effects in both the cell lines were examined, focusing mainly on the activation of inflammatory and oxidative stress responses. Inhibitory studies were also performed to identify the possible mediators responsible for the endothelial responses. Results showed that DEP was able to induce oxidative stress, IL6 and IL6R release in BEAS cells and a consequent endothelial dysfunction, as evidenced by the increased expression of ICAM1 and VCAM1 in HPMEC-ST1.6R. These outcomes evidence that vascular effects induced by DEP might derive from the inflammatory response of the lung epithelial cells and are modulated by the particle physico-chemical properties.

In conclusion, the present work highlights the important role of particle chemical composition in triggering noteworthy adverse outcomes. We evidenced that particles from different emission sources and fuels may exert respiratory and cardiovascular effects at different level according to their composition. Thus, more complex strategies should be explored to reduce the biological impact caused by the emission of diesel engine and biomass-propelled heating systems and prevent hazardous health effects.

Introduction

1. Airborne pollution

Airborne pollution represents the most important environmental and public health risk, due to its effect on worldwide air quality and climate. The World Health Organization (WHO) reports that each year more than 7 million premature deaths can be attributed to various respiratory and cardiovascular diseases related to the effects of air pollution, including lung cancer. Among these there are 4.2 million of deaths (60%) addressed to the exposure to outdoor air pollution (WHO, 2014).

Particulate matter (PM) is one of the main contributors to air quality and the most damaging not only for human health but also for ecosystems, on which it has a great impact.

Particulate emissions have increased globally in recent years. In order to reduce air pollution impact, it is important to understand its causes, how particles are transported and altered in the atmosphere, how their chemical composition changes over time, and how they affect human health, ecosystems, the climate and thus, society and the economy.

Greater attention should be paid to this environmental concern, possibly by implementing effective measures to reduce air pollution and its effects and promoting international, national and local policies. Furthermore, technological development and personal behavioral changes are required, in order to reduce emissions (Guerreiro et al., 2018).

1.1. PM physico-chemical characteristics

The term “Particulate Matter” (PM) refers to a complex mixture of solid and liquid particles suspended in the air. Different number, size, shape, surface area, chemical composition, solubility, and origin can characterize inhaled particles and thus, influence the resulting health effects (Pope and Dockery, 2006).

1.1.1. Size

Among all these characteristics, the dimension strongly influences the probability of deposition, the deposition site and the retention of particles in the airways. For these reasons, the aerodynamic diameter is the main criteria used to describe the particles.

According to the “aerodynamic equivalent diameter” (AED), which determine the particles settling velocity, we can divide particles in different categories: PM₁₀ (diameter less than $<10\ \mu\text{m}$), PM_{2.5} ($<2.5\ \mu\text{m}$), and PM_{0.1} ($<0.1\ \mu\text{m}$) respectively. Considering their size, particles can be classified also as “course”, “fine” or “ultrafine”. The term “course” refers to all the particles with a diameter between 2.5 and $10\ \mu\text{m}$, while “fine” indicate particles with a diameter less than $2.5\ \mu\text{m}$.

Finally, particles smaller than 0.1 μm are defined as “ultrafine” (Anderson et al., 2012).

Coarse particles derive primarily from suspension or resuspension of soil, dust or other crustal materials from roads, farming, volcanos or windstorms. They include also sea salts, pollen, spores, and other plant fragments.

Fine particles instead, originate mainly from industrial and combustion processes, such as vehicle use of gasoline and biomass burning. They include also product generated by conversion from primary to secondary emissions.

Finally, ultrafine particles originate mainly from combustion processes, such as vehicle exhaust and atmospheric photochemical reactions (Pope and Dockery, 2006).

1.1.2. Chemical composition

Airborne particles are composed of several chemical and/or biological elements that can interact with each other and possibly be adsorbed on cells (Figure 1). Among these, there are elemental and organic carbon, volatile organic compounds (VOC), polycyclic aromatic hydrocarbons (PAH), inorganic ions and mineral matter (such as sulphates, nitrates, oxides of aluminum, titanium, iron, ammonium, silicon, sodium, potassium, calcium, magnesium, and chloride), acids and metals (including lead, copper, manganese, nickel and cadmium) (Cheung et al., 2011; Kim et al., 2015; World Health Organization, 2013). The biological components, also called *bioaerosols*, are a combination of viable and non-viable microorganisms such as allergens, fungal spores, endotoxins, cell fragments, fragmented pollen, and non-agglomerated bacteria (Morakinyo et al., 2016).

PM composition can also be influenced by emission sources, meteorological conditions, season, time, and location (Morakinyo et al., 2016; Cesari et al., 2018; Longhin et al., 2013; Perrone et al., 2013).

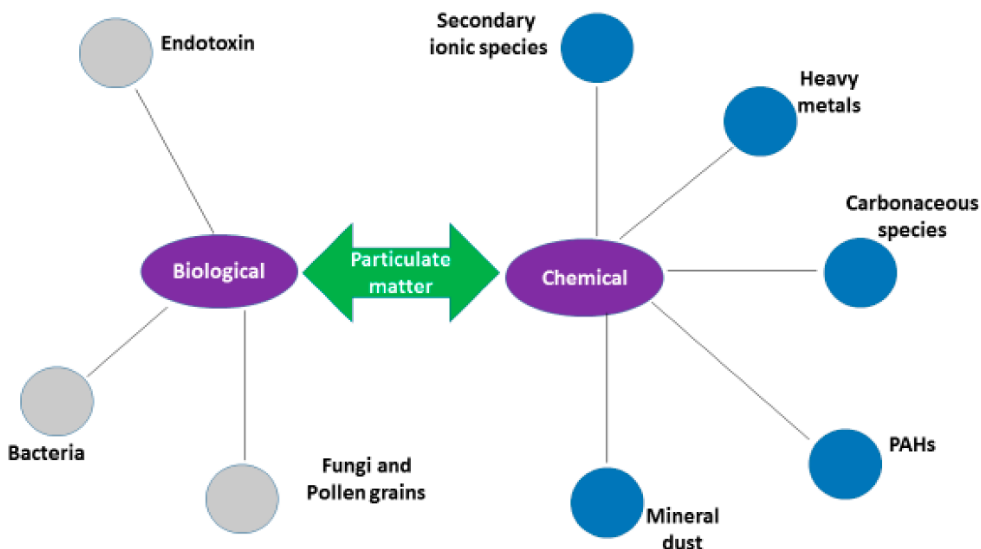


Figure 1. Biological and chemical components of particulate matter (Morakinyo et al., 2016).

Several toxicological studies report the adverse health effects induced by the chemical compounds adsorbed on PM and numerous candidates, including sulphates, transition metals, PAH and ultrafine particles have been suggested. However, the relation between a specific PM chemical compound and the adverse outcome is still unclear.

1.1.3. Particle deposition and lung defense mechanisms

Once inhaled, the particles can spread and settle in the respiratory system and, the smaller a particle is, the deeper it will penetrate to reach the alveoli. Here, due to the low metabolism of the alveolar cells, the absorbed organic pollutants are transferred into the circulatory flow. Considering this, PM can also be classified into three groups accordingly to the deposition area: inhalable, thoracic and respirable particles (Figure 2). Inhalable particles penetrate the upper respiratory tract (nose, throat and larynx); thoracic particles pass the larynx and reach the tracheobronchial tract (trachea, bronchi, bronchioles); respirable particles instead, easily reach the alveoli and the gas exchange region of the lung (Wang et al., 2009).

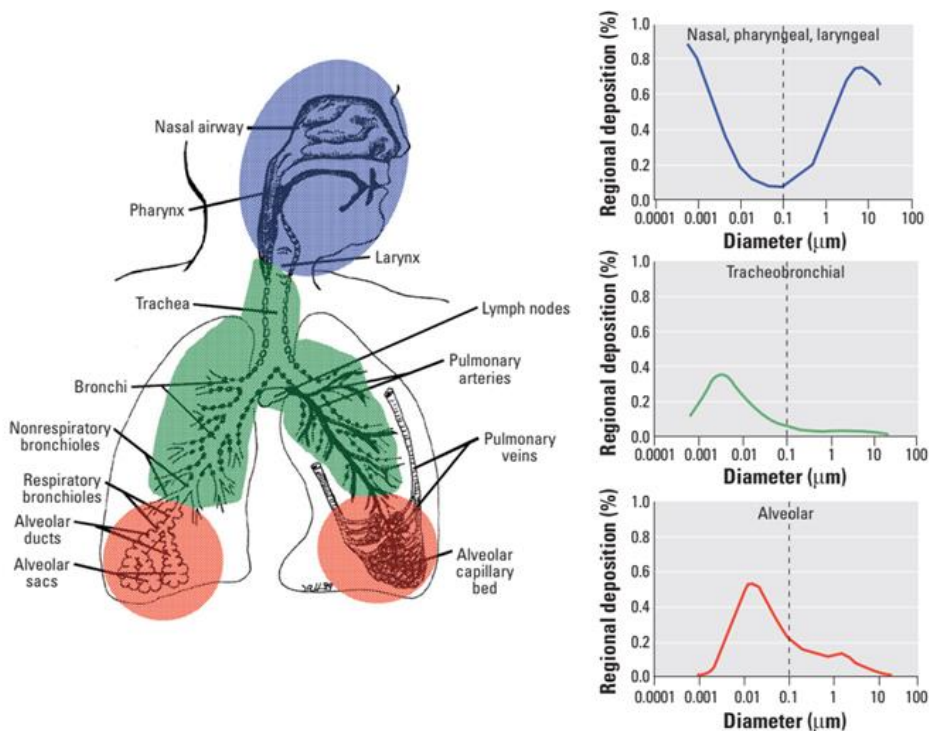


Figure 2. Predicted fractional deposition of inhaled particles in the nasopharyngeal, tracheobronchial, and alveolar region of the human respiratory tract during nose breathing (Oberdörster et al., 2005).

Once deposited on the lung surface, particles may remain intact or be partially or totally dissolved.

Some particles (like salt particles) might dissolve upon contact with aqueous solutions, and the dissolved ions be uptake by cells through ion channels. Once internalized, they exert a short and quickly response. On the other hand, insoluble particles are phagocytosed by cells activating an intracellular signaling cascade and promoting an extended response (Salvi and Holgate, 1999). Finally, organic compounds adsorbed on particles can be transported and transferred directly to the cells through the plasma membrane and then, trigger some intracellular signaling pathways (Penn et al., 2005).

Deposited particles can be cleared by two mechanisms: mucociliary clearance and phagocytosis. Mucociliary clearance is the lung first defense line and is responsible for the removal of most the inhaled particles in the tracheobronchial airways. Immunologic, phagocytic, and enzymatic defenses also contribute to this process. Under physiological conditions the insoluble particles removal occurs within 24 hours. During pathological conditions, (such as respiratory diseases like asthma and

COPD) the process is impaired, particle retention increases, and adverse health effects occur.

Phagocytosis represent the primary clearance mechanism in the alveolar region and is responsible for the removal of any materials, including airborne particles and microorganisms. Phagocytic cells (i.e., macrophages, monocytes and leukocytes) are localized throughout the respiratory system. Phagocytosis efficiency decreases accordingly to particle size. Thus, ultrafine particles (UFP) can be retained in the alveolar region for years (Environmental Protection Agency, 2003; Murgia et al., 2014).

In recent years increasing attention has been given to the study of UFP by monitoring of personal exposure, as well as discovering their toxicological impact by means of experimental studies (Wallace and Ott, 2011). Their increasing consideration is mostly due to their ability to deeply penetrate in the lungs and interact with the alveolar epithelium. Moreover, they can potentially cross the respiratory barrier and finally reach more distal organs (Möller et al., 2008).

1.2. PM sources

Several natural and anthropogenic sources might be responsible of PM emission in the atmosphere. Natural sources include volcanoes, forest fires, living vegetation, dust storms and sea spray (Anderson et al., 2012; Misra et al., 2001). Anthropogenic sources instead include vehicle emissions, abrasion of brakes and tires, tobacco smoke, solid fuel combustion (including biomass and heavy oil) and industrial and agricultural processes (Srimuruganandam and Shiva Nagendra, 2012).

Moreover, PM can be classified as “primary” if particles are directly emitted in the atmosphere by road transport, combustion and other industrial processes, or “secondary” if particles derived from chemical reactions among different primary particulates in the atmosphere (RW et al., 2010; Vicente and Alves, 2018). Primary and secondary PM can be transported in the atmosphere over long distances and eliminated via gravitational sedimentation, aggregation with other particles or meteorological conditions (such as rainfall) (Baldacci et al., 2015).

In conclusion, the first exposure route to airborne particles is inhalation. Consequently, chronic alterations and numerous acute cyto- and genotoxic effects could rise from PM exposure. Among these, cardiopulmonary diseases exacerbation remains the most palpable effect. Considering this, studies on inhalation toxicology focusing on the understanding of the molecular mechanism that occur in the airways as consequence of air pollution exposure are getting more important.

2. Combustion-derived particles: case of study

2.1. Biomass-derived particles

Exposure to wildfire and other biomass smoke is increasingly recognized as a significant public health concern considering that about 3 billion people are exposed to biomass smoke in the world (Silva et al., 2015). Indeed, biomass combustion for residential cooking, heating and lighting is nowadays documented as main source of energy and major contributor to PM emissions, especially in developing countries. The use of solid biomass as sustainability source is increasing also in Europe, where has been promoted as measure to mitigate gas emissions by replacing fossil fuels. As consequence, in 2015 was estimated that in Europe residential combustion has been accountable for > 45% of total PM_{2.5} emissions (Vicente and Alves, 2018). In order to reach energy sustainability, renewable sources like pellet and wood are commonly used as fuel for combustion appliances (Venturini et al., 2018).

The term “biomass smoke” refers to emissions from different combustion appliances. In literature has been described a high variability in airborne particles emitted by combustion appliances. Different factors are certainly responsible for the observed variability: appliance, type of fuel, combustion technologies and operating conditions.

Considering that emissions are highly technology-dependent, the choice of appliance is important. The type of appliances commonly used are fireplace (that can be open or closed), stove and boiler (Vicente and Alves, 2018). Moreover, old and new models of appliance differ in combustion technology, and air supply and thus, in the emitted particles (Kocbach Bølling et al., 2009). Automated combustion technologies characterized by high energy efficiency and reduced pollutant emissions have been developed with a better performance compared to traditional ones (Meyer, 2012). However, traditional old type appliances still represent the most used (Gonçalves et al., 2012).

PM from these appliances is highly dependent on the type of fuel and the moisture content (Kocbach Bølling et al., 2009). Different type of biomass can be used as fuel: crop residues, wood, logs, pellet, charcoal, spring sandstorms or resuspension of local soil and animal dung are all referred as biomass (Capistrano et al., 2016; Dilger et al., 2016; Jin et al., 2016; Marchetti et al., 2019; Muala et al., 2015; Kasurinen et al., 2017).

2.1.1. Biomass-particles: physico-chemical properties

Physical and chemical properties of particles derived from biomass combustion differ considerably. They usually have a diameter between 0.1 and 1 μm (Vicente and Alves, 2018). Based on their chemical composition and morphology, they can

be classified into three different groups: spherical organic carbon particles, aggregated soot particles and inorganic ash particles. However, we should consider that during combustion the different particle classes may co-exist and interact to each other.

Spherical organic carbon particles are usually formed during incomplete combustion processes, characterized by low temperature. They are composed of several organic compounds, including high quantities of oxygenated water-soluble organic species, monosaccharide anhydrides, low levels of elemental carbon and a reduced content of inorganic constituents, such as potassium, sulphur and chlorine. This type of particles is usually emitted from an open fireplace or a conventional stove.

Solid carbon aggregates (soot) are generated during incomplete combustion with air-starved conditions at high temperatures (~800-1000°C) using conventional stoves, open fireplaces or boilers. These particles are characterized by a graphitic structure with concentric carbon layers. Moreover, soot particles are composed of high level of elemental carbon, low level of organic carbon and high levels of PAHs compared to the spherical organic carbon. The most abundant PAHs are naphthalene, acenaphthene, fluorene, phenanthrene, anthracene, fluoranthene, pyrene, benzo(a)pyrene (B(a)P) and fluoranthene.

Finally, *inorganic ash particles* are generated during complete combustion processes at high-temperature. They are frequently emitted from boilers or stove with modern technology and good oxygen supply. Particles resulting from this process are alkali salts of potassium/sodium-sulphates and chlorides and are characterized by low organic and elemental carbon content and small amounts of trace elements (like Zn) (Kocbach Bølling et al., 2009).

Therefore, particles emitted from combustion processes consist of a complex mixture of several organic and inorganic compounds, characterized by different physical and chemical properties, which greatly influence the harmful biological effects. Indeed, the biological responses activated, are related to both physical characteristics (such as particle size and number, surface area, density, morphology and mass concentration) and chemical properties. As known, the content of metals and organic compounds strongly affect the particle-elicited adverse outcomes. Among metals vanadium, zinc, iron, copper and nickel have been suggested to play a crucial role in the adverse health effects observed after exposure to combustion-derived particles (CDPs). Regarding organic compounds, PAHs, quinones, aldehydes, ketones, organic acids and various chlorinated organics can seriously contribute to the harmful biological effects.

Most importantly, combustion technology, quality and type of fuel and combustion conditions are accountable for these different physico-chemical properties. Thus, several factors should be taken in to account to prevent the hazardous effects related to exposure to biomass burning (Vicente and Alves, 2018). In this

perspective, acquire importance also the necessity to use high quality fuels, with a precise classification and qualitative standard on raw material and to standardize the burning appliances in order to obtain cleaner systems. This is essential indeed, to optimize the combustion efficiency, avoid technical problems and possibly reduce the hazardous health effects (Venturini et al., 2018). Furthermore, lack of ventilation in homes frequently exacerbate the harmful effects of the emitted particles.

Bølling et colleagues (2009) compared the physicochemical properties of particles emitted from diverse combustion appliances reporting their correlation to the adverse health effects. The researchers concluded that combustion conditions and CDPs physicochemical properties strongly influence results on biological endpoint investigated. Attention was to particles derived from incomplete combustion processes that seems to be more toxic compared to the ones generated under controlled combustion conditions.

2.1.2. Health effects

Exposure to PM from biomass combustion has been associated with harmful health outcomes, including increased mortality and hospital admissions for cardio-respiratory illnesses (Uski et al., 2014). In recent years emissions from household combustion of biomass fuels has been classified as “probably carcinogenic to humans” (group 2A) by the International Agency for Research on Cancer (“IARC Monographs on the Evaluation of Carcinogenic Risks to Humans,” 2010). Taking this into account, indoor pollution and the associated adverse health effects is getting more important.

Although the particles derived from biomass represent the main source of particulate air pollution in many countries and their toxicity is of increasing interest, relatively few toxicological studies have been published on the health effects associated with exposure to such particles.

Taken together these studies suggest that risk assessment for biomass-derived particles is not enough, considering that toxicity of the emitted PM vary significantly accordingly to several factors.

2.2. Diesel exhaust particles

In urban area the main source of combustion processes is represented by UFP deriving from tire and brake wearing and, above all, from diesel exhaust particles (DEP) deriving from incomplete combustion of the diesel engine. DEP particles, composed of a carbonaceous core and several chemicals adsorbed on it, including organic compounds, metals, sulphur compounds, aldehydes and ashes, are indeed, a worldwide problem given the intensity of vehicle traffic in large and small population centers (Zerboni et al., 2019; Bengalli et al., 2019).

The organic fraction is composed of methanol, ethylene, formaldehyde, aliphatic compounds and more complex molecules such as benzene, naphthalene, pyrene, anthracene and their functionalized derivatives. They can be traces of fuel and lubrication oil that survived to combustion, but also compounds newly formed from combusted precursor. Metal and metal-oxides derive mainly from lubrication, fuel additives and engine wear, such as zinc, magnesium, cerium, iron, manganese, platinum and copper.

Particles emitted by diesel engines have commonly a dimension between 10 and 30 nm, but they can also form agglomerate of 1 and 2 μm , depending on the type of engine (Steiner et al., 2016; Bengalli et al., 2019).

These particles are characterized not only by a small size, but also by a large surface area that allow them to penetrate deeply in the lung and affect the respiratory system (Li and Nel, 2006).

Numerous factors can impact on DEP chemical and physical properties. Among them, there are type and operation mode, fuel and lubrication oil type, oil additives, load, temperature and filtration devices.

In the last decades, there has been a huge increase in diesel-fueled vehicle with pre-EURO 5 technologies (that are known for their high PM emissions). Therefore, an increased DEP emission compared to gasoline-fueled vehicles has been observed. Even if, in recent years new engines that emit less PM and gaseous compounds have been developed, old technology cars are still commonly used.

Furthermore, actions to remove PM using a diesel particulate filter (DPF) provoke an increase of NO_x and cause the formation of different kinds of particles (Steiner et al., 2016; Schwarze et al., 2013).

Considering this, extensive research on DEP effects on human health has been carried out. Environmental and toxicological studies of UFP derived from diesel engines combustion, are currently performed using different type of DEP: diesel exhaust particles from light duty passenger cars and standard reference materials (SRM) furnished by The National Institute of Standards and Technology (NIST, United States)(Braun et al., 2007).

In 2012, the discharge of diesel engines has been classified by IARC as carcinogenic to humans (Group 1). Thus, there are enough scientific evidences to support the existence of a strong correlation between DEP exposure and the development of cancer in humans ("IARC: diesel engine exhaust carcinogenic.," 2012). Moreover, DEP exposure is associated to an increased incidence of allergies, asthma, rhinitis, cardiovascular disorders, mutagenesis and carcinogenesis (Bengalli et al., 2017).

3. Impacts of air pollution on health

Air pollution has a noteworthy impact on human health, principally in urban areas. PM short-term effects are usually observed within 48 h after exposure and include acute eye and nose irritation, respiratory symptoms, fatigue, headache, and neurophysiological symptoms (Tseng et al., 2017).

Chronic exposure instead, is responsible of reducing life expectancy. Epidemiologic data have revealed that air pollution is the main cause of premature death and is linked to increased mortality and morbidity (Guerreiro et al., 2018; Tseng et al., 2017). It is also involved in the pathogenesis of several pulmonary and cardiovascular diseases. Among pulmonary effects decreased lung function, exacerbation of asthma, allergy, chronic obstructive pulmonary disease (COPD), fibrosis and lung cancer have been reported (Anderson et al., 2012; Kocbach Bølling et al., 2009). Cardiac and vascular diseases are also a frequently consequence of prolonged exposure to air pollution. Among these, there are atherosclerosis, ischemic stroke, thrombotic effects, congestive heart failure and myocardial ischemia (Wang et al., 2017; WHO, 2014). Furthermore, evidences have demonstrated that maternal exposure is related to adverse impacts on pregnancy, fertility, new-born and children. New-onset type 2 diabetes in adults, obesity, systemic inflammation, ageing, and neurodegenerative diseases, like Alzheimer's disease and dementia, have also been associated to PM exposure.

All these data support the carcinogenic potential of PM highlighted in 2013 by IARC ("IARC: Outdoor air pollution a leading environmental cause of cancer deaths," 2013).

Several toxicological studies have been performed in the last decades in order to clarify the close relationship between PM exposure and adverse effects on human health, allowing us to formulate many hypotheses on the mechanisms by which PM, directly or indirectly, can cause health damage (World Health Organization, 2013).

Unfortunately, there are still no evidence about a possible safe concentration of PM exposure or a threshold suggesting that above it, adverse effects may occur. Taking this into consideration it is imperative to avoid, reduce and prevent emissions of air pollutant considering the World Health Organization guidelines for planning and implementing health long-term policies.

4. *In vitro* systems

Considering that PM can reach the lung by inhalation, studies on *in vitro* model derived from lung tissue might provide useful information on the negative effects produced by PM exposure.

Epithelial cells and alveoli, which are in direct contact with pollutants, are the first targets for exposure studies on inhaled substances deriving from environmental or occupational sources. Thus, cell culture models for inhalation toxicology are focused mainly on epithelial cells.

Different human cell lines are currently used to test the harmful effects of inhaled particles on the human respiratory system, especially bronchial and alveolar epithelial cells. Additionally, pulmonary endothelial cells and monocyte permit to investigate possible cardiovascular events and immunomodulatory responses that occur after exposure to PM (Dong et al., 2017; Hiemstra et al., 2018).

For inhalation toxicology, particles are usually added as suspension to the culture medium in which lung cells are submerged. This process can change the particle properties and cause particle-particle interactions and binding to the medium components. Although it is well known that inhaled particles can easily reach the alveoli, the mechanism by which the particles really interact with cells remains unknown. This is a consequence of the lack of an appropriate exposure system.

Despite the numerous advantages given by *in vitro* systems, there are indeed, some concerns related to their use, due to the different exposure modes between *in vivo* (aerosol) and *in vitro* (particles suspended) models, but also to the difficulty of appropriately correlate particle doses used in cellular systems to the real exposure concentrations.

Most of the studies performed on environmental chemicals and particles are based on monoculture system models in which cells are exposed to particles in submerged conditions. Furthermore, in recent years modern systems for inhalation toxicology studies have been developed to recreate more realistic conditions, such as the air-liquid interface (ALI). ALI exposure system represents an alternative method to the submerged system for inhalation toxicology studies. This system allows the direct exposure of cells to an aerosol containing the particles. However, its use for PM studies is still limited due to the reduced efficiency of particles deposition. Moreover, complex strategies are necessary to define well the composition of the particles to which cells are exposed. For this reason, this system is currently used mainly for studying commercial nanoparticles, that possess a well-defined chemical composition and size (Kim et al., 2013).

In order to investigate the biological interactions and the effects of combustion-derived particles (CDPs) on the respiratory system and pulmonary endothelium, different human cell lines were used for the studies here presented.

The A549 cell line is derived from the human lung adenocarcinoma. These cells exhibit a phenotype like the type II pneumocytes (alveolar cells) and are characterized by the presence of lamellar bodies, surfactant proteins, a distinct polarization, tight junctions and extensive cytoplasmic extensions (Foster et al., 1998; Murgia et al., 2014).

The cell line is widely used in the research to test PM cytotoxic effects and has been confirmed to be a valid model for lung and particle toxicity studies. Moreover, A549 cells have also been incorporated into more complex 3D tri-culture and tetra-culture (together with endothelial cells, macrophages and dendritic cells) *in vitro* models, that mimic the tissue organization better than a monoculture (Klein et al., 2017; Murgia et al., 2014).

In this study, we described the biological effects of PM₁₀s emitted indoor from the burning of three different biomasses on human alveolar epithelial cells. Cytotoxic, genotoxic and pro-carcinogenic effects were studied (Chapters 1 and 2).

As bronchial epithelial cells, two different cell lines were used: HBEC-3KT and BEAS-2B cells.

HBEC3-KT cells are human normal cells immortalized with the cell cycle protein cdk4 and the catalytic subunit of the telomerase enzyme (human telomerase reverse transcriptase, hTERT). hTERT stabilizes the telomere length allowing then, to extend the cell proliferation in culture without trigger the oncogenic transformation. It also allows to retain the cell normal differentiation profile and/or function. HBEC3-KT cells do not form colonies in soft agar and do not promote tumors development in mice. Compared to BEAS-2B, HBEC-3KT have been generated without viral oncoproteins, which may lead cells to become malignant after numerous passages *in vitro* (Ramirez et al., 2004; Vaughan et al., 2006).

Using HBEC3-KT, in this work (Chapter 3) we elucidate genotoxic and pro-carcinogenic effects of biomass combustion-derived particles. Epithelial bronchial cells have been exposed not only to biomass particles as such, but also to their respective organic and inorganic fractions, in order to characterize and compare the relative role of the particle core versus extractable organic compounds.

BEAS-2B are epithelial bronchial cells obtained by autopsy on healthy subjects and then transfected with DNA sequences of an adenovirus, the Simian Virus 40 (SV40). In the present work, we exposed BEAS-2B cells to DEP particles to study the role of epithelial-released mediators in the endothelial cells activation (Chapter 4).

Finally, human microvascular endothelial cells were used. This type of cells resides on the luminal side of blood vessels and cooperates to the several interactions that occur between blood and tissues. For this reason, they play an important role in numerous physiological and pathological processes. Thus, their use is indispensable to recreate *in vitro* experimental models of inflammation, angiogenesis, wound healing, atherosclerosis and cancer.

Thus, to investigate the role of endothelial cells, *HPMEC-ST1.6R* cells were chosen for our study. They are endothelial cells originating from the pulmonary microcirculation. Compared to other endothelial cells often used *in vitro* (such as HUVEC cells), HPMEC-ST1.6R cells, coming directly from a lung district, recreate a more realistically situation like that *in vivo*. HPMEC-ST1.6R cells were generated by co-transfection with a plasmid encoding for hTERT and the SV40 large T-antigen.

They exhibit several unique specific characteristics that define endothelial cells, including the high constitutive production of von Willebrand factor (vWF) and the expression of adhesion molecules such as the platelet endothelial cell adhesion molecule (PECAM-1, CD31), the intercellular cell adhesion molecule 1 (ICAM-1, CD54), the vascular adhesion molecule (VCAM-1, CD106), and E-selectin (E-sel) (Unger et al., 2002).

In the present work (Chapter 4), we evaluate DEP effects at the endothelial level using conditioned media (supernatants of BEAS-2B cells exposed to DEP and then used for the treatment of HPMEC-ST1.6R cells).

5. *In vitro* toxicological studies

In the last decades, several epidemiological studies have been performed to explain the association between particle exposure and adverse effects on human health and clarify the mechanisms of particle toxicology, also linking chemical and physical properties of PM with the biological responses obtained with *in vitro* systems. *In vitro* studies aim indeed, to provide additional information on the particle toxic properties, considering them as a complex mixture of compounds.

Numerous *in vitro* studies have demonstrated the toxic effects of biomass particles and DEP on human or animal cell models, reporting that such particles cause cytotoxicity, inflammation, oxidative stress, plasma membrane impairment, xenobiotic metabolism response activation, DNA damage, cell cycle de-regulation and EMT activation (Danielsen et al., 2011; Happo et al., 2013; Jalava et al., 2012; Bølling et al., 2012; Velali et al., 2018; Farina et al., 2013; Gualtieri et al., 2011; Longhin et al., 2016; Robertson et al., 2012; Rossner et al., 2016; Sancini et al., 2014; Uski et al., 2012; Yang et al., 2016; Nemmar et al., 2003; Bersaas et al., 2016; Rynning et al., 2018). Moreover, few studies compared DEP and biomass-derived particles reporting that DEP is more toxic and mutagenic (Künzi et al., 2015; Yang et al., 2010).

Some literature studies have also correlated the chemical composition of PM with the effects on health, as evidenced by different biological endpoints (Dilger et al., 2016; Líbalová et al., 2014; Perrone et al., 2013; Tarantini et al., 2011; Totlandsdal et al., 2015, 2014; Yang et al., 2016; Låg et al., 2016; Knaapen et al., 2002).

In the present work, attention was given to some of the main toxicological mechanisms activated following exposure to PM, such as inflammation, oxidative stress, DNA damage, cell cycle de-regulation and EMT activation.

PM toxicity may be mediated mainly by two mechanisms: by triggering directly an inflammatory response or by promoting reactive oxygen species (ROS) formation within pulmonary cells that subsequently cause oxidative stress and inflammation.

Inflammation is indeed, a common denominator in the adverse outcome associated with PM exposure. Literature studies have confirmed that airborne particles trigger an inflammatory response in epithelial and endothelial cells, which is characterized by the secretion of pro-inflammatory cytokines such as interleukin-1 β (IL-1 β), interleukin-6 (IL-6), interleukin-8 (IL-8) and tumor necrosis factor- α (TNF- α). Inflammatory response can be triggered by different compounds adsorbed on PM, such as metals, PAHs but also biological components (like endotoxins) (Møller et al., 2014; Tseng et al., 2017).

Inflammation can lead also to enhanced ROS production, DNA damage and inhibition of apoptosis. Inflamed cells are indeed, effective in generating ROS and other reactive species, promoting oxidative damage and carcinogenesis (Valavanidis et al., 2013).

In recent years has been proposed that one of the main mechanisms through which PM exert harmfulness is oxidative stress (Møller et al., 2014). Oxidative stress is a consequence of the imbalance between the production of cellular oxidant species and the antioxidant capability and is characterized by the generation of ROS. ROS species can be produced by cells both in physiological conditions and in response to an environmental insult. These species are transient but highly cytotoxic and lead to a state of cellular oxidative stress. *In vitro* and *in vivo* studies have demonstrated that PM promote oxidative stress and the upregulation of antioxidant enzymes, such as heme oxygenase (HO-1) and superoxide dismutase (Tseng et al., 2017).

DNA is regarded as an important target for oxidative stress response. During PM-induced oxidative stress response, the antioxidant defense system can induce free radical formation that generate a huge number of oxidative modifications in DNA, including strand break and base oxidations. Oxidative DNA damage may be implicated in different steps of cancer development. (Valavanidis et al., 2013).

Cell cycle progression can be altered not only in response to numerous genotoxic insults, but also to protein structural dysfunctions. Oxidative DNA damage has been reported one of the mechanisms responsible for cell cycle de-regulation. Indeed, DNA damage triggers checkpoints protein kinases activation and stop cells from going on in the cell cycle. The activated G1/S, G2/M and metaphase/anaphase (M/A) transition checkpoints might be diverse according to the type of damage (Figure 3).

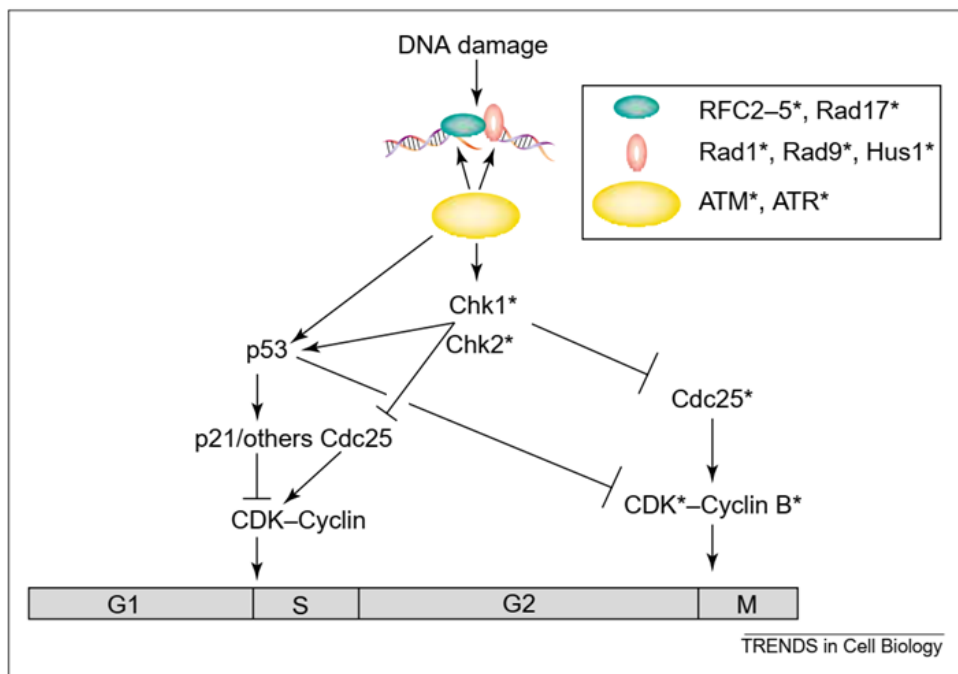


Figure 3. DNA-integrity checkpoint pathways (Pearce and Humphrey, 2001).

Their function is to mediate cell cycle arrest at G1, S, or G2 phases, induce DNA repair and avoid transmissions of DNA damages to daughter cells.

DNA damage response is characterized by the protein kinases ATM (ataxia telangiectasia mutated) and ATR (ATM and Rad3 related) activation. They rapidly localize to the damage site and promote a cell signaling cascade that leads to the phosphorylation of numerous substrates. Activated substrates can act on different processes: DNA repair, cell-cycle blockage or apoptosis (Longhin et al., 2013; Pearce and Humphrey, 2001).

Another important process activated following exposure to PM is the epithelial-to-mesenchymal transition (EMT). It is a key program associated with both physiological and pathological processes, including embryogenesis, organ development, wound healing and tissue repair, tumor development and metastasis.

During EMT, epithelial cells undergo numerous biochemical changes, losing cellular polarity and cell-to-cell contacts, re-organizing the cytoskeleton and differentiating into a mesenchymal-cell phenotype. The loss of epithelial markers such as E-cadherin and ZO-1 and acquisition of mesenchymal markers such as N-cadherin and Vimentin, are considered as crucial events in EMT process. In particular, the so called “cadherin switch”, that consist of E-cadherin down-

regulation and N-cadherin up-regulation, is an important step and involve several genetic and epigenetic alterations (Figure 4).

The mesenchymal phenotype acquired is characterized by increased motility, invasiveness and resistance to apoptosis (Kalluri and Weinberg, 2009; Thiery et al., 2009).

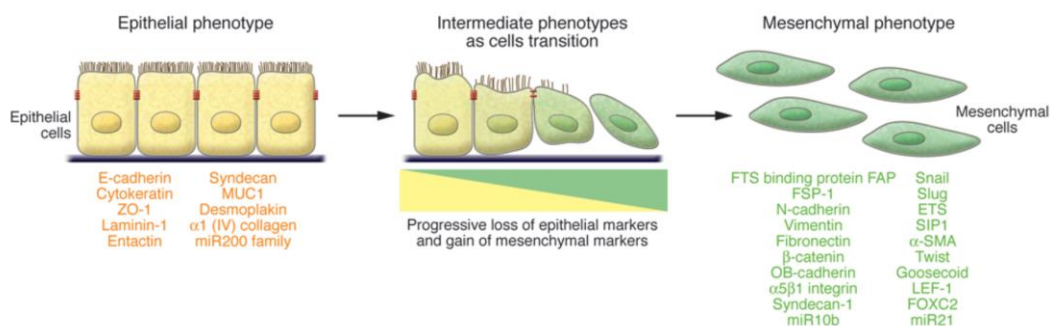


Figure 4. EMT. An EMT involves a functional transition of polarized epithelial cells into mobile and ECM component–secreting mesenchymal cells (Kalluri and Weinberg, 2009).

In recent years, increasing evidence have suggested that this process can be activated following exposure to PM and lead to lung cancer development (Bersaas et al., 2016; Rynning et al., 2018; Yang et al., 2017).

Cancer is a worldwide leading cause of death resulting also from environmental exposure. However, the specific connections between PM exposure and cancer progression remains not clear.

Cancer is a long-term process that involve several distinct phases. Although the detailed sequencing is not still fully explained, carcinogenesis involves tumor initiation, tumor formation and progression, matrix remodeling, intravasation, extravasation and finally metastasis. Important typical hallmarks are genetic instability, chronic inflammatory response, increased migration, proliferation, insensitivity to anti-growth signals, replicative immortality, dysregulated metabolism, resistance to apoptosis, angiogenesis, invasiveness and metastasis.

Both cancer cells and stromal cells synthetize chemokines and cytokines that act by autocrine or paracrine mechanisms to sustain tumor development, inducing angiogenesis and facilitating the evasion of the immune system. Regarding to lung cancer, which has been associated to exposure to airborne pollution, the release of IL-8 by tumor cells has been reported to be a key step. The cytokines release indeed, promote angiogenesis, an important step in malignant transformation (Øvrevik et al., 2017; Raman et al., 2007; Fidler, 2002).

6. Perspectives

A large amount of data is available in literature on the biological mechanisms activated by exposure to airborne pollutant. Their aim is to clearly understand the molecular mechanisms involved and possibly correlate them to adverse outcomes. Anyway, several questions are still unsolved. A high variability has been indeed observed in the resulting biological effects due to PM complexity and its variability in structure and chemical composition.

Knowing the cellular mechanisms and the hazardous PM components responsible for their activation is a crucial step to understand the possible clinical outcomes and to define more efficient strategies to reduce harmful effects and also to implement air quality measures and guidelines in order to finally reduce air pollution.

In this perspective, in this work a comparative analysis of PMs, derived from combustion of different sources, has been performed in order to understand the specific biological effects induced and associating them to the particle physico-chemical properties.

References

- Anderson, J.O., Thundiyil, J.G., Stolbach, A., 2012. Clearing the Air: A Review of the Effects of Particulate Matter Air Pollution on Human Health. *J. Med. Toxicol.* 8, 166–175. <https://doi.org/10.1007/s13181-011-0203-1>
- Baldacci, S., Maio, S., Cerrai, S., Sarno, G., Băiz, N., Simoni, M., Annesi-Maesano, I., Viegi, G., 2015. Allergy and asthma: Effects of the exposure to particulate matter and biological allergens. *Respir. Med.* <https://doi.org/10.1016/j.rmed.2015.05.017>
- Bengalli, R., Longhin, E., Marchetti, S., Proverbio, M.C., Battaglia, C., Camatini, M., 2017. The role of IL-6 released from pulmonary epithelial cells in diesel UFP-induced endothelial activation. *Environ. Pollut.* 231, 1314–1321. <https://doi.org/10.1016/j.envpol.2017.08.104>
- Bengalli, R., Zerboni, A., Marchetti, S., Longhin, E., Priola, M., Camatini, M., Mantecca, P., 2019. In vitro pulmonary and vascular effects induced by different diesel exhaust particles. *Toxicol. Lett.* <https://doi.org/10.1016/j.toxlet.2019.01.017>
- Bersaas, A., Arnoldussen, Y.J., Sjøberg, M., Haugen, A., Mollerup, S., 2016. Epithelial-mesenchymal transition and FOXA genes during tobacco smoke carcinogen induced transformation of human bronchial epithelial cells. *Toxicol. Vitro.* 35, 55–65. <https://doi.org/10.1016/j.tiv.2016.04.012>
- Bølling, A.K., Totlandsdal, A.I., Sallsten, G., Braun, A., Westerholm, R., Bergvall, C., Boman, J., Dahlman, H.J., Sehlstedt, M., Cassee, F., Sandstrom, T., Schwarze, P.E., Herseth, J.I., 2012. Wood smoke particles from different combustion phases induce similar pro-inflammatory effects in a co-culture of monocyte and pneumocyte cell lines. *Part. Fibre Toxicol.* <https://doi.org/10.1186/1743-8977-9-45>
- Braun, A., Mun, B.S., Huggins, F.E., Huffman, G.P., 2007. Carbon speciation of diesel exhaust and urban particulate matter NIST standard reference materials with C(1s) NEXAFS spectroscopy. *Environ. Sci. Technol.* <https://doi.org/10.1021/es061044w>
- Capistrano, S.J., Zakarya, R., Chen, H., Oliver, B.G., 2016. Biomass smoke exposure enhances rhinovirus-induced inflammation in primary lung fibroblasts. *Int. J. Mol. Sci.* 17. <https://doi.org/10.3390/ijms17091403>
- Cesari, D., De Benedetto, G.E., Bonasoni, P., Busetto, M., Dinoi, A., Merico, E., Chirizzi, D., Cristofanelli, P., Donateo, A., Grasso, F.M., Marinoni, A., Pennetta, A., Contini, D., 2018. Seasonal variability of PM_{2.5} and PM₁₀ composition and sources in an urban background site in Southern Italy. *Sci. Total Environ.* 612, 202–213. <https://doi.org/10.1016/j.scitotenv.2017.08.230>
- Cheung, K., Daher, N., Kam, W., Shafer, M.M., Ning, Z., Schauer, J.J., Sioutas, C.,

2011. Spatial and temporal variation of chemical composition and mass closure of ambient coarse particulate matter (PM_{10-2.5}) in the Los Angeles area. *Atmos. Environ.* <https://doi.org/10.1016/j.atmosenv.2011.02.066>
- Danielsen, P.H., Møller, P., Jensen, K.A., Sharma, A.K., Wallin, H., Bossi, R., Autrup, H., Mølhav, L., Ravanat, J.-L., Briedé, J.J., de Kok, T.M., Loft, S., 2011. Oxidative stress, DNA damage, and inflammation induced by ambient air and wood smoke particulate matter in human A549 and THP-1 cell lines. *Chem. Res. Toxicol.* 24, 168–84.
- Dilger, M., Orasche, J., Zimmermann, R., Paur, H.-R., Diabaté, S., Weiss, C., 2016. Toxicity of wood smoke particles in human A549 lung epithelial cells: the role of PAHs, soot and zinc. *Arch. Toxicol.* 90, 3029–3044. <https://doi.org/10.1007/s00204-016-1659-1>
- Dong, T.T.T., Hinwood, A.L., Callan, A.C., Zosky, G., Stock, W.D., 2017. In vitro assessment of the toxicity of bushfire emissions: A review. *Sci. Total Environ.* 603–604, 268–278. <https://doi.org/10.1016/j.scitotenv.2017.06.062>
- Environmental Protection Agency, 2003. Particle Pollution and Your Health. United States.
- Farina, F., Sancini, G., Longhin, E., Mantecca, P., Camatini, M., Palestini, P., 2013. Milan PM₁ induces adverse effects on mice lungs and cardiovascular system. *Biomed Res. Int.* 2013. <https://doi.org/10.1155/2013/583513>
- Fidler, I.J., 2002. The organ microenvironment and cancer metastasis. *Differentiation.* <https://doi.org/10.1046/j.1432-0436.2002.700904.x>
- Foster, K.A., Oster, C.G., Mayer, M.M., Avery, M.L., Audus, K.L., 1998. Characterization of the A549 cell line as a type II pulmonary epithelial cell model for drug metabolism. *Exp. Cell Res.* <https://doi.org/10.1006/excr.1998.4172>
- Gonçalves, C., Alves, C., Pio, C., 2012. Inventory of fine particulate organic compound emissions from residential wood combustion in Portugal. *Atmos. Environ.* <https://doi.org/10.1016/j.atmosenv.2011.12.013>
- Gualtieri, M., Øvrevik, J., Møllerup, S., Asare, N., Longhin, E., Dahlman, H.J., Camatini, M., Holme, J.A., 2011. Airborne urban particles (Milan winter-PM_{2.5}) cause mitotic arrest and cell death: Effects on DNA, mitochondria, AhR binding and spindle organization. *Mutat. Res. - Fundam. Mol. Mech. Mutagen.* 713, 18–31. <https://doi.org/10.1016/j.mrfmmm.2011.05.011>
- Guerreiro, C., de Leeuw, F., Ortiz, A.G., Viana, M., Colette, A., 2018. Air quality in Europe — 2018 report, EEA Report. <https://doi.org/10.2800/62459>
- Happo, M.S., Uski, O., Jalava, P.I., Kelz, J., Brunner, T., Hakulinen, P., Mäki-Paakkanen, J., Kosma, V.M., Jokiniemi, J., Obernberger, I., Hirvonen, M.R., 2013. Pulmonary inflammation and tissue damage in the mouse lung after exposure to PM samples from biomass heating appliances of old and modern technologies. *Sci. Total Environ.* 443, 256–266.

- <https://doi.org/10.1016/j.scitotenv.2012.11.004>
- Hiemstra, P.S., Grootaers, G., van der Does, A.M., Krul, C.A.M., Kooter, I.M., 2018. Human lung epithelial cell cultures for analysis of inhaled toxicants: Lessons learned and future directions. *Toxicol. Vitro*. 47, 137–146.
<https://doi.org/10.1016/j.tiv.2017.11.005>
- IARC: diesel engine exhaust carcinogenic., 2012. . *Cent. Eur. J. Public Health*.
- IARC: Outdoor air pollution a leading environmental cause of cancer deaths, 2013. 51, 229–235.
- IARC Monographs on the Evaluation of Carcinogenic Risks to Humans, 2010. 95.
- Jalava, P.I., Happonen, M.S., Kelz, J., Brunner, T., Hakulinen, P., Mäki-Paakkanen, J., Hukkanen, A., Jokiniemi, J., Obernberger, I., Hirvonen, M.R., 2012. In vitro toxicological characterization of particulate emissions from residential biomass heating systems based on old and new technologies. *Atmos. Environ*. 50, 24–35. <https://doi.org/10.1016/j.atmosenv.2012.01.009>
- Jin, W., Su, S., Wang, B., Zhu, X., Chen, Y., Shen, G., Liu, J., Cheng, H., Wang, X., Wu, S., Zeng, E., Xing, B., Tao, S., 2016. Properties and cellular effects of particulate matter from direct emissions and ambient sources. *J. Environ. Sci. Heal. - Part A Toxic/Hazardous Subst. Environ. Eng*. 51, 1075–1083.
<https://doi.org/10.1080/10934529.2016.1198632>
- Kalluri, R., Weinberg, R.A., 2009. The basics of epithelial-mesenchymal transition. *J. Clin. Invest*. <https://doi.org/10.1172/JCI39104>
- Kasurinen, S., Jalava, P.I., Happonen, M.S., Sippula, O., Uski, O., Koponen, H., Orasche, J., Zimmermann, R., Jokiniemi, J., Hirvonen, M.R., 2017. Particulate emissions from the combustion of birch, beech, and spruce logs cause different cytotoxic responses in A549 cells. *Environ. Toxicol*.
<https://doi.org/10.1002/tox.22369>
- Kim, J.S., Peters, T.M., O’Shaughnessy, P.T., Adamcakova-Dodd, A., Thorne, P.S., 2013. Validation of an in vitro exposure system for toxicity assessment of air-delivered nanomaterials. *Toxicol. Vitro*.
<https://doi.org/10.1016/j.tiv.2012.08.030>
- Kim, K.H., Kabir, E., Kabir, S., 2015. A review on the human health impact of airborne particulate matter. *Environ. Int*.
<https://doi.org/10.1016/j.envint.2014.10.005>
- Klein, S.G., Cambier, S., Hennen, J., Legay, S., Serchi, T., Nelissen, I., Chary, A., Moschini, E., Krein, A., Blömeke, B., Gutleb, A.C., 2017. Endothelial responses of the alveolar barrier in vitro in a dose-controlled exposure to diesel exhaust particulate matter. *Part. Fibre Toxicol*. 14, 1–17.
<https://doi.org/10.1186/s12989-017-0186-4>
- Knaapen, A.M., Shi, T., Borm, P.J.A., Schins, R.P.F., 2002. Soluble metals as well as the insoluble particle fraction are involved in cellular DNA damage induced by particulate matter. *Mol. Cell. Biochem*.

- <https://doi.org/10.1023/A:1015970023889>
- Kocbach Bølling, A., Pagels, J., Yttri, K.E., Barregard, L., Sallsten, G., Schwarze, P.E., Boman, C., 2009. Health effects of residential wood smoke particles: the importance of combustion conditions and physicochemical particle properties. *Part. Fibre Toxicol.* 6, 29.
- Künzi, L., Krapf, M., Daher, N., Dommen, J., Jeannet, N., Schneider, S., Platt, S., Slowik, J.G., Baumlin, N., Salathe, M., Prévôt, A.S.H., Kalberer, M., Strähl, C., Dübgen, L., Sioutas, C., Baltensperger, U., Geiser, M., 2015. Toxicity of aged gasoline exhaust particles to normal and diseased airway epithelia. *Sci. Rep.* <https://doi.org/10.1038/srep11801>
- Låg, M., Øvrevik, J., Totlandsdal, A.I., Lilleaas, E.M., Thormodsæter, A., Holme, J.A., Schwarze, P.E., Refsnes, M., 2016. Air pollution-related metals induce differential cytokine responses in bronchial epithelial cells. *Toxicol. Vitr.* <https://doi.org/10.1016/j.tiv.2016.07.004>
- Li, N., Nel, A.E., 2006. The cellular impacts of diesel exhaust particles: Beyond inflammation and death. *Eur. Respir. J.* <https://doi.org/10.1183/09031936.06.00025006>
- Líbalová, H., Krčková, S., Uhlířová, K., Kléma, J., Ciganek, M., Rössner, P., Šrám, R.J., Vondráček, J., Machala, M., Topinka, J., 2014. Analysis of gene expression changes in A549 cells induced by organic compounds from respirable air particles. *Mutat. Res. - Fundam. Mol. Mech. Mutagen.* 770, 94–105. <https://doi.org/10.1016/j.mrfmmm.2014.10.002>
- Longhin, E., Gualtieri, M., Capasso, L., Bengalli, R., Mollerup, S., Holme, J.A., Øvrevik, J., Casadei, S., Di Benedetto, C., Parenti, P., Camatini, M., 2016. Physico-chemical properties and biological effects of diesel and biomass particles. *Environ. Pollut.* 215, 366–375. <https://doi.org/10.1016/j.envpol.2016.05.015>
- Longhin, Eleonora, Holme, J.A., Gutzkow, K.B., Arlt, V.M., Kucab, J.E., Camatini, M., Gualtieri, M., 2013. Cell cycle alterations induced by urban PM_{2.5} in bronchial epithelial cells: Characterization of the process and possible mechanisms involved. *Part. Fibre Toxicol.* <https://doi.org/10.1186/1743-8977-10-63>
- Longhin, E., Pezzolato, E., Mantecca, P., Holme, J.A., Franzetti, A., Camatini, M., Gualtieri, M., 2013. Season linked responses to fine and quasi-ultrafine Milan PM in cultured cells. *Toxicol. Vitr.* 27, 551–559. <https://doi.org/10.1016/j.tiv.2012.10.018>
- Marchetti, S., Longhin, E., Bengalli, R., Avino, P., Stabile, L., Buonanno, G., Colombo, A., Camatini, M., Mantecca, P., 2019. In vitro lung toxicity of indoor PM₁₀ from a stove fueled with different biomasses. *Sci. Total Environ.* 649, 1422–1433. <https://doi.org/10.1016/j.scitotenv.2018.08.249>
- Meyer, N.K., 2012. Particulate, black carbon and organic emissions from small-

- scale residential wood combustion appliances in Switzerland. *Biomass and Bioenergy*. <https://doi.org/10.1016/j.biombioe.2011.09.023>
- Misra, C., Geller, M., Shah, P., Sioutas, C., 2001. Development and Evaluation of a Continuous Coarse(PM sub (10)-PM sub (2. 5)) Particle Monitor. *J. Air & Waste Manag. Assoc.*
- Møller, P., Danielsen, P.H., Karottki, D.G., Jantzen, K., Roursgaard, M., Klingberg, H., Jensen, D.M., Christophersen, D.V., Hemmingsen, J.G., Cao, Y., Loft, S., 2014. Oxidative stress and inflammation generated DNA damage by exposure to air pollution particles. *Mutat. Res. - Rev. Mutat. Res.* <https://doi.org/10.1016/j.mrrev.2014.09.001>
- Möller, W., Felten, K., Sommerer, K., Scheuch, G., Meyer, G., Meyer, P., Häussinger, K., Kreyling, W.G., 2008. Deposition, retention, and translocation of ultrafine particles from the central airways and lung periphery. *Am. J. Respir. Crit. Care Med.* <https://doi.org/10.1164/rccm.200602-301OC>
- Morakinyo, O.M., Mokgobu, M.I., Mukhola, M.S., Hunter, R.P., 2016. Health outcomes of exposure to biological and chemical components of inhalable and respirable particulate matter. *Int. J. Environ. Res. Public Health.* <https://doi.org/10.3390/ijerph13060592>
- Muala, A., Rankin, G., Sehlstedt, M., Unosson, J., Bosson, J.A., Behndig, A., Pourazar, J., Nyström, R., Pettersson, E., Bergvall, C., Westerholm, R., Jalava, P.I., Happonen, M.S., Uski, O., Hirvonen, M.-R., Kelly, F.J., Mudway, I.S., Blomberg, A., Boman, C., Sandström, T., 2015. Acute exposure to wood smoke from incomplete combustion - indications of cytotoxicity. *Part. Fibre Toxicol.* 12, 33. <https://doi.org/10.1186/s12989-015-0111-7>
- Murgia, X., De Souza Carvalho, C., Lehr, C.M., 2014. Overcoming the pulmonary barrier: New insights to improve the efficiency of inhaled therapeutics. *Eur. J. Nanomedicine.* <https://doi.org/10.1515/ejnm-2014-0019>
- Nemmar, A., Nemery, B., Hoet, P.H.M., Vermeylen, J., Hoylaerts, M.F., 2003. Pulmonary Inflammation and Thrombogenicity Caused by Diesel Particles in Hamsters: Role of Histamine. *Am. J. Respir. Crit. Care Med.* <https://doi.org/10.1164/rccm.200306-801OC>
- Oberdörster, G., Oberdörster, E., Oberdörster, J., 2005. Nanotoxicology: An emerging discipline evolving from studies of ultrafine particles. *Environ. Health Perspect.* <https://doi.org/10.1289/ehp.7339>
- Øvrevik, J., Refsnes, M., Låg, M., Brinckmann, B.C., Schwarze, P.E., Holme, J.A., 2017. Triggering Mechanisms and Inflammatory Effects of Combustion Exhaust Particles with Implication for Carcinogenesis. *Basic Clin. Pharmacol. Toxicol.* 121, 55–62. <https://doi.org/10.1111/bcpt.12746>
- Pearce, A.K., Humphrey, T.C., 2001. Integrating stress-response and cell-cycle checkpoint pathways. *Trends Cell Biol.* [https://doi.org/10.1016/S0962-8924\(01\)02119-5](https://doi.org/10.1016/S0962-8924(01)02119-5)

- Penn, A., Murphy, G., Barker, S., Henk, W., Penn, L., 2005. Combustion-derived ultrafine particles transport organic toxicants to target respiratory cells. *Environ. Health Perspect.* <https://doi.org/10.1289/ehp.7661>
- Perrone, M.G., Gualtieri, M., Consonni, V., Ferrero, L., Sangiorgi, G., Longhin, E., Ballabio, D., Bolzacchini, E., Camatini, M., 2013. Particle size, chemical composition, seasons of the year and urban, rural or remote site origins as determinants of biological effects of particulate matter on pulmonary cells. *Environ. Pollut.* 176, 215–227. <https://doi.org/10.1016/j.envpol.2013.01.012>
- Pope, C.A., Dockery, D.W., 2006. Health Effects of Fine Particulate Air Pollution: Lines that Connect. *J. Air Waste Manage. Assoc.* 56, 709–742. <https://doi.org/10.1080/10473289.2006.10464485>
- Raman, D., Baugher, P.J., Thu, Y.M., Richmond, A., 2007. Role of chemokines in tumor growth. *Cancer Lett.* <https://doi.org/10.1016/j.canlet.2007.05.013>
- Ramirez, R.D., Sheridan, S., Girard, L., Sato, M., Kim, Y., Pollack, J., Peyton, M., Zou, Y., Kurie, J.M., DiMaio, J.M., Milchgrub, S., Smith, A.L., Souza, R.F., Gilbey, L., Zhang, X., Gandia, K., Vaughan, M.B., Wright, W.E., Gazdar, A.F., Shay, J.W., Minna, J.D., 2004. Immortalization of human bronchial epithelial cells in the absence of viral oncoproteins. *Cancer Res.* <https://doi.org/10.1158/0008-5472.CAN-04-3703>
- Robertson, S., Gray, G.A., Duffin, R., McLean, S.G., Shaw, C.A., Hadoke, P.W.F., Newby, D.E., Miller, M.R., 2012. Diesel exhaust particulate induces pulmonary and systemic inflammation in rats without impairing endothelial function ex vivo or in vivo. *Part. Fibre Toxicol.* <https://doi.org/10.1186/1743-8977-9-9>
- Rossner, P., Strapacova, S., Stolcpartova, J., Schmutzerova, J., Milcova, A., Neca, J., Vlkova, V., Brzicova, T., Machala, M., Topinka, J., 2016. Toxic effects of the major components of diesel exhaust in human alveolar basal epithelial cells (A549). *Int. J. Mol. Sci.* 17. <https://doi.org/10.3390/ijms17091393>
- RW, A., GW, F., HR, A., RM, H., B, A., 2010. Urban ambient particle metrics and health: a time-series analysis. *Epidemiology.*
- Rynning, I., Neca, J., Vrbova, K., Libalova, H., Rossner, P., Holme, J.A., Gützkow, K.B., Afanou, A.K.J., Arnoldussen, Y.J., Hrubá, E., Skare, Ø., Haugen, A., Topinka, J., Machala, M., Møllerup, S., 2018. In Vitro Transformation of Human Bronchial Epithelial Cells by Diesel Exhaust Particles: Gene Expression Profiling and Early Toxic Responses. *Toxicol. Sci.* 166, 51–64. <https://doi.org/10.1093/toxsci/kfy183>
- Salvi, S., Holgate, S.T., 1999. Mechanisms of particulate matter toxicity. *Clin. Exp. Allergy.* <https://doi.org/10.1046/j.1365-2222.1999.00576.x>
- Sancini, G., Farina, F., Battaglia, C., Cifola, I., Mangano, E., Mantecca, P., Camatini, M., Palestini, P., 2014. Health risk assessment for air pollutants: Alterations in lung and cardiac gene expression in mice exposed to milano winter fine

- particulate matter (PM_{2.5}). *PLoS One* 9.
<https://doi.org/10.1371/journal.pone.0109685>
- Schwarze, P.E., Totlandsdal, A.I., Låg, M., Refsnes, M., Holme, J.A., Øvrevik, J., 2013. Inflammation-related effects of diesel engine exhaust particles: Studies on lung cells in vitro. *Biomed Res. Int.* <https://doi.org/10.1155/2013/685142>
- Silva, R., Oyarzún, M., Olloquequi, J., 2015. Pathogenic Mechanisms in Chronic Obstructive Pulmonary Disease Due to Biomass Smoke Exposure. *Arch. Bronconeumol.* (English Ed. <https://doi.org/10.1016/j.arbr.2015.04.013>
- Srimuruganandam, B., Shiva Nagendra, S.M., 2012. Source characterization of PM₁₀ and PM_{2.5} mass using a chemical mass balance model at urban roadside. *Sci. Total Environ.* <https://doi.org/10.1016/j.scitotenv.2012.05.082>
- Steiner, S., Bisig, C., Petri-Fink, A., Rothen-Rutishauser, B., 2016. Diesel exhaust: current knowledge of adverse effects and underlying cellular mechanisms. *Arch. Toxicol.* <https://doi.org/10.1007/s00204-016-1736-5>
- Tarantini, A., Maître, A., Lefèbre, E., Marques, M., Rajhi, A., Douki, T., 2011. Polycyclic aromatic hydrocarbons in binary mixtures modulate the efficiency of benzo[a]pyrene to form DNA adducts in human cells. *Toxicology* 279, 36–44. <https://doi.org/10.1016/j.tox.2010.09.002>
- Thiery, J.P., Acloque, H., Huang, R.Y.J., Nieto, M.A., 2009. Epithelial-Mesenchymal Transitions in Development and Disease. *Cell.* <https://doi.org/10.1016/j.cell.2009.11.007>
- Totlandsdal, A.I., Låg, M., Lilleaas, E., Cassee, F., Schwarze, P., 2015. Differential proinflammatory responses induced by diesel exhaust particles with contrasting PAH and metal content. *Environ. Toxicol.* <https://doi.org/10.1002/tox.21884>
- Totlandsdal, A.I., Øvrevik, J., Cochran, R.E., Herseth, J.I., Bølling, A.K., Låg, M., Schwarze, P., Lilleaas, E., Holme, J.A., Kubátová, A., 2014. The occurrence of polycyclic aromatic hydrocarbons and their derivatives and the proinflammatory potential of fractionated extracts of diesel exhaust and wood smoke particles. *J. Environ. Sci. Heal. - Part A Toxic/Hazardous Subst. Environ. Eng.* <https://doi.org/10.1080/10934529.2014.854586>
- Tseng, C.Y., Wang, J.S., Chao, M.W., 2017. Causation by Diesel Exhaust Particles of Endothelial Dysfunctions in Cytotoxicity, Pro-inflammation, Permeability, and Apoptosis Induced by ROS Generation. *Cardiovasc. Toxicol.* <https://doi.org/10.1007/s12012-016-9364-0>
- Unger, R.E., Krump-Konvalinkova, V., Peters, K., James Kirkpatrick, C., 2002. In vitro expression of the endothelial phenotype: Comparative study of primary isolated cells and cell lines, including the novel cell line HPMEC-ST1.6R. *Microvasc. Res.* <https://doi.org/10.1006/mvres.2002.2434>
- Uski, O., Jalava, P.I., Happonen, M.S., Leskinen, J., Sippula, O., Tissari, J., Mäki-Paakkanen, J., Jokiniemi, J., Hirvonen, M.R., 2014. Different toxic mechanisms

- are activated by emission PM depending on combustion efficiency. *Atmos. Environ.* <https://doi.org/10.1016/j.atmosenv.2014.02.036>
- Uski, O.J., Happonen, M.S., Jalava, P.I., Brunner, T., Kelz, J., Obernberger, I., Jokiniemi, J., Hirvonen, M.-R., 2012. Acute systemic and lung inflammation in C57Bl/6J mice after intratracheal aspiration of particulate matter from small-scale biomass combustion appliances based on old and modern technologies. *Inhal. Toxicol.* 24, 952–965. <https://doi.org/10.3109/08958378.2012.742172>
- Valavanidis, A., Vlachogianni, T., Fiotakis, K., Loridas, S., 2013. Pulmonary oxidative stress, inflammation and cancer: Respirable particulate matter, fibrous dusts and ozone as major causes of lung carcinogenesis through reactive oxygen species mechanisms. *Int. J. Environ. Res. Public Health* 10, 3886–3907. <https://doi.org/10.3390/ijerph10093886>
- Vaughan, M.B., Ramirez, R.D., Wright, W.E., Minna, J.D., Shay, J.W., 2006. A three-dimensional model of differentiation of immortalized human bronchial epithelial cells. *Differentiation*. <https://doi.org/10.1111/j.1432-0436.2006.00069.x>
- Velali, E., Papachristou, E., Pantazaki, A., Besis, A., Samara, C., Labrianidis, C., Lialiaris, T., 2018. In vitro cellular toxicity induced by extractable organic fractions of particles exhausted from urban combustion sources - Role of PAHs. *Environ. Pollut.* 243, 1166–1176. <https://doi.org/10.1016/j.envpol.2018.09.075>
- Venturini, E., Vassura, I., Agostini, F., Pizzi, A., Toscano, G., Passarini, F., 2018. Effect of fuel quality classes on the emissions of a residential wood pellet stove. *Fuel*. <https://doi.org/10.1016/j.fuel.2017.09.017>
- Vicente, E.D., Alves, C.A., 2018. An overview of particulate emissions from residential biomass combustion. *Atmos. Res.* 199, 159–185. <https://doi.org/10.1016/j.atmosres.2017.08.027>
- Wallace, L., Ott, W., 2011. Personal exposure to ultrafine particles. *J. Expo. Sci. Environ. Epidemiol.* <https://doi.org/10.1038/jes.2009.59>
- Wang, J., Huang, J., Wang, L., Chen, C., Yang, D., Jin, M., Bai, C., Song, Y., 2017. Urban particulate matter triggers lung inflammation via the ROS-MAPK- NF- κ B signaling pathway. *J. Thorac. Dis.* <https://doi.org/10.21037/jtd.2017.09.135>
- Wang, X., Chancellor, G., Evenstad, J., Farnsworth, J.E., Hase, A., Olson, G.M., Sreenath, A., Agarwal, J.K., 2009. A novel optical instrument for estimating size segregated aerosol mass concentration in real time. *Aerosol Sci. Technol.* <https://doi.org/10.1080/02786820903045141>
- WHO, 2014a. World Health Organization releases 7 million premature deaths annually linked to air pollution. Accessed June 21, 2018. <http://www.who.int/mediacentre/news/releases/2014/air-pollution/en/>
- WHO, 2014b. World Health Organization releases 7 million premature deaths

- annually linked to air pollution. Accessed June 21.2018.
<http://www.who.int/mediacentre/news/releases/2014/air-pollution/en/>
<https://doi.org/9789241511353>
- World Health Organization, 2013. Health Effects of Particulate Matter: Policy implications for countries in eastern Europe, Caucasus and central Asia. *J. Korean Med. Assoc.* <https://doi.org/10.5124/jkma.2007.50.2.175>
- Yang, D., Ma, M., Zhou, W., Yang, B., Xiao, C., 2017. Inhibition of miR-32 activity promoted EMT induced by PM2.5 exposure through the modulation of the Smad1-mediated signaling pathways in lung cancer cells. *Chemosphere* 184, 289–298. <https://doi.org/10.1016/j.chemosphere.2017.05.152>
- Yang, L., Liu, G., Lin, Z., Wang, Y., He, H., Liu, T., Kamp, D.W., 2016. Pro-inflammatory response and oxidative stress induced by specific components in ambient particulate matter in human bronchial epithelial cells. *Environ. Toxicol.* 31, 923–936. <https://doi.org/10.1002/tox.22102>
- Yang, X.Y., Igarashi, K., Tang, N., Lin, J.M., Wang, W., Kameda, T., Toriba, A., Hayakawa, K., 2010. Indirect- and direct-acting mutagenicity of diesel, coal and wood burning-derived particulates and contribution of polycyclic aromatic hydrocarbons and nitropolycyclic aromatic hydrocarbons. *Mutat. Res. - Genet. Toxicol. Environ. Mutagen.* <https://doi.org/10.1016/j.mrgentox.2009.10.010>
- Zerboni, Bengalli, Baeri, Fiandra, Catelani, Mantecca, 2019. Mixture Effects of Diesel Exhaust and Metal Oxide Nanoparticles in Human Lung A549 Cells. *Nanomaterials.* <https://doi.org/10.3390/nano9091302>

Chapter 1:

***In vitro* lung toxicity of indoor PM10 from a stove fueled with different biomasses**

Sara Marchetti^{1*}, Eleonora Longhin¹, Rossella Bengalli¹, Pasquale Avino², Luca Stabile³, Giorgio Buonanno^{3,4,5}, Anita Colombo¹, Marina Camatini¹, Paride Mantecca¹

¹POLARIS Research Centre, Department of Earth and Environmental Sciences, University of Milano-Bicocca, Piazza della Scienza 1, 20126 Milano, Italy

²DiAAA, University of Molise, via De Sanctis, 86100 Campobasso, Italy

³Department of Civil and Mechanical Engineering, University of Cassino and Southern Lazio, Via Di Biasio 43, 03043 Cassino (FR) Italy

⁴University of Naples "Parthenope", Via Ammiraglio Ferdinando Acton, 38, 80133 Napoli, Italy

⁵Queensland University of Technology, GPO Box 2434, Brisbane, Qld 4001, Australia

*Corresponding author: Sara Marchetti, e-mail: s.marchetti16@campus.unimib.it, tel: +390264482928

Published in **Science of the Total Environment**
(DOI: 10.1016/j.scitotenv.2018.08.249)

Abstract

Biomass combustion significantly contributes to indoor and outdoor air pollution and to the adverse health effects observed in the exposed populations. Besides, the contribution to toxicity of the particles derived from combustion of different biomass sources (pellet, wood, charcoal), as well as their biological mode of action, are still poorly understood. In the present study, we investigate the toxicological properties of PM₁₀ particles emitted indoor from a stove fueled with different biomasses.

PM₁₀ was sampled by gravimetric methods and particles were chemically analyzed for Polycyclic Aromatic Hydrocarbons (PAHs) and elemental content. Human lung A549 cells were exposed for 24 h to 1–10 µg/cm² PM and different biological endpoints were evaluated to comparatively estimate the cytotoxic, genotoxic and pro-inflammatory effects of the different PMs.

Pellet PM decreased cell viability, inducing necrosis, while charcoal and wood ones mainly induced apoptosis. Oxidative stress-related response and cytochrome P450 enzymes activation were observed after exposure to all the biomasses tested. Furthermore, after pellet exposure, DNA lesions and cell cycle arrest were also observed. The severe genotoxic and pro-necrotic effects observed after pellet exposure were likely the consequence of the high metal content. By administering the chelating agent TPEN, the genotoxic effects were indeed rescued. The higher content in PAHs measured in wood and charcoal PMs was likely the reason of the enhanced expression of metabolizing and oxidative stress-related enzymes, like CYP1B1 and HO-1, and the consequent increase in apoptotic cell death.

These data suggest that combustion particles from different biomass sources may impact on lung cells according to different pathways, finally producing different toxicities. This is strictly related to the PM chemical composition, which reflects the quality of the combustion and the fuel in particular. Further studies are needed to clarify the role of particle dimension and the molecular mechanisms behind the harmful effects observed.

Keywords: Biomass, PM₁₀, Air pollution, Indoor, Lung cells, Cytotoxicity

Abbreviations

PM: Particulate matter; ROS: Reactive oxygen species; PAHs: polycyclic aromatic hydrocarbons; UFP: ultrafine particles; HO-1: hemeoxygenase 1; TPEN: N,N,N',N'-tetrakis(2pyridylmethyl)ethylenediamine; CDPs: combustion-derived particles; Zn: Zinc; Pb: lead; CYP1A1: Cytochrome P450, family 1, subfamily A, polypeptide 1; CYP1B1: Cytochrome P450 Family 1 Subfamily B Member 1; B[a]P: Benzo[a]pyrene; p-ATM: phosphorylated form of Ataxia Telangiectasia Mutated; γ H2AX: Phosphorylated histone H2AX; GC/MS: gas chromatography-mass spectrometry; SIM: single ion monitoring; INAA: Instrumental Neutron Activation Analysis; TEM: transmission electron microscopy; SEM: scanning electron microscopy; RT: room temperature; PBS: Phosphate Buffered Saline; PI: Propidium Iodide; IL: Interleukin; O/N: overnight; TBS: Tris-Buffered Saline; TBS-T: TBS with 0.1% Tween20; SE: standard error of mean; OM: optical microscopy.

1. Introduction

The burning of biomass fuels for domestic heating is one of the most significant sources of particulate air pollutants during winter in the developed countries (Li et al., 2017; Secrest et al., 2016). Its role has increased in the last years as consequence of a general effort in improving the use of renewable energy sources and lower costs. Emissions from biomass combustion significantly contribute to the air pollution events and could cause severe health effects in adult and children (Samburova et al., 2016). Indoor air quality can differ with type of housing ventilation, energy technology (type of oven or stove used), environmental pollutant concentration and exposure time. Airborne and combustion particle exposure has been associated with increased lung cancer risk, exacerbation of respiratory diseases and cardiovascular impairment (Jalava et al., 2012; Sussan et al., 2014; Swiston et al., 2008). Furthermore, the International Agency for Research on Cancer (IARC), has classified biomass fuel combustion as probably carcinogenic to humans (Category 2A) ("IARC Monographs on the Evaluation of Carcinogenic Risks to Humans," 2010).

Previous studies have investigated the toxicological effects of particles derived from biomass combustion in *in vitro* and *in vivo* systems, reporting ROS formation, activation of the response to polycyclic aromatic hydrocarbons (PAHs), DNA damage and cell death (Dilger et al., 2016; Happo et al., 2013; Muala et al., 2015). The results on inflammatory responses are controversial, since some papers report only minor activation (Kasurinen et al., 2017; Muala et al., 2015), while others highlight release of interleukins and activation of MAPK (Corsini et al., 2017; Uski et al., 2012). One reason of such differences might be related to the use of particles derived from different biomasses and combustion processes. In fact, particles collected from combustion of wood, animal dung, crop residues (Muala et al., 2015), coals (Capistrano et al., 2016), logs (Kasurinen et al., 2017), spring sandstorms or resuspension of local soil (Jin et al., 2016) are all referred as biomass. Therefore, the particle composition can be different depending on fuel type (Muala et al., 2015) and its properties, including content of ash and moisture (Jin et al., 2016), chemical composition, combustion conditions (Lamberg et al., 2013) and combustion appliances used (Kocbach Bølling et al., 2009).

Recently, we reported low biological effects for biomass ultrafine particles (UFPs) produced by a modern boiler propelled with high quality certified pellet. Particle chemical characterization showed that this effect was associated to a low content of harmful compounds such as PAHs and metals (Longhin et al., 2016).

To date, the comprehension of the toxic effects induced by biomass particles emitted from different fuels is still poor. However, it is known that the physicochemical properties related to the content of transition metals and PAHs are associated to different cytotoxic properties, that could be responsible for the

several adverse health effects caused by PM exposure (Jin et al., 2016; Yang et al., 2016).

This study intends to investigate how different fuels (i.e. pellet, charcoal and wood) used to propel the same stove (commonly used) may affect the properties of the emitted particles and their toxic potential.

Particulate matter (PM₁₀) was sampled on filters by gravimetric technique and PAHs, metals content and particles morphology were investigated. The cytotoxic effect of PM₁₀ was analyzed on the human alveolar A549 cells, that represent an extensively used model for inhalation toxicology purposes, and in particular for the PM cytotoxic effect (Chirino et al., 2017; Choi et al., 2016; Gualtieri et al., 2012; Kasurinen et al., 2017; Rossner et al., 2016). Cell viability, inflammatory response, antioxidant activity, xenobiotic metabolism activation, cell cycle alterations and DNA damage were evaluated.

Our data demonstrate that combustion particles deriving from different biomasses can activate different toxicological pathways, pointing out the role of the particle physico-chemical properties on the cytotoxic effects produced and the molecular mechanisms involved.

2. Materials and methods

2.1. Particles sampling

PMs were collected on filters through a gravimetric technique. The measurements were performed in a 20 m³ room (with doors and windows closed) equipped with an open fireplace for 4 h. The fuel (pellet, charcoal or wood) was burnt in the open fireplace and continuously fed during the experiment. Three combustion tests were carried out for each fuel. Thus, PMs for biological investigation were sampled on Teflon filter, while particles for the chemical analysis were collected on laden quartz filters. PM₁₀ concentrations were obtained after proper filter conditioning before and after particle samplings (Buonanno et al., 2011, 2009).

The gravimetric sampler used was made up of a volumetric rotating pump Zambelli 6000 Plus (equipped with temperature and atmospheric pressure sensors to measure normalized sampling volume) and a Zambelli PM₁₀ impactor (working at a nominal fixed flow rate of 2.3 m³h⁻¹ according to the EN 12341) to collect particles on low porosity filters for post-hoc analysis and PM₁₀ mass concentration evaluation.

2.2. Particles characterization

2.2.1. Polycyclic aromatic hydrocarbons (PAHs)

The following PAHs were determined: acenaphthene, acenaphthylene, fluorene, phenanthrene, anthracene, fluoranthene, pyrene, benzo(a)anthracene, chrysene, benzo(b)fluoranthene, benzo(j)fluoranthene, benzo(k)fluoranthene, benzo(e)pyrene, benzo(a)pyrene, perylene, indeno(1,2,3,c,d)pyrene, dibenzo(a,h)anthracene and benzo(g,h,i)perylene. PAHs were quantified by gas chromatography-mass spectrometry (GC/MS) with an isotopic dilution method (Stabile et al., 2018). In particular, filters were spiked before the extraction with 5 ng of perdeuterated PAHs (L429-IS Internal Standard D-IPA Stock Solution, Wellington Laboratories, Guelph, Canada); then the PAHs were Soxhlet-extracted in hexane for 24 h and the samples obtained were concentrated on a rotary evaporator (40 °C, 3.00×10^4 Pa) to 3–5 mL. Finally, the samples were automatically purified, by means of gel permeation chromatography, and concentrated, using an AccuPrep MPS & AccuVap Inline (J2 Scientific, Columbia, MO, USA).

GC/MS analysis was performed by an Ultra Trace gas chromatograph coupled with a TSQ mass spectrometer (Thermo Fischer Scientific, St Peters, MO, USA) used in single ion monitoring (SIM) mode. The column Meta-XLB (60 m length, 0.25 mm internal diameter, 0.25 μm film thickness; Teknokroma, Barcelona, Spain) was used for the separation, and He (99.9995% purity) was used as carrier gas. The temperatures for the injector, transfer line and ion source were set as 260 °C, 280 °C and 250 °C, respectively. The following oven temperature program was adopted: isothermal oven temperature of 60 °C for 1 min; thermal gradient of 20 °C min^{-1} up to 250 °C; isothermal oven temperature of 250 °C for 10 min; thermal gradient of 15 °C min^{-1} up to 300 °C; isothermal oven temperature of 300 °C for 15 min; thermal gradient of 5 °C min^{-1} up to 325 °C; isothermal oven temperature of 325 °C for 10 min. Each native PAH was quantified using its perdeuterated isotopologues as internal standard, except for acenaphthene (quantified using perdeuterated acenaphthylene), fluorene, anthracene (quantified using perdeuterated phenanthrene), pyrene (quantified using perdeuterated fluoranthene) and benzo(e)pyrene (quantified using perdeuterated benzo(a)pyrene). To calculate the extraction and purification recovery, 5 ng of recovery standard (L429-RS Recovery Standard D-IPA Stock Solution, Wellington Laboratories) were added before injection into the GC/MS. Recovery was calculated as the percentage ratio between the internal standard (added before the extraction) and the recovery standard (added before the injection in GC/MS). Perdeuterated acenaphthene was used to calculate the recovery of acenaphthylene and phenanthrene; perdeuterated pyrene was used to calculate the recovery of fluoranthene, benzo(a)anthracene and chrysene; perdeuterated benzo(e)pyrene was used to calculate the recovery of benzo(b)fluoranthene,

benzo(k)fluoranthene, benzo(a)pyrene, perylene, indeno(1,2,3,c,d)pyrene, dibenzo(a,h)anthracene and benzo(g,h,i)perylene.

2.2.2. Elements

The inorganic composition was investigated by a nuclear non-destructive technique: the Instrumental Neutron Activation Analysis (INAA). In particular, PMs (placed into the polyethylene tubes; Kartell, Milan, Italy) were irradiated by a Triga Mark II nuclear reactor of the ENEA-Casaccia Laboratories (1 MW power) (Capannesi et al., 2009). The irradiation was performed in the rotating rack, called Lazy Susan, which can give uniform neutron irradiation to the sample due to the continuous rotation. After neutron irradiation, the radionuclides begin to decay emitting γ -rays. The half-life time ($t_{1/2}$), which is characteristic of nuclides produced, was adopted as criterion for element detection (Avino et al., 2000). Basically, the γ -ray emission of nuclides with long $t_{1/2}$ is negligible after short irradiation (Rabbit) (Avino et al., 2011). However, nuclides with short $t_{1/2}$ were not detected because the sample was very active after the end of irradiation and the cooling time (3–5 days) is greater than the nuclide half-life; moreover, the nuclide activities with long half-lives hide the contribution (Avino et al., 2013, 2011). An 8 h long irradiation in the Lazy Susan was performed at a neutron flux of $2.6 \times 10^{12} \text{ n s}^{-1} \text{ cm}^{-2}$. At the end of irradiation, the samples were highly active and, according to the half-life of each elements, only few elements, such as As, Cd, Cr, Cu, Hg, Ni, Se and Zn could be analyzed, whereas Pb was separately analyzed by Inductively Coupled Plasma Atomic Emission Spectroscopy (ICP-AES). For the analysis, primary and secondary standards were used: primary standards (Carlo Erba, Milano, Italy) were Al, As, Br, Cl, Cu, I, Mg, Mn, Na, and V, whereas, as secondary standards, three reference materials (SRMs) such as SRM 2709 (S. Joaquim Soil) and SRM 98a (Plastic Clay) from the National Institute of Standards and Technology (NIST), and a SRM GRX-4 (Soil) from the US Geochemical Survey (USGS) were involved in this study. To guarantee the quality assurance and quality control (QA/QC) of the measurements performed, three SRMs along with the 8 primary standards were adopted: SRM 2709, SRM 98a, and SRM GRX-4. After irradiation, γ -ray spectrometry measurements of different durations were carried out using a Ge (HP) Canberra detector (Meriden, CT, USA) (full width at half maximum 1.68 keV at 1.332 keV) connected to a multichannel analyzer equipped with software packages (Canberra Genie 2k) for a γ -spectra analysis.

2.3. Particles extraction for biological investigations

Particles for *in vitro* exposures were obtained by extraction from Teflon filters according to a standardized procedure previously reported (Longhin et al., 2013). Briefly, filters from the same fuel were pooled in a glass vial and PM was extracted

by an ultrasound bath (SONICA Soltec, Milan, Italy) by replicating four 20 min cycles using 2 mL of pure sterile water for each cycle. PM10 water suspensions were then collected in sterile tubes previously weighed, dried into a desiccator and the resulting pellet weighed to determine the mass of particles extracted. Finally, samples were stored at -20°C until use. For biological investigations, particles were suspended in sterilized water to obtain aliquots at a final concentration of $2\ \mu\text{g}/\mu\text{L}$ just before use. PM suspensions were sonicated for 30 s just prior to cells exposure.

2.4. Morphological characterization of extracted particles

After extraction from the Teflon filters, a morphological characterization of the particles was performed by transmission electron microscopy (TEM) and scanning electron microscopy (SEM). Briefly, aliquots of $8\ \mu\text{L}$ of sonicated particle suspensions at $25\ \mu\text{g}/\text{mL}$ in pure water and 1% Isopropyl alcohol were respectively, pipetted on 200-mesh formvar-coated copper grids and aluminum stubs and dried at room temperature (RT). Samples were observed by a Jeol JEM 1220 TEM, operating at 80 kV, and a Tescan VEGA 5136XM, operating at 20kV. Images were digitally acquired and elaborated through dedicated softwares.

2.5. Cell culture and exposure

A549 cells, a human lung adenocarcinoma epithelial cell line, were obtained from the American Type Culture Collection (ATCC[®] CCL-185, American Type Culture Collection, Manassas, USA). Cells were cultured in OptiMEM I Reduced Serum Medium (Gibco, Life Technologies, Monza, Italy) supplemented with 10% heat-inactivated fetal bovine serum (FBS, Gibco) and Penicillin/Streptomycin (100 x, Euroclone, Pero, Italy) in a 5% CO_2 atmosphere at 37°C .

For particle exposure, cells (passages 39 to 55) were seeded at a concentration of 2×10^4 cells/ cm^2 (12-well plates) or 1.6×10^4 cells/ cm^2 (6-well plates), and grown up to 80% confluence for 24 h. At the optimal confluence, the culture medium was replaced with 1% FBS supplemented OptiMEM medium and cells exposed for 24 h at 37°C to different doses (1, 2.5, 5, 7.5 and $10\ \mu\text{g}/\text{cm}^2$) for cellular metabolic activity evaluation and to $5\ \mu\text{g}/\text{cm}^2$ ($50\ \mu\text{g}/\text{mL}$) PM10 for the following experiments. The same treatment was repeated for all the particles. Unexposed cells were used as control. Cells were exposed also to $14\ \mu\text{M}$ benzo[a]pyrene (B[a]P, Sigma Aldrich, Saint Louis, MO, USA) for xenobiotic metabolism activation studies or $1.65\ \mu\text{M}$ Etoposide (Sigma Aldrich) for DNA damage studies, as positive control (data not showed).

2.6. Cell viability

A549 cell viability was evaluated after 24 h of exposure to increasing PM₁₀ concentrations (1–10 µg/cm²) for each biomass particles by means of Alamar Blue assay. After exposure, the medium was removed, cells were rinsed twice with Phosphate Buffered Saline (PBS) and incubated for 3 h in 10% Alamar Blue (Invitrogen, Burlington, ON, Canada) supplemented OptiMEM complete medium. The absorbance, proportional to cell metabolic activity, was assessed with a multiplate spectrophotometer reader (Tecan, Männedorf, Switzerland) at excitation and emission wavelengths of 570 and 630 nm respectively.

To provide additional data on biomass cytotoxicity, cell viability was evaluated also by fluorescence microscopy following cells staining with Hoechst 33342 (1 mg/mL) and Propidium Iodide (PI, 1 mg/mL). Briefly, after cells exposure to 5 µg/cm² PM, supernatants were harvested to recover floating cells, whereas attached cells were collected after trypsinization. Trypsinized and floating cells were then centrifuged at 1200 rpm, pooled, re-suspended in complete medium and stained 1:1 with Hoechst and PI for 20 min at RT in the dark. Cells were finally, centrifuged, re-suspended in FBS and smeared on a glass slide to quickly dry. Cell morphology was evaluated using a fluorescence microscope (Zeiss Axioplan). Cells were scored and classified on the different nuclear morphology as: viable (Hoechst positive and PI negative, with intact plasma membrane and without nuclear anomalies), necrotic (PI positive), apoptotic (bright Hoechst-stained with condensed and/or fragmented nuclei) and mitotic (Hoechst positive with chromosome condensation). At least 300 cells for each sample were scored. Additional cytofluorimetric analyses were performed on cells stained with Annexin V/PI to assess the cell death modality (see Additional file 2).

2.7. Pro-inflammatory cytokines release

Intracellular and released protein levels of the pro-inflammatory cytokine Interleukin 6 (IL-6) and the chemokine IL-8 were measured by commercial enzyme-linked immunosorbent assay (ELISA) kits (IL-6, IL-8, Life Technologies). At the end of the exposure, cell supernatants were collected and centrifuged at 12000 rpm for 6 min at 4 °C to remove debris. The exposed cells were scraped and lysed on ice in RIPA buffer (150 mM NaCl, 1% TritonX-100, 0.5% sodium deoxycholate, 0.1% SDS, 50 mM Tris pH 8.0) and 0.1% of proteases inhibitor, added just before use. The supernatants and cell lysates were stored at –80 °C until measurement. Cytokine analysis was performed according to the manufacturer's instructions. The absorbance of each sample was measured at 450 nm and the amount of proteins in pg/mL quantified by a plate reader (Multiplate Reader Ascent, Thermo Scientific, USA), based on a standard curve.

2.8. Protein extraction and immunoblotting

After exposure, cells for immunoblotting were rinsed twice, scraped and lysed on ice in RIPA buffer and 0.1% of proteases inhibitor, added just before use. Total cellular lysates were centrifuged at 12000 rpm for 15 min and the protein content evaluated by the bicinchoninic acid assay (Sigma Aldrich) according to the manufacturer's instructions. Equal amounts of proteins (30 μ g) were loaded onto 12% SDS-PAGE gels, separated and transferred on nitrocellulose membranes. Equal loading was assessed by Ponceau S red staining of protein bands on nitrocellulose. Membranes were rinsed three times with water and Tris-Buffered Saline (TBS) with 0.1% Tween20 (TBS-T) and then, incubated for 1 h with Blocking buffer, TBS-T supplemented with 5% w/v bovine serum albumin (BSA; Sigma) or milk (Skim milk powder, Fluka, Sigma). Membranes were incubated overnight (O/N) at 4 °C with the specific primary antibody (HO-1 P249 Antibody, 1:1000, Cell Signaling Technology, Danvers, USA; Cytochrome P450 1A1 1:500 and CYP1B1, 1:500, Novus Biologicals, Littleton, CO, United States). The day after, membranes were rinsed three times with TBS-T and incubated with specific HRP-linked secondary antibodies in Blocking buffer for 1 h at RT (anti-rabbit IgG, 1:2000, Cell Signaling). Finally, membranes were rinsed as previously described, and exposed to Chemiluminescent Substrate (Euroclone). Monoclonal anti- β -Actin antibody (Cell Signaling, 1:1000) was used as loading control. Digital images were taken by a luminescence reader (Biospectrum-UVP, LLC, Upland, CA, United States) and densitometry analysis performed with dedicated software (Vision Works LS).

2.9. DNA damage analysis

Phosphorylated histone H2AX (γ H2AX) and phosphorylated form of Ataxia Telangiectasia Mutated (p-ATM) were used as marker of DNA damage and analysis was performed by flow cytometry. After exposure, cells were trypsinized, washed and fixed with 1% paraformaldehyde in PBS at 4 °C for 15 min. Cells were gently re-suspended in 90% cold methanol and stored O/N at -80 °C prior to analysis. The samples were centrifuged at 1600 rpm for 6 min to discharge the methanol, washed once in PBS supplemented with 0.5% BSA and then, incubated with the specific antibody in PBS supplemented with 0.5% BSA and 0.2% Triton X-100. Alexa Fluor 488 conjugated γ H2AX antibody (1:100, Cell Signaling) and a p-ATM mouse monoclonal antibody (1:100, Santa Cruz Biotechnology, Dallas, Texas, USA) were used. Cells stained for γ H2AX were incubated for 4 h at RT, washed once in PBS 0.5% BSA, re-suspended in PBS and analyzed by the CytoFLEX 13/3. Cells stained for p-ATM were incubated with the primary antibody O/N at 4 °C. The day after, cells were washed once in PBS 0.5% BSA and incubated with the secondary antibody (Alexa Fluor 594 goat anti-mouse IgG, 1:500 dilution, Invitrogen/Molecular Probes, Eugene, Oregon, USA) in PBS 0.5% BSA, 0.2% Triton X-100 for 90 min at RT in the

dark. Finally, cells were washed once, re-suspended in PBS and analyzed at the flow cytometer. The fluorescence of 10,000 events was detected using 525 (γ H2AX) or 617 (p-ATM) nm band pass filter. The same cytometer setting was maintained for staining on independent experiment. Data were analyzed as mean percentage of positive cells for the staining.

Immunofluorescence analyses of p-ATM and γ H2AX nuclear foci were also performed to confirm the cytofluorimetric analysis (see Additional file 3).

2.10. Cell cycle analysis

The cell cycle progression of PM-treated cells was investigated after 24 h of exposure by DNA-staining. At the end of the exposure, cells were trypsinized, collected and pooled with the harvested medium. They were then, centrifuged at 1200 rpm for 6 min, fixed in 90% ethanol and stored at -20°C until analysis. The cell cycle of unexposed control cells was analyzed too.

For the analysis, cells were centrifuged at 1600 rpm for 6 min to discharge the ethanol and resuspended in PBS and RNase DNase-free (1 mg/mL, Sigma-Aldrich, Italy) was added for 30 min at 37°C . Finally, the fluorescent dye PI was added to stain DNA of cells for 7 min in the dark. Fluorescence was measured by flow cytometer (CytoFLEX 13/3) using 617 nm band pass filters and the analysis performed with the dedicated software (CytExpert software). A total of 10,000 events per sample were analyzed. We maintained the same cytometer setting for all the independent experiments performed. For the analysis, cells in different cell cycle phases were selected and analyzed as mean percentage of cells in each phase.

2.11. Treatment with metal chelator

The metal chelator TPEN (N,N,N',N'-tetrakis(2-pyridylmethyl)ethylenediamine, Sigma) was used, since its high affinity for Zn^{2+} . TPEN was firstly dissolved in EtOH and used for incubating cells at the final concentration of $3\ \mu\text{M}$. This concentration has been selected after preliminary set up experiments. Particles were pre-incubated with TPEN for 1 h before the cells treatment and then added to cell medium. After 24 h exposure, cell cycle analysis was performed, as previously described (see par. 2.10).

2.12. Statistical analysis

Mean and standard error of mean (SE) of at least three independent experiments, carried out following the same experimental conditions, are reported. Statistical analyses were performed using GraphPad Prism 6 software, using One-way or Two-

way ANOVA with Dunn's or Dunnett's post hoc multiple comparisons tests. Values of $p < 0.05$ were considered statistically significant.

3. Results

3.1. Biomass PM10 chemico-physical characterization

The average mass fraction of PAHs emitted by pellet, charcoal and wood PMs are summarized in Table 1. A high PAH concentration was measured in PM10 emitted by charcoal and wood combustion processes with respect to pellet. BaP, recognized as the most cancerogenic PAH, was measured and its concentration resulted to be 4.03 ng_{BaP}/mg_{PM10}, 27.8 ng_{BaP}/mg_{PM10}, 62 ng_{BaP}/mg_{PM10} for pellet, charcoal and wood, respectively.

Table 1. Average mass fractions of PAH on PM10 (ng/mgPM10) emitted by pellet, charcoal and wood combustion processes.

Polycyclic Aromatic Hydrocarbons (PAHs)	Pellet	Charcoal	Wood
Fluoranthene	22.7	173	124
Pyrene	25.3	197	219
Benzo[a]anthracene	5.1	38.8	54.4
Crysene	8.05	61.1	100
Benzo[b]fluoranthene	3.93	29.9	106
Benzo[k]fluoranthene	1.24	15	33.2
Benzo[e]pyrene	1.43	11.5	24.6
Benzo[a]pyrene	4.03	27.8	62
Perylene	0.76	7.44	13.3
Indeno[1.2.3.c.d]pyrene	1.74	12.4	49.1
Dibenzo[a.h]anthracene	0.69	4.55	1.94
Benzo[g.h.i]perylene	1.88	13.1	45.3
Total	76.85	591.6	832.8

Higher metal amounts were detected in PM10 emitted by pellet combustion compared to charcoal and wood, including As, Cd and Ni, which belong to Group 1 carcinogenic compounds (“IARC: Outdoor air pollution a leading environmental cause of cancer deaths,” 2013), as summarized in Table 2. A negligible (lower than the detection limit) As amount was measured in charcoal and wood samples, whereas its concentration in PM10 emitted by pellet combustion was equal to 0.09 ng_{As}/μg_{PM10}. Ni and Cd concentration was 12.4 ng_{Ni}/μg_{PM10} and 0.43 ng_{Cd}/μg_{PM10}, 5.7 ng_{Ni}/μg_{PM10} and 0.17 ng_{Cd}/μg_{PM10} and 7.2 ng_{Ni}/μg_{PM10} and 0.24 ng_{Cd}/μg_{PM10}, for pellet, charcoal and wood combustion, respectively.

Table 2. Average mass fractions of inorganic elements on PM10 (ng/μgPM10) emitted by pellet, charcoal and wood combustion processes.

Metals	Pellet	Charcoal	Wood
As	0.09	<LOD	<LOD
Cd	0.43	0.17	0.24
Cr	6.2	5.5	5.1
Cu	3.5	2.8	4.1
Hg	7.9	2.3	3.1
Ni	12.4	5.7	7.2
Pb	19.3	2.9	0
Se	4.2	5.9	5.2
Zn	42.8	14.7	28.2
Total	96.82	39.97	53.14

The particle morphology examined after filters extraction is reported in more detail in the additional Figure 1 [see Additional file 1]. It is evident that the particles deriving from the combustion of the different biomasses significantly differ in size and shape, with pellet PM samples showing more particles with dimension in the ultrafine range. The PMs derived from charcoal and wood combustion appeared larger and with very irregular shapes (Figure 1).

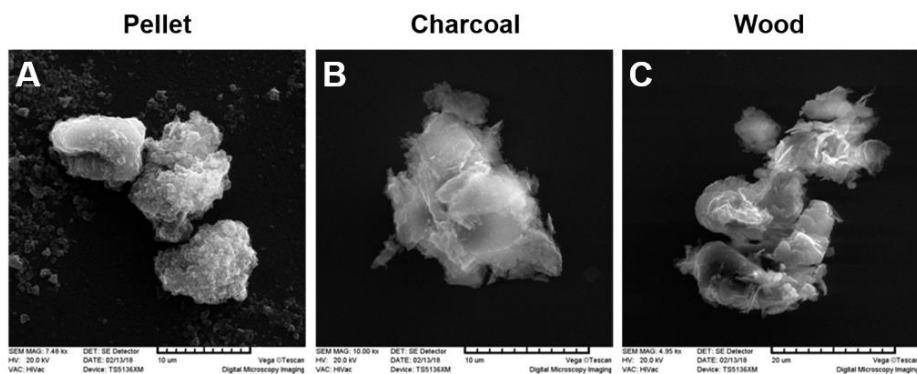


Figure 1. Morphological characterization of biomass PM₁₀. Scanning Electron Microscopy (SEM) analysis on particles extracted from the sampling filters and suspended in sterile water: pellet (A), charcoal (B), and wood (C).

3.2. Biomass PM₁₀ biological effects

3.2.1. Cell viability

The cytotoxic effects were investigated by Alamar Blue assay (Figure 2) and Hoechst/PI staining (Figure 3) after 24 h exposure to PM₁₀ from 1 µg/cm² to 10 µg/cm². A dose-dependent decrease in cell viability was observed (Figure 2), with significant differences in comparison to control starting from 5 µg/cm² for pellet PM and from 7.5 µg/cm² for wood (Two-way ANOVA; $p < 0.05$). Cell viability was not affected after exposure to all the charcoal PM doses tested.

The dose of 5 µg/cm², showing low or no effects in the metabolic assay, was selected for the further experiments.

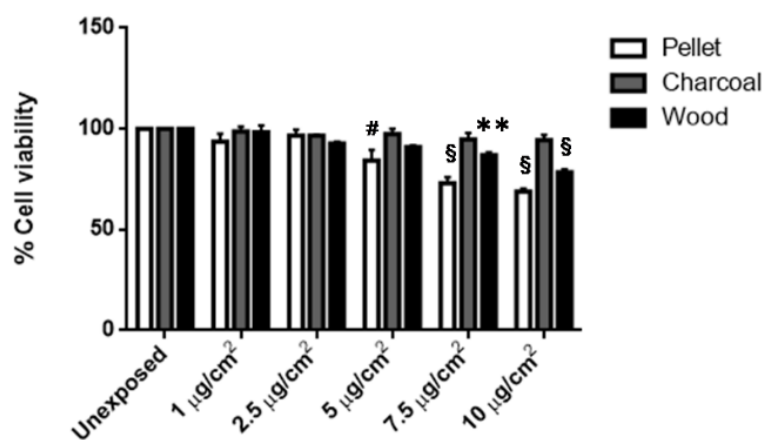


Figure 2. Cell viability assessed by Alamar Blue assay after 24 h exposure to increasing biomass PM concentrations: 0 (unexposed), 1, 2.5, 5, 7.5 and 10 µg/cm². Histograms represent the mean ± SE of

at least three independent experiments. Statistical analysis was performed by Two-way ANOVA with Dunnett's multiple comparison test. $^{\S}p < 0.0001$, $^{\#}p < 0.001$ and $^{**}p < 0.01$ vs control cells.

The differential cell count of the Hoechst/PI stained A549 cells, after exposure to 5 $\mu\text{g}/\text{cm}^2$ PMs for 24 h, suggested a significant decrease in the number of viable cells. In parallel a significant increase in necrotic cells (>14%) was induced by pellet, while charcoal and wood PMs significantly increased the number of apoptotic cells (>13% and 11% respectively) (Figure 3).

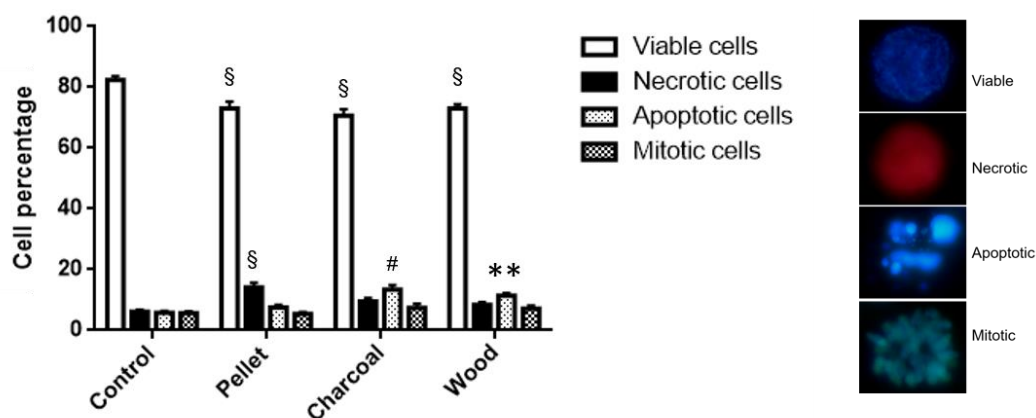


Figure 3. Cell viability assessed by Hoechst/PI staining after 24 h exposure to 5 $\mu\text{g}/\text{cm}^2$ biomass PMs. The differential cell count (viable, necrotic, apoptotic and mitotic cells) was based on the nuclei staining and morphology (see the right side of the panel). The data represent mean \pm SE of three independent experiments. Statistical analysis was performed by Two-way ANOVA with Dunnett's multiple comparison test. $^{\S}p < 0.0001$, $^{\#}p < 0.001$ and $^{**}p < 0.01$ vs control cells.

A more sensitive method was used to better discriminate the type of death mechanisms induced by biomass PMs [see Additional file 2]. Thanks to the cytofluorimetric analysis of the Annexin V/PI staining, we were able to discriminate between necrosis and early or late apoptosis. The results confirmed necrosis as the main mechanism of cell death activated by pellet PM. As shown in the Additional Figure 2, charcoal and wood PMs, activated also the apoptotic process, with a slight increased number of cells in early and late apoptosis compared to control and pellet exposed cells.

3.2.2. Synthesis and release of pro-inflammatory cytokines

To investigate the inflammatory response, the release of two key pro-inflammatory mediators, IL-6 and IL-8, was measured after A549 cells exposure to 5 $\mu\text{g}/\text{cm}^2$ PM10 for 24 h. No significant increase in IL-6 and IL-8 secretion was obtained after exposure to all the biomass PMs (Figure 4A and C). Only a slight increase of IL-6 was observed in pellet-exposed cells (Figure 4A). The intracellular levels of the proteins were also analyzed (Figure 4B and D). IL-8 expression significantly increased in

pellet-exposed cells (One-way ANOVA; $p < 0.05$), while charcoal and wood did not affect IL-8 levels. IL-6 intracellular concentration is higher in the cells exposed to all PMs. Anyway, such increase was not statistically significant (Figure 4B).

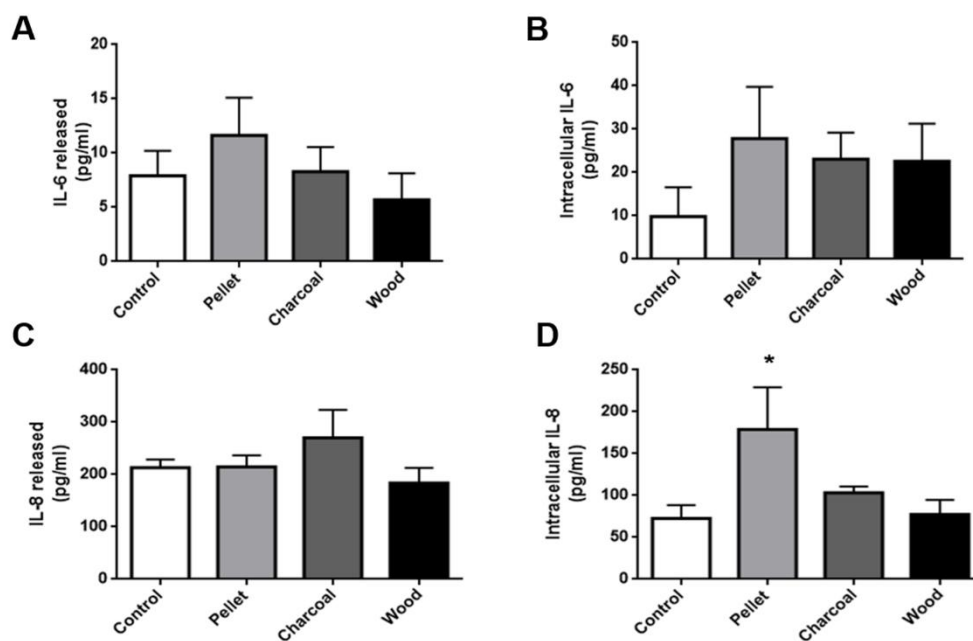


Figure 4. Pro-inflammatory effects induced by biomass PMs after exposure to $5 \mu\text{g}/\text{cm}^2$. A) IL-6 secretion. B) Intracellular level of IL-6. C) IL-8 secretion. D) Intracellular level of IL-8. Results are expressed as mean \pm SE of five independent experiments. Statistical analysis was performed by One-way ANOVA with Dunnett's multiple comparison test. * $p < 0.05$ vs control cells.

3.2.3. Antioxidant response

The activation of the anti-oxidant response was also evaluated. The expression of hemeoxygenase 1 protein (HO-1) was assessed by Western Blot. As showed in Figure 5, a statistically significant increase in HO-1 expression was observed after exposure to all the three PMs, with wood particles inducing the highest effect.

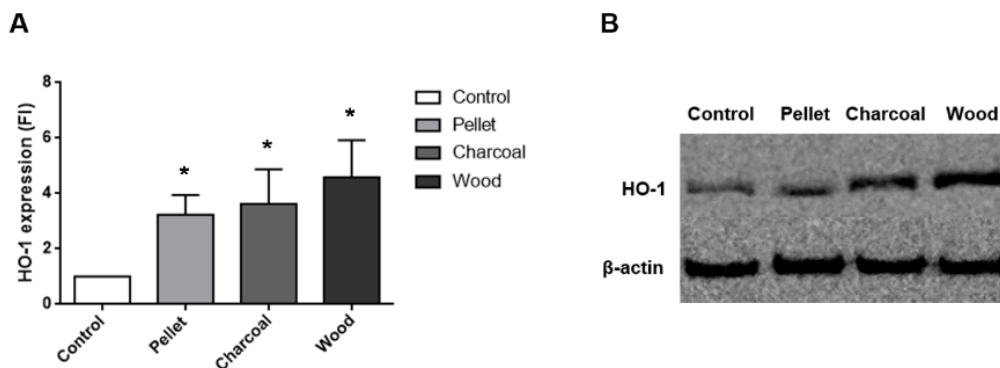


Figure 5. Expression of the oxidative stress marker HO-1. A) Protein analysis after exposure to biomass PMs. Data are presented as mean \pm SE of five independent experiments. Statistical analysis was performed by One-way ANOVA with Dunn's multiple comparison test. * $p < 0.05$ vs control cells. B) Representative immunoblotting images displaying HO-1 expressed from A549 cells exposed for 24 h to 5 $\mu\text{g}/\text{cm}^2$. β -Actin was used as control.

3.2.4. Xenobiotic metabolism activation

The expression of the enzymes CYP1A1 and CYP1B1, involved in PAHs metabolism, was analyzed. As shown in Figure 6A, CYP1A1 protein level was not significantly increased by biomass PMs exposure at the dose and time point investigated. On the contrary, positive results were obtained for CYP1B1, with a mild increase of the protein level in cells exposed to pellet, a strong, although not statistically significant, increase in cells exposed to charcoal, and a definite statistically significant increment in cells exposed to wood PM (Figure 6B).

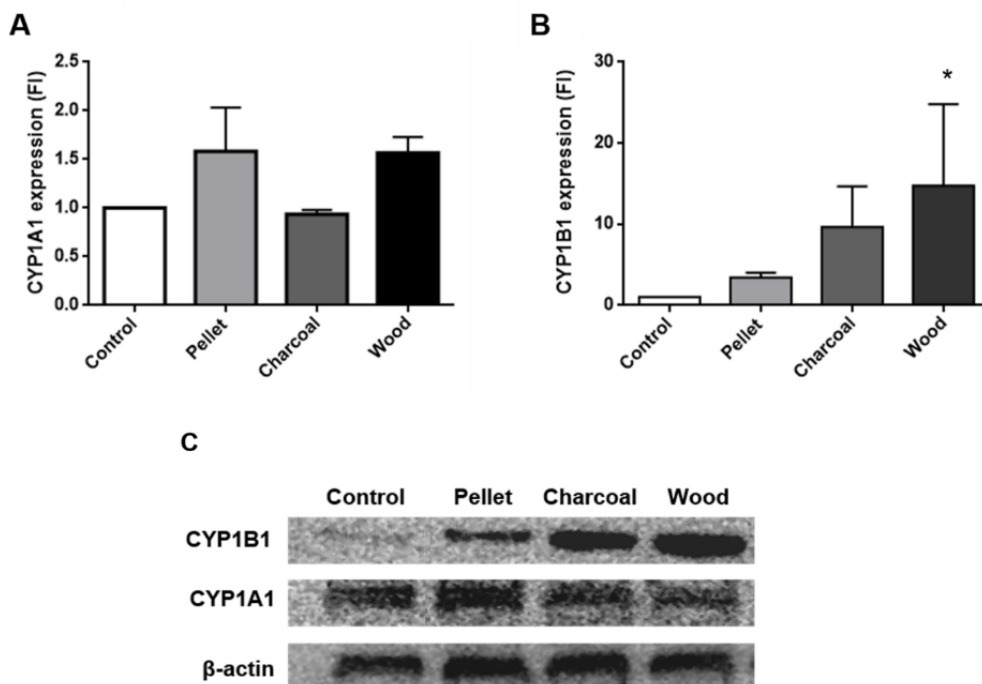


Figure 6. Activation of PAH-metabolizing enzymes cytochromes P450 (CYPs). A, B) Histograms represent CYP1A1 and CYP1B1 expression respectively. Data are presented as mean \pm SE of three independent experiments. Statistical analysis was performed by One-way ANOVA with Dunn's multiple comparison test. * $p < 0.05$ vs control cells. C) Representative immunoblotting images displaying CYP1A1 and CYP1B1 expressed from A549 cells exposed for 24 h to $5 \mu\text{g}/\text{cm}^2$. All the data were normalized to β -actin.

3.2.5. DNA damage

DNA strand breaks were evaluated by the quantification of the activated form of ATM (p-ATM). To determine if p-ATM activation is followed by H2AX phosphorylation, which reflects the activation of DNA repair mechanisms, cells were also stained and scored for γ H2AX. As shown in Figure 7, only the exposure to pellet PM led to a significant augmented expression of p-ATM compared to the control cells, but it is associated only to a slight activation of γ H2AX. It is noteworthy that A549 cells showed high background levels of γ H2AX, possibly masking eventual increases induced by PM exposure (Figure 7B). A representative immunofluorescence image showing the foci of DNA damage (p-ATM) after the exposure to Pellet PM is reported in the additional Figure 3 [see Additional file 3].

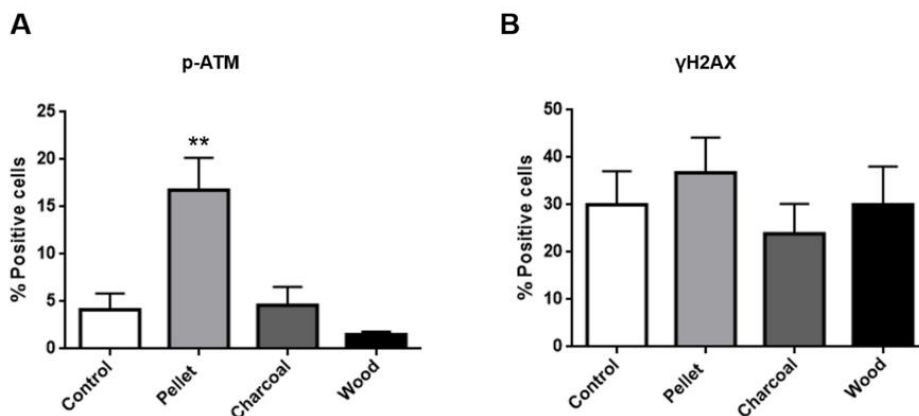


Figure 7. Induction of ATM and H2AX phosphorylation in A549 cells following exposure to biomass PMs. The histograms show the percentage of positive cells for p-ATM expression (A) and for γ H2AX expression (B). Data are presented as mean \pm SE of three independent experiments. Statistical analysis was performed by One-way ANOVA with Dunnett's multiple comparison test. ** $p < 0.01$ vs control cells.

3.2.6 Cell cycle analysis

A549 cells exposed to $5 \mu\text{g}/\text{cm}^2$ of charcoal and wood PMs did not show cell cycle alterations, while those exposed to pellet PM did (Figure 8A). Pellet-exposed cells presented a significant increase in G0-G1 phase (from 62.27% of control cells to 76.47%), with a parallel decrease in S and G2-M phases. These results confirm the genotoxic effect, already evidenced by DNA repair system activation, specifically produced by pellet PM.

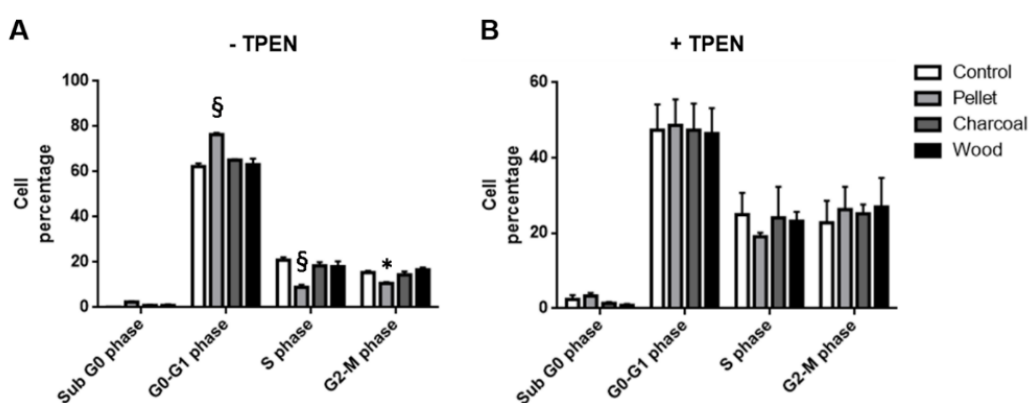


Figure 8. Cell percentage in each phase of the cycle (SubG0, G1, S, G2/M) after exposure to $5 \mu\text{g}/\text{cm}^2$ biomass PMs pre-incubated (B) or not (A) with TPEN. A) Cells exposed to PMs. B) Cells exposed to PMs pre-incubated with TPEN. Data are presented as mean \pm SE of four independent experiments. Statistical analysis was performed by Two-Way ANOVA with Dunnett's multiple comparison test. [§] $p < 0.0001$ and * $p < 0.05$ vs control cells.

The metal chelator TPEN (N,N,N',N'-tetrakis(2-pyridylmethyl)ethylenediamine) was used to investigate the role of Zinc in the pellet-induced cell cycle alterations. TPEN per se had a slight but not significant effect on the cell cycle, but it was able to completely rescue the alterations induced by pellet PM (Figure 8B).

4. Discussion

There is today a general awareness that the atmospheric PM-induced biological effects could depend on the particle physico-chemical composition and on the sources of emissions, but still much remains to be explained about the role of specific combustion processes and fuels in determining the toxicity of the emitted particles. In this perspective, more research is needed to understand the toxicological properties of combustion-derived particles (CDPs), the specific biological mechanism of action and their role in the adverse health effects observed in the exposed populations.

In the present work, we compared the chemical composition and the biological effects of three different biomass CDPs, sampled indoor as PM₁₀ during combustion of pellet, charcoal and wood, using the same stove. PM₁₀s were analyzed for PAHs and metals content and their cytotoxic, pro-inflammatory and genotoxic effects were evaluated *in vitro* on human lung A549 cells.

Charcoal and wood PMs mainly induced the xenobiotic response enzymes activation and cell apoptosis. Interestingly, pellet particles displayed a different toxicological mechanism, inducing a mild inflammatory response, DNA damage and cell cycle arrest in G1 phase and the consequent cell death by necrosis. Such a difference in the toxicological profiles was likely dependent on the different relative abundances of PAHs and heavy and transition metals observed in the PMs. Indeed, pellet PM contained higher amounts of metals compared to charcoal and wood that, on the contrary, resulted enriched in PAHs.

Among metals, Zinc (Zn) was the most abundant in all samples, but with a concentration in pellet particles 1.5- and 3-fold higher than in wood and charcoal, respectively. Also lead (Pb) concentration presented great differences among the particles, being 6-fold higher in pellet than in charcoal, while it was not detected in wood particles. A higher cytotoxicity of Zn-enriched biomass particles, compared to particles with lower Zn content, was already suggested (Uski et al., 2015), and ZnO particles were shown to induce cell apoptosis or necrosis, according to the cell exposure to lower or higher doses respectively (Zhang et al., 2012). A correlation between cytotoxicity and Pb content in airborne PM was also reported, so as for other metals, such as Cd, As, Cr, and Cu (Michael et al., 2013; Perrone et al., 2010; Van Den Heuvel et al., 2016), and a definitely higher concentration of this metal in pellet PM in respect to wood and charcoal ones.

On the contrary, charcoal and wood particles displayed a PAH content approximately 10-fold higher than pellet ones. Such lower metal content, together with the relatively high PAH content may be responsible of the reduced cytotoxicity and the slightly increased apoptotic event in charcoal and wood exposed cells. This is also in agreement with previous studies, showing that high concentrations of PAHs in urban PM are strongly associated with apoptosis (Uski et al., 2014; Yang et al., 2016), and that PAH-coated carbon particles are able to induce apoptosis in tracheal epithelial cells, while pristine particles are not (Lindner et al., 2017). All together, these observations suggest that the particle-adsorbed chemicals might activate different cell death mechanisms.

The activation of the inflammatory pathway was also investigated as important cell response to biomass PM, possibly involved in necrotic and/or apoptotic processes (Nemmar et al., 2013; Wallach et al., 2013). The levels of IL-6 and IL-8, two main pro-inflammatory mediators, were measured in both the intracellular and the extracellular compartments. At the subtoxic dose tested, no significant responses were observed, except for a slight increase in the intracellular level of IL-6 after exposure to all PMs and a statistically significant increase in the intracellular IL-8 in pellet PM-exposed cells (Figure 4). In literature, the results concerning the biomass particles inflammatory potential are controversial. In A549 cells exposed to diverse wood/biomass particles, low pro-inflammatory cytokines release has been generally reported (Corsini et al., 2017; Danielsen et al., 2011; Dilger et al., 2016). Also in RAW264.7 macrophages wood smoke particles were found to induce cell death with only minor inflammatory response (Muala et al., 2015). In a previous study on ambient PM, we observed that IL-8 response was induced by the fine PM fraction (PM₁), mainly as a consequence of the metal content - As and Zn in particular - as demonstrated by PCA analysis (Perrone et al., 2010). Metals in general are known to induce inflammatory responses, thus the increased IL-8 expression in cells exposed to pellet PM may be related to the higher metal content displayed. The differences between IL-8 intracellular and extracellular expression could be due to an inhibitory effect of the PM on the secretion of IL-8 soluble form. A mismatch between IL-8 gene expression and lack of augmented extracellular release has previously been reported following exposure to urban PM_{2.5} (Alfaro-Moreno et al., 2009; Kocbach et al., 2008). This IL-8 suppression could be due to PAHs or other chemicals present in the PM, as reported also by previous studies (Fuentes-Mattei et al., 2010; Totlandsdal et al., 2014).

Since the biomass PMs, especially charcoal and wood ones, are enriched in PAHs, we evaluated the activation of two main enzymes of the cytochrome P450 superfamily, CYP1A1 and CYP1B1, that are involved in the xenobiotic metabolism response (Dilger et al., 2016; Rossner et al., 2016). We found a significant induction of CYP1B1 in wood CDPs-exposed cells, in agreement with the highest PAH content. Pellet CDPs did not induce a significant activation of CYP enzymes, accordingly to

the lower PAH levels. Although it may seem unexpected, the overall lower induction of CYP1A1 is in agreement with previous studies, in which CYP1B1 resulted more responsiveness than CYP1A1 in A549 cells exposed to urban PM_{2.5} and Benzo[a]pyrene (B[a]P) (Genies et al., 2013; Gualtieri et al., 2012). Furthermore, according to Genies (2016), A549 response to PAHs could be influenced by their behavior in a mixture of compounds. Individual PAHs indeed, upregulate in different ways the two enzymes, but their toxic properties could be inhibited or enhanced when they are combined. Since PM is a complex mixture of PAHs, the differences in the concentration of individual PAHs could be therefore responsible for the different responses observed after exposure to biomass PMs. Interestingly, in previous papers the induction of CYP1B1, and not of CYP1A1, was observed after exposure to urban PM_{2.5} and PM₁₀ in both *in vitro* (A549 cells) and *in vivo* systems (Gualtieri et al., 2012; Farina et al., 2013). It may be supposed that specific PAHs and/or the presence of other molecules (e.g. TCDD) may contribute in the expression of such enzyme. Moreover, according to Hukkanen and colleagues (2000) the expression of CYP1B1 by TCDD (2,3,7,8- tetrachlorodibenzo-p-dioxin) is less dependent on AHR. Interestingly it has also been reported that CYP1B1 mRNA is the most sensitive target across different cell models compared to CYP1A1 and other three less frequently used AhR target genes (TIPARP, AHRR, ALDH3A1), while CYP1A1 mRNA induction is strictly AhR-dependent (Strapáčová et al., 2018).

Oxidative stress is a main mechanism of PM-mediated cytotoxicity, able to induce cellular damage by targeting several cellular components, including proteins, lipids and nucleic acids. Both PAHs and metals are able to induce ROS production (Crobeddu et al., 2017; Yang et al., 2016), and in response to oxidative stress cells might react modulating the expression of heme oxygenase 1 (HO-1), one of the key enzyme involved in the anti-oxidant activity (Dilger et al., 2016). Not surprisingly, our results showed that all biomass PMs were able to activate the anti-oxidant response, inducing a statistical significant increase of the HO-1 expression, independently from their chemical compositions.

Since the PM-induced oxidative stress may result in genotoxic effects, the presence of DNA lesions was then evaluated by quantifying the expression of p-ATM and γ H2AX. One of the main signalling pathways that help cells to respond to DNA insults involves the ataxia-telangiectasia mutated (ATM) kinase, which is activated by double strand breaks (DSBs) induced by radiations, oxidative stress and genotoxins (Maréchal and Zou, 2013; Smith et al., 2010). ATM activation triggers a cascade of events that lead to the phosphorylation of different substrates, including H2AX, BRCA1, Chk1/2 and p53, involved in DNA repair, cell-cycle arrest or apoptosis processes. The key event deriving from ATM activation is the phosphorylation of the histone H2AX (γ H2AX), that is required for the activation of DNA repair proteins to the damage site (Maréchal and Zou, 2013; Sánchez-Pérez et al., 2009).

Although DNA primary lesions generally occur after 6 h of exposure, our results indicate that also after 24 h it is possible to observe genotoxic lesions. Similar evidences have been observed also in other previous works, even at reduced concentrations compared to the one selected for our research (Gualtieri et al., 2011; Longhin et al., 2013; Marabini et al., 2017). Such differences in the timing of the response to DNA damage may be due to the delayed bioavailability of PAHs carried out by the CDPs. Since PAHs are adsorbed onto the carbonaceous particles, their effects on the cell metabolic response can take place only after the endocytosis and the consequent availability of the xenobiotics at the level of the smooth endoplasmic reticulum (SER), where the metabolism enzymatic systems are located.

Our results indicate an increased expression of p-ATM and a slight modulation of γ H2AX only after pellet exposure, suggestive of DNA lesions, followed by the tentative to activate the DNA repairing machinery. This partial activation might be responsible of the significant cell cycle arrest in G1 phase and cell death by necrosis induced by pellet CDPs.

The reason why no DNA damages were revealed after wood and charcoal exposure may reside in the fact that ROS generation by PAHs involves their conversion into quinones, which are able to generate bulky DNA adducts, not recognized by ATM. On the contrary, metals, generating hydroxyl radicals, could trigger the accumulation of DNA strand breaks that finally activate ATM (Henkler et al., 2010; Rudolf and Cervinka, 2011).

The cell-signaling pathway activated in presence of oxidative DNA damage has been suggested as one of the mechanisms behind cell cycle arrest. DNA damage indeed, activates different checkpoints, finally inhibiting cell cycle progression. Besides, the activated checkpoint may depend on the type of damage (Cuadrado et al., 2006; Gualtieri et al., 2011; Liang et al., 2009). In the present study, only the samples exposed to pellet CDPs showed a significant cell cycle modification, with many cells blocked in G1 phase. This is in accordance with previous data, in which the arrest in G0 checkpoint is reported to be associated to DNA damage and increased cellular levels of p53 (Liang et al., 2009; Kastan et al., 1991). Other studies demonstrated the PM-induced arrest of cell cycle in G1 (Reyes-Zárate et al., 2016; Zhang et al., 2007) and in G2/M phase (Longhin et al., 2013), as a function of the variable chemical composition. The amount and type of PAHs was probably the main responsible of to the mitotic arrest, while the higher amount of metals in pellet CDPs could be responsible for the arrest in G1 phase, as already suggested (Steenhof et al., 2011). It was reasonable to suspect that Zinc, present in a very high concentration in pellet PM, contributes significantly to the cytotoxic and genotoxic effects of this PM type, even considering the significant cell cycle rescue achieved after incubation with the Zinc chelator probe, TPEN (Figure 8B). Zinc, and in general transition metals, are known to significantly induce oxidative DNA damage through

Fenton reaction-generated ROS, with the consequent accumulation of DNA lesions preventing cells to enter S phase. From the literature, it is known that PM samples containing high Zn concentrations display elevated toxic properties (Torvela et al., 2014; Uski et al., 2015) and that Zn ions and Zn nanoparticles produce significant DNA damage (Pati et al., 2016; Rudolf and Cervinka, 2011). Of course, the very high content of other heavy metals, e.g. Pb and Mercury (Hg), does not allow us to exclude an involvement also of these elements in the enhanced toxicity observed after treatment with pellet CDPs.

In a recent publication we reported that UFPs obtained from the combustion of high- quality certified pellet in a modern automatic 25 kW boiler did not induce significant toxicity in human bronchial cells at concentrations similar to those used in the present study, contrary to diesel exhaust particles, which displayed cytotoxic and genotoxic effects (Longhin et al., 2016). These results clearly point out that the quality of the biomass used, and the combustion technology may drastically influence the quality of the emitted particles, with the size and the relative abundance of metals and PAHs as the main physico-chemical variables affected.

5. Conclusions

According to the main evidences of the present study, the physico-chemical properties of the biomass CDPs, reflecting the efficiency of the combustion systems and the biomass fuel quality, do not only influences the acute toxicity, but even the cellular mechanism of action, pointing out the need of further exploring the adverse outcome pathways. In this regard, recently the Air Liquid Interface (ALI) exposure systems received attention as an alternative method to the submerged system in studying the biological effects of ultrafine particles (Loxham et al., 2015) and nanoparticles (Kim et al., 2013). Nevertheless, the widespread adoption of ALI systems is still limited for PM by the minimal efficiency of particles deposition and by the complex strategy needed to characterize the composition of the particles delivered to the cells (Kim et al., 2013). Besides, studies on the comparative biological effects of the UFPs deriving from controlled combustion processes, using 3D lung in vitro systems exposed at the ALI, will be of high relevance to depict the hazardous behavior of the different biomass CDPs.

In conclusion, different adverse biological outcomes can result from the exposure to biomass CDPs and the present data confirm that the amount of metals is crucial in inducing acute effects related to cytotoxicity and genotoxicity, while PAHs are responsible for the induction of the xenobiotic metabolizing systems and the oxidative stress cell responses. Since these variable effects induced by solid biomass CDPs, the chemical composition of particles and their toxicological profiles should be known in order to suggest efficient strategies for the prevention of the adverse

health effects in indoor exposure, but also for the management of outdoor air quality at local level.

Further investigations are of course needed to better define the molecular mechanisms of action but, at the same time, more stringent regulations are required to guarantee high quality biomass fuels and safer combustion technologies.

Acknowledgments

SM performed the experiments and manuscript writing. EL performed the particles extraction, supervised the flow cytometry analysis, interpreted the results and contributed to writing the manuscript. RB performed the TPEN analysis, interpreted the results and helped with the writing of the manuscript. PA conducted the chemical analysis. LS conducted the PM sampling and helped with the writing of the manuscript. GB defined the experimental plan, conducted the PM sampling and helped with the writing of the manuscript. AC helped with the particle morphological characterization, supervised all the experiments and contributed to writing the manuscript. MC defined the experimental plan, supervised all the experiments and contributed to writing the manuscript. PM performed the morphological analysis, supervised all the experiments and contributed to writing the manuscript. All authors read and approved the final manuscript.

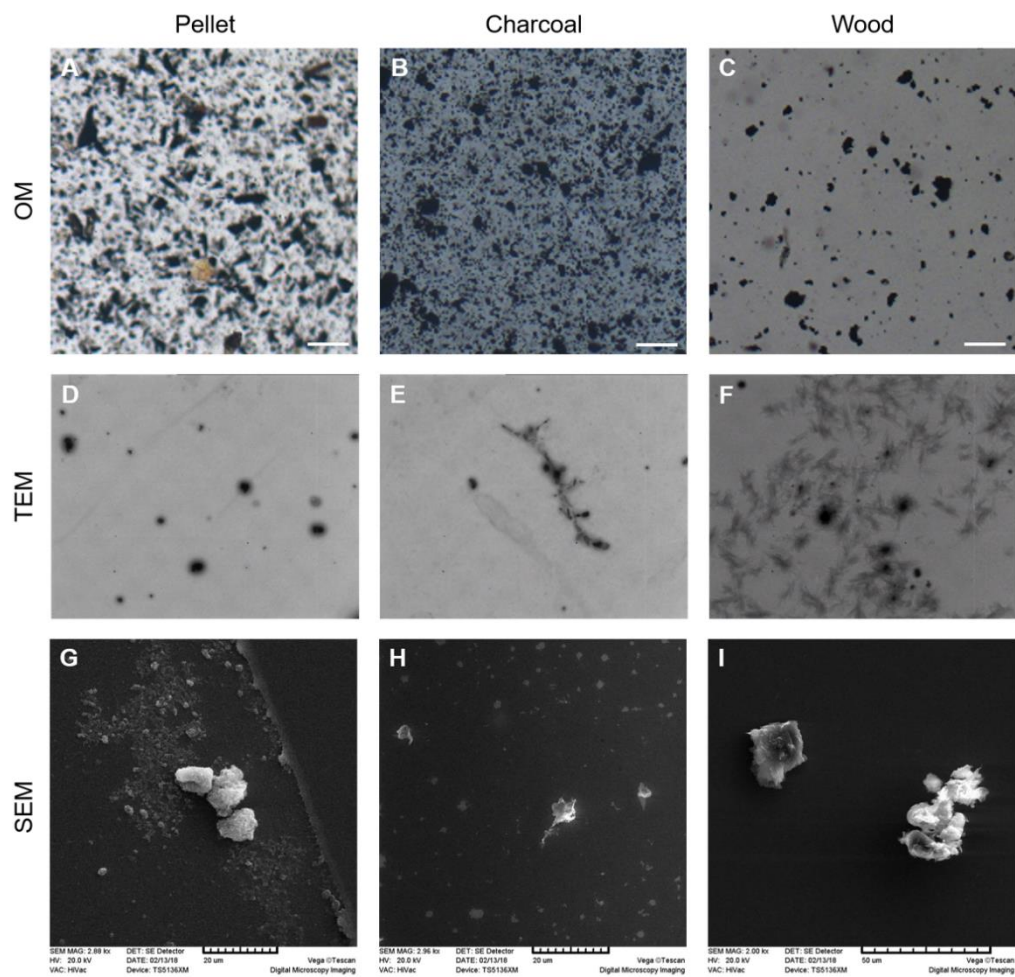
Funding

This study has been supported by the grants of the Cariplo Foundation to MC (proj. ID 2013-1038) and the Italian Ministry of Foreign Affairs and International Cooperation to PM (proj. ID PGR00786).

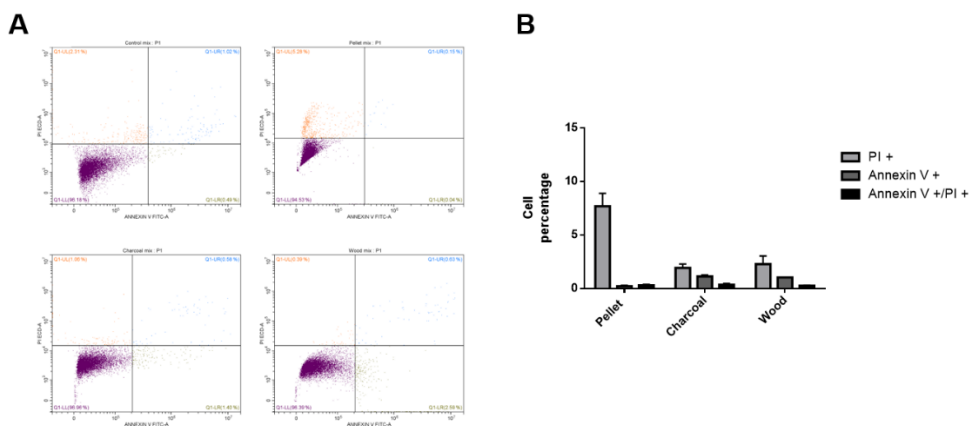
Conflicts of interest

The authors declare no conflicts of interest.

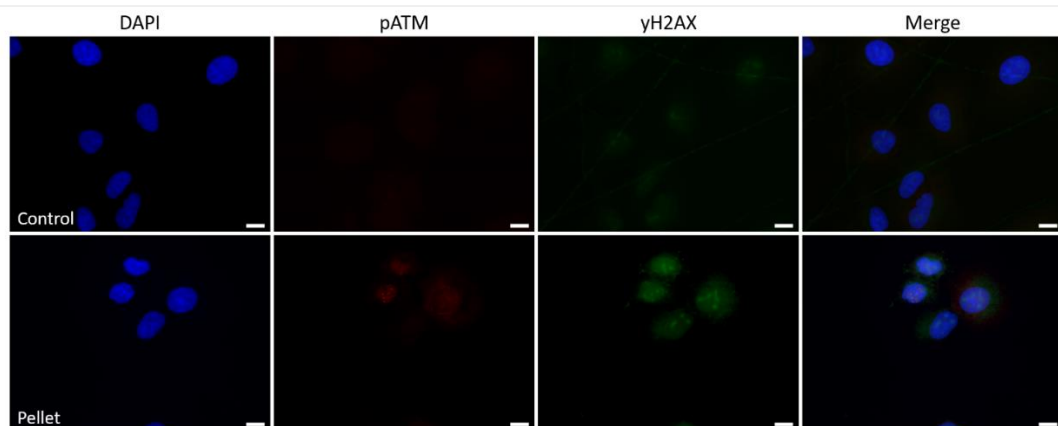
Appendix A. Supplementary data



Additional file 1: Morphological characterization of biomass PMs: optical microscopy (OM), Transmission (TEM) and Scanning Electron Microscopy (SEM) analysis. (A, B and C) scale bars = 50 μm ; (D and E) magnification = 3k; (F) magnification = 2.5k.



Additional file 2: A) Dot plots representing the percentage of positive cells for each staining. PI+: necrotic cells (Q1-UL), PI+/Annexin V+: late apoptotic cells (Q1-UR), Annexin +: early apoptotic cells (Q1-LR), PI-/Annexin V-: viable cells (Q1-LL). B) Percentage of necrotic or apoptotic (early and late) cells after 24 h of exposure to 5 $\mu\text{g}/\text{cm}^2$ biomass PMs. Annexin V/PI staining was performed according to the manufacturer's instructions (Invitrogen/Molecular Probes).



Additional file 3: Representative immunofluorescence image of p-ATM (red) and γ H2AX (green) foci in cells exposed to Pellet PM. The immunofluorescence was performed according to Gualtieri et al., 2011. Bars = 10 μ m.

References

- Alfaro-Moreno, E., Torres, V., Miranda, J., Martínez, L., García-Cuellar, C., Nawrot, T.S., Vanaudenaerde, B., Hoet, P., Ramírez-López, P., Rosas, I., Nemery, B., Osornio-Vargas, A.R., 2009. Induction of IL-6 and inhibition of IL-8 secretion in the human airway cell line Calu-3 by urban particulate matter collected with a modified method of PM sampling. *Environ. Res.* 109, 528–535. doi:10.1016/j.envres.2009.02.010
- Avino, P., Capannesi, G., Renzi, L., Rosada, A., 2013. Instrumental neutron activation analysis and statistical approach for determining baseline values of essential and toxic elements in hairs of high school students. *Ecotoxicol. Environ. Saf.* 92, 206–214. doi:10.1016/j.ecoenv.2013.01.029
- Avino, P., Capannesi, G., Rosada, A., 2011. Ultra-trace nutritional and toxicological elements in Rome and Florence drinking waters determined by Instrumental Neutron Activation Analysis. *Microchem. J.* 97, 144–153. doi:10.1016/j.microc.2010.08.007
- Avino, P., Carconi, P.L., Lepore, L., Moauro, A., 2000. Nutritional and environmental properties of algal products used in healthy diet by INAA and ICP-AES. *J. Radioanal. Nucl. Chem.* doi:10.1023/A:1006721811478
- Buonanno, G., Dell'Isola, M., Stabile, L., Viola, A., 2011. Critical aspects of the uncertainty budget in the gravimetric PM measurements. *Measurement: Journal of the International Measurement Confederation* 44, 139–147. doi:10.1016/j.measurement.2010.09.037
- Buonanno, G., Dell'Isola, M., Stabile, L., Viola, A., 2009. Uncertainty budget of the SMPS-APS system in the measurement of PM 1, PM2.5, and PM10. *Aerosol Sci. Technol.* 43, 1130–1141. doi:10.1080/02786820903204078
- Capannesi, G., Rosada, A., Avino, P., 2009. Elemental characterization of impurities at trace and ultra-trace levels in metallurgical lead samples by INAA. *Microchem. J.* 93, 188–194. doi:10.1016/j.microc.2009.07.004
- Capistrano, S.J., Zakarya, R., Chen, H., Oliver, B.G., 2016. Biomass smoke exposure enhances rhinovirus-induced inflammation in primary lung fibroblasts. *Int. J. Mol. Sci.* 17. doi:10.3390/ijms17091403
- Chirino, Y.I., García-Cuellar, C.M., García-García, C., Soto-Reyes, E., Osornio-Vargas, Á.R., Herrera, L.A., López-Saavedra, A., Miranda, J., Quintana-Belmares, R., Pérez, I.R., Sánchez-Pérez, Y., 2017. Airborne particulate matter in vitro exposure induces cytoskeleton remodeling through activation of the ROCK-MYPT1-MLC pathway in A549 epithelial lung cells. *Toxicol. Lett.* 272, 29–37. doi:10.1016/j.toxlet.2017.03.002
- Choi, Y., Park, K., Kim, I., Kim, S.D., 2016. Combined toxic effect of airborne heavy metals on human lung cell line A549. *Environ. Geochem. Health* doi:10.1007/s10653-016-9901-6

- Corsini, E., Ozgen, S., Papale, A., Galbiati, V., Lonati, G., Fermo, P., Corbella, L., Valli, G., Bernardoni, V., Dell'Acqua, M., Becagli, S., Caruso, D., Vecchi, R., Galli, C.L., Marinovich, M., 2017. Insights on wood combustion generated proinflammatory ultrafine particles (UFP). *Toxicol. Lett.* 266, 74–84. doi:10.1016/j.toxlet.2016.12.005
- Crobeddu, B., Aragao-Santiago, L., Bui, L.C., Boland, S., Baeza Squiban, A., 2017. Oxidative potential of particulate matter 2.5 as predictive indicator of cellular stress. *Environ. Pollut* 230, 125–133. doi:10.1016/j.envpol.2017.06.051
- Cuadrado, M., Martinez-Pastor, B., Murga, M., Toledo, L.I., Gutierrez-Martinez, P., Lopez, E., Fernandez-Capetillo, O., 2006. ATM regulates ATR chromatin loading in response to DNA double-strand breaks. *J. Exp. Med.* 203, 297–303. doi:10.1084/jem.20051923
- Danielsen, P.H., Møller, P., Jensen, K.A., Sharma, A.K., Wallin, H., Bossi, R., Autrup, H., Mølhav, L., Ravanat, J.-L., Briedé, J.J., de Kok, T.M., Loft, S., 2011. Oxidative stress, DNA damage, and inflammation induced by ambient air and wood smoke particulate matter in human A549 and THP-1 cell lines. *Chem. Res. Toxicol.* 24, 168–84.
- Dilger, M., Orasche, J., Zimmermann, R., Paur, H.-R., Diabaté, S., Weiss, C., 2016. Toxicity of wood smoke particles in human A549 lung epithelial cells: the role of PAHs, soot and zinc. *Arch. Toxicol* 90, 3029–3044. doi:10.1007/s00204-016-1659-1
- Farina, F., Sancini, G., Battaglia, C., Tinaglia, V., Mantecca, P., Camatini, M., Palestini, P., 2013. Milano summer particulate matter (PM10) triggers lung inflammation and extra pulmonary adverse events in mice. *PLoS ONE* 8. doi:10.1371/journal.pone.0056636
- Fuentes-Mattei, E., Rivera, E., Gioda, A., Sanchez-Rivera, D., Roman-Velazquez, F.R., Jimenez-Velez, B.D., 2010. Use of human bronchial epithelial cells (BEAS-2B) to study immunological markers resulting from exposure to PM2.5 organic extract from Puerto Rico. *Toxicol. Appl. Pharmacol.* 243, 381–389. doi:10.1016/j.taap.2009.12.009
- Genies, C., Jullien, A., Lefebvre, E., Revol, M., Maitre, A., Douki, T., 2016. Inhibition of the formation of benzo[a]pyrene adducts to DNA in A549 lung cells exposed to mixtures of polycyclic aromatic hydrocarbons. *Toxicol. in Vitro* 35, 1–10. doi:10.1016/j.tiv.2016.05.006
- Genies, C., Maître, A., Lefèbvre, E., Jullien, A., Chopard-Lallier, M., Douki, T., 2013. The extreme variety of genotoxic response to benzo[a]pyrene in three different human cell lines from three different organs. *PLoS ONE* 8, 1–11. doi:10.1371/journal.pone.0078356
- Gualtieri, M., Longhin, E., Mattioli, M., Mantecca, P., Tinaglia, V., Mangano, E., Carla, M., Bestetti, G., Camatini, M., Battaglia, C., 2012. Gene expression profiling of A549 cells exposed to Milan PM2.5. *Toxicol. Lett.* 209, 136–145.

- doi:10.1016/j.toxlet.2011.11.015
- Gualtieri, M., Øvrevik, J., Møllerup, S., Asare, N., Longhin, E., Dahlman, H.J., Camatini, M., Holme, J.A., 2011. Airborne urban particles (Milan winter-PM2.5) cause mitotic arrest and cell death: effects on DNA, mitochondria, AhR binding and spindle organization. *Mutation Research - Fundamental and Molecular Mechanisms of Mutagenesis* 713, 18–31. doi:10.1016/j.mrfmmm.2011.05.011
- Happo, M.S., Uski, O., Jalava, P.I., Kelz, J., Brunner, T., Hakulinen, P., Mäki-Paakkanen, J., Kosma, V.M., Jokiniemi, J., Obernberger, I., Hirvonen, M.R., 2013. Pulmonary inflammation and tissue damage in the mouse lung after exposure to PM samples from biomass heating appliances of old and modern technologies. *Sci. Total Environ.* 443, 256–266. doi:10.1016/j.scitotenv.2012.11.004
- Henkler, F., Brinkmann, J., Luch, A., 2010. The role of oxidative stress in carcinogenesis induced by metals and xenobiotics. *Cancers* 2, 376–396. doi:10.3390/cancers2020376
- Hukkanen, J., Lassila, A., Päivärinta, K., Valanne, S., Sarpola, S., Hakkola, J., Pelkonen, O., Raunio, H., 2000. Induction and regulation of xenobiotic-metabolizing cytochrome P450s in the human A549 lung adenocarcinoma cell line. *Am. J. Respir. Cell Mol. Biol.* 22, 360–366. doi:10.1165/ajrcmb.22.3.3845
- IARC: Outdoor air pollution a leading environmental cause of cancer deaths, 2013. 51, 229–235.
- IARC Monographs on the Evaluation of Carcinogenic Risks to Humans, 2010. 95.
- Jalava, P.I., Happo, M.S., Kelz, J., Brunner, T., Hakulinen, P., Mäki-Paakkanen, J., Hukkanen, A., Jokiniemi, J., Obernberger, I., Hirvonen, M.R., 2012. In vitro toxicological characterization of particulate emissions from residential biomass heating systems based on old and new technologies. *Atmos. Environ* 50, 24–35. doi:10.1016/j.atmosenv.2012.01.009
- Jin, W., Su, S., Wang, B., Zhu, X., Chen, Y., Shen, G., Liu, J., Cheng, H., Wang, X., Wu, S., Zeng, E., Xing, B., Tao, S., 2016. Properties and cellular effects of particulate matter from direct emissions and ambient sources. *Journal of Environmental Science and Health - Part A Toxic/Hazardous Substances and Environmental Engineering* 51, 1075–1083. doi:10.1080/10934529.2016.1198632
- Kastan, M.B., Onyekwere, O., Sidransky, D., Vogelstein, B., Craig, R.W., 1991. Participation of p53 protein in the cellular response to DNA Damage. *Cancer Res.* 51, 6304–6311.
- Kasurinen, S., Jalava, P.I., Happo, M.S., Sippula, O., Uski, O., Koponen, H., Orasche, J., Zimmermann, R., Jokiniemi, J., Hirvonen, M.R., 2017. Particulate emissions from the combustion of birch, beech, and spruce logs cause different cytotoxic responses in A549 cells. *Environmental Toxicology*. doi:10.1002/tox.22369
- Kim, J.S., Peters, T.M., O’Shaughnessy, P.T., Adamcakova-Dodd, A., Thorne, P.S.,

2013. Validation of an in vitro exposure system for toxicity assessment of air-delivered nanomaterials. *Toxicol. in Vitro*. doi:10.1016/j.tiv.2012.08.030
- Kocbach, A., Totlandsdal, A.I., Låg, M., Refsnes, M., Schwarze, P.E., 2008. Differential binding of cytokines to environmentally relevant particles: a possible source for misinterpretation of in vitro results? *Toxicol. Lett.* 176, 131–137. doi:10.1016/j.toxlet.2007.10.014
- Kocbach Bølling, A., Pagels, J., Yttri, K.E., Barregard, L., Sallsten, G., Schwarze, P.E., Boman, C., 2009. Health effects of residential wood smoke particles: the importance of combustion conditions and physicochemical particle properties. *Particle and fibre toxicology* 6, 29.
- Lamberg, H., Tissari, J., Jokiniemi, J., Sippula, O., 2013. Fine particle and gaseous emissions from a small-scale boiler fueled by pellets of various raw materials. *Energy and Fuels* 27, 7044–7053. doi:10.1021/ef401267t
- Li, Q., Jiang, J., Wang, S., Rumchev, K., Mead-Hunter, R., Morawska, L., Hao, J., 2017. Impacts of household coal and biomass combustion on indoor and ambient air quality in China: current status and implication. *Sci. Total Environ.* 576, 347–361. doi:10.1016/j.scitotenv.2016.10.080
- Liang, Y., Lin, S.-Y., Brunicardi, F.C., Goss, J., Li, K., 2009. DNA damage response pathways in tumor suppression and cancer treatment. *World J. Surg.* 33, 661–666. doi:10.1007/s00268-008-9840-1
- Lindner, K., Ströbele, M., Schlick, S., Webering, S., Jenckel, A., Kopf, J., Danov, O., Sewald, K., Buj, C., Creutzenberg, O., Tillmann, T., Pohlmann, G., Ernst, H., Ziemann, C., Hüttmann, G., Heine, H., Bockhorn, H., Hansen, T., König, P., Fehrenbach, H., 2017. Biological effects of carbon black nanoparticles are changed by surface coating with polycyclic aromatic hydrocarbons. *Particle and fibre toxicology* 14, 8. doi:10.1186/s12989-017-0189-1
- Longhin, E., Gualtieri, M., Capasso, L., Bengalli, R., Mollerup, S., Holme, J.A., Øvrevik, J., Casadei, S., Di Benedetto, C., Parenti, P., Camatini, M., 2016. Physicochemical properties and biological effects of diesel and biomass particles. *Environ. Pollut* 215, 366–375. doi:10.1016/j.envpol.2016.05.015
- Longhin, E., Pezzolato, E., Mantecca, P., Holme, J.A., Franzetti, A., Camatini, M., Gualtieri, M., 2013. Season linked responses to fine and quasi-ultrafine Milan PM in cultured cells. *Toxicol. in Vitro* 27, 551–559. doi:10.1016/j.tiv.2012.10.018
- Loxham, M., Morgan-Walsh, R.J., Cooper, M.J., Blume, C., Swindle, E.J., Dennison, P.W., Howarth, P.H., Cassee, F.R., Teagle, D.A.H., Palmer, M.R., Davies, D.E., 2015. The effects on bronchial epithelial mucociliary cultures of coarse, fine, and ultrafine particulate matter from an underground railway station. *Toxicol. Sci.* 145, 98–107. doi:10.1093/toxsci/kfv034
- Marabini, L., Ozgen, S., Turacchi, S., Aminti, S., Arnaboldi, F., Lonati, G., Fermo, P., Corbella, L., Valli, G., Bernardoni, V., Dell'Acqua, M., Vecchi, R., Becagli, S.,

- Caruso, D., Corrado, L.G., Marinovich, M., 2017. Ultrafine particles (UFPs) from domestic wood stoves: genotoxicity in human lung carcinoma A549 cells. *Mutation Research - Genetic Toxicology and Environmental Mutagenesis* 820, 39–46. doi:10.1016/j.mrgentox.2017.06.001
- Maréchal, A., Zou, L., 2013. DNA damage sensing by the ATM and ATR kinases. *Cold Spring Harb. Perspect. Biol.* 5, 1–17. doi:10.1101/cshperspect.a012716
- Michael, S., Montag, M., Dott, W., 2013. Pro-inflammatory effects and oxidative stress in lung macrophages and epithelial cells induced by ambient particulate matter. *Environ. Pollut* 183, 19–29. doi:10.1016/j.envpol.2013.01.026
- Muala, A., Rankin, G., Sehlstedt, M., Unosson, J., Bosson, J.A., Behndig, A., Pourazar, J., Nyström, R., Pettersson, E., Bergvall, C., Westerholm, R., Jalava, P.I., Happo, M.S., Uski, O., Hirvonen, M.-R., Kelly, F.J., Mudway, I.S., Blomberg, A., Boman, C., Sandström, T., 2015. Acute exposure to wood smoke from incomplete combustion - indications of cytotoxicity. *Particle and Fibre Toxicology* 12, 33. doi:10.1186/s12989-015-0111-7
- Nemmar, A., Holme, J.A., Rosas, I., Schwarze, P.E., Alfaro-Moreno, E., 2013. Recent advances in particulate matter and nanoparticle toxicology: a review of the in vivo and in vitro studies. *Biomed. Res. Int.* 2013, 279371. doi:10.1155/2013/279371
- Pati, R., Das, I., Mehta, R.K., Sahu, R., Sonawane, A., 2016. Zinc-oxide nanoparticles exhibit genotoxic, clastogenic, cytotoxic and actin depolymerization effects by inducing oxidative stress responses in macrophages and adult mice. *Toxicol. Sci.* 150, 454–472. doi:10.1093/toxsci/kfw010
- Perrone, M.G., Gualtieri, M., Ferrero, L., Porto, C. Lo, Udisti, R., Bolzacchini, E., Camatini, M., 2010. Seasonal variations in chemical composition and in vitro biological effects of fine PM from Milan. *Chemosphere* 78, 1368–1377. doi:10.1016/j.chemosphere.2009.12.071
- Reyes-Zárate, E., Sánchez-Pérez, Y., Gutiérrez-Ruiz, M.C., Chirino, Y.I., Osornio-Vargas, Á.R., Morales-Bárceñas, R., Souza-Arroyo, V., García-Cuellar, C.M., 2016. Atmospheric particulate matter (PM10) exposure-induced cell cycle arrest and apoptosis evasion through STAT3 activation via PKC ζ and Src kinases in lung cells. *Environ. Pollut* 214, 646–656. doi:10.1016/j.envpol.2016.04.072
- Rossner, P., Strapacova, S., Stolcpartova, J., Schmuczerova, J., Milcova, A., Neca, J., Vlkova, V., Brzicova, T., Machala, M., Topinka, J., 2016. Toxic effects of the major components of diesel exhaust in human alveolar basal epithelial cells (A549). *Int. J. Mol. Sci.* 17. doi:10.3390/ijms17091393
- Rudolf, E., Cervinka, M., 2011. Stress responses of human dermal fibroblasts exposed to zinc pyrithione. *Toxicol. Lett.* 204, 164–173. doi:10.1016/j.toxlet.2011.04.028
- Samburova, V., Connolly, J., Gyawali, M., Yatavelli, R.L.N., Watts, A.C., Chakrabarty, R.K., Zielinska, B., Moosmüller, H., Khlystov, A., 2016. Polycyclic aromatic

- hydrocarbons in biomass-burning emissions and their contribution to light absorption and aerosol toxicity. *Sci. Total Environ.* 568, 391–401. doi:10.1016/j.scitotenv.2016.06.026
- Sánchez-Pérez, Y., Chirino, Y.I., Osornio-Vargas, A.R., Morales-Bàrcenas, R., Gutiérrez-Ruiz, C., Vázquez-López, I., García-Cuellar, C.M., 2009. DNA damage response of A549 cells treated with particulate matter (PM₁₀) of urban air pollutants. *Cancer Lett.* 278, 192–200. doi:10.1016/j.canlet.2009.01.010
- Secrest, M.H., Schauer, J.J., Carter, E.M., Lai, A.M., Wang, Y., Shan, M., Yang, X., Zhang, Y., Baumgartner, J., 2016. The oxidative potential of PM_{2.5} exposures from indoor and outdoor sources in rural China. *Sci. Total Environ.* 571, 1477–1489. doi:10.1016/j.scitotenv.2016.06.231
- Smith, J., Mun Tho, L., Xu, N., A. Gillespie, D., 2010. The ATM-Chk2 and ATR-Chk1 pathways in DNA damage signaling and cancer. *Advances in Cancer Res.* 108, 73–112. doi:10.1016/B978-0-12-380888-2.00003-0
- Stabile, L., Buonanno, G., Avino, P., Frattolillo, A., Guerriero, E., 2018. Indoor exposure to particles emitted by biomass-burning heating systems and evaluation of dose and lung cancer risk received by population. *Environ. Pollut* 235, 65–73. doi:10.1016/j.envpol.2017.12.055
- Steenhof, M., Gosens, I., Strak, M., Godri, K.J., Hoek, G., Cassee, F.R., Mudway, I.S., Kelly, F.J., Harrison, R.M., Lebret, E., Brunekreef, B., Janssen, N.A., Pieters, R.H., 2011. In vitro toxicity of particulate matter (PM) collected at different sites in the Netherlands is associated with PM composition, size fraction and oxidative potential - the RAPTES project. *Particle and Fibre Toxicology* 8, 26. doi:10.1186/1743-8977-8-26
- Strapáčová, S., Brenerová, P., Krčmář, P., Andersson, P., van Ede, K.I., van Duursen, M.B.M., van den Berg, M., Vondráček, J., Machala, M., 2018. Relative effective potencies of dioxin-like compounds in rodent and human lung cell models. *Toxicology* 404–405, 33–41. doi:10.1016/j.tox.2018.05.004
- Sussan, T.E., Ingole, V., Kim, J.H., McCormick, S., Negherbon, J., Fallica, J., Akulian, J., Yarmus, L., Feller-Kopman, D., Wills-Karp, M., Horton, M.R., Breyse, P.N., Agrawal, A., Juvekar, S., Salvi, S., Biswal, S., 2014. Source of biomass cooking fuel determines pulmonary response to household air pollution. *Am. J. Respir. Cell Mol. Biol.* 50, 538–548. doi:10.1165/rcmb.2013-0201OC
- Swiston, J.R., Davidson, W., Attridge, S., Li, G.T., Brauer, M., Van Eeden, S.F., 2008. Wood smoke exposure induces a pulmonary and systemic inflammatory response in firefighters. *Eur. Respir. J.* 32, 129–138. doi:10.1183/09031936.00097707
- Torvela, T., Uski, O., Karhunen, T., Jalava, P., Sippula, O., Tissari, J., Hirvonen, M., Jokiniemi, J., 2014. Reference Particles for Toxicological Studies of Wood Combustion: Formation, Characteristics, and Toxicity Compared to Those of Real Wood Combustion Particulate Mass.

- Totlandsdal, A.I., Øvrevik, J., Cochran, R.E., Herseth, J.I., Bølling, A.K., Låg, M., Schwarze, P., Lilleaas, E., Holme, J.A., Kubátová, A., 2014. The occurrence of polycyclic aromatic hydrocarbons and their derivatives and the proinflammatory potential of fractionated extracts of diesel exhaust and wood smoke particles. *Journal of Environmental Science and Health - Part A Toxic/Hazardous Substances and Environmental Engineering*. doi:10.1080/10934529.2014.854586
- Uski, O., Jalava, P.I., Happonen, M.S., Leskinen, J., Sippula, O., Tissari, J., Mäki-Paakkanen, J., Jokiniemi, J., Hirvonen, M.R., 2014. Different toxic mechanisms are activated by emission PM depending on combustion efficiency. *Atmos. Environ* 89, 623–632. doi:10.1016/j.atmosenv.2014.02.036
- Uski, O., Jalava, P.I., Happonen, M.S., Torvela, T., Leskinen, J., Mäki-Paakkanen, J., Tissari, J., Sippula, O., Lamberg, H., Jokiniemi, J., Hirvonen, M.-R., 2015. Effect of fuel zinc content on toxicological responses of particulate matter from pellet combustion in vitro. *The Sci. Total Environ*. 511, 331–340.
- Uski, O.J., Happonen, M.S., Jalava, P.I., Brunner, T., Kelz, J., Obernberger, I., Jokiniemi, J., Hirvonen, M.-R., 2012. Acute systemic and lung inflammation in C57Bl/6J mice after intratracheal aspiration of particulate matter from small-scale biomass combustion appliances based on old and modern technologies. *Inhal. Toxicol*. 24, 952–965. doi:10.3109/08958378.2012.742172
- Van Den Heuvel, R., Den Hond, E., Govarts, E., Colles, A., Koppen, G., Staelens, J., Mampaey, M., Janssen, N., Schoeters, G., 2016. Identification of PM10 characteristics involved in cellular responses in human bronchial epithelial cells (Beas-2B). *Environ. Res*. 149, 48–56. doi:10.1016/j.envres.2016.04.029
- Wallach, D., Kang, T.-B., Kovalenko, A., 2013. Concepts of tissue injury and cell death in inflammation: a historical perspective. *Nat. Rev. Immunol*. 14, 51–59. doi:10.1038/nri3561
- Yang, L., Liu, G., Lin, Z., Wang, Y., He, H., Liu, T., Kamp, D.W., 2016. Pro-inflammatory response and oxidative stress induced by specific components in ambient particulate matter in human bronchial epithelial cells. *Environ. Toxicol*. 31, 923–936. doi:10.1002/tox.22102
- Zhang, J., Ghio, A.J., Gao, M., Wei, K., Rosen, G.D., Upadhyay, D., 2007. Ambient particulate matter induces alveolar epithelial cell cycle arrest: role of G1 cyclins. *FEBS Lett*. 581, 5315–5320.
- Zhang, J., Song, W., Guo, J., Zhang, J., Sun, Z., Ding, F., Gao, M., 2012. Toxic effect of different ZnO particles on mouse alveolar macrophages. *J. Hazard. Mater* 219–220, 148–155. doi:10.1016/j.jhazmat.2012.03.069

Chapter 2:

Combustion-derived particles from biomass sources differently promote epithelial to mesenchymal transition on A549 cells

Sara Marchetti¹ *, Rossella Bengalli¹, Pamela Floris¹, Anita Colombo¹, Paride Mantecca¹

¹POLARIS Research Centre, Department of Earth and Environmental Sciences, University of Milano-Bicocca, Piazza della Scienza 1, 20126 Milano, Italy

*Corresponding author: Sara Marchetti, e-mail: s.marchetti16@campus.unimib.it, tel: +390264482928

Manuscript in submission (Environmental Pollution)

Abstract

Combustion-derived particles (CDPs) are linked to several respiratory diseases, including lung cancer. Epithelial-to-mesenchymal transition (EMT) is a crucial step in lung cancer progression, involving several morphological and phenotypical changes. The study aims at exploring how exposure to CDPs from different biomass sources might be involved in cancer development, focusing mainly on the effects linked to EMT and invasion on human A549 lung cells.

CDPs were collected from a stove fueled with pellet, charcoal or wood respectively. A time course and dose response evaluation on cell viability and pro-inflammatory response was performed to select the optimal conditions for EMT-related studies. A significant release of IL-8, which has been reported to support EMT activation, was found after 72 h of exposure to 2.5 µg/cm² CDPs. Thus, the process activation was then examined by evaluating the expression of some typical EMT markers and the possible enhanced migration and invasiveness.

Long-term exposure revealed that CDPs differentially modulated cell viability, migration and invasion as well as the expression of proteins linked to EMT. Results showed a reduction in the epithelial marker E-cadherin and a parallel increase in the mesenchymal marker N-cadherin after exposure to charcoal and wood mainly. Migration and invasion were also increased.

In conclusion, results suggest that organic compounds such as PAHs might play a crucial role in inducing pro-carcinogenic effects on epithelial cells.

Keywords: combustion-derived particles, epithelial to mesenchymal transition activation, biomass, interleukin 8, lung cancer.

biochemical changes, losing cellular polarity and adhesion contacts (Yang et al., 2017; Zou et al., 2013) and re-organizing the cytoskeleton (Liu et al., 2013). Finally, cells differentiate into a mesenchymal-cell phenotype, which is described by improved motility, invasiveness and resistance to apoptosis (Kalluri and Weinberg, 2009). Several genes have been reported as key regulators for cancer progression. EMT indeed, is characterized by loss of epithelial markers, like E-cadherin and ZO-1, and gain of mesenchymal-type proteins, like Vimentin and N-cadherin (Bersaas et al., 2016; Thiery et al., 2009).

Furthermore, even soluble factors, including growth factor and cytokines such as tumor growth factor beta (TGF- β) and interleukin-8 (IL-8), could contribute to promote and/or maintain an EMT phenotype (Palena et al., 2012; Xiao and He, 2010).

The increased release of cytokines and chemokines is a common response after PM exposure (Sun, 2010; Van Eeden et al., 2001) and chronic inflammation due to airborne particles could lead to lung remodeling (Ohbayashi, 2002).

Biomass sources represent the most frequently fuels used for domestic heating. However, to our knowledge only Longhin et al., (Longhin et al., 2016b) have investigated their potential carcinogenic risk focusing on EMT as crucial pathological process activated. Nevertheless, few studies have been performed on cigarette smoke-induced EMT (Bersaas et al., 2016; Milara et al., 2013; Shen et al., 2014).

We have previously shown that the compositions of particles emitted from the same combustion technology activate different toxicological responses *in vitro* (Marchetti et al., 2019). In the present study, we assessed long-term toxicity and EMT process activation induced by different CDPs on human lung epithelial cells (A549). Our hypothesis was to identify the possible mechanisms by which CDPs may exert their pro-carcinogenic properties and thus, increase the risk of cancer. Attention was given to EMT activation and the consequent increase in motility and invasiveness that suggests that PAHs more than metals may be effective. The study points out the importance of select biomass fuels as energy source considering both composition and biological activity, in order to reduce lung cancer risk.

2. Materials and methods

2.1. CDPs sampling and extraction

Samplings were performed using an open fireplace fueled for 4 hours with pellet, charcoal or wood respectively. Briefly, CDPs were collected on Teflon filter using a gravimetric sampler made up of a volumetric rotating pump Zambelli 6000 Plus and a Zambelli PM10 impactor gravimetric sampler (FAI Instruments, Rome, Italy). Filters from the same fuel were pooled and particles mechanically detached by

replicating four 20-min ultrasonic cycles in 2 mL of pure sterile water using an ultrasound bath (Sonica Soltec, Milan, Italy). The obtained suspensions were then aliquoted in sterile tubes, dried in a desiccator and stored at -20 °C until use. Finally, CDPs were resuspended to the concentration of 2 µg/µL in sterile water just prior to cell exposure. More details on CDPs sampling and physico-chemical characterization have been reported in our previous study (Marchetti et al., 2019).

2.2. Cell culture

Human alveolar epithelial cell line A549 was purchased from the American Type Culture Collection (ATCC® CCL-185, American Type Culture Collection, Manassas, USA). Cells were cultured in Optimem medium supplemented with 10% heat-inactivated Fetal Bovine Serum (FBS) and penicillin/streptomycin (0.1 mg/mL) at 37 °C in humidified atmosphere with 5 % CO₂. The cell line was splitted every Monday, Wednesday and Friday.

For CDP exposure, A549 cells were cultured in Optimem medium with 1 % FBS. All the *in vitro* experiments were performed at least in triplicate.

2.3. Cell viability

A549 viability was assessed by means of Alamar Blue (Life Technologies, Monza, Italy) assay accordingly to manufacturer's instruction, as previously described (Marchetti et al., 2019). Depending on the incubation time, A549 cells were seeded at different density (100.000 cell/well for 24 h of exposure, 50000 cell/well for 48 h and 25000 cell/well for 72 h) and exposed to the different CDPs after 24 hours. For each source, cells were exposed to different doses (1, 2.5 and 5 µg/cm²) for 24, 48 and 72 h. Then, a solution containing 1:10 of Alamar Blue reagent and cell medium was added into each well. After 3 h of incubation, media absorbance was read to the spectrophotometer (TECAN Infinite Pro) at 570 and 630 nm wavelengths and compared to control values.

2.4. ELISA

Supernatants from A549 cells were collected after exposure to CDPs, centrifuged to remove particles (12000 rpm, 6 min, 4 °C) and stored at -20 °C until analysis. IL-8 protein levels were detected after 48 and 72 h of exposure by sandwich ELISA according to the manufacturer's instructions (Life Technologies). Absorbance was measured by Multiplate Reader Ascent (Thermo Scientific, USA) at the wavelengths of 450 and 650 nm and the amount of proteins expressed in pg/mL based on a standard curve.

2.5. BPDE DNA bulky adducts detection

After a 72 h of exposure to 2.5 $\mu\text{g}/\text{cm}^2$, DNA was extracted from A549 cell pellets using the FlexiGene DNA kit (Qiagen) and quantified by spectrophotometry. DNA adduct detection was performed using the OxiSelect BPDE DNA Adduct ELISA Kit (Cell Biolabs, San Diego, USA), an enzyme immunoassay that allow detection of benzo(a)pyrene diol epoxide (BPDE)-DNA adducts. Briefly, extracted DNA was diluted to 4 $\mu\text{g}/\text{mL}$ in TE Buffer (10 mM Tris, pH 8.0, 1 mM EDTA). DNA samples and BPDE-DNA standards were then added in duplicate to the well of the plate and incubated overnight (O/N) at room temperature (RT) with DNA Binding Solution. The day after, samples were rinsed with PBS and incubated with assay diluent for 1h at RT. Then, after washing, Anti-BPDE-I Antibody was added for 1h. Finally, samples were incubated with Secondary Antibody-HRP conjugate for 1h, and then substrate and stop solution to develop the colorimetric enzyme reaction. Absorbance was read at 450 nm and the amount of BPDE DNA Adduct expressed as fold change compared to the control cells.

2.6. Protein expression analysis

For protein expression evaluation, cells were exposed for 72 h to 2.5 $\mu\text{g}/\text{cm}^2$ CDPs in 6-well plates. After treatment, cells were lysed on ice with RIPA buffer (150 mM NaCl, 1 % Triton X-100, 0.5 % sodium deoxycholate, 0.1 % SDS, 50 mM Tris pH 8.0) and 0.1 % of proteases inhibitor, added just before use. Lysates were then, centrifuged at 12000 rpm for 15 min to remove debris and particles. Finally, protein concentration was assessed by bicinchoninic acid assay (Sigma Aldrich), according to the manufacturer instructions. Thirty μg of proteins were loaded onto 10 % SDS-PAGE gels, separated and transferred on nitrocellulose membranes. Membranes were incubated for 1 h with blocking buffer, composed of Tris-Buffered Saline (TBS) with 0.1% Tween20 (TBS-T) supplemented with 5 % w/v bovine serum albumin (BSA; Sigma) or milk (Skim milk powder, Fluka, Sigma). Afterward, membranes were incubated O/N at 4 °C with the following rabbit monoclonal antibodies: ZO-1, E-cadherin, N-cadherin, Vimentin, (1:1000, Cell Signaling Technology, Danvers, USA), CYP1A1 and CYP1B1 (1:500, Novus Biologicals, Littleton, CO, United States). The following day, membranes were washed three times with TBS-T and then incubated with the specific HRP-linked secondary antibodies (anti-rabbit IgG, 1:2000, Cell Signaling) in Blocking buffer for 1 h at RT. Finally, after washing, proteins were detected by enhanced chemiluminescent (ECL, Euroclone) and digital images taken by means of a luminescence reader (Biospectrum-UVP, LLC, Upland, CA, United States). The dedicated software (Vision Works LS) was used to perform densitometry analysis. As loading control, monoclonal anti- β -Actin antibody (Cell Signaling, 1:1000) was used.

2.7. Immunofluorescence microscopy

The analysis of the expression of E-cadherin and N-cadherin, as epithelial and mesenchymal markers respectively, was evaluated also through immunofluorescence analysis.

Cells (25000 cells/well) were seeded on a 6-multiwell having coverslides on the bottom. After 24 h of incubation, cells were treated with the different CDPs (2.5 $\mu\text{g}/\text{cm}^2$) for 72h. After treatment cells were washed twice with PBS and then, fixed with 4% paraformaldehyde for 20 min. For staining, cells were washed with PBS and permeabilized with PBTS (1X PBS + 0.3% TritonX100 and 5% BSA) for 30 min. After permeabilization, cells were stained with the antibody mAb rabbit anti-E-cadherin (24E10) (1:200; Cell Signaling) or anti-N-cadherin (1:200; Cell Signaling) in antibody dilution buffer (1X PBS + 1% BSA + 0.3% Triton X-100) O/N at 4°C. The secondary antibody goat anti-rabbit Alexa Fluor488 (Molecular Probe, Life Technologies, Monza, Milano, Italy) was added for 2 h at RT after washes. Cells stained with E-cadherin were also stained for 20 min with rhodamine phalloidin (Cytoskeleton Inc., Denver, CO, US) for the evaluation of actin changes. Cells were finally counterstained with DAPI (Molecular Probe, Life Technologies, Monza, Italy) for 2 min and after washing, mounted with ProLong™ Gold Antifade Mountant (Life Technologies) on glass slides. The analysis of fluorescence was evaluated through an AxioObserver Z1 Cell Imaging station (Carl-ZEISS Spa, Milano, Italy) and images were elaborated with the dedicated software ZEN 2.3 Blue edition.

2.8. Migration and invasion assays

To assess cell motility and invasiveness, 62.5×10^3 A549 cells were seeded in a 24-well plate on polycarbonate membrane inserts with 8 μm pore size. CytoSelect 24 - Well Cell Migration and CytoSelect 24-Well Cell Invasion assays were performed according the manufacturer's manuals (Cell BioLabs). Briefly, cell suspensions were placed in upper chamber of inserts in OptiMem medium without serum for O/N starvation. 500 μL of media containing 10 % FBS were added to the well. The day after, media were replaced and cells treated with 2.5 $\mu\text{g}/\text{cm}^2$ CDPs for 72h in OptiMem medium supplemented with 1% FBS. Migratory/invasiveness cells pass through basement membrane layer to the bottom chamber of the insert. Non-migratory/invasiveness cells (upper chamber) were removed and inserts incubated with cell stain solution for 10 min at RT. After that, cells were washed several times with sterile water and allow to dry. Finally, extraction solution was added for 10 min incubation. Absorbance was read with a spectrophotometer at 560 nm and migration/invasion of exposed cells expressed as fold change compared to the control cells.

2.9. Statistical analysis

The data represent mean and standard error of mean (SEM) of three independent experiments carried out at the same experimental conditions. Statistical analysis was performed using GraphPad Prism 6 software, using One-way or Two-way ANOVA with Tukey's, Dunn's or Dunnett's post hoc multiple comparisons tests. Values of $p < 0.05$ were considered statistically significant.

3. Results

Viability assay showed that pellet induced a dose response mortality, with effects visible already after 24 h of exposure, as previously reported (Marchetti et al., 2019). The cytotoxic response is increased after 48 and 72 h, showing 2.5 $\mu\text{g}/\text{cm}^2$ as sub-lethal dose (Figure 1). Charcoal instead, did not induce significant effects on cell viability except for a slight reduction after long-term exposure (Figures 1B and C). Regarding wood, a decreased viability was observed after 72 h of exposure to 5 $\mu\text{g}/\text{cm}^2$ (Figure 1C).

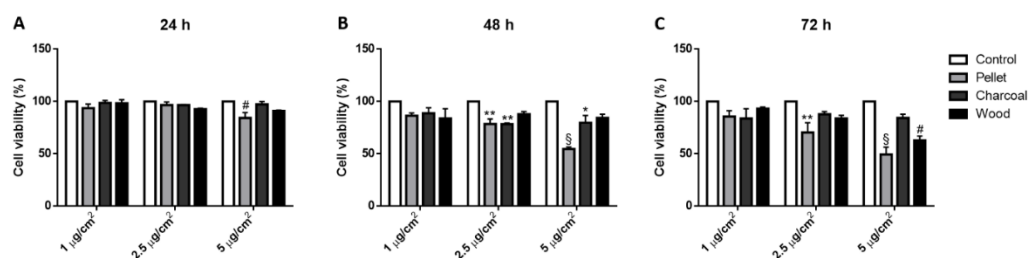


Figure 1. Cell viability. A549 viability was assessed after 24 (A), 48 (B) and 72 h (C) of exposure to increasing doses of CDPs (1, 2.5 and 5 $\mu\text{g}/\text{cm}^2$). Histograms represent cell viability expressed as percentage compared to the control (expressed as 100%). Each bar shows mean \pm SEM of three independent experiments (N=3). Statistical analysis was performed by Two-way ANOVA with Tukey's multiple comparisons test tests. $§p < 0.0001$, $\#p < 0.001$, $**p < 0.01$ and $*p < 0.05$ vs control cells.

As a measure of CDPs-induced pro-inflammatory effects and as possible soluble factor involved in promoting EMT, the release of IL-8 was detected after 48 h and 72 h of exposure. Although the activation of the inflammatory response was not detected after 24 h of exposure to CDPs, here IL-8 secretion was discovered augmented both at 48 and at 72 h of exposure. Indeed, results showed an increased release in time of the cytokine with all CDPs and doses tested. Charcoal and pellet in particular, seemed the most potent CDPs, inducing IL-8 release at 2.5 $\mu\text{g}/\text{cm}^2$ respectively 9 and 8 times more than control.

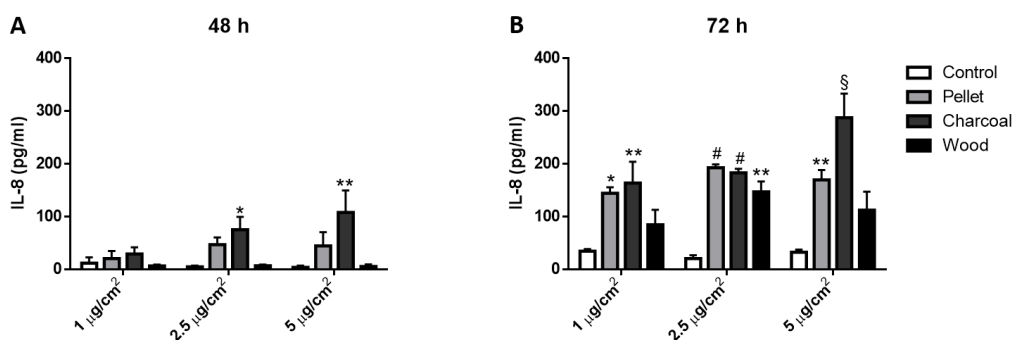


Figure 2. Pro-inflammatory response. IL-8 protein secretion after 48 (A) and 72 h (B) of A549 exposure to increasing CDPs doses (1, 2.5 and 5 $\mu\text{g}/\text{cm}^2$). Each bar shows mean \pm SEM of three independent experiments (N=3). Statistical analysis was performed by Two-way ANOVA with Tukey's multiple comparisons tests. $^{\S}p<0.0001$, $^{\#}p<0.001$, $^{**}p<0.01$ and $^{*}p<0.05$ vs control cells.

Considering results on cell viability and IL-8 release, 72h of exposure and the dose of 2.5 $\mu\text{g}/\text{cm}^2$ were selected to perform the following experiments.

The metabolic activation of PAHs adsorbed on CDPs and PAH-induced DNA bulky adduct formation was then studied. A statistically significant increase in CYP1A1 protein activity was detected only in cells exposed to wood, while a slight effect was exerted on CYP1B1 by all CDPs (Figure 3A). However, no BPDE-DNA bulky adduct were detected, regardless the type of biomass source (Supplementary figure1).

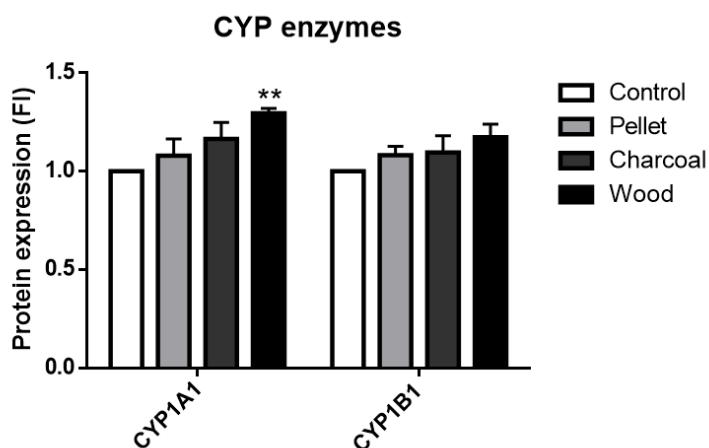


Figure 3. CYP1A1 and CYP1B1 protein expression in A549 cells after 72 h of exposure to 2.5 $\mu\text{g}/\text{cm}^2$. Each bar shows mean \pm SEM of three independent experiments (N=3). Statistical analysis was performed by One-way ANOVA with Sidak's multiple comparisons test. $^{**}p<0.01$ vs control cells.

EMT-proteins expression on A549 cells was also evaluated in order to verify if CDPs might modulate the process activation. After exposure to CDPs, the levels of expression of epithelial markers were not influenced (Figure 4A). However,

mesenchymal markers (Figure 4B) were found modulated. In particular, charcoal significantly increased both N-cadherin and modulated Vimentin, although it is not significant. Wood instead, significantly increased only the expression of Vimentin. No significant effects were detected after exposure to pellet.

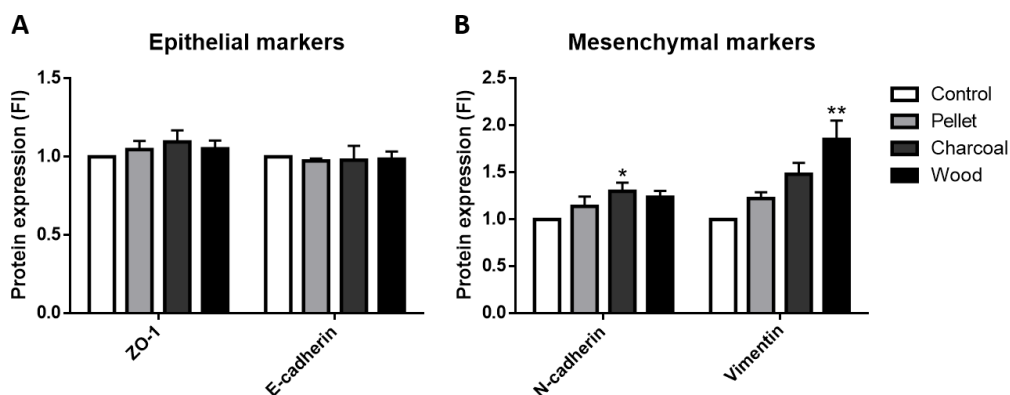


Figure 4. EMT-related proteins expression on A549 cells after 72h of exposure to 2.5 µg/cm². A) Epithelial-type proteins: ZO-1 and E-cadherin. B) Mesenchymal-type proteins: N-cadherin and Vimentin. Each bar shows mean ± SEM of three independent experiments (N=3). Statistical analysis was performed by One-way ANOVA with Dunnett's or Dunn's multiple comparisons test. ***p*<0.01 and **p*<0.05 vs control cells.

The expression of epithelial and mesenchymal markers in CDPs exposed cells was detected also by immunostaining (Figure 5 and 6). Here, we observed that in the exposed cells, especially pellet and charcoal, E-cadherin is delocalized and expressed in the cytoplasm, not only in the plasma membrane. This delocalization after exposure to CDPs suggest a reduction in the cell-to-cell contacts. A cytoskeletal remodelling was also observed with augmented expression of stress fibers, actin ruffles and focal adhesion complexes (Figure 5 and Supplementary figure 2), as evidenced by the actin staining.

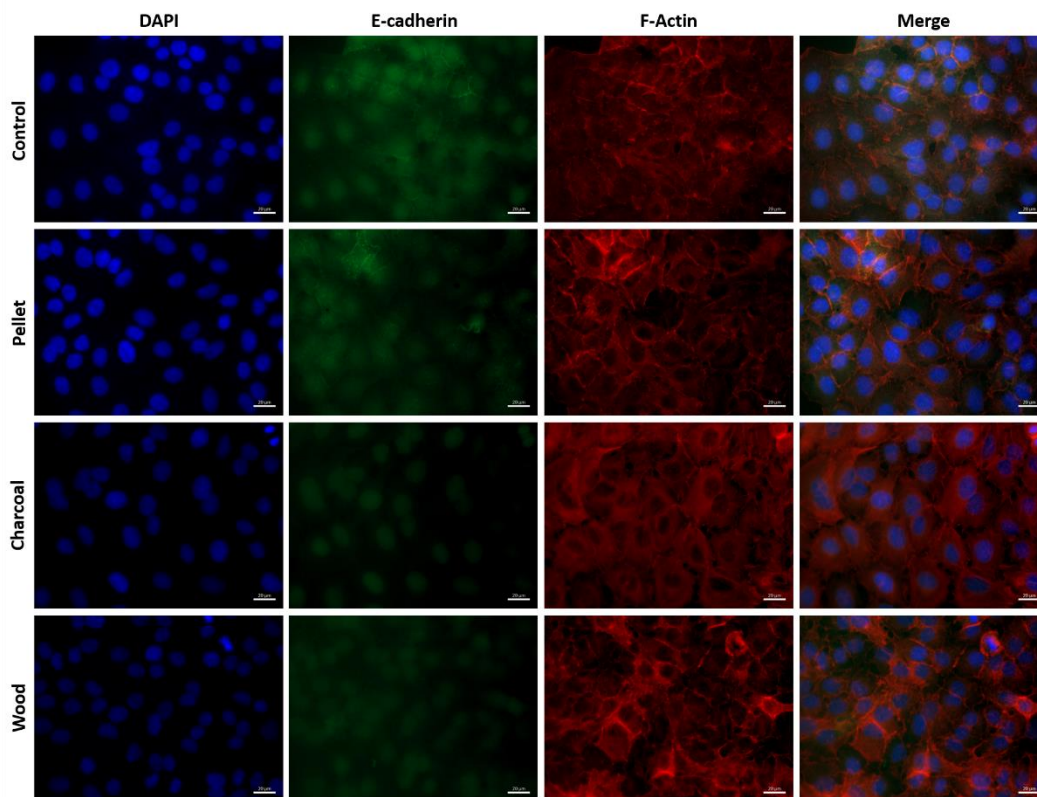


Figure 5. Immunofluorescence of the EMT epithelial marker E-cadherin on A549 cells after 72h of exposure to CDPs ($2.5 \mu\text{g}/\text{cm}^2$). Nuclei are stained with DAPI (blue); E-cadherin with rabbit anti-E-cadherin (green) antibody and F-actin with rhodamine-phalloidin (red). Scale bar= $20 \mu\text{m}$.

N-cadherin, the mesenchymal marker, was instead increased upon CDPs exposure (Figure 6), mainly after charcoal and wood exposure, confirming western blot analysis.

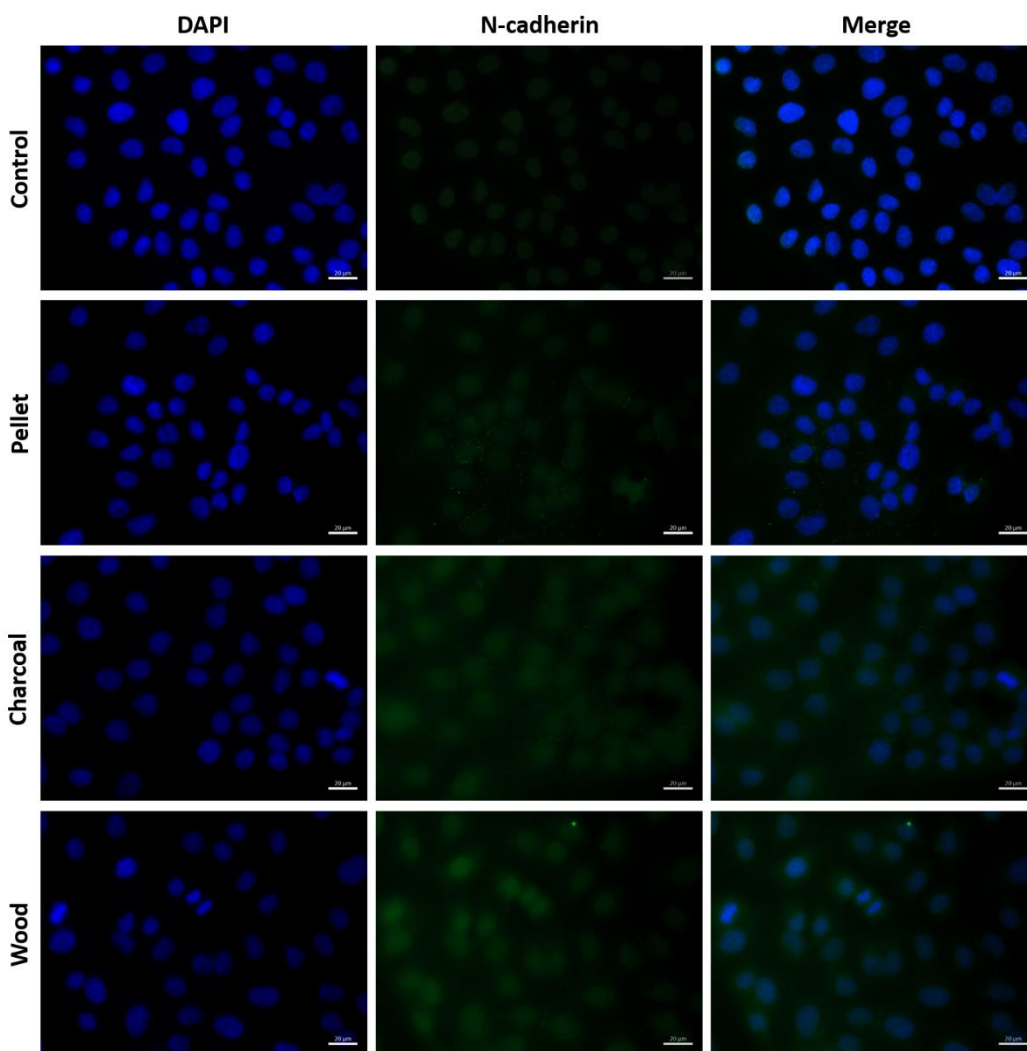


Figure 6. Immunofluorescence of the EMT mesenchymal marker N-cadherin on A549 cells after 72h of exposure to CDPs ($2.5 \mu\text{g}/\text{cm}^2$). Nuclei are stained with DAPI (blue) and N-cadherin with anti-body rabbit anti-N-cadherin (green). Scale bar= $20 \mu\text{m}$.

Transwell assays were then performed to assess if CDPs could stimulate A549 migration and invasiveness activity (Figure 7). As showed in figure 7A, migration of charcoal and wood-exposed cells was significantly enhanced compared to the control. Furthermore, we conducted a transwell invasion assay. Results showed that A549 cells exposed to charcoal significantly enhanced their ability to invade (Figure 7B), degrading the basement membrane matrix proteins in the layer, and ultimately passing through the pores of the polycarbonate membrane. No effects on invasion were found instead after exposure to wood. About pellet, only slight differences in migration and invasion were detected compared to the control.

Taken together, the results suggested that charcoal was the most effective in promoting A549 cell migration and invasion *in vitro*.

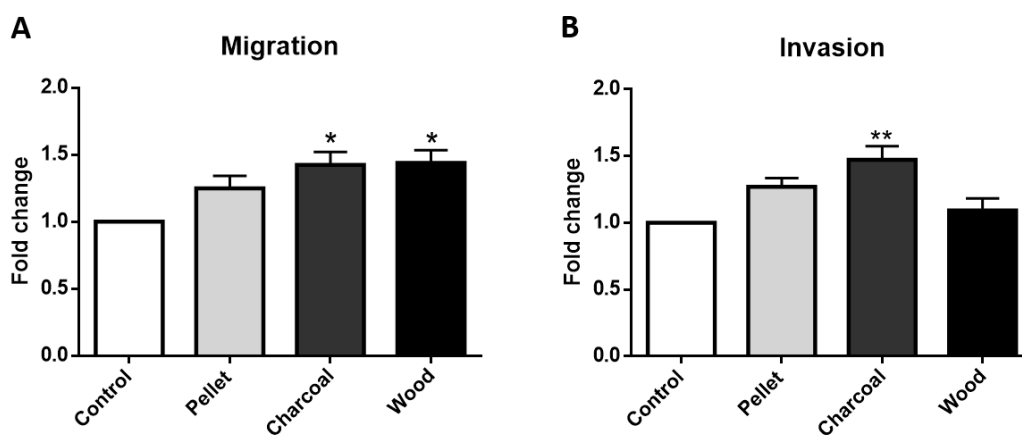


Figure 7. Effects of CDPs on A549 migration (A) and invasion (B) after 72 h of exposure to 2.5 $\mu\text{g}/\text{cm}^2$. Each bar shows mean \pm SEM of three independent experiments (N=3). Statistical analysis was performed by One-way ANOVA with Dunnett's multiple comparisons test. ** $p < 0.01$ and * $p < 0.05$ vs control cells.

4. Discussion

The dramatic impact of air pollution, especially of airborne PM and UFP, on human health it has already been scientifically demonstrated (WHO, 2014) and many evidences on the effects of these compounds in the development of lung cancer has been given. However, there are still few information about the mechanisms that are involved in the development of such pathology after exposure to particles emitted in the atmosphere.

CDPs, including PM derived from biomass burning, are considered one of the major risk factors for the development of respiratory diseases, including lung cancer (Fullerton et al., 2008).

This evidence poses a huge concern for worldwide population health safety and implies both ethical and economic issues that must be urgently dealt. Furthermore, the data from *in vivo* and *in vitro* air monitoring and clinical studies push researchers, but also policy makers and international agencies, to find new strategies for reducing particle emissions in the atmosphere.

The use of combustibles that produce CDPs with less impacting chemical composition on human health could be helpful in reducing the morbidity and mortality related to the onset of lung tumours. In this perspective, *in vitro* studies could be a useful model to understand the key event factors, the molecular mechanisms and the biological responses associated to CDPs exposure.

In lung cancer, epithelial cells play an important role during lung remodeling, which could lead to progression of respiratory diseases. Since there are many missing information about the specific role played by CDPs in the development of lung cancer, here we aimed to investigate some mechanisms reported to be involved on it and their possible activation following exposure to CDPs. Thus, to design this work, we selected lung epithelial A549 cells to investigate the potential carcinogenic properties of CDPs and to assess the underlying mechanism. A549 cell line is a widely and currently accepted experimental model for *in vitro* inhalation toxicology studies. Furthermore, A549 cells maintain alveolar type II cells characteristics, such as secretion of cytokines, surfactant production and phase I and phase II enzymes for xenobiotic biotransformation similar to lung tissue (Deng et al., 2014; Orona et al., 2014).

The lung epithelial cells were subjected to sub-toxic exposure of PM₁₀ derived from different biomass sources, such as pellet, charcoal and wood, having different chemical composition. Effects of CDPs on A549 cell viability, inflammatory response, xenobiotics enzyme activation, DNA bulky adducts formation, expression of epithelial and mesenchymal protein markers, migration and invasion were investigated. Previous works have demonstrated that exposure to PM₁₀ and PM_{2.5} modulates the expression of different genes involved in xenobiotic transformation, inflammation and EMT pathways and that the upregulation or downregulation of these genes is related to the variable chemical composition of PM sampled in different seasons (Gualtieri et al., 2012; Yue et al., 2015) or derived from different emission sources (Longhin et al., 2016b).

CDPs contains several chemical compounds, both organic and inorganic, including PAHs. Among these, some PAHs have been reported indeed to be carcinogenic and largely contribute to cancer risks, including benzo[a]pyrene (B[a]P). In recent years increasing evidence have described the crucial role of PAHs in lung carcinogenesis (Yue et al., 2015; Zhang et al., 2016). Here we analyzed the role of PAHs present in the CDPs mixtures considering their genotoxic properties and particularly their possible involvement in EMT activation promotion. Since DNA damage and mutation appearance mainly explained PAHs carcinogenic properties, we firstly analyzed the possible formation of DNA adduct, reported to be their main way to affect DNA (Genies et al., 2016).

We have previously observed that at early time points (24h) DNA damage occur only after pellet exposure, which is the CDP with the most abundant content of metals, especially Zn⁺ compared to the other biomasses (Marchetti et al., 2019).

At late time points, 48 and 72 h, it seems that cells respond also to PAHs content, as evidenced by CYP1A1 expression. In fact, wood particles at 72 h induce a significant upregulation of this xenobiotic transformation marker (Figure 3). Reduced effect instead, were detected after exposure to pellet particles that had no significant effect on the mechanisms investigated. The effect of PAHs-induced

biological responses at 24 h of exposure could be at lower extent because PAHs are adsorbed on carbonaceous particles and their effects are exerted in relation to the bioavailability of PAHs bound to PM and to the mechanism of particles and PAHs interactions. On the counterpart, metals adsorbed on PM, such as Zn^{+} , can solubilize in the cell culture medium and exert their effect (e.g. DNA damage) at earlier time points as previously observed (Marchetti et al., 2019).

After CYPs expression evaluation, we measured the formation of DNA adducts of benzo[a]pyrene diol epoxide (BPDE), which has been reported to be strictly connected to CYP1A1 expression [29,30]. However, DNA adducts were not detected, confirming that PAHs, when in a complex mixture, interact with each other in several ways in terms of toxicity, potentiating or inhibiting their action, as suggested by Tarantini and Billet (Billet et al., 2018; Tarantini et al., 2011).

Lung cancer results from a variety of interactions and biological processes, including activation of a strong inflammatory response, vessel development, cell migration and proliferation and finally, invasion (Fidler, 2002). The imbalance caused by CPDs exposure to lung cells could contribute to the development of cancer through the cell transformation from epithelial to mesenchymal phenotype. Epithelial-to-mesenchymal transition (EMT) is a phenotypic switch that promote the acquisition of a fibroblastoid-like morphology by epithelial cancer cells, resulting in enhanced cell motility and invasiveness, increased metastatic propensity and resistance to therapies (Xiao and He, 2010). Cells undergoing EMT are also known to increase the secretion of specific mediators, including cytokines, chemokines and growth factors, which could play an important role in cancer progression and invasion (Yue et al., 2015; Zhang et al., 2016). Invasion is defined as cell movement through a 3D matrix, and it requires migration and proteolysis of extracellular matrix components (Kramer et al., 2013).

In vitro alterations, associated with an invasive phenotype induced by PM₁₀, were observed in cells exposed to particles with the higher content of PAHs. Wood and mostly charcoal indeed, significantly enhanced cell migration and invasion, as well as increase IL-8 secretion in A549 cells, suggesting that biomass combustion may be a noteworthy contributor in lung cancer development and progression. Our data suggest that the upregulation of N-cadherin and Vimentin, as well as the loss of E-cadherin and disassembly of actin concur to the migration and invasiveness of lung cells exposed to charcoal and wood CDPs.

Data from invasion assay are in accordance with the work of Morales-Barcenas (Morales-Bárcenas et al., 2015), in which the authors found alterations in A549 after exposure to sub-toxic dose of PM₁₀ (10 $\mu\text{g}/\text{cm}^2$) and a more aggressive *in vitro* phenotype, with an increase in protease activity and invasiveness. Furthermore, previous data (Yue et al., 2015) have evidenced that higher content of PAHs could promote EMT in A549 cells exposed to PM₁₀ and PM_{2.5} collected from peri-urban North China. The authors found that the winter PAH-bound PM promote lung

cancer and that these particles had the characteristics of coal. CDPs chemical composition have similarities with PM_{2.5} sampled in winter (PM_{2.5w}), as evidenced by the content of PAHs and metals, while particles sampled in summer usually have a major content of crustal elements and biogenic fraction (Gualtieri et al., 2010; Longhin et al., 2013). Moreover, it has been previously demonstrated (Gualtieri et al., 2012) that PM_{2.5w} and BaP shared the down-regulation of the E-cadherin gene (CDH1) associated to the EMT and the up-regulation of other genes involved in this pathways.

As previously mentioned, hallmarks for EMT include dissolution of cell–cell contacts, production of transcription factors able to inhibit or delocalize Epithelial cadherin (E-cadherin) expression, increased expression of mesenchymal markers (e.g. N-cadherin and Vimentin), induction of focal adhesion turnover and secretion of proteolytic enzymes involved in matrix degradation, such as the matrix metalloproteinases (MMPs). Disruption of the actin cytoskeleton could induce an epithelial transition in metastatic cancer cells (Shankar and Nabi, 2015). During EMT the remodeling of actin cytoskeleton and focal adhesion formation are associated. Focal adhesions link the cytoskeleton to the extracellular matrix (ECM) and allow the cell to respond to its environment. Focal adhesions are also sites of localized signal transduction events that modulate processes such as cell proliferation, differentiation and migration. Changes in cell morphology, such as membrane ruffles and filopodia formation might be a consequence of the cytoskeletal remodeling (Yilmaz and Christofori, 2009). Moreover, Arjonen and colleagues (Arjonen et al., 2011) reported that filipodia-inducing genes are involved in cancer progression. They also related the altered expression of integrins to negative prognosis in human cancer.

In this regard, a migrating phenotype results in an increase of F-actin fibers (Vallenius, 2013), as observed after exposure to CPDs. Authors have previously found that PM₁₀ exposure *in vitro* increases these fibers through the stabilization of p21 (Sánchez-Pérez et al., 2014). This change in actin organization and polymerization promote cells migration, giving them characteristics of cancer cells. IL-8 is a well-known pro-inflammatory cytokine released after PM exposure (Wu et al., 2018). Nevertheless, it is important to highlight that the development of an EMT phenotype indeed could also depend on variety of external soluble factors, such as cytokines, growth factors or components of the extracellular matrix (ECM) which are provided by the tumor microenvironment (Raman et al., 2007; Zhang et al., 2016). These signals can derive from many cells that are within the tumor stroma (e.g. endothelial cells, immune cell, fibroblasts) and they can be capable to induce EMT in the neighboring cancer cells. Furthermore, cancer cells themselves may reprogram the surrounding tumoral tissue by producing cytokines and other soluble mediators that promote tumor growth, dissemination and invasion and that can induce and/or maintain EMT in tumor cells (Fidler, 2002). Well-established

signals that promote EMT in various tumor cell models are induced by TGF- β and growth factors including FGF, EGF and HGF (Xiao and He, 2010). Zhang et al. (Zhang et al., 2016), reported that by silencing IL-8 and other inflammatory markers, migration is drastically reduced on A549 cells exposed to B[a]P.

The IL-8/IL-8 receptor (IL-8R) axis has been demonstrating to have a role on the induction and/or maintenance of EMT by an autocrine loop and in the remodeling of the tumor microenvironment (Palena et al., 2012). Data from our work evidenced that there is a significant release of IL-8 from cells exposed to CDPs at 48 and 72h. Charcoal and wood PM were even capable to stimulate EMT proteins modulation, as evidenced by E-cadherin, N-cadherin and Vimentin expression and by the migration and invasion assays data.

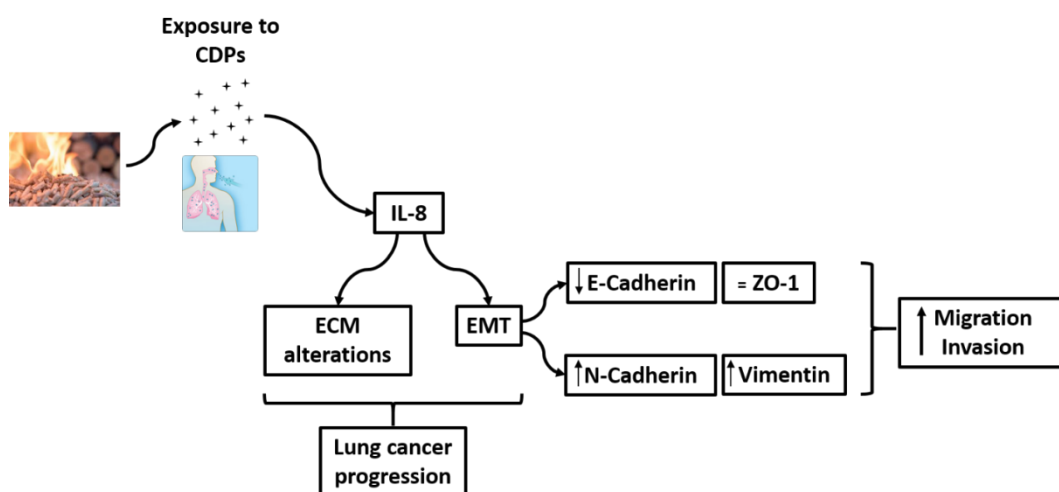
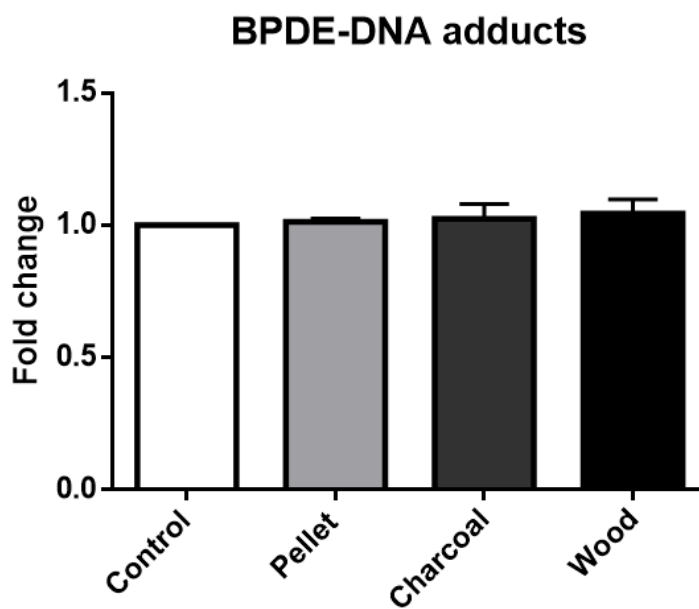


Figure 8. Graphical scheme of the experimental design and the mechanisms involved in the A549 cells response to CDPs exposure.

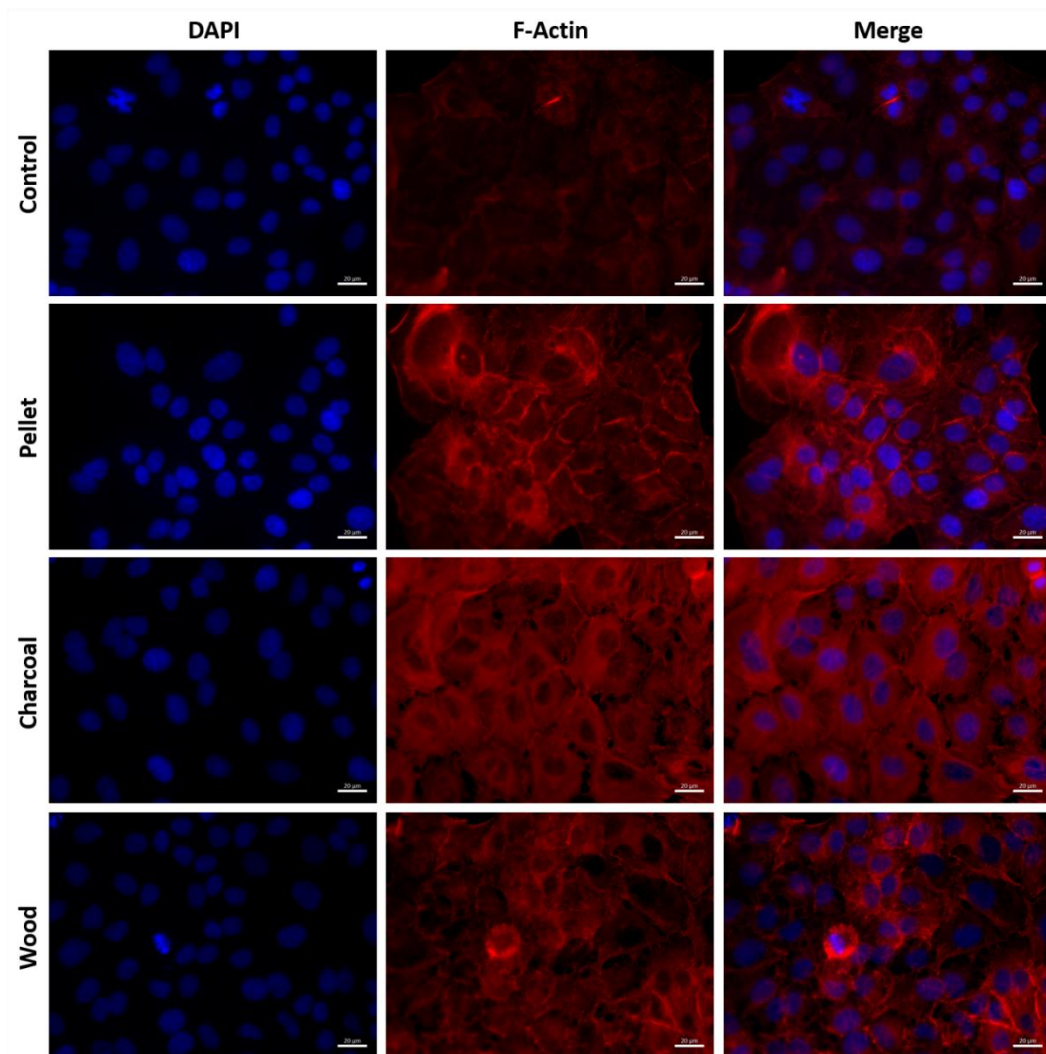
To conclude, our results support the hypothesis that exposure to CDPs with high content of PAHs promote cell migration and invasiveness also by creating a tumor microenvironment in which IL-8 secretion support the development and/or maintenance of EMT that can be used by cancer cells for invasion (Figure 8).

In this perspective, IL-8 could be a potential target for the therapy of lung cancer, even if other cytokines and even mi-RNA that are present in the cell condition medium could be involved in EMT development (Longhin et al., 2016a).

Supplementary data



Supplementary figure 1. BPDE adduct formation in A549 cells after 72 h of exposure to 2.5 $\mu\text{g}/\text{cm}^2$. Each bar shows mean \pm SEM of three independent experiments (N=3). Statistical analysis was performed by One-way ANOVA with Dunnett's multiple comparisons test.



Supplementary figure 2. Immunofluorescence on A549 cells after 72h of exposure to CDPs ($2.5 \mu\text{g}/\text{cm}^2$). Nuclei are stained with DAPI (blue) and F-actin with rhodamine-phalloidin (red). Scale bar= $20 \mu\text{m}$.

References

- Abbas, I., Garçon, G., Saint-Georges, F., Andre, V., Gosset, P., Billet, S., Goff, J. Le, Verdin, A., Mulliez, P., Sichel, F., Shirali, P., 2013. Polycyclic aromatic hydrocarbons within airborne particulate matter (PM_{2.5}) produced DNA bulky stable adducts in a human lung cell coculture model. *J. Appl. Toxicol.* <https://doi.org/10.1002/jat.1722>
- Arjonen, A., Kaukonen, R., Ivaska, J., 2011. Filopodia and adhesion in cancer cell motility. *Cell Adhes. Migr.* <https://doi.org/10.4161/cam.5.5.17723>
- Bersaas, A., Arnoldussen, Y.J., Sjøberg, M., Haugen, A., Mollerup, S., 2016. Epithelial-mesenchymal transition and FOXA genes during tobacco smoke carcinogen induced transformation of human bronchial epithelial cells. *Toxicol. Vitro.* 35, 55–65. <https://doi.org/10.1016/j.tiv.2016.04.012>
- Billet, S., Abbas, I., Goff, J. Le, Verdin, A., André, V., Lafargue, P.E., Hachimi, A., Cazier, F., Sichel, F., Shirali, P., Garçon, G., 2008. Genotoxic potential of Polycyclic Aromatic Hydrocarbons-coated onto airborne Particulate Matter (PM_{2.5}) in human lung epithelial A549 cells. *Cancer Lett.* 270, 144–155. <https://doi.org/10.1016/j.canlet.2008.04.044>
- Billet, S., Landkocz, Y., Martin, P.J., Verdin, A., Ledoux, F., Lepers, C., André, V., Cazier, F., Sichel, F., Shirali, P., Gosset, P., Courcot, D., 2018. Chemical characterization of fine and ultrafine PM, direct and indirect genotoxicity of PM and their organic extracts on pulmonary cells. *J. Environ. Sci. (China)* 71, 168–178. <https://doi.org/10.1016/j.jes.2018.04.022>
- Chen, Y.C., Statt, S., Wu, R., Chang, H.T., Liao, J.W., Wang, C.N., Shyu, W.C., Lee, C.C., 2016. High mobility group box 1-induced epithelial mesenchymal transition in human airway epithelial cells. *Sci. Rep.* <https://doi.org/10.1038/srep18815>
- Deng, X., Zhang, F., Wang, L., Rui, W., Long, F., Zhao, Y., Chen, D., Ding, W., 2014. Airborne fine particulate matter induces multiple cell death pathways in human lung epithelial cells. *Apoptosis.* <https://doi.org/10.1007/s10495-014-0980-5>
- Duan, H., Leng, S., Pan, Z., Dai, Y., Niu, Y., Huang, C., Bin, P., Wang, Y., Liu, Q., Chen, W., Zheng, Y., 2009. Biomarkers measured by cytokinesis-block micronucleus cytome assay for evaluating genetic damages induced by polycyclic aromatic hydrocarbons. *Mutat. Res. - Genet. Toxicol. Environ. Mutagen.* <https://doi.org/10.1016/j.mrgentox.2009.06.002>
- Fidler, I.J., 2002. The organ microenvironment and cancer metastasis. *Differentiation.* <https://doi.org/10.1046/j.1432-0436.2002.700904.x>
- Fullerton, D.G., Bruce, N., Gordon, S.B., 2008. Indoor air pollution from biomass fuel smoke is a major health concern in the developing world. *Trans. R. Soc. Trop. Med. Hyg.* <https://doi.org/10.1016/j.trstmh.2008.05.028>

- Genies, C., Jullien, A., Lefebvre, E., Revol, M., Maitre, A., Douki, T., 2016. Inhibition of the formation of benzo[a]pyrene adducts to DNA in A549 lung cells exposed to mixtures of polycyclic aromatic hydrocarbons. *Toxicol. Vitro.* 35, 1–10. <https://doi.org/10.1016/j.tiv.2016.05.006>
- Gualtieri, M., Longhin, E., Mattioli, M., Mantecchia, P., Tinaglia, V., Mangano, E., Carla, M., Bestetti, G., Camatini, M., Battaglia, C., 2012. Gene expression profiling of A549 cells exposed to Milan PM2.5. *Toxicol. Lett.* 209, 136–145. <https://doi.org/10.1016/j.toxlet.2011.11.015>
- Gualtieri, M., Øvrevik, J., Holme, J.A., Perrone, M.G., Bolzacchini, E., Schwarze, P.E., Camatini, M., 2010. Differences in cytotoxicity versus pro-inflammatory potency of different PM fractions in human epithelial lung cells. *Toxicol. Vitro.* 24, 29–39. <https://doi.org/10.1016/j.tiv.2009.09.013>
- IARC: Outdoor air pollution a leading environmental cause of cancer deaths, 2013. 51, 229–235.
- IARC Monographs on the Evaluation of Carcinogenic Risks to Humans, 2010. 95.
- IARC Working Group on the Evaluation of Carcinogenic Risks to Humans, 2010a. Household use of solid fuels and high-temperature frying. IARC Monogr. Eval. Carcinog. Risks Hum.
- IARC Working Group on the Evaluation of Carcinogenic Risks to Humans, 2010b. Some non-heterocyclic polycyclic aromatic hydrocarbons and some related exposures. IARC Monogr. Eval. Carcinog. Risks Hum.
- Kalluri, R., Weinberg, R.A., 2009. The basics of epithelial-mesenchymal transition. *J. Clin. Invest.* <https://doi.org/10.1172/JCI39104>
- Kim, K.H., Jahan, S.A., Kabir, E., 2011. A review of diseases associated with household air pollution due to the use of biomass fuels. *J. Hazard. Mater.* <https://doi.org/10.1016/j.jhazmat.2011.05.087>
- Kramer, N., Walzl, A., Unger, C., Rosner, M., Krupitza, G., Hengstschläger, M., Dolznig, H., 2013. In vitro cell migration and invasion assays. *Mutat. Res. - Rev. Mutat. Res.* <https://doi.org/10.1016/j.mrrev.2012.08.001>
- Liu, N., Li, Y., Su, S., Wang, N., Wang, H., Li, J., 2013. Inhibition of cell migration by ouabain in the A549 human lung cancer cell line. *Oncol. Lett.* <https://doi.org/10.3892/ol.2013.1406>
- Longhin, E., Capasso, L., Battaglia, C., Proverbio, M.C., Cosentino, C., Cifola, I., Mangano, E., Camatini, M., Gualtieri, M., 2016a. Integrative transcriptomic and protein analysis of human bronchial BEAS-2B exposed to seasonal urban particulate matter. *Environ. Pollut.* 209, 87–98. <https://doi.org/10.1016/j.envpol.2015.11.013>
- Longhin, E., Gualtieri, M., Capasso, L., Bengalli, R., Mollerup, S., Holme, J.A., Øvrevik, J., Casadei, S., Di Benedetto, C., Parenti, P., Camatini, M., 2016b. Physico-chemical properties and biological effects of diesel and biomass particles. *Environ. Pollut.* 215, 366–375.

- <https://doi.org/10.1016/j.envpol.2016.05.015>
- Longhin, E., Pezzolato, E., Mantecca, P., Holme, J.A., Franzetti, A., Camatini, M., Gualtieri, M., 2013. Season linked responses to fine and quasi-ultrafine Milan PM in cultured cells. *Toxicol. Vitro*. 27, 551–559.
<https://doi.org/10.1016/j.tiv.2012.10.018>
- Marchetti, S., Longhin, E., Bengalli, R., Avino, P., Stabile, L., Buonanno, G., Colombo, A., Camatini, M., Mantecca, P., 2019. In vitro lung toxicity of indoor PM10 from a stove fueled with different biomasses. *Sci. Total Environ.* 649, 1422–1433. <https://doi.org/10.1016/j.scitotenv.2018.08.249>
- Milara, J., Peiró, T., Serrano, A., Cortijo, J., 2013. Epithelial to mesenchymal transition is increased in patients with COPD and induced by cigarette smoke. *Thorax*. <https://doi.org/10.1136/thoraxjnl-2012-201761>
- Morales-Bárceñas, R., Chirino, Y.I., Sánchez-Pérez, Y., Osornio-Vargas, Á.R., Melendez-Zajgla, J., Rosas, I., García-Cuellar, C.M., 2015. Particulate matter (PM10) induces metalloprotease activity and invasion in airway epithelial cells. *Toxicol. Lett.* <https://doi.org/10.1016/j.toxlet.2015.06.001>
- Ohbayashi, H., 2002. Matrix metalloproteinases in lung diseases. *Curr. Protein Pept. Sci.* 3, 409–21.
- Orona, N.S., Astort, F., Maglione, G.A., Saldiva, P.H.N., Yakisich, J.S., Tasat, D.R., 2014. Direct and indirect air particle cytotoxicity in human alveolar epithelial cells. *Toxicol. Vitro*. <https://doi.org/10.1016/j.tiv.2014.02.011>
- Palena, C., Hamilton, D.H., Fernando, R.I., 2012. Influence of IL-8 on the epithelial-mesenchymal transition and the tumor microenvironment. *Futur. Oncol.* <https://doi.org/10.2217/fon.12.59>
- Raman, D., Baugher, P.J., Thu, Y.M., Richmond, A., 2007. Role of chemokines in tumor growth. *Cancer Lett.* <https://doi.org/10.1016/j.canlet.2007.05.013>
- Sánchez-Pérez, Y., Chirino, Y.I., Osornio-Vargas, Á.R., Herrera, L.A., Morales-Bárceñas, R., López-Saavedra, A., González-Ramírez, I., Miranda, J., García-Cuellar, C.M., 2014. Cytoplasmic p21CIP1/WAF1, ERK1/2 activation, and cytoskeletal remodeling are associated with the senescence-like phenotype after airborne particulate matter (PM10) exposure in lung cells. *Toxicol. Lett.* <https://doi.org/10.1016/j.toxlet.2013.11.018>
- Sarigiannis, D.A., Karakitsios, S.P., Zikopoulos, D., Nikolaki, S., Kermenidou, M., 2015. Lung cancer risk from PAHs emitted from biomass combustion. *Environ. Res.* 137, 147–156. <https://doi.org/10.1016/j.envres.2014.12.009>
- Shankar, J., Nabi, I.R., 2015. Actin cytoskeleton regulation of epithelial mesenchymal transition in metastatic cancer cells. *PLoS One*. <https://doi.org/10.1371/journal.pone.0119954>
- Shen, H.J., Sun, Y.H., Zhang, S.J., Jiang, J.X., Dong, X.W., Jia, Y.L., Shen, J., Guan, Y., Zhang, L.H., Li, F.F., Lin, X.X., Wu, X.M., Xie, Q.M., Yan, X.F., 2014. Cigarette smoke-induced alveolar epithelial-mesenchymal transition is mediated by

- Rac1 activation. *Biochim. Biophys. Acta - Gen. Subj.*
<https://doi.org/10.1016/j.bbagen.2014.01.033>
- Sun, J., 2010. Matrix Metalloproteinases and Tissue Inhibitor of Metalloproteinases Are Essential for the Inflammatory Response in Cancer Cells. *J. Signal Transduct.* 2010, 1–7. <https://doi.org/10.1155/2010/985132>
- Tarantini, A., Maître, A., Lefèbvre, E., Marques, M., Rajhi, A., Douki, T., 2011. Polycyclic aromatic hydrocarbons in binary mixtures modulate the efficiency of benzo[a]pyrene to form DNA adducts in human cells. *Toxicology* 279, 36–44. <https://doi.org/10.1016/j.tox.2010.09.002>
- Thiery, J.P., Acloque, H., Huang, R.Y.J., Nieto, M.A., 2009. Epithelial-Mesenchymal Transitions in Development and Disease. *Cell.*
<https://doi.org/10.1016/j.cell.2009.11.007>
- Uski, O., Jalava, P.I., Happonen, M.S., Torvela, T., Leskinen, J., Mäki-Paakkanen, J., Tissari, J., Sippula, O., Lamberg, H., Jokiniemi, J., Hirvonen, M.-R., 2015. Effect of fuel zinc content on toxicological responses of particulate matter from pellet combustion in vitro. *Sci. Total Environ.* 511, 331–40.
- Vallenius, T., 2013. Actin stress fibre subtypes in mesenchymal-migrating cells. *Open Biol.* <https://doi.org/10.1098/rsob.130001>
- Van Den Heuvel, R., Den Hond, E., Govarts, E., Colles, A., Koppen, G., Staelens, J., Mampaey, M., Janssen, N., Schoeters, G., 2016. Identification of PM10 characteristics involved in cellular responses in human bronchial epithelial cells (Beas-2B). *Environ. Res.* 149, 48–56.
<https://doi.org/10.1016/j.envres.2016.04.029>
- Van Eeden, S.F., Tan, W.C., Suwa, T., Mukae, H., Terashima, T., Fujii, T., Qui, D., Vincent, R., Hogg, J.C., 2001. Cytokines involved in the systemic inflammatory response induced by exposure to particulate matter air pollutants (PM10). *Am. J. Respir. Crit. Care Med.* <https://doi.org/10.1164/ajrccm.164.5.2010160>
- WHO, 2014. World Health Organization releases 7 million premature deaths annually linked to air pollution. Accessed June 21.2018.
<http://www.who.int/mediacentre/news/releases/2014/air-pollution/en/>
- Wu, W., Jin, Y., Carlsten, C., 2018. Inflammatory health effects of indoor and outdoor particulate matter. *J. Allergy Clin. Immunol.*
<https://doi.org/10.1016/j.jaci.2017.12.981>
- Xiao, D., He, J., 2010. Epithelial mesenchymal transition and lung cancer. *J. Thorac. Dis.*
- Yang, D., Ma, M., Zhou, W., Yang, B., Xiao, C., 2017. Inhibition of miR-32 activity promoted EMT induced by PM2.5 exposure through the modulation of the Smad1-mediated signaling pathways in lung cancer cells. *Chemosphere* 184, 289–298. <https://doi.org/10.1016/j.chemosphere.2017.05.152>
- Yilmaz, M., Christofori, G., 2009. EMT, the cytoskeleton, and cancer cell invasion. *Cancer Metastasis Rev.* <https://doi.org/10.1007/s10555-008-9169-0>

- Yue, H., Yun, Y., Gao, R., Li, G., Sang, N., 2015. Winter Polycyclic Aromatic Hydrocarbon-Bound Particulate Matter from Peri-urban North China Promotes Lung Cancer Cell Metastasis. *Environ. Sci. Technol.* 49, 14484–14493. <https://doi.org/10.1021/es506280c>
- Zhang, J., Chang, L., Jin, H., Xia, Y., Wang, L., He, W., Li, W., Chen, H., 2016. Benzopyrene promotes lung cancer A549 cell migration and invasion through up-regulating cytokine IL8 and chemokines CCL2 and CCL3 expression. *Exp. Biol. Med.* <https://doi.org/10.1177/1535370216644530>
- Zou, W., Zou, Y., Zhao, Z., Li, B., Ran, P., 2013. Nicotine-induced epithelial-mesenchymal transition via Wnt/ β -catenin signaling in human airway epithelial cells. *Am. J. Physiol. - Lung Cell. Mol. Physiol.* <https://doi.org/10.1152/ajplung.00094.2012>

Chapter 3:

Biological effects of combustion-derived particles from different sources on human bronchial epithelial cells

Marchetti S.¹, Mollerup S.², Gutzkow K. B.³, Skuland T., A.⁴, Refsnes M.⁴, Colombo A.¹, Øvrevik J.⁴, Mantecca P.¹, Holme J. A.⁴

¹POLARIS Research Centre, Department of Earth and Environmental Sciences, University of Milano-Bicocca, Piazza della Scienza 1, 20126 Milano, Italy;

²Section for Toxicology and Biological Working Environment, Department of Biological and Chemical Working Environment, National Institute of Occupational Health, Oslo N-0033, Norway

³Department of Molecular Biology, Division of Infection Control, Norwegian Institute of Public Health, PO Box 4404 Nydalen, Oslo N-0403, Norway

⁴Department of Air Pollution and Noise, Domain of Infection Control, Environment and Health, Norwegian Institute of Public Health, PO Box 4404, Nydalen, N-0403 Oslo, Norway

Manuscript in preparation

1. Introduction

In recent years, biomass burning has been recognized as an important public health issue and suggested to be one of the main sources of outdoor and indoor air pollutants. Particulate matter (PM) formed during this process is regarded as a central contributor for the adverse health effects (Dong et al., 2017; Sigsgaard et al., 2015). So far most of the studies related to air pollution-induced health effects are focusing on industrial or traffic-related PM (Forchhammer et al., 2012; Heßelbach et al., 2017). They have illustrated that the toxic properties of PM are highly depending on source (Bølling et al., 2012; Cassee et al., 2013; Corsini et al., 2017; Jalava et al., 2012). Although some studies on combustion-derived particles (CDPs) derived from biomass burning have been published (Bølling et al., 2012; Corsini et al., 2013; Muala et al., 2015; Noël et al., 2016), less is known regarding the specific role of various biomass burning processes and/or sources for PM-induced toxicity.

The WHO has suggested that more than 4 million of deaths per year may be attributable to illness related to exposure to CDPs. Exposure to CDPs is found to be involved in the pathogenesis of several respiratory and cardiovascular diseases, including lung cancer (World Health Organization, 2016). CDPs may affect the respiratory system in different ways, according to their size and chemical composition (Dong et al., 2017). Particles with a diameter $\leq 10 \mu\text{m}$ (PM₁₀) are of greatest interest, as they will reach important parts of the respiratory system.

CDPs are composed of a complex mixture of toxic compounds absorbed on their carbonaceous core, highly depending on the sources. Among these, organic chemicals (e.g. polycyclic aromatic hydrocarbons, PAHs), transition metals (including copper, lead, zinc and cadmium), and biological components (such as allergens or microbial compounds) have been found to have a particularly harmful potential (Billet et al., 2018; Bølling et al., 2012; Corsini et al., 2013; Dilger et al., 2016; Sarigiannis et al., 2015; Stabile et al., 2018).

Studies on CDP-toxicity have traditionally focused on particle induced formation of reactive oxygen species (ROS) and the resulting oxidative damage (Forchhammer et al., 2012; Nakayama Wong et al., 2011) which include cytotoxicity (De Oliveira Alves et al., 2014; Jalava et al., 2012), inflammatory responses (Bølling et al., 2012; Danielsen et al., 2009) and genotoxic effects (Danielsen et al., 2011; De Oliveira Alves et al., 2014). Recent studies have revealed that as PM toxicity and the mechanisms involved are not only depending on the particle core, but also on components adsorbed as well as the health end point in study (Danielsen et al., 2009; Dilger et al., 2016). The particle morphology and relative amount and composition of organic chemicals and transition metals varies with the biomass as well as with the burning processes (Longhin et al., 2016; Marchetti et al., 2019). The

precise role of the combustion process on particle properties linked to various biological endpoints is still not fully clarified.

In a previous study (Marchetti et al., 2019) we evaluated the physico-chemical properties and the cytotoxic and genotoxic effects of combustion-derived particles (PM₁₀) from different biomass sources.

Here we elucidate the role potentially played by these CDPs in various processes linked to *in vitro* lung carcinogenesis, using human bronchial epithelial cells (HBEC3-KT). These cells have previously been found to be a particularly relevant cell line for mechanistic studies regarding genotoxic and pro-carcinogenic effects of diesel exhausted particles (Rynning et al., 2018), cigarette smoke concentrate and PAH such as benzo[*a*]pyrene (B[*a*]P) in lung epithelium (Bersaas et al., 2016).

As in our study on A549 cells (Marchetti et al., 2019), HBEC3-KT cells were exposed to pristine particles from combustion of pellet, charcoal and wood. In order to elucidate the contribution of the particle-associated organic compounds, CDP-derived organic fractions and the remaining washed particles were also tested. More specifically, we studied effects on cell migration, modulation of genes involved in several PM-activated processes (such as xenobiotic metabolism, oxidative stress, inflammatory response and epithelial-to-mesenchymal-transition), DNA damage and cell cycle de-regulations. The present research points out the importance of understand the potential risk for CDPs in promoting lung cancer and reveal a mechanistic basis for preventing and/or targeting the ones that could represent a serious risk for lung cancer development.

2. Materials and methods

2.1. Biomass particles: sampling and extraction for biological experiments

CDPs (PM₁₀) samples were collected from an open fireplace fueled for 4 h with pellet, charcoal or wood respectively as previously described (Marchetti et al., 2019). Samplings were performed on Teflon filters by a gravimetric sampler made up of a volumetric rotating pump Zambelli 6000 Plus and a Zambelli PM₁₀ impactor gravimetric sampler (FAI Instruments). Filters were stored at minus 20°C until manipulation. Samples collected from combustion of the same fuel were pooled and particles extracted. Briefly, particles were detached from filters in pure sterile water by replicating four 20 min ultrasonic cycles using an ultrasound bath (Sonica Soltec). Each cycle was performed using 2 mL of sterile water, which were collected and replaced every time. Particle suspensions were pooled to obtain a sample representative of the sampling campaign, aliquoted in sterile tubes and then dried in a desiccator. Resulting pellets were stored at minus 20°C until further use. Particles for cell exposure were resuspended in sterile water (2 µg/µL) and then,

sonicated before each experiment. Data on CDPs chemical and morphological characterization have been published previously (Marchetti et al., 2019).

In addition, organic extract and washed particles were used, in order to elucidate and compare the relative role of the particle core versus coated organic compounds. The two fractions were obtained by acetonitrile extraction according to the protocol described by Longhin (2013). Briefly, CDPs were resuspended in acetonitrile (Sigma Aldrich) and sonicated for 20 min in an ultrasound bath. The extracted organic fractions and the resulting washed particles were separated by centrifugation (12 000 rpm for 12 min at 4°C). The supernatant (organic fraction) and the centrifuged pellet (washed particles), were then dried in a desiccator. Finally, the organic fraction was dissolved in dimethyl sulfoxide (DMSO) to the concentration of 10 µg/µL (referring to the original particle weight) in order to minimize the effect of solvent when adding to cell culture, while the washed particles was re-suspended in sterile water to obtain 2 µg/µL (referring to the original particle weight).

2.2. Chemical analysis (ongoing)

2.3. Cell culture: maintenance and treatments

The hTERT and Cdk4 immortalized human bronchial epithelial HBEC3-KT cells were a generous gift of Dr. John D. Minna (Ramirez et al., 2004). Cells were routinely maintained in LHC-9 medium (Thermo Fisher Scientific) on collagen-coated dishes at 37°C with 5% CO₂. Cells were seeded at different concentrations according to the type of experiments to be carried out. Cells were then, exposed to CDPs or extracts for 24 h and results were compared to the respective controls.

2.4. Cytotoxicity assay

Cell viability was assessed with Alamar Blue assay after 24, 48 and 72 h of exposure. HBEC3-KT were seeded in 96-well culture plates at a density of 7 x 10³ cells/well and exposed to CDPs and to the respective organic fraction and washed particles. Different doses (corresponding to 1, 2.5, 5, 7.5 and 10 µg/cm² of original particle weight) were tested. The Alamar Blue assay was performed accordingly to the manufacturer's instructions. After exposure, culture media were replaced with Alamar reagent (Thermo Fisher Scientific) and fresh media at the concentration of 1:10 for 3 h of incubation at 37°C with 5% CO₂. The relative number of living cells when compared to control (set as 100%) was estimated by reading the absorbance of each sample at 570 and 630 nm (SpectraMax i3, Molecular Devices).

2.5. Cell migration

Cell migration studies were performed by the scratch wound closure assay using the IncuCyte Zoom Live Cell Imaging microscope (Essen BioScience). Cells were seeded on collagen-coated ImageLock 96-well plates (Essen Bioscience) at a density of 1×10^4 cells/well and after 24 h, a scratch wound was made in each well using the Wound Maker tool (Essen BioScience). Finally, cells were exposed to $2.5 \mu\text{g}/\text{cm}^2$ CDPs and respective fractions and images acquired every hour for up to 24 h to monitor closure of the wound. Migration was assessed by the dedicated software (Essen Bioscience).

2.6. Gene expression

Cells for RNA analysis were seeded into collagen coated 6-well plates at a concentration of 3×10^5 cells/well and exposed to CDPs at a concentration of $2.5 \mu\text{g}/\text{cm}^2$. At the end of the exposure, cells were washed with ice-cold PBS and stored at minus 80°C until RNA isolation.

Total RNA was extracted from samples with the RNA-Solv Reagent (Omega Bio-tek) and reverse transcribed with the qScript cDNA Synthesis kit (Quanta Biosciences). Gene expression analysis was performed by real-time PCR. PCR reactions were run on StepOnePlus using PerfeCTa SYBR green fast mix (Quanta Biosciences) and the following program: initial denaturation at 95°C for 30 s, then 40 cycles of 95°C for 3 s and 60°C for 30 s, followed by a melting curve. For each PCR plate, known amounts of the corresponding product with the same primer sets were run as standard curve. The amount of target cDNA in each sample was calculated by the $\Delta\Delta\text{C}_t$ method, normalized to the expression of β -Actin and expressed as fold change relative to control cells. Primers sequences used in this study are reported in supplementary data.

2.7. Measurement of cytokine IL-1 β release

Cell culture supernatants were analyzed to assess CDPs potential to induce release of the pro-inflammatory cytokine IL-1 β by enzyme-linked immunosorbent assay (ELISA). Supernatants were collected after exposure, centrifuged (12 000 rpm, 6 min and 4°C) to remove debris and particles and stored at minus 20°C until the analysis.

The release of IL-1 β was detected according to the manufacturer's manual (Human IL-1 β /IL-1F DuoSet Kit, R&D). Absorbance was measured at 450 nm and 620 nm respectively, and the amount of IL-1 β protein in pg/ml quantified by a TECAN plate reader with the dedicated software (Magellan V 1.10, Phoenix Research Product).

2.8. COMET analysis

COMET analysis/single cell gel electrophoresis (SCGE) were performed as previously described (Gutzkow et al., 2013). In short, $1,5 \times 10^5$ cells/well were seeded in 12-well plates and exposed for 24 h to the following CDPs doses: 1, 2.5 and 5 $\mu\text{g}/\text{cm}^2$. After exposure, cells were trypsinized and collected (1×10^6 cells/mL) in PBS before resuspension in 0.75% soft agar (LMP) solution. DNA single-strand breaks (SSBs) and alkali-labile sites were detected. Oxidative DNA-damage was also evaluated by means of formamidopyrimidine-DNA-glycosylase (FPG) enzyme. Cells were loaded in duplicates (7 $\mu\text{L}/\text{sample}$) onto GelBond films and lysed overnight (ON) at 4°C. The day after, films were pre-treated for 1 h at 4°C in enzyme buffer and then for 1 h at 37°C with and without 0.5 $\mu\text{g}/\text{mL}$ FPG in enzyme buffer (40 mM HEPES, 0.1 M KCl and 0.5 mM Na₂-EDTA, pH 7.6) supplemented with 0.2 mg/mL BSA. Samples were then, transferred to cold electrophoresis solution (0.3 M NaOH, 0.01 M Na₂EDTA, pH > 13) for 40 min at 10°C for DNA unwinding. After electrophoresis (~0.8 V/cm, 25 min, 10°C) and neutralization with PBS, films were fixed in ethanol and dried. Rehydrated DNA samples were finally, stained with SYBR Gold (diluted 1:1000 in TE-buffer pH 8) and scored with Comet IV software (Perceptives) at 20x magnification using a Leica DMLB microscope. Fifty comets per gel were randomly counted. DNA damage was quantified as tail intensity (% fluorescence in the comet tail).

2.9. Flow cytometry

Cell cycle analysis was performed on cells exposed to the same doses tested for SCGE assay. After exposure for 24 h on 12-well plates, cells were collected, centrifuged (250 g, 10 min, 4°C), added PBS with 0,2% paraformaldehyde and stored at 4°C. DNA was stained with the fluorescent dye Hoechst 33258 (1 $\mu\text{g}/\text{mL}$) in the dark for 20 min at 4°C. Fluorescence was measured by flow cytometer (ZE5 Cell Analyzer, Bio-Rad) using 405 nm band pass filters and the analysis performed with the dedicated software (FlowJo_V10). Apoptotic index was also determined. In order to discriminate different cell cycle phases, DNA content (stained with Hoechst) and cell size (forward light scatter) were considered. In this assay, apoptotic cells correspond to the sub-G1 peak of the Hoechst histogram.

2.10. Statistical analysis

The data represent mean and standard error of mean (SEM) of three independent experiments carried out at the same experimental conditions. For migration studies, we chose one experiment and presented it as representative of the five technical replicates (eight biological replicates for each experiment). Significant differences were analyzed on 6 and 15 h of exposure.

Statistical analyses were performed using GraphPad Prism 6 software, using One-way or Two-way ANOVA with Dunnett's or Tukey's post hoc multiple comparisons tests. Values of $p < 0.05$ were considered statistically significant.

3. Results

Time course and dose response of CDP-induced toxicity was performed on HBEC3-KT cells to select optimal conditions for the study. The results on cells exposed for 24 h revealed a statistically significant toxicity only with the higher dose of particles from burning pellet and wood (Figure 1A). Similar effects were observed after 48 h (Figure 1B). After 72 h of exposure, the pellet particles reduced the number of viable cells to approximately 65%, while charcoal and wood resulted in a viability of 80%.

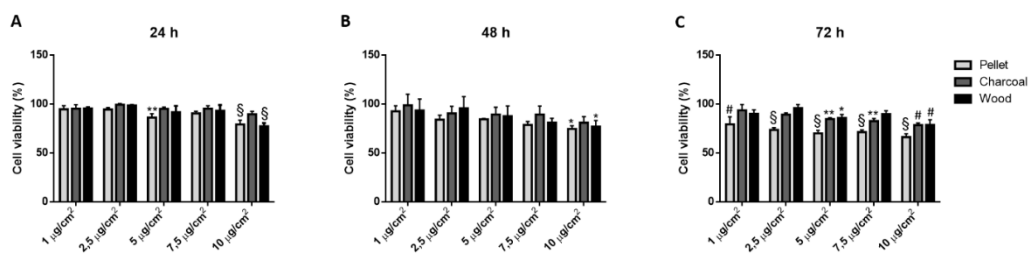


Figure 1. Alamar Blue assay. HBEC3-KT cell viability was evaluated after 24 (A), 48 (B) and 72 h (C) of exposure to increasing doses of CDPs. Histograms show the percentage of viable cells compared to the unexposed control (100%). Statistical analysis was performed by Two-way ANOVA with Dunnett's multiple comparisons tests. § $p < 0.0001$, # $p < 0.001$, ** $p < 0.01$ and * $p < 0.05$ vs control cells.

Viability was assessed also after exposure to CDP-derived organic fractions and washed particles. After 24 h exposure, statistically significant effects were seen after exposure to the pellet organic fraction (Figure 2A). More pronounced cytotoxic effects were seen after longer exposure times. A time-dependent decrease in viability was detected also after exposure to charcoal and wood organic fractions (Figures 2B and C). Interesting differences between particles were observed, while the organic fraction originating from the pellet and wood particles were more cytotoxic than the corresponding washed particles, the opposite appeared to be true for charcoal (Figures 2D, E and F).

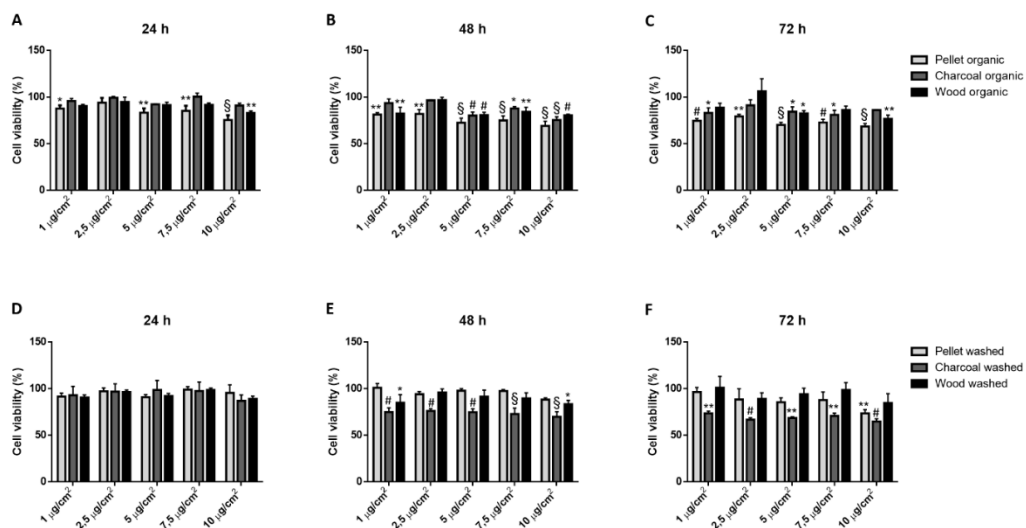


Figure 2. Alamar Blue assay on cells exposed to organic fractions and washed particles. Cell viability was assessed after 24, 48 and 72 h of exposure to increasing doses of CDP-derived organic extracts (A, B, C) and washed particles (D, E, F) corresponding to the concentration of the original particles as indicated in the figure. Histograms show the percentage of viable cells compared to the control (100 %). Statistical analysis was performed by Two-way ANOVA with Dunnett's multiple comparisons tests. § $p < 0.0001$, # $p < 0.001$, ** $p < 0.01$ and * $p < 0.05$ vs control cells.

The cells ability to migrate after exposure to 2.5 $\mu\text{g}/\text{cm}^2$ CDPs for up to 24 h was evaluated in a scratch wound closure assay (Figure 3). Most importantly, during this time no or only minor cytotoxic effects following exposure to the different samples could be seen. After 6 h of exposure, only pellet and wood significantly affected migration compared to the control. After 15 h instead, all particles induced alteration in migration, with wood as the most potent and charcoal as the less.

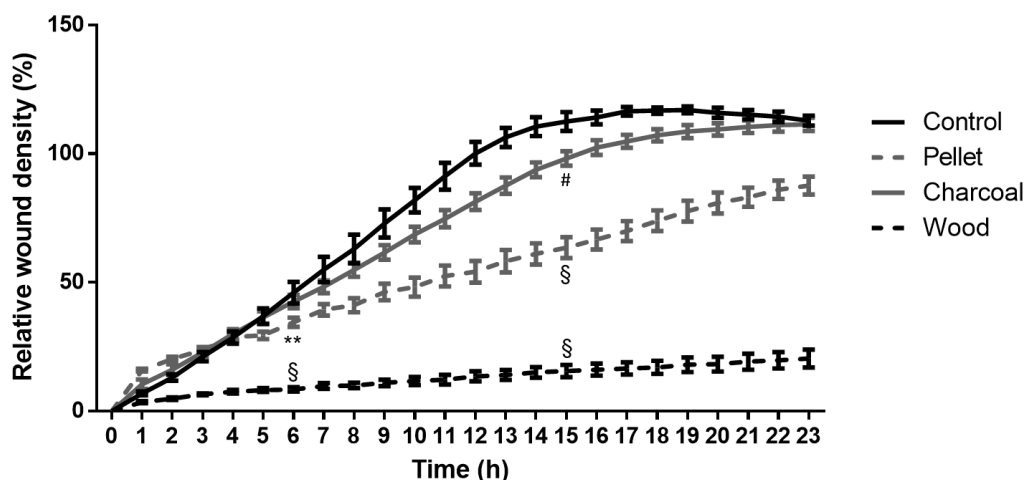


Figure 3. Cell migration. HBEC3-KT migration was assessed by scratch wound closure assay after exposure to CDPs at a concentration corresponding to $2.5 \mu\text{g}/\text{cm}^2$. Data display the relative wound density measured every hour up to 24 h of a representative experiment. Reduction in migration after 6 and 15 h of CDPs exposure was statistically significant according to Two-way ANOVA with Dunnett's multiple comparisons tests. $^{\S}p < 0.0001$, $^{\#}p < 0.001$ and $^{**}p < 0.01$ vs control cells.

Migration was studied also after exposure to organic fractions and washed particles (Figure 4). While a slight effect on migration was observed after exposure to washed particles (Figure 4B), showing wood as the most potent and pellet as the less, a consistent decrease was observed treating with organic extracts (Figure 4A). Since data on the organic fractions are comparable to those observed with CDPs as such, it might be assumed that organic compounds are primarily responsible of the effects. However, there was no correlation with the PAH content as charcoal had no effects. Most interestingly, preliminary experiments with the AhR-inhibitor (Antagonist III, GNF351, Sigma-Aldrich) suggested that an inhibition of AhR markedly reduced the migration process supporting the notion that the receptor is needed in this process (Bui et al., 2016).

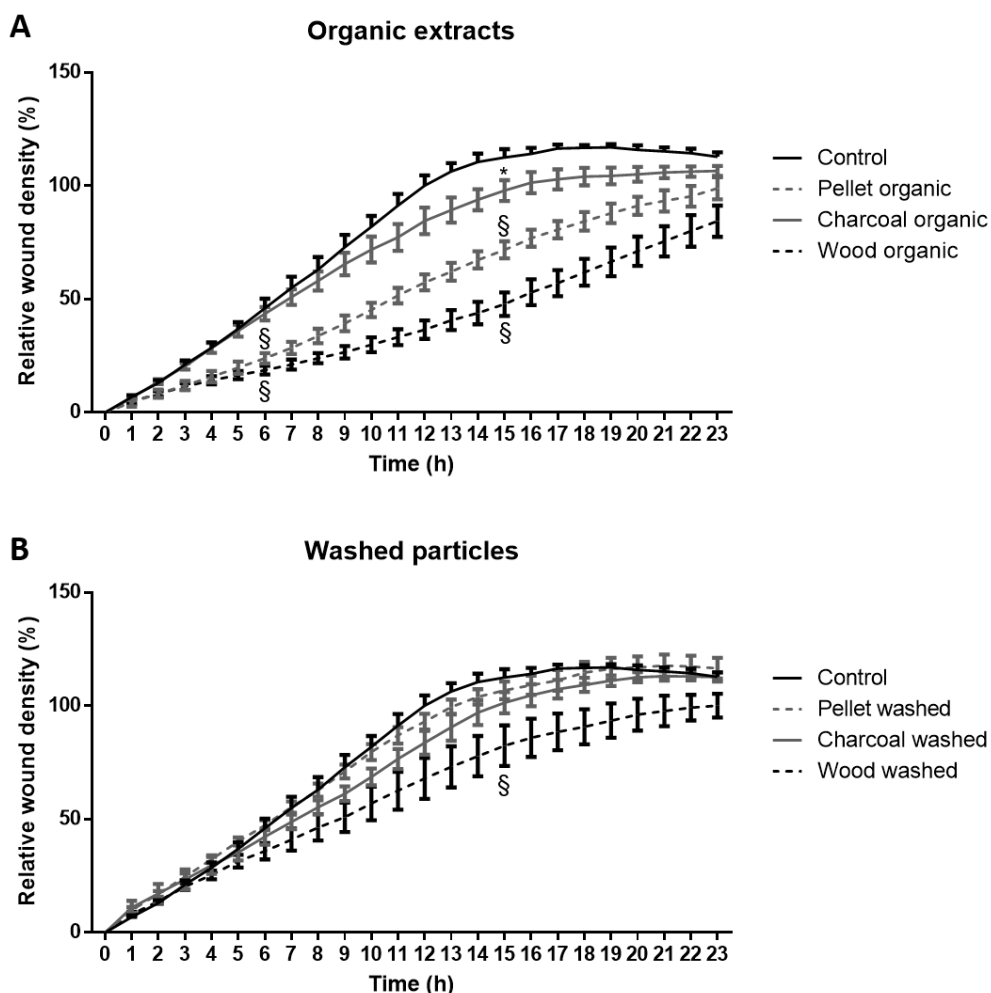


Figure 4. Cell migration. Migration was assessed by scratch wound closure assay after exposure to the CDP-derived organic (A) and washed fractions (B). Data display the relative wound density measured every hour up to 24 h of a representative experiment. Reduction in migration after 6 and 15 h of exposure is statistically significant according to Two-way ANOVA with Dunnett's multiple comparisons tests. § $p < 0.0001$ and * $p < 0.05$ vs control cells.

Modulation of genes involved in several CDP-activated pathways, i.e. xenobiotic metabolism (CYP1A1, CYP1B1 and AHRR), oxidative stress (HO-1), inflammatory response (IL-1B, IL-8, IL-6 and COX2), and EMT (SerpinB2, CDH1, CDH2 and Vim) was then examined.

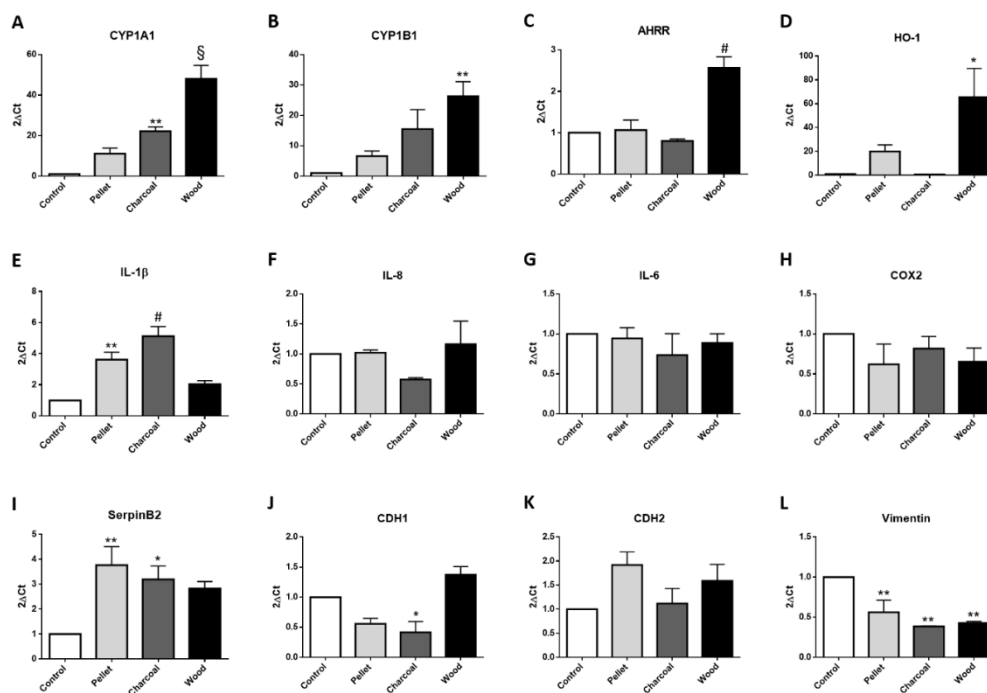


Figure 5. Gene expression analysis. Modulation of genes related to xenobiotic metabolism (A, B, C), oxidative stress (D), inflammatory response (E, F, G, H), and EMT (I, J, K, L) was explored after 24 h of exposure to CDPs at a concentration corresponding to 2.5 $\mu\text{g}/\text{cm}^2$. Statistical analysis was performed by One-way ANOVA with Dunnett's multiple comparisons tests. § $p < 0.0001$, # $p < 0.001$, ** $p < 0.01$ and * $p < 0.05$ vs control cells.

A statistically significant increase in the AhR-linked CYP1A1 and CYP1B1 gene transcripts was observed (Figures 5A and B). CYP1A1 was induced also by charcoal. Besides, AhR repressor (AhRR) was significantly up-regulated in HBEC3-KT after exposure to wood (Figure 5C). Furthermore, oxidative stress response assessed by heme oxygenase 1 (HO-1) expression, showed a significant increase after exposure particles from wood (Figure 5D). Pellet also appeared to be able to activate the expression of this gene, although the increase was not significant.

Regarding the inflammatory response genes, only interleukin (IL)-1 β (Figure 5E) was significantly altered. A significantly increased expression of this gene was observed after exposure to pellet and charcoal CDPs. No significant effects were detected on IL-8, IL-6 and Cyclooxygenase 2 (COX2; Figures 5F, G and H). Finally, panels I, J, K and L displays the relative expression of plasminogen activator inhibitor-2 (Serpin2B) and EMT-related genes. While the expression of SERPINB2 was induced, VIM was inhibited by all CDPs, with the largest effects detected after exposure to charcoal and wood. In contrast, E-cadherin (CDH1) was only down-regulated by

charcoal. No significant alterations of the gene encoding N-cadherin (CDH2) expression were observed.

Analysis of effects on gene expression of organic fractions and washed particles are shown in Supplementary materials (Figures 1 and 2).

The focus of the remaining part of the study was on CDPs only. Based on the gene expression analysis, the release of IL-1 β as into the cell culture medium was explored (Figure 6A) after exposure to different CDP doses (1, 2.5 and 5 $\mu\text{g}/\text{cm}^2$). The studies showed that particles from pellet, charcoal and wood increased the release of IL-1 β , with wood particles as the most potent.

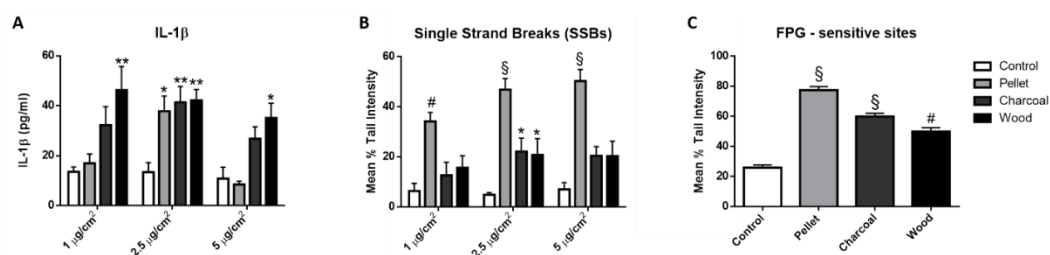


Figure 6. IL-1 β release and DNA damage. A) IL-1 β release assessed after 24 h of exposure to CDPs (1, 2.5 and 5 $\mu\text{g}/\text{cm}^2$). Statistical analysis was performed by Two-way ANOVA with Tukey's multiple comparisons test. ** $p < 0.01$ and * $p < 0.05$ vs control cells B) Single strand breaks (SSBs) on cells exposed to increasing CDPs doses. DNA damage was assessed by SCGE assay. Histogram shows DNA-damage expressed as tail intensity (%). Statistical analysis was performed by Two-way ANOVA with Dunnett's multiple comparisons tests. $^{\S}p < 0.0001$, $^{\#}p < 0.001$ and * $p < 0.05$ vs control cells. C) FPG – sensitive sites on cells exposed to 5 μg CDPs/ cm^2 . Histogram shows tail intensity expressed as percentage. Statistical analysis was performed by One-way ANOVA with Dunnett's multiple comparisons tests. $^{\S}p < 0.0001$ and * $p < 0.05$ vs control cells.

To elucidate DNA damaging potential of the CDPs, cells were exposed to three different doses of particles (1, 2.5 and 5 $\mu\text{g}/\text{cm}^2$) for 24 h and analyzed by single cell gel electrophoresis (SCGE). Data in Figure 6B shows that pellet induced a statistically significant increase in tail intensity in a dose-response manner, suggesting the presence of SSBs. The effects obtained after exposure to charcoal and wood were less marked, but a significant increase was observed after exposure to 2.5 $\mu\text{g}/\text{cm}^2$. Next, the presence of oxidative lesions was assessed by addition of formamidopyrimidine-DNA-glycosylase (FPG), which is an enzyme that detects oxidated purine bases (8-oxoG) in addition to other base oxidations. As seen in Figure 6C, FPG-sensitive sites significantly increased following exposure to all CDPs, again with particles from pellet burning as the most potent.

The presence of DNA damage often results in alterations of the cell cycle. Here, particles from pellet burning changed the cell cycle profile as measured after 24 h (Figures 5A, B and C). A very marked reduction in G1 phase cell percentage was observed after exposure to pellet (2.5 and 5 $\mu\text{g}/\text{cm}^2$) at this time point. A parallel

increase in S and/or G2 phases was indicated, suggesting an accumulation of cells cycle in late S and/or early G2, as confirmed by Figure 7D. Finally, the apoptotic index was evaluated (Figure 7E), showing that pellet induced a significant increase in the fraction of apoptotic cells.

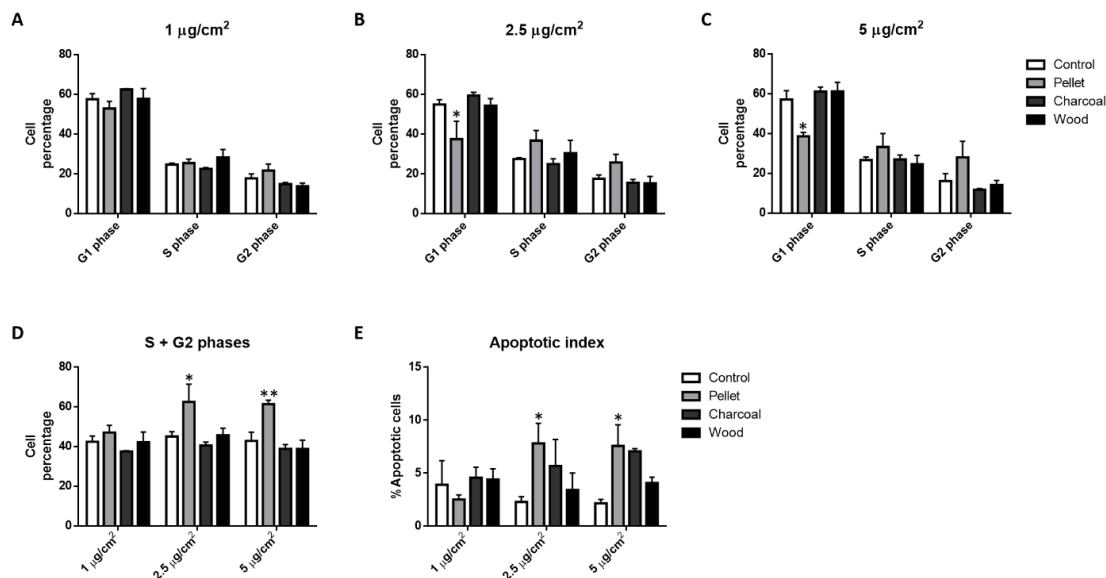


Figure 7. Cell cycle investigation and apoptotic index. A, B, C) Cell percentage in each phase of the cycle after 24 h exposure to increasing doses (1, 2.5 and 5 µg/cm²) of CDPs. D) Histogram represents percentage of cells in S and G2 phases at all tested doses. E) Histogram represents percentage of apoptotic cells at all tested doses. Statistical analysis was performed by Two-way ANOVA with Dunnett's multiple comparisons tests. ** $p < 0.01$ and * $p < 0.05$ vs control cells.

4. Discussion

CDPs-elicited health effects are influenced by several factors, related not only to the chemical composition, but also to particles aerodynamics properties, such as size, density and shape. These characteristics are reported to be associated to type of appliances (traditional or modern), differences in biomass type and operating condition, which can affect the physico-chemical properties of the emitted particles in several ways (Kocbach Bølling et al., 2009; Uski et al., 2014; Vicente and Alves, 2018, Longhin et al. 2016). Understanding the genotoxic and pro-carcinogenic effects of particles emitted from a stove propelled with different fuels is important in order to identify the ones that can cause harmful effects on lung cells.

In a previous study on A549 cells, we found pellet as the more cytotoxic and genotoxic, inducing necrosis, a mild inflammatory response, DNA damage and cell cycle de-regulation. Charcoal and wood instead, causes apoptosis and the activation of the xenobiotic enzyme CYP1A1 (Marchetti et al., 2019). To increase

the understanding of CDP-induced lung cells injuries, the HBEC3-KT cell line was used as a representative model of normal human bronchial epithelial cells (Bersaas et al., 2016).

The CDPs used had been collected from an open fireplace fueled with pellet, charcoal and wood, respectively. CDPs from charcoal and wood-derived samples were larger when compared to pellet, which conversely had more particles in the ultrafine range (Marchetti et al., 2019). Moreover, while wood and charcoal CDPs have a high amount of PAHs (10 and 8-fold higher than in pellet), pellet particles were characterized by a higher concentration of metals (2-fold higher than in charcoal and wood). These results are in line with other studies on traditional appliances describing particles with a high concentration of PAHs and metals, compared to CDPs emitted from modern stoves. Vicente et al. (2015), reported indeed significant differences in chemical composition between particles collected from modern stoves or old type appliances. Moreover, Longhin et al. (2016) described particles emitted from a modern and automatic stove, which possess a low content of organic compounds and exert a low biological effect on human lung cells.

Several studies have pointed out that there might be a link between environmental pollution and effects on cell migration (Longhin et al., 2018; Rey-Barroso et al., 2014; Yang et al., 2017; Yue et al., 2015), as its regulation is a key factor for dissemination of metastatic cells during tumor progression. Reduced cell migration has been described in post-EMT human mammary epithelial cells (Schaeffer et al., 2014), and in murine lung epithelial cells exposed to diesel particles (LaGier et al., 2013). In contrast, augmented migratory potential for condensate tobacco smoke (Bersaas et al., 2016) and diesel exhaust PM transformed (Rynning et al., 2018) was reported on HBEC cells. Furthermore, following short-term exposure, was also found a reduction in cell migration after exposure to ultrafine diesel particles, while biomass particles were ineffective (Longhin et al., 2016). Similarly, we here report that exposure to PM, and their organic fractions reduced migration. Considering that washed particles had only a slight effect, while the organic fractions had results comparable to those observed with CDPs as such, it might be proposed that organic compounds are primarily responsible of the effects. Particles with a high PAHs content have been reported to potentiate lung cancer cell metastasis *in vitro* by promoting cell migration and invasion (Yue et al., 2015). Moreover, following exposure to PAHs such as B[a]P and diesel PM, we have found that the expression of EMT marker genes was modified in transformed colonies which were able to grow in soft agar (Bersaas et al., 2016; Rynning et al., 2018). Interestingly, we have also reported changes in EMT related to short-term exposures to diesel PM (Longhin et al., 2016). In this study, significantly reduced migration was observed in HBEC3-KT cells exposed to diesel, while no effect on migration was detected in biomass PM treated cells. In contrast to the present study, diesel PM mediated

inhibition of migration was accompanied by a decrease in the expression of CDH1, although with different kinetics. Here we reported alterations in the EMT process, with a reduction/delay in migration and alterations in the expression of important EMT genes. However, the relative potency of our particles with regard to reduced migration (wood > pellet > charcoal) did not correspond to the particles PAH content. On the other hand, results on pellet might be explained by the high metal content. Yang et al. (2017), reported indeed that increased migration might be promoted also by metals, not only by PAHs. Additionally, results from gene expression imply that there might be other chemical compounds, other than PAHs and metals, that also are important for the migration process.

The effects of CDPs related to the expression of AhR-linked genes *CYP1A1*, *CYP1B1*, *AHRR* showed charcoal and wood giving higher responses than pellet PM. These results are in accordance with the particles relative levels of PAHs. The relative increase in *SERPINB2* expression were opposite. As *SERPINB2* seems to be regulated via AhR non-canonical signaling (Sekine et al., 2009), the results indicate that various ligands may differentially regulate these two pathways.

The ROS-related effects addressed by assessing HO-1 expression indicated that particles derived from wood induced oxidative stress, while pellet particles resulted in a slight, but not statistically significant effect. SCGE assay showed that all the particles caused oxidative DNA-damage, as measured as FPG-sensitive sites, with pellet as the most potent. Although oxidative stress also has been linked to inflammatory responses, the relative response observed (wood > charcoal > pellet) did not directly reflect the oxidative damage measured by either HO-1 nor oxidative DNA damage.

With regards to inflammation, results following exposure of particles at different concentrations revealed that all the CDPs induced IL-1 β release, and that wood particles were the most potent. The relative response might be associated with particle PAH content. However, the results on gene expression following exposure to organic fractions and washed particles suggest that different compounds may be involved.

In the present study, pellet was the most toxic CDPs measured as reduction in number of viable cells. Studies on flow cytometry revealed that this reduction could be due to an accumulation of cells in G2/M phase. CPDs derived from pellet combustion were also a more potent inducer of apoptosis when compared to the other CPDs.

The studies with the comet assay showed that the pellet-derived particles gave more DNA damage, as measured as both single strand breaks as well as oxidative DNA damage. It is well-known that DNA damage including SSB and oxidative damage will reduce DNA replication synthesis (Jackson and Bartek, 2009). Thus, the increased DNA damage could explain the observed accumulation of cells in S-phase/G2 phase following exposure to pellet.

As pellet CDPs, compared to charcoal and wood derived particles contain little PAHs but more metals, the toxic effects observed after exposure to pellet particles could be related to their metal content. In line with this suggestion, Perrone and colleagues (2010) proposed that metals could be responsible for the oxidative stress response activation and the genotoxic damages reported on A549 cells. Furthermore, Van Den Heuvel (2016) reported a positive correlation between metals, reduction in cell viability and DNA damage supporting Perrone's observations.

5. Conclusions

CDPs-induced toxic cellular effects were investigated in terms of cytotoxicity, inflammation and EMT-related effects, DNA damage, and genotoxicity. Differences in the toxicological profile could be associated with the organic and metal content of the different CDPs that might lead to activation of different cellular mechanisms involved in lung cancer progression. Specifically, pellet and wood-derived CDPs showed more genotoxic and carcinogenic properties than charcoal. Thus, fuel type acquires importance with respect to the harmfulness of the emitted particles. However, the correlation between the chemical content and the biological effects is still unclear. It might be anticipated that several compounds simultaneously contribute to the physiological changes reported, including possibly compounds other than PAHs and metals commonly measured.

Further studies are needed to elucidate the role of metals and PAHs in the biological effects induced by CPDs, in order to take into account preventive measures on the propel type of fuel used.

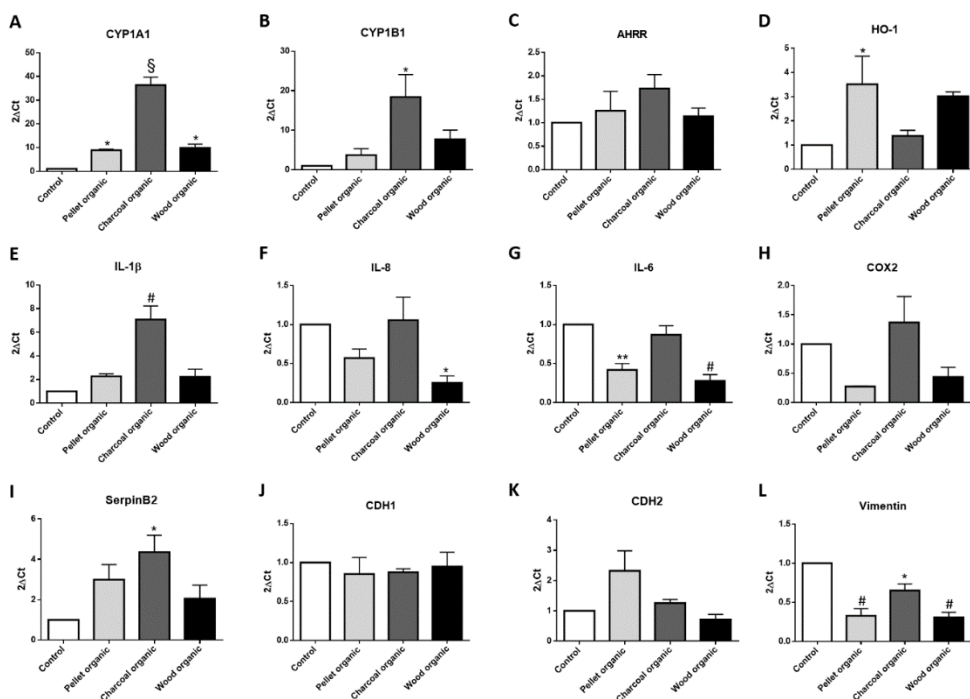
Acknowledgements

The authors want to thank Rita Bæra (National Institute of Occupational Health), Leni Ekeren and Hans J. Dahlman (Norwegian Institute of Public Health, Oslo, Norway) for technical assistance throughout the study.

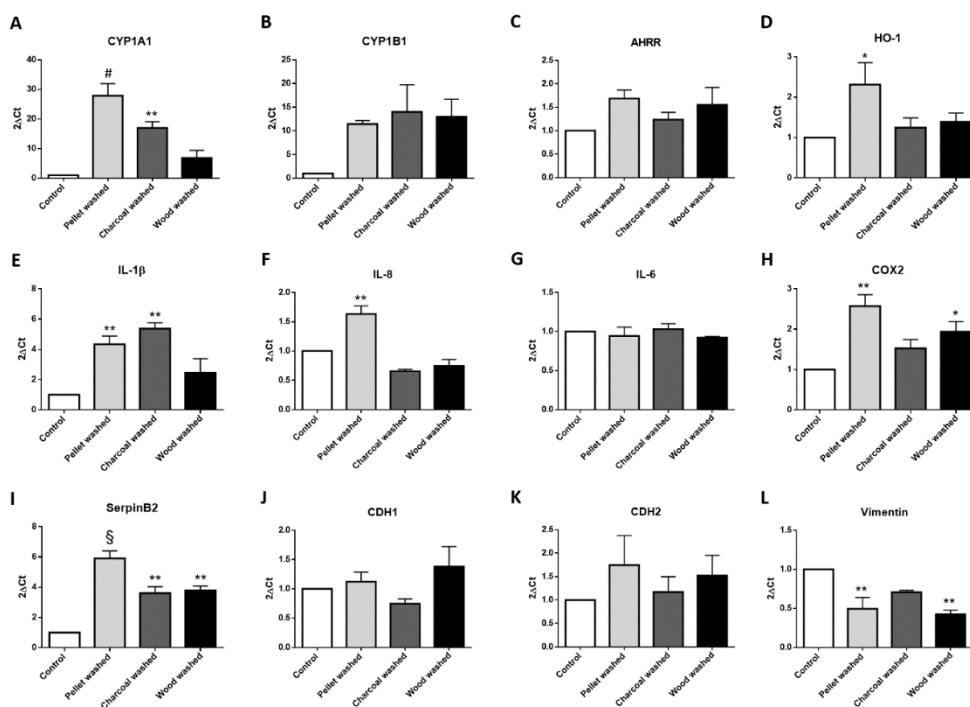
Supplementary data

Supplementary table 1. Primer sequences of investigated genes.

CYP1A1	<i>Fwd</i>	CATCCCCACAGCACAACA
	<i>Rev</i>	CAGGGGTGAGAAACCGTTCA
CYP1B1	<i>Fwd</i>	CTGGATTTGGAGAACGTACCG
	<i>Rev</i>	TGATCCAATTCTGCCTGCAC
AhRR	<i>Fwd</i>	GAAGGGACGATATTTTATGCATCAG
	<i>Rev</i>	CACGTGGATGTAGTCATAAATGTTCTG
HO-1	<i>Fwd</i>	GGGTGATAGAAGAGGCCAAGA
	<i>Rev</i>	AGCTCCTGCAACTCCTCAA
IL1-β	<i>Fwd</i>	CTAAACAGATGAAAGTGCTCC
	<i>Rev</i>	GGTCATTCTCCTGGAAGG
IL-6	<i>Fwd</i>	ATCCTCGACGGCATCTCA
	<i>Rev</i>	TTTACCAGGCAAGTCTCCT
IL-8	<i>Fwd</i>	TTGGCAGCCTTCTGATTTT
	<i>Rev</i>	AACTTCTCCACAACCCTCTG
COX2	<i>Fwd</i>	ATCACAGGCTTCCATTGACC
	<i>Rev</i>	CAGGATACAGCTCCACAGCA
SerpinB2	<i>Fwd</i>	TGTGGGTTCATGCAGCAGAT
	<i>Rev</i>	AAGCTCGCAGACTTCTCACC
Vimentin	<i>Fwd</i>	TCCAAACTTTTCTCCTGAA
	<i>Rev</i>	CGTGATGCTGAGAAGTTTCG
CDH1	<i>Fwd</i>	ACGCCGAGAGCTACACGTTCA
	<i>Rev</i>	TCCTTTGTGACCGGTGCAATC
CDH2	<i>Fwd</i>	TCCAACGGGGACTGCACAGAT
	<i>Rev</i>	GGCGTTCTTTATCCC GGCGTT
β-Actin	<i>Fwd</i>	GACGACATGGAGAAATCTG
	<i>Rev</i>	ATGATCTGGGTCATCTTCTC



Supplementary figure 1. Gene expression analysis on cells exposed to organic fractions. Modulation of genes related to xenobiotic metabolism (A, B, C), oxidative stress (D) inflammatory response (E, F, G, H), and EMT (I, J, K, L) was explored after 24 h of exposure to the CDP-derived organic fractions at a concentration corresponding to 2.5 $\mu\text{g}/\text{cm}^2$. Statistical analysis was performed by One-way ANOVA with Dunnett's multiple comparisons tests. $^{\S}p < 0.0001$, $^{\#}p < 0.001$, $^{**}p < 0.01$ and $^{*}p < 0.05$ vs control cells.



Supplementary figure 2. Gene expression analysis on cells exposed to washed particles. Modulation of genes related to xenobiotic metabolism (A, B, C), oxidative stress (D) inflammatory response (E, F, G, H), and EMT (I, J, K, L) was explored after 24 h of exposure to washed particles at a concentration corresponding to 2.5 $\mu\text{g}/\text{cm}^2$. Statistical analysis was performed by One-way ANOVA with Dunnett's multiple comparisons tests. $^{\S}p < 0.0001$, $^{\#}p < 0.001$, $^{**}p < 0.01$ and $^{*}p < 0.05$ vs control cells.

References

- Bersaas, A., Arnoldussen, Y.J., Sjøberg, M., Haugen, A., Møllerup, S., 2016. Epithelial-mesenchymal transition and FOXA genes during tobacco smoke carcinogen induced transformation of human bronchial epithelial cells. *Toxicol. Vitro*. 35, 55–65.
<https://doi.org/10.1016/j.tiv.2016.04.012>
- Billet, S., Landkocz, Y., Martin, P.J., Verdin, A., Ledoux, F., Lepers, C., André, V., Cazier, F., Sichel, F., Shirali, P., Gosset, P., Courcot, D., 2018. Chemical characterization of fine and ultrafine PM, direct and indirect genotoxicity of PM and their organic extracts on pulmonary cells. *J. Environ. Sci. (China)* 71, 168–178.
<https://doi.org/10.1016/j.jes.2018.04.022>
- Bølling, A.K., Totlandsdal, A.I., Sallsten, G., Braun, A., Westerholm, R., Bergvall, C., Boman, J., Dahlman, H.J., Sehlstedt, M., Cassee, F., Sandstrom, T., Schwarze, P.E., Herseth, J.I., 2012. Wood smoke particles from different combustion phases induce similar pro-inflammatory effects in a co-culture of monocyte and pneumocyte cell lines. *Part. Fibre Toxicol.* <https://doi.org/10.1186/1743-8977-9-45>
- Bui, L.C., Tomkiewicz, C., Pierre, S., Chevallier, A., Barouki, R., Coumoul, X., 2016. Regulation of Aquaporin 3 Expression by the AhR Pathway Is Critical to Cell Migration. *Toxicol. Sci.* <https://doi.org/10.1093/toxsci/kfv221>
- Cassee, F.R., Héroux, M.E., Gerlofs-Nijland, M.E., Kelly, F.J., 2013. Particulate matter beyond mass: Recent health evidence on the role of fractions, chemical constituents and sources of emission. *Inhal. Toxicol.* 25, 802–812.
<https://doi.org/10.3109/08958378.2013.850127>
- Corsini, E., Budello, S., Marabini, L., Galbiati, V., Piazzalunga, A., Barbieri, P., Cozzutto, S., Marinovich, M., Pitea, D., Galli, C.L., 2013. Comparison of wood smoke PM_{2.5} obtained from the combustion of FIR and beech pellets on inflammation and DNA damage in A549 and THP-1 human cell lines. *Arch. Toxicol.* 87, 2187–2199.
<https://doi.org/10.1007/s00204-013-1071-z>
- Corsini, E., Ozgen, S., Papale, A., Galbiati, V., Lonati, G., Fermo, P., Corbella, L., Valli, G., Bernardoni, V., Dell'Acqua, M., Becagli, S., Caruso, D., Vecchi, R., Galli, C.L., Marinovich, M., 2017. Insights on wood combustion generated proinflammatory ultrafine particles (UFP). *Toxicol. Lett.* 266, 74–84.
<https://doi.org/10.1016/j.toxlet.2016.12.005>
- Danielsen, P.H., Loft, S., Kocbach, A., Schwarze, P.E., Møller, P., 2009. Oxidative damage to DNA and repair induced by Norwegian wood smoke particles in human A549 and THP-1 cell lines. *Mutat. Res. - Genet. Toxicol. Environ. Mutagen.* 674, 116–122.
<https://doi.org/10.1016/j.mrgentox.2008.10.014>
- Danielsen, P.H., Møller, P., Jensen, K.A., Sharma, A.K., Wallin, H., Bossi, R., Autrup, H., Mølhave, L., Ravanat, J.L., Briedé, J.J., De Kok, T.M., Loft, S., 2011. Oxidative stress, DNA damage, and inflammation induced by ambient air and wood smoke particulate matter in human A549 and THP-1 cell lines. *Chem. Res. Toxicol.* <https://doi.org/10.1021/tx100407m>
- De Oliveira Alves, N., De Souza Hacon, S., De Oliveira Galvão, M.F., Simões Peixotoc, M., Artaxo, P., De Castro Vasconcellos, P., De Medeiros, S.R.B., 2014. Genetic damage of organic matter in the Brazilian Amazon: A comparative study between intense and

- moderate biomass burning. *Environ. Res.* 130, 51–58.
<https://doi.org/10.1016/j.envres.2013.12.011>
- Dilger, M., Orasche, J., Zimmermann, R., Paur, H.R., Diabaté, S., Weiss, C., 2016. Toxicity of wood smoke particles in human A549 lung epithelial cells: the role of PAHs, soot and zinc. *Arch. Toxicol.* 90, 3029–3044. <https://doi.org/10.1007/s00204-016-1659-1>
- Dong, T.T.T., Hinwood, A.L., Callan, A.C., Zosky, G., Stock, W.D., 2017. In vitro assessment of the toxicity of bushfire emissions: A review. *Sci. Total Environ.* 603–604, 268–278. <https://doi.org/10.1016/j.scitotenv.2017.06.062>
- Forchhammer, L., Loft, S., Roursgaard, M., Cao, Y., Riddervold, I.S., Sigsgaard, T., Møller, P., 2012. Expression of adhesion molecules, monocyte interactions and oxidative stress in human endothelial cells exposed to wood smoke and diesel exhaust particulate matter. *Toxicol. Lett.* 209, 121–128.
<https://doi.org/10.1016/j.toxlet.2011.12.003>
- Gutzkow, K.B., Langleite, T.M., Meier, S., Graupner, A., Collins, A.R., Brunborg, G., 2013. High-throughput comet assay using 96 minigels. *Mutagenesis* 28, 333–340.
<https://doi.org/10.1093/mutage/get012>
- Heßelbach, K., Kim, G.J., Flemming, S., Häupl, T., Bonin, M., Dornhof, R., Günther, S., Merfort, I., Humar, M., 2017. Disease relevant modifications of the methylome and transcriptome by particulate matter (PM 2.5) from biomass combustion. *Epigenetics* 12, 779–792. <https://doi.org/10.1080/15592294.2017.1356555>
- Jackson, S.P., Bartek, J., 2009. The DNA-damage response in human biology and disease. *Nature*. <https://doi.org/10.1038/nature08467>
- Jalava, P.I., Happonen, M.S., Kelz, J., Brunner, T., Hakulinen, P., Mäki-Paakkanen, J., Hukkanen, A., Jokiniemi, J., Obernberger, I., Hirvonen, M.R., 2012. In vitro toxicological characterization of particulate emissions from residential biomass heating systems based on old and new technologies. *Atmos. Environ.* 50, 24–35.
<https://doi.org/10.1016/j.atmosenv.2012.01.009>
- Kocbach Bølling, A., Pagels, J., Yttri, K.E., Barregard, L., Sallsten, G., Schwarze, P.E., Boman, C., 2009. Health effects of residential wood smoke particles: the importance of combustion conditions and physicochemical particle properties. *Part. Fibre Toxicol.* 6, 29.
- LaGier, A.J., Manzo, N.D., Dye, J.A., 2013. Diesel exhaust particles induce aberrant alveolar epithelial directed cell movement by disruption of polarity mechanisms. *J. Toxicol. Environ. Heal. - Part A Curr. Issues*.
<https://doi.org/10.1080/15287394.2013.738169>
- Longhin, E., Camatini, M., Bersaas, A., Mantecca, P., Mollerup, S., 2018. The role of SerpinB2 in human bronchial epithelial cells responses to particulate matter exposure. *Arch. Toxicol.* 92, 2923–2933. <https://doi.org/10.1007/s00204-018-2259-z>
- Longhin, E., Gualtieri, M., Capasso, L., Bengalli, R., Mollerup, S., Holme, J.A., Øvrevik, J., Casadei, S., Di Benedetto, C., Parenti, P., Camatini, M., 2016. Physico-chemical properties and biological effects of diesel and biomass particles. *Environ. Pollut.* 215, 366–375. <https://doi.org/10.1016/j.envpol.2016.05.015>
- Longhin, E., Holme, J.A., Gutzkow, K.B., Arlt, V.M., Kucab, J.E., Camatini, M., Gualtieri, M., 2013. Cell cycle alterations induced by urban PM2.5 in bronchial epithelial cells:

- Characterization of the process and possible mechanisms involved. Part. *Fibre Toxicol.* <https://doi.org/10.1186/1743-8977-10-63>
- Marchetti, S., Longhin, E., Bengalli, R., Avino, P., Stabile, L., Buonanno, G., Colombo, A., Camatini, M., Mantecca, P., 2019. In vitro lung toxicity of indoor PM10 from a stove fueled with different biomasses. *Sci. Total Environ.* 649, 1422–1433. <https://doi.org/10.1016/j.scitotenv.2018.08.249>
- Muala, A., Rankin, G., Sehlstedt, M., Unosson, J., Bosson, J.A., Behndig, A., Pourazar, J., Nyström, R., Pettersson, E., Bergvall, C., Westerholm, R., Jalava, P.I., Happonen, M.S., Uski, O., Hirvonen, M.-R., Kelly, F.J., Mudway, I.S., Blomberg, A., Boman, C., Sandström, T., 2015. Acute exposure to wood smoke from incomplete combustion - indications of cytotoxicity. Part. *Fibre Toxicol.* 12, 33. <https://doi.org/10.1186/s12989-015-0111-7>
- Nakayama Wong, L.S., Aung, H.H., Lamé, M.W., Wegesser, T.C., Wilson, D.W., 2011. Fine particulate matter from urban ambient and wildfire sources from California's San Joaquin Valley initiate differential inflammatory, oxidative stress, and xenobiotic responses in human bronchial epithelial cells. *Toxicol. Vitro.* 25, 1895–1905. <https://doi.org/10.1016/j.tiv.2011.06.001>
- Noël, A., Xiao, R., Perveen, Z., Zaman, H.M., Rouse, R.L., Paulsen, D.B., Penn, A.L., 2016. Incomplete lung recovery following sub-acute inhalation of combustion-derived ultrafine particles in mice. Part. *Fibre Toxicol.* 13, 10. <https://doi.org/10.1186/s12989-016-0122-z>
- Perrone, M.G., Gualtieri, M., Ferrero, L., Porto, C. Lo, Udisti, R., Bolzacchini, E., Camatini, M., 2010. Seasonal variations in chemical composition and in vitro biological effects of fine PM from Milan. *Chemosphere* 78, 1368–1377. <https://doi.org/10.1016/j.chemosphere.2009.12.071>
- Ramirez, R.D., Kurie, J., Michael DiMaio, J., Vaughan, M.B., Milchgrub, S., Smith, A., Gandia, G., Sheridan, S., Shay, J.W., Minna, J.D., 2004. O-205 Immortalization of normal human bronchial epithelial cells (NHBE) in the absence of viral oncoproteins. *Lung Cancer* 41, S60–S61. [https://doi.org/10.1016/s0169-5002\(03\)91863-0](https://doi.org/10.1016/s0169-5002(03)91863-0)
- Rey-Barroso, J., Alvarez-Barrientos, A., Rico-Leo, E., Contador-Troca, M., Carvajal-Gonzalez, J.M., Echarri, A., Del Pozo, M.A., Fernandez-Salguero, P.M., 2014. The Dioxin receptor modulates Caveolin-1 mobilization during directional migration: Role of cholesterol. *Cell Commun. Signal.* <https://doi.org/10.1186/s12964-014-0057-7>
- Rynning, I., Neca, J., Vrbova, K., Libalova, H., Rossner, P., Holme, J.A., Gützkow, K.B., Afanou, A.K.J., Arnoldussen, Y.J., Hrubá, E., Skare, Ø., Haugen, A., Topinka, J., Machala, M., Mollerup, S., 2018. In Vitro Transformation of Human Bronchial Epithelial Cells by Diesel Exhaust Particles: Gene Expression Profiling and Early Toxic Responses. *Toxicol. Sci.* 166, 51–64. <https://doi.org/10.1093/toxsci/kfy183>
- Sarigiannis, D.A., Karakitsios, S.P., Zikopoulos, D., Nikolaki, S., Kermenidou, M., 2015. Lung cancer risk from PAHs emitted from biomass combustion. *Environ. Res.* 137, 147–156. <https://doi.org/10.1016/j.envres.2014.12.009>
- Schaeffer, D., Somarelli, J.A., Hanna, G., Palmer, G.M., Garcia-Blanco, M.A., 2014. Cellular

- Migration and Invasion Uncoupled: Increased Migration Is Not an Inexorable Consequence of Epithelial-to-Mesenchymal Transition. *Mol. Cell. Biol.* 34, 3486–3499. <https://doi.org/10.1128/mcb.00694-14>
- Sekine, H., Mimura, J., Oshima, M., Okawa, H., Kanno, J., Igarashi, K., Gonzalez, F.J., Ikuta, T., Kawajiri, K., Fujii-Kuriyama, Y., 2009. Hypersensitivity of Aryl Hydrocarbon Receptor-Deficient Mice to Lipopolysaccharide-Induced Septic Shock. *Mol. Cell. Biol.* <https://doi.org/10.1128/mcb.00337-09>
- Sigsgaard, T., Forsberg, B., Annesi-Maesano, I., Blomberg, A., Bølling, A., Boman, C., Bønløkke, J., Brauer, M., Bruce, N., Héroux, M.-E., Hirvonen, M.-R., Kelly, F., Künzli, N., Lundbäck, B., Moshhammer, H., Noonan, C., Pagels, J., Sallsten, G., Sculier, J.-P., Brunekreef, B., 2015. Health impacts of anthropogenic biomass burning in the developed world. *Eur. Respir. J.* 46, 1577–1588. <https://doi.org/10.1183/13993003.01865-2014>
- Stabile, L., Buonanno, G., Avino, P., Frattolillo, A., Guerriero, E., 2018. Indoor exposure to particles emitted by biomass-burning heating systems and evaluation of dose and lung cancer risk received by population. *Environ. Pollut.* 235, 65–73. <https://doi.org/10.1016/j.envpol.2017.12.055>
- Uski, O., Jalava, P.I., Happonen, M.S., Leskinen, J., Sippula, O., Tissari, J., Mäki-Paakkanen, J., Jokiniemi, J., Hirvonen, M.R., 2014. Different toxic mechanisms are activated by emission PM depending on combustion efficiency. *Atmos. Environ.* <https://doi.org/10.1016/j.atmosenv.2014.02.036>
- Van Den Heuvel, R., Den Hond, E., Govarts, E., Colles, A., Koppen, G., Staelens, J., Mampaey, M., Janssen, N., Schoeters, G., 2016. Identification of PM10 characteristics involved in cellular responses in human bronchial epithelial cells (Beas-2B). *Environ. Res.* 149, 48–56. <https://doi.org/10.1016/j.envres.2016.04.029>
- Vicente, E.D., Alves, C.A., 2018. An overview of particulate emissions from residential biomass combustion. *Atmos. Res.* 199, 159–185. <https://doi.org/10.1016/j.atmosres.2017.08.027>
- Vicente, E.D., Duarte, M.A., Tarelho, L.A.C., Nunes, T.F., Amato, F., Querol, X., Colombi, C., Gianelle, V., Alves, C.A., 2015. Particulate and gaseous emissions from the combustion of different biofuels in a pellet stove. *Atmos. Environ.* 120, 15–27. <https://doi.org/10.1016/j.atmosenv.2015.08.067>
- World Health Organization, 2016. Household air pollution and health | Fact sheet N°292 [WWW Document]. WHO.
- Yang, D., Ma, M., Zhou, W., Yang, B., Xiao, C., 2017. Inhibition of miR-32 activity promoted EMT induced by PM2.5 exposure through the modulation of the Smad1-mediated signaling pathways in lung cancer cells. *Chemosphere* 184, 289–298. <https://doi.org/10.1016/j.chemosphere.2017.05.152>
- Yue, H., Yun, Y., Gao, R., Li, G., Sang, N., 2015. Winter Polycyclic Aromatic Hydrocarbon-Bound Particulate Matter from Peri-urban North China Promotes Lung Cancer Cell Metastasis. *Environ. Sci. Technol.* 49, 14484–14493. <https://doi.org/10.1021/es506280c>

Chapter 4:

The role of IL-6 released from pulmonary epithelial cells in diesel UFP-induced endothelial activation

Rossella Bengalli^{1,*}, Eleonora Longhin¹, Sara Marchetti¹, Maria C. Proverbio²,
Cristina Battaglia³, Marina Camatini¹

¹Polaris Research Centre, Dept. of Earth and Environmental Sciences, University of Milano-Bicocca, Piazza della Scienza, 1, 20126, Milan, Italy

²Department of Physiopathology and Transplantation, University of Milan, Via Fratelli Cervi 93, 20090, Segrate, Italy

³Department of Medical Biotechnology and Translational Medicine (BIOMETRA), University of Milan, via F.lli Cervi 93, 20090, Segrate, Italy

*Corresponding author: Rossella Bengalli, e-mail: rossella.bengalli@unimib.it, tel: +390264482928

Published in **Environmental Pollution**
(DOI: 10.1016/j.envpol.2017.08.104)

Abstract

Diesel exhaust particles (DEP) and their ultrafine fraction (UFP) are known to induce cardiovascular effects in exposed subjects. The mechanisms leading to these outcomes are still under investigation, but the activation of respiratory endothelium is likely to be involved. Particles translocation through the air-blood barrier and the release of mediators from the exposed epithelium have been suggested to participate in the process. Here we used a conditioned media *in vitro* model to investigate the role of epithelial-released mediators in the endothelial cells activation.

Diesel UFP were sampled from a Euro 4 vehicle run over a chassis dyno and lung epithelial BEAS-2B cells were exposed for 20 h (dose 5 $\mu\text{g}/\text{cm}^2$). The exposure media were collected and used for endothelial HPMEC-ST1.6R cells treatment for 24 h. The processes related to oxidative stress and inflammation were investigated in the epithelial cells, accordingly to the present knowledge on DEP toxicity. The release of IL-6 and VEGF was significantly augmented in diesel exposed cells. In endothelial cells, VCAM-1 and ICAM-1 adhesion molecules levels were increased after exposure to the conditioned media. By interfering with IL-6 binding to its endothelial receptor, we demonstrate the role of this interleukin in inducing the endothelial response.

Keywords: conditioned media; diesel ultrafine particles; endothelial activation; IL-6; inflammation.

1. Introduction

Diesel exhaust particles (DEP) exposure has been associated to both severe respiratory health effects, such as chronic inflammation and lung cancer (Lewtas, 2007), and cardiovascular diseases such as hypertension and atherosclerosis (BéruBé et al., 2007; Lee et al., 2014). Ultrafine particles (UFP, <100 nm) represent in number the largest fraction of particles emitted by diesel combustion (Nemmar et al., 2013), and arise particular interest for their peculiar properties. UFP have a greater surface area compared to larger particles, providing greater possibilities of interaction with biological systems, and adhesion for harmful chemicals produced by combustion. Furthermore small particles have been shown to evade the pulmonary clearance, reaching the distal parts of the respiratory system and gaining access to the systemic circulation (Nemmar et al., 2013).

Studies on humans have evidenced that after 24 h exposure to DEP there is a persistent impairment of the respiratory endothelium, which occurs in the presence of mild systemic inflammation, and may cause adverse vascular effects (Törnqvist et al., 2007).

The translocation across the air-blood barrier is one of the proposed mechanisms by which diesel and PM_{0.1} (particulate matter ≤ 100 nm) might lead to cardiovascular diseases. This hypothesis suggests that, once in the circulation, UFP directly interact with the cells of vascular endothelium inducing oxidative stress and inflammation, which determine the activation of response pathways related to endothelial dysfunction (Mills et al., 2009). However the evidences on particles translocation are still conflicting (Stone et al., 2016) and some studies show that only a low percentage of carbonaceous UFP reaches the circulation in exposed animals and humans (Klepczyńska-Nyström et al., 2012; Kreyling et al., 2009). Thus, other processes are likely to concur to the vascular response observed.

The release of mediators and signalling factors from the epithelium in response to particles exposure has been suggested as an alternative mechanism inducing endothelial activation (Kelly and Fussell, 2015). Mediators released by *in vitro* and *in vivo* systems in response to diesel exposure include IL-6, IL-8, IL-13, CXCL1/Gro- α , IL-1 β , TNF- α (Kelly and Fussell, 2015; Schwarze et al., 2013).

Endothelial activation is characterized by the increase of the adhesion molecules ICAM-1, VCAM-1 and E-selectin, which enable the adhesion of monocytes to the vascular endothelium, an early step in the formation of atherosclerotic plaques (Galkina and Ley, 2007; Mestas and Ley, 2008). Several studies have addressed the effects of diesel exposure on endothelial cells, and the relation with possible cardiovascular effects. In the HUVEC tube cells, diesel particles have been shown to induce the release of vascular endothelial growth factor VEGF-A and the redistribution of the adherens junction molecule VE-cadherin from the cell membrane to the cytoplasm, thus increasing vascular permeability (Tseng et al.,

2016). In another study (Li et al., 2010), diesel particles activated the expression of VCAM-1 adhesion molecule through NF- κ B signalling pathway in HAEC endothelial cells, and consequently stimulated the monocyte binding to the endothelial cells monolayer. However these papers and most of the *in vitro* studies are focused on the direct effects of particles on cardiac and endothelial cells (Tseng et al., 2015), using particles concentrations that might not be reflect real conditions (1-100 $\mu\text{g}/\text{ml}$, equal to 0.1-10 $\mu\text{g}/\text{cm}^2$ in our exposure model). Only few works investigate the indirect vascular effects caused by the respiratory epithelium exposed to particles (Gorr et al., 2015; Totlandsdal et al., 2008; Weldy et al., 2011).

Here we set up a conditioned media *in vitro* system, where lung epithelial cells are exposed to diesel UFP and the supernatants used to treat endothelial cells. The biological effects in both the cell lines have been investigated and inhibitory studies have been performed to individuate the possible mediators responsible for endothelial responses.

2. Materials and methods

2.1. Preparation of diesel particles

UFP sampling and preparation for biological investigations have been previously described (Longhin et al., 2016). Briefly, DEP were sampled on Teflon filters (Whatman, Maidstone, UK), from a Euro 4 light duty vehicle without DPF run over a chassis dyno. A Dekati gravimetric impactor (DGI-1570, Finland) was used to remove the bigger aggregates. After sampling filters were preserved at $-20\text{ }^{\circ}\text{C}$, until particles extraction was performed by sonication in an ice-cold water-bath (SONICA Soltec, Milan, Italy). Particle suspensions were dried into a desiccator, weighed and stored at $-20\text{ }^{\circ}\text{C}$. Samples were re-suspended in sterile water (final concentration 2 mg/ml) just before use. UFP physico-chemical characterization has been previously reported (Longhin et al., 2016).

2.2. Cells culture and exposure

BEAS-2B cells were maintained in LHC-9 medium (Gibco, Life Technologies, Monza, Italy) at $37\text{ }^{\circ}\text{C}$ with 5% of CO_2 . Cells for experiments (passages 13 to 27) were seeded at a concentration of 2.7×10^5 cells/well in 6-well plates and treated the day after with $5\text{ }\mu\text{g}/\text{cm}^2$ of diesel UFP. The concentration of $5\text{ }\mu\text{g}/\text{cm}^2$ of diesel UFP has been chosen because it was the lower tested dose that induced a significant effect in the *in vitro* system here used after a single acute exposure. After 20 h of exposure, the media were collected, and the cellular responses analysed.

HPMEC-ST1.6R cells were received from Dr. Ronald E. Unger (Institute of Pathology, Medical University of Mainz, Johannes Gutenberg University, Mainz, Germany) and

maintained in M199 medium (Euroclone, Italy), supplemented with 15% inactivated fetal bovine serum (FBS; Gibco, Life Technologies), 2mM L-Glutamine (Sigma Aldrich, Milan, Italy), 20 µg/ml ECGS (Endothelial Cell Growth Supplement) (Sigma Aldrich), 20 µg/ml Na Heparin (Sigma Aldrich), 25 mM Hepes (Sigma Aldrich) and 100 U/ 100 µg/ml Penicillin/Streptomycin (Euroclone) and were grown at 37 °C with 5% of CO₂. Cells for experiments (passages 26 to 37) were seeded at a concentration of 1.5 x 10⁵ cells/well in 6-well plates and treated the day after with 40% of media collected from epithelial cells diluted in M199 medium. The ratio between BEAS-2B medium (LHC-9) and HPMEC medium (M199) for HPMEC exposure has been preliminary selected in the set-up of the *in vitro* system here used. HPMEC-ST1.6R cells exposure lasted for 24 h.

2.3. ROS formation

The oxidative potential of diesel UFP was determined after 1 h of exposure using the 5-(and-6)-Carboxy-2',7'-Dichlorofluorescein Diacetate (carboxy-DCF-DA, Molecular Probes, Life Technologies) probe, that becomes fluorescent when is oxidized by intracellular reactive oxygen species (ROS). Before exposure, BEAS-2B cells were incubated at 37 °C with DCFH-DA 5 µM in PBS for 20 minutes. After incubation, cells were washed twice with PBS and exposed to 5 µg/cm² of diesel UFP in fresh media for 1 h. The samples were then washed with PBS and the fluorescent signal, proportional to ROS formation in the cells, was measured with a multiplate spectrophotometer reader (Tecan, Männedorf, Switzerland, excitation/emission wavelengths: 492/525 nm). As positive control, cells were exposed to 10 µM H₂O₂ (data not shown). Data were expressed as fold increase (FI) of exposed sample over control (untreated cells).

2.4. RNA extraction and QPCR

BEAS-2B cells were collected after 20 h of exposure to 5 µg/cm² of diesel UFP, lysed, and stored in QIAzol Lysis reagent (Qiagen, Hilden, Germany) until RNA extraction. Total RNA was extracted using the miRNeasy extraction kit (Qiagen) and eluted in RNase free-water, according to the manufacturer's guidelines. Quality and quantity of the total RNA samples were evaluated with 2100 Bioanalyzer (Agilent, Santa Clara, CA) and Nanodrop 1000 (Thermo Fisher Scientific, Wilmington, DE), respectively. According to previous investigations, we focused the gene expression analysis on 11 selected genes involved in inflammation (*IL1A*), oxidative stress (aldehyde dehydrogenase 3A1, *ALDH3A1*; heme oxygenase 1, *HMOX1*; thioredoxin reductase 1, *TXNRD1*) and mitogen-activated protein kinase (MAPK) signaling (*IGFBP1*, *EPGN*, *GREM1*, *LIF*, *DAPP1*, *FOSL1*). A customized RT² PCR profiler system (Qiagen, Hilden, Germany) with Sybr green as reporter dye has been used. The

expression of each gene within each sample was normalized using the average expression levels of three housekeeping genes (*ACTB*, *B2M*, *GAPDH*). The fold change was calculated for each conditions using the $2^{-\Delta\Delta Ct}$ method comparing ΔCt of UFP treated cells to ΔCt of control untreated cells. Data of two independent experiments are reported.

2.5. Western blotting

After 24 h of exposure to conditioned media, HPMEC-ST1.6R cells were scraped and lysed on ice in RIPA buffer (150 mM NaCl, 1% TritonX-100, 0.5% sodium deoxycholate, 0.1% SDS, 50 mM Tris pH 8.0 and 0.1% of protease inhibitors, added just before use). The total protein content was evaluated by the bicinchoninic acid assay (Sigma Aldrich) according to the manufacturer's instruction. Equal amounts of proteins were loaded onto 10% SDS-PAGE (Sodium Dodecyl Sulphate - PolyAcrylamide Gel Electrophoresis) gels, separated and transferred on nitrocellulose membranes. Equal loading was assessed by Ponceau red staining of membranes. The membranes were then blocked for 1 h (Tris-buffered saline, TBS, 0.1% Tween20, 5% (w/v) Bovine Serum Albumin, BSA) and incubated at 4 °C overnight with specific primary antibody diluted according to datasheets (CD54/ICAM-1, VCAM-1 and β -actin for loading control, 1:1000, Cell Signalling Technology, Danvers, USA). The day after, membranes were washed in TBS, 0.1% Tween20 and incubated with specific HRP-linked secondary antibodies for 1 h at RT (anti-rabbit IgG, 1:2000, Cell Signalling). After detection with Chemiluminescent Peroxidase Substrate (Euroclone), digital images were taken by a luminescence reader (Biospectrum-UVP, Upland, USA) and densitometry analysis performed with dedicated software (VisionWorks LS).

2.6. Protein arrays

A panel of protein involved in the MAPK and angiogenesis pathways were investigated by antibody arrays (Proteome Profiler Human Phospho-MAPK Array Kit cod. ARY002B, Proteome Profiler Human Angiogenesis Array Kit cod. ARY007; R&D Systems, Minneapolis, USA). This method allows to detect simultaneously the relative phosphorylation of 24 different kinases or the expression of 55 angiogenesis related proteins which are captured by relative different antibodies spotted in duplicate on a nitrocellulose membrane. Levels of proteins are then assessed using phospho-specific antibodies and chemiluminescent detection. After exposure well plates with cells were stored overnight at -80 °C. Cells were then scraped on ice in provided lysis buffer, homogenized using a syringe with needle, rocked at 2-8 °C for 30 minutes and centrifuged (5 min, 14000 x g at 4 °C). Total amount of proteins was assessed by bicinchoninic acid assay (Sigma Aldrich)

and membrane arrays were processed according to the manufacturer's instructions. Briefly, during incubation of membranes with provided blocking buffer for 1 h at room temperature (RT), 300 µg of total proteins of each sample were incubated with Detection antibody for the same time. Subsequently, the mixtures sample/detection antibody were pipetted onto different membranes and incubated overnight at 4 °C on a platform shaker. The day after, membranes were washed 3 times with wash buffer and incubated with Streptavidin-HRP for 30 minutes at RT. The signal intensities for each antigen-specific antibody spots, proportional to the relative concentration of the antigen in the sample, were detected by chemiluminescence and recorded by a luminescence reader (Biospectrum-UVP). Densitometry analysis was performed with dedicated software (VisionWorks LS-UVP). Data were expressed as signal intensity corrected by the signals of positive and negative controls following manufacturer's guidelines, and fold increase (FI) of diesel exposed samples over unexposed (control) are reported in false colour scale.

2.7. ELISA

After exposure, the supernatants of BEAS-2B and HPMEC-ST1.6R cells were collected and protein levels were determined by sandwich ELISA according to the manufacturer's guidelines (IL-6, IL-6R, VEGF, IL-8, MCP-1, TNF- α , Life Technologies). The absorbance of each sample was measured by Multiplate Reader Ascent (Thermo Scientific, USA) at 450 nm and 630 nm, and the amount of proteins in pg/ml calculated on the basis of a standard curve.

2.8. Inhibitory studies

IL-6 antibody (aIL-6) has been used to specifically prevent the binding of this molecule with its receptors on endothelial cells. aIL-6 (1 µg/ml) was added to BEAS-2B supernatants for 2 h at room temperature, and then the supernatants were used for HPMEC-ST1.6R cells exposure for further 24 h. Endothelial cells responses were thus assessed.

2.9. Statistical analyses

Mean and standard error of mean (SEM) of at least three independent experiments are reported. Statistical analyses were performed using Sigma Stat 3.1 software, using t-test. Values of $p < 0.05$ were considered statistically significant.

3. Results

3.1. Effects on epithelial cells

Diesel UFP exposure ($5 \mu\text{g}/\text{cm}^2$) activated oxidative stress response and MAPK signalling in epithelial cells. ROS formation in BEAS-2B cells was observed 1 h after exposure to diesel UFP, with a fold increase of 1.6 over control (**Figure 1**).

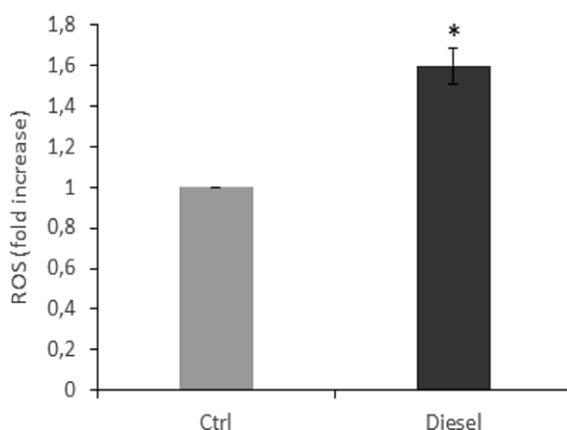


Figure 1. ROS formation in BEAS-2B cells after 1 h exposure to diesel UFP ($5 \mu\text{g}/\text{cm}^2$), measured by carboxy-DCF-DA fluorescence. *Statistically significant according to unpaired t-test $p < 0.05$.

The analysis of gene expression by qPCR evidenced the up-regulation of oxidative stress responsive genes *HMOX1* and *TXNRD1*, and a strong over-expression of *ALDH3A1*, involved in the metabolism of peroxidised lipids (Table 1). Additionally we observed over-expressed levels of several genes related to the MAPK pathway (Table 1).

Table 1

Gene expression in epithelial cells exposed to diesel UFP. FC: fold change.

<i>Gene Symbol (assay ID)^a</i>	<i>FC</i>	<i>FC (min-max)</i>	<i>Biological relevance</i>
<i>ALDH3A1 (PPH07009A)</i>	9.25	7.53-10.96	oxidative stress
<i>CXCL2 (PPH00552F)</i>	1.43	1.26-1.60	MAPK
<i>DAPP1 (PPH00006A)</i>	3.02	1.82-4.22	MAPK
<i>EPGN (PPH19098A)</i>	4.99	3.60-6.38	MAPK
<i>FOSL1 (PPH00145C)</i>	2.82	2.76-2.87	MAPK
<i>GREM1 (PPH01941B)</i>	4.64	3.87-5.40	MAPK
<i>HMOX1 (PPH00161F)</i>	2.53	1.63-3.44	oxidative stress
<i>IER3 (PPH10008F)</i>	2.16	1.51-2.81	MAPK, oxidative stress
<i>IGFBP1 (PPH02046E)</i>	18.11	17.38-18.84	MAPK
<i>IL1A (PPH00690A)</i>	2.58	2.21-2.95	MAPK, inflammation
<i>LIF (PPH00813F)</i>	3.21	2.80-3.63	MAPK
<i>NFE2L2 (PPH06070A)</i>	1.88	1.66-2.11	MAPK
<i>TNFAIP3 (PPH00063A)</i>	2.28	1.93-2.63	inflammation
<i>TXNRD1 (PPH02104F)</i>	2.47	1.48-3.45	oxidative stress
<i>VEGFA (PPH00251C)</i>	1.14	0.90-1.39	MAPK, angiogenesis

^a ID for RT2 qPCR primer assays (Qiagen).

To further confirm the activation of MAPK pathway, we measured the level of 24 proteins involved. By mean of protein array (**Figure 2**), we observed slightly increased levels of the phosphorylated form of almost all the proteins in the pathway. Remarkable increases were reported for Akt proteins (FI was 4.1 and 3.2 for Akt1 and Akt2 respectively, 3.2 for Akt *pan* = all Akts) and for ERK2 (FI was 2.6).

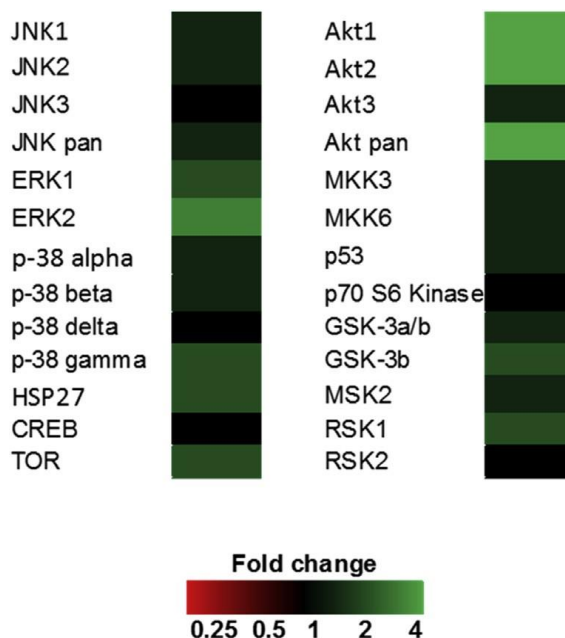


Figure 2. MAPK proteins phosphorylation in BEAS-2B cells after 20 h exposure to diesel UFP (5 mg/cm²), measured by chemiluminescent detection of proper phospho-MAPK protein array. “pan” indicates all the forms of that protein. Fold changes of protein expression, increased (green), decreased (red) or equal (black) compared to untreated cells are reported. (For interpretation of the references to colour in this figure legend, the reader is referred to the web version of this article.)

To assess the modulation of factors renowned to be relevant for inflammation and vascular signalling, we measured the release of cytokines and proteins in the BEAS-2B cells media by ELISA. The secretion of IL-6 and VEGF proteins was found to be significantly increased in cells exposed to diesel UFP (Figure 3) while the levels of IL-8, MCP-1 and TNF- α were not significantly modified respect to control (data not shown).

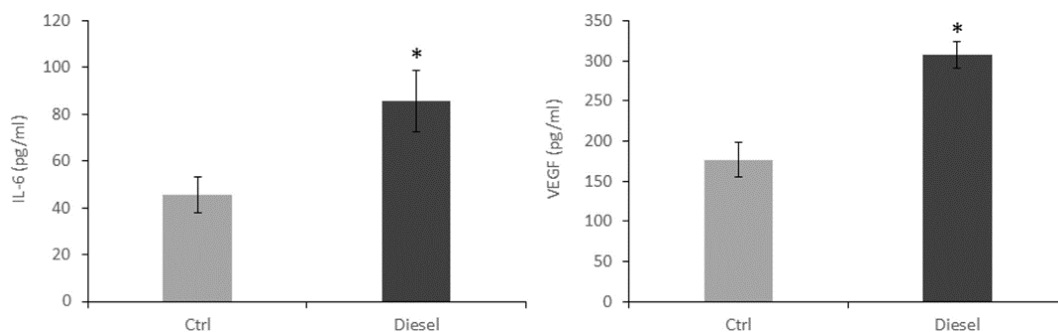


Figure 3. Proteins secretion (IL-6 and VEGF) from BEAS-2B cells after 20 h exposure to diesel UFP (5 mg/cm²), measured by ELISA. *Statistically significant according to unpaired t-test $p < 0.05$.

3.2. Effects on endothelial cells

HPMEC-ST1.6R cells were treated for 24 h with the media collected from epithelial cultures. The analysis of MAPK (Figure 4a) and angiogenesis (Figure 4b) pathways activation in HPMEC cells by protein arrays showed a very weak modulation, involving only few proteins with a fold change between 0.6 and 1.4.

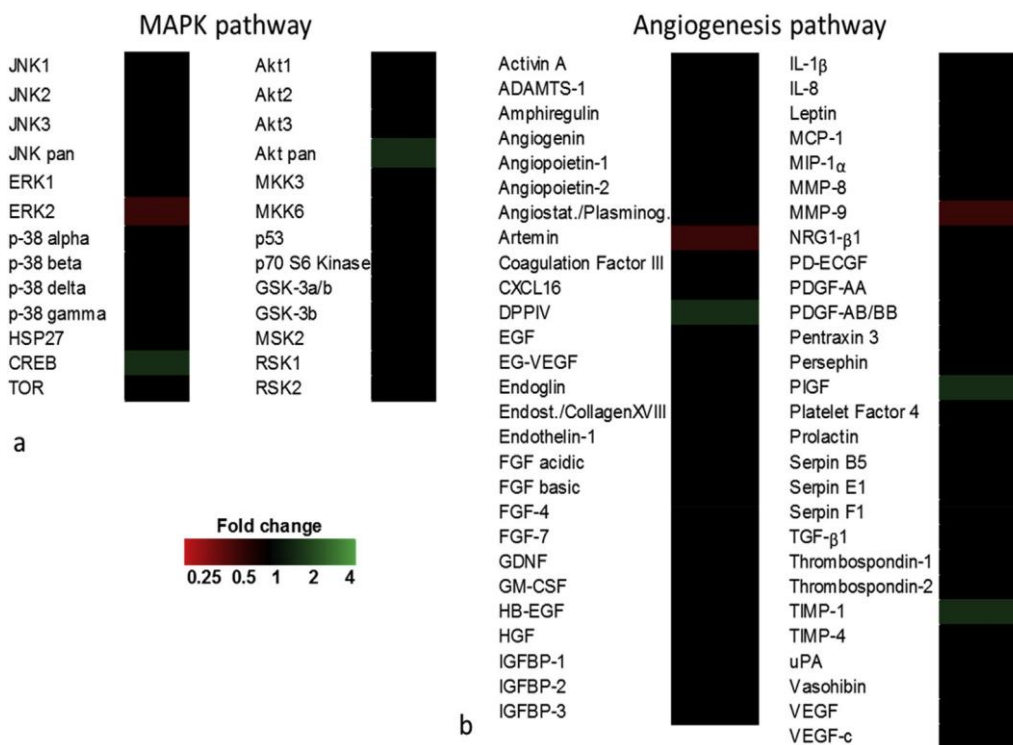


Figure 4. MAPK (a) and angiogenesis (b) pathways activation in HPMEC cells after 24 h exposure to conditioned media, measured by chemiluminescent detection of protein arrays. Fold changes of protein expression, increased (green), decreased (red) or equal (black) compared to untreated cells are reported. (For interpretation of the references to colour in this figure legend, the reader is referred to the web version of this article.)

ICAM-1 and VCAM-1 protein expression was investigated as typical markers of endothelial activation, and found significantly augmented in HPMEC-ST1.6R cells indirectly exposed to diesel particles (Figure 5).

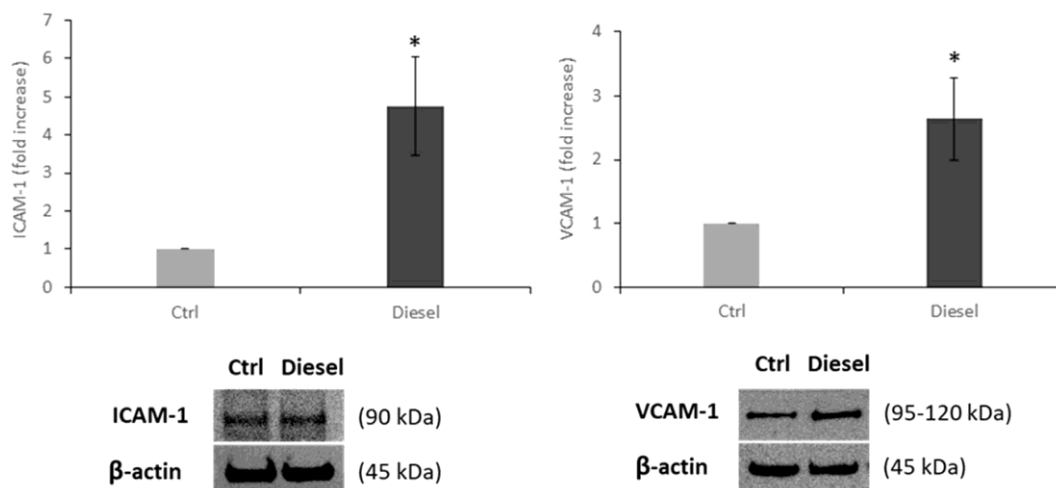


Figure 5. ICAM-1 and VCAM-1 protein expression in HPMEC-ST1.6R cells after 24 h exposure to conditioned media, measured by western blotting. The protein expression is normalized over the housekeeping protein β -actin and data are presented as fold increase over the control. *Statistically significant according to unpaired t-test $p < 0.05$.

3.3. Mechanisms of endothelial activation

Both VEGF and IL-6 signalling can activate ICAM-1 and VCAM-1 transcription in endothelial cells. VEGF-dependent modulation goes through MAPK cascade signalling (Maitland et al., 2010; Radisavljevic et al., 2000). Since we found that this pathway is weakly modulated in our samples, we focused on IL-6 as a possible mediator responsible for endothelial activation. IL-6 interacts with endothelial cells through the so called trans-signalling pathway: IL-6 circulating in the serum forms a complex with the soluble form of interleukin-6 receptor (IL-6R), and then binds to the gp130 receptor on endothelial cells membrane (Barnes et al., 2011; Rose-John, 2012). Thus, in order to verify the role of IL-6 signalling in the modulation of adhesion molecules in our model, we first measured IL-6R levels in BEAS-2B supernatants and then we interfered with the binding of IL-6 to gp130 receptor by adding IL-6 antibody to supernatants. The results showed that IL-6R was significantly increased in diesel UFP exposed cells compared to control (Figure 6).

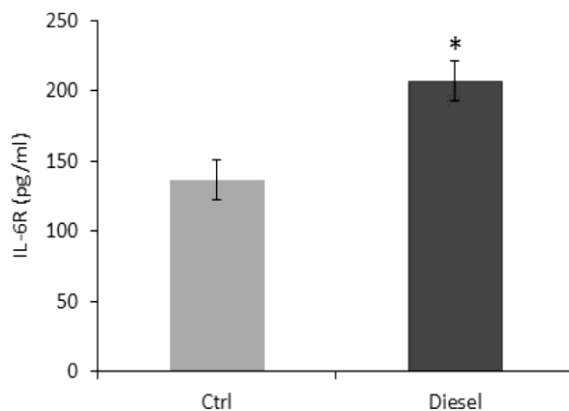


Figure 6. IL-6R levels in BEAS-2B cells supernatants after 20 h exposure to diesel UFP (5 mg/cm²), measured by ELISA. *Statistically significant according to unpaired t-test $p < 0.05$.

When IL-6 antibody was added to the media, a not significant increase of ICAM-1 and VCAM-1 levels was observed in control cells, suggesting that the antibody may present some affinity for IL-6R and/or gp130, and thus may partly work as an agonist to gp130 receptor (Figure 7). Anyway, in samples exposed to diesel-conditioned media, the addition of IL-6 antibody reduced ICAM-1 and VCAM-1 over-expression, indicating the role of IL-6 in their modulation (Figure 7).

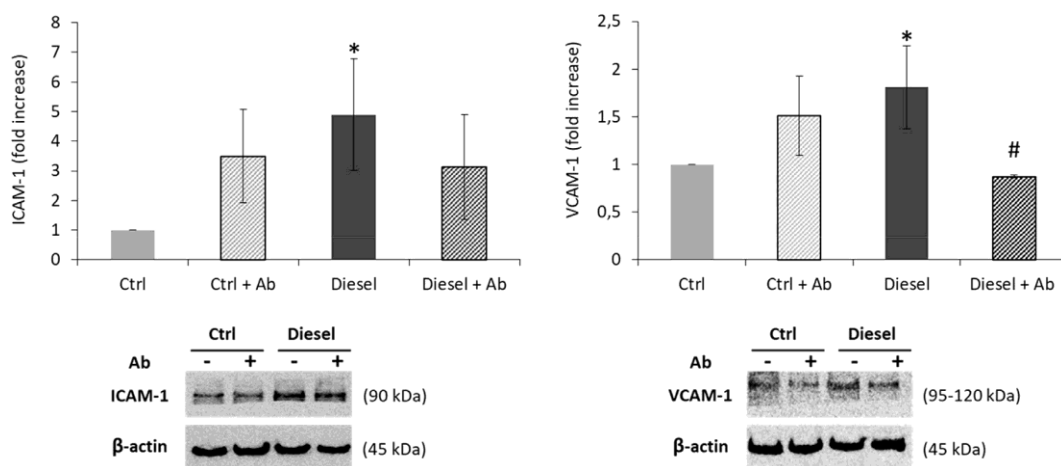


Figure 7. ICAM-1 and VCAM-1 protein expression in HPMEC cells after 24 h exposure to conditioned media, with (+Ab) and without IL-6 antibody interference, measured by western blotting. The protein expression is normalized over the housekeeping protein β -actin and data are presented as fold increase over the control. *Statistically significant respect to untreated cells (Ctrl) according to unpaired t-test $p < 0.05$. # Statistically significant respect to cells exposed to diesel-conditioned media (Diesel) according to unpaired t-test $p < 0.05$.

4. Discussion

In this research we have used an *in vitro* model based on conditioned media to investigate the mechanisms of diesel particles-induced vascular effects. A possible mechanism based on our results is proposed below (Figure 8).

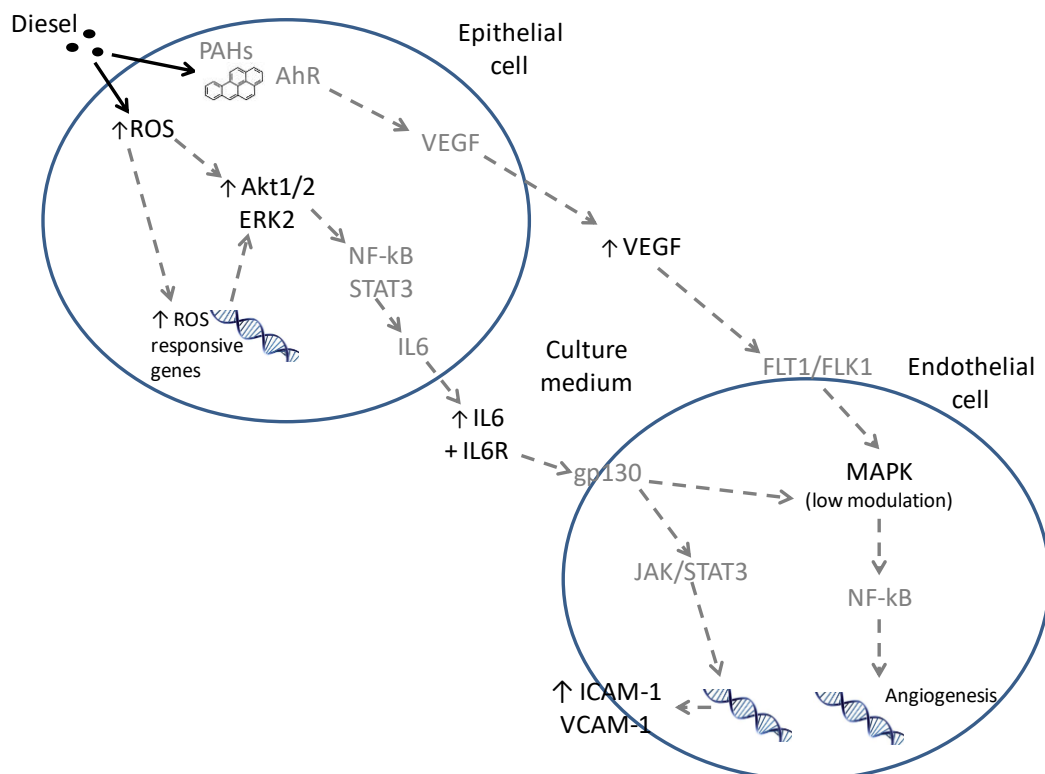


Figure 8. Summary of the events measured in BEAS-2B and HPMEC-ST1.6R cells, and possible correlations among them. In black: measured events. Possibly involved factors (in grey) and signalling/correlations (broken arrows) are suggested according to the literature. PAH: polycyclic aromatic hydrocarbons.

BEAS-2B lung epithelial cells directly exposed to particles exhibited higher levels of ROS and the activation of oxidative stress-responsive genes. The strongest modulated gene was *ALDH3A1*, an AhR-responsive gene participating in xenobiotic metabolism and involved in the detoxification of aldehydes generated by lipid peroxidation. The modulation of this gene has been previously reported in animals and cells exposed to different types of combustion particles, and indicates the role of organic compounds, mostly polycyclic aromatic hydrocarbons (PAHs), in driving cellular oxidative effects (Líbalová et al., 2014; Noël et al., 2016).

Other oxidative stress-responsive genes here modulated are *NFE2L2* transcription factor and its targets HMOX1 and TXNRD1, enzymes with a protective role against oxidative stress. Among genes with altered expression, several were related to MAPK pathway, e.g. *IGFBP1*, *EPGN*, *GREM1*, *LIF*, *DAPP1*, *FOSL1*, *IL1A* and *CXCL2*. MAPK pathway activation was then validated at protein level by the increased expression of phosphorylated active forms, in particular of Akt1/2 and ERK2. These proteins, known to respond mainly to growth factors signal, were also shown to be directly activated by ROS (Zhang et al., 2016). They are involved in the regulation of many processes including metabolism, proliferation, cell survival, growth, angiogenesis and cytokine production (Zhang et al., 2016). Akt has been reported to activate NF- κ B, a renowned factor inducing cytokines transcription (Dan et al., 2008), and interestingly it has been shown to directly modulate IL-6 levels, through NF- κ B and STAT3 regulation (Malanga et al., 2015).

IL-6 secretion by lung epithelial cells exposed to diesel particles was previously reported (Nemmar et al., 2013) and here confirmed. Mediators found in other studies e.g. IL-8 and MCP-1, were not modulated. Increased levels of VEGF were instead measured. Interestingly, aryl hydrocarbon receptor (AhR) agonists were reported to upregulate VEGF secretion from bronchial epithelial cells (Tsai et al., 2015). This mechanism might be of great importance for cardiovascular diseases induced by diesel particles, as AhR is largely recognized to be a main receptor of diesel-adsorbed organic compounds (Pálková et al., 2015). VEGF is a potent inducer of angiogenesis, through the interaction with FLT1, KDR, or NRP1 receptors on endothelial cells membrane, and the subsequent activation of RAS and MAPK kinases signalling cascades (Maitland et al., 2010). In our case, we found a very weak modulation of MAPK pathway and angiogenesis-related proteins in endothelial cells exposed to conditioned media. We assumed that the levels of VEGF released (around 300 pg/ml) were too low to induce a significant response, since much higher concentrations of VEGF (10-100 ng/ml) are normally used to investigate its effects on endothelial cells (Chang et al., 2000; Tseng et al., 2015).

In our model, the levels of adhesion molecules ICAM-1 and VCAM-1 were significantly increased in endothelial cells exposed to conditioned media. ICAM-1/VCAM-1 over-expression is a marker of endothelial activation and leads to monocyte/lymphocyte recruitment and infiltration into the sub-endothelium (Tedgui and Mallat, 2006). It occurs in response of several stimuli and has been reported in cells, animals and humans exposed to diesel or ambient particles (Araujo and Nel, 2009; Hemmingsen et al., 2011; Krishnan et al., 2013; Salvi et al., 1999). The increased expression of these molecules in endothelial cells can be induced by IL-6 trans-signalling (Barnes et al., 2011). This pathway occurs in cells that do not express the interleukin-6 receptor IL-6R, like endothelial cells. In humans, soluble IL-6R exists in the serum, released by several cell types, and bind to IL-6 forming an IL-6/sIL-6R complex. This complex can bind to gp130 receptor on

endothelial cells membrane and activate STAT3 and its target genes, including ICAM-1 and VCAM-1 (Rose-John, 2012). Thus, here we first assessed the availability of IL-6R in BEAS-2B supernatants and found its overexpression after diesel exposure. Then we successfully inhibited ICAM-1 and VCAM-1 over-expression induced by diesel by interfering with IL-6/gp130 binding by the addition of IL-6 antibody to epithelial cells media. Our results demonstrate the role of IL-6 released by the epithelial cells in inducing the observed effects on endothelial cells.

Previous *in vitro* studies compared direct and indirect effects of particles on endothelial cells or cardiomyocytes (Gorr et al., 2015; Totlandsdal et al., 2008; Weldy et al., 2011). Although in all these papers both direct and indirect effects were reported, there was general agreement that the particles concentrations used for direct exposure of endothelial cells likely overestimate the *in vivo* concentration found in the vascular system, due to the small fraction of translocated particles. Besides, the pathways of translocation into the bloodstream are still not clear, as well as the modifications that particles may undergo along this process, making the direct exposure experiments poorly representative of the real situation (Gorr et al., 2015). On the other hand, indirect effects involving the release of inflammatory factors from the exposed lung look highly relevant for the vascular outcomes, and it is possible that the small fraction of translocated particles contributes to this complex mechanism.

Previous investigations to individuate the mediators responsible for indirect effects to the vascular system gave divergent results, further highlighting the complexity of this issue. In a model involving bronchial cells directly exposed to diesel particles and cardiomyocytes exposed to conditioned media, MCP-1 was individuated as the main contributor to the cardiomyocyte dysfunction observed (Gorr et al., 2015), while in another model the role of IL-1 was demonstrated by the use of an IL-1 receptor antagonist (Totlandsdal et al., 2008). With an interesting but slightly different approach, plasma from healthy human volunteers exposed to DEP was used to treat endothelial cells, and significant increase of VCAM-1 mRNA was observed (Channell et al., 2012). In a follow-up study, the same authors measured IL-6 and TNF- α in plasma as possible mediators of endothelial effects, but these markers were not increased (Schisler et al., 2015). These proteins were however found to be augmented in plasma of exposed humans in other studies (Hilt et al., 2002; Törnqvist et al., 2007; Xu et al., 2013). It is likely that the mediators released might differ according to several factors such as particles properties (Li et al., 2010; Totlandsdal et al., 2015), exposure dose and, in particular with regard to human exposure, genetic polymorphism and health status of the subjects investigated (Ljungman et al., 2009; Stenfors et al., 2004). As a last consideration, the mediators found in peripheral blood might not be the same factors released by the lung and acting at local level on the pulmonary vessels, which might respond by releasing other mediators.

In conclusion, here we show that a conditioned media model is capable to induce a response in endothelial cells indirectly exposed to diesel UFP, consisting in the modulation of the adhesion molecules ICAM-1 and VCAM-1. We demonstrate that IL-6 released by epithelial cells after diesel UFP exposure is responsible for the effects observed in endothelial cells. Our approach might be useful to investigate local mediators involved in initial endothelial activation, which may have further consequences. The relatively low dose and the exposure time here used caused limited responses both in epithelial and endothelial cells. Further investigations, involving a similar model undergoing repeated exposures, might provide interesting results also regarding the role of VEGF.

Acknowledgments

This study has been supported by Cariplo Foundation (Grant no. 2013-1038).

References

- Araujo, J.A., Nel, A.E., 2009. Particulate matter and atherosclerosis: role of particle size, composition and oxidative stress. Part. Fibre Toxicol. 6, 24. doi:10.1186/1743-8977-6-24
- Barnes, T.C., Anderson, M.E., Moots, R.J., 2011. The many faces of interleukin-6: the role of IL-6 in inflammation, vasculopathy, and fibrosis in systemic sclerosis. *Int. J. Rheumatol.* 2011, 721608. doi:10.1155/2011/721608
- BéruBé, K., Balharry, D., Sexton, K., Koshy, L., Jones, T., 2007. Combustion-derived nanoparticles: Mechanisms of pulmonary toxicity. *Clin. Exp. Pharmacol. Physiol.* 34, 1044–1050. doi:10.1111/j.1440-1681.2007.04733.x
- Chang, Y.S., Munn, L.L., Hillsley, M. V., Dull, R.O., Yuan, J., Lakshminarayanan, S., Gardner, T.W., Jain, R.K., Tarbell, J.M., 2000. Effect of Vascular Endothelial Growth Factor on Cultured Endothelial Cell Monolayer Transport Properties. *Microvasc. Res.* 59, 265–277. doi:10.1006/mvres.1999.2225
- Channell, M.M., Paffett, M.L., Devlin, R.B., Madden, M.C., Campen, M.J., 2012. Circulating factors induce coronary endothelial cell activation following exposure to inhaled diesel exhaust and nitrogen dioxide in humans: evidence from a novel translational in vitro model. *Toxicol. Sci.* 127, 179–86. doi:10.1093/toxsci/kfs084
- Dan, H.C., Cooper, M.J., Cogswell, P.C., Duncan, J.A., Ting, J.P.-Y., Baldwin, A.S., 2008. Akt-dependent regulation of NF- κ B is controlled by mTOR and Raptor in association with IKK. *Genes Dev.* 22, 1490–500. doi:10.1101/gad.1662308
- Galkina, E., Ley, K., 2007. Vascular Adhesion Molecules in Atherosclerosis. *Arterioscler. Thromb. Vasc. Biol.* 27, 2292–2301. doi:10.1161/ATVBAHA.107.149179
- Gorr, M.W., Youtz, D.J., Eichenseer, C.M., Smith, K.E., Nelin, T.D., Cormet-Boyaka, E., Wold, L.E., 2015. In vitro particulate matter exposure causes direct and lung-mediated indirect effects on cardiomyocyte function. *Am. J. Physiol. - Hear. Circ. Physiol.* 309, H53–H62. doi:10.1152/ajpheart.00162.2015
- Hemmingsen, J.G., Møller, P., Nøjgaard, J.K., Roursgaard, M., Loft, S., 2011. Oxidative Stress, Genotoxicity, And Vascular Cell Adhesion Molecule Expression in Cells Exposed to Particulate Matter from Combustion of Conventional Diesel and Methyl Ester Biodiesel Blends. *Environ. Sci. Technol.* 45, 8545–8551. doi:10.1021/es200956p
- Hilt, B., Qvenild, T., Holme, J., Svendsen, K., Ulvestad, B., 2002. Increase in interleukin-6 and fibrinogen after exposure to dust in tunnel construction workers. *Occup. Environ. Med.* 59, 9–12. doi:10.1136/oem.59.1.9
- Kelly, F.J., Fussell, J.C., 2015. Linking ambient particulate matter pollution effects with oxidative biology and immune responses. *Ann. N. Y. Acad. Sci.* 1340, 84–94. doi:10.1111/nyas.12720
- Klepczyńska-Nyström, A., Sanchez-Crespo, A., Andersson, M., Falk, R., Lundin, A., Larsson, B.-M., Svartengren, M., 2012. The pulmonary deposition and retention of indium-111 labeled ultrafine carbon particles in healthy individuals. *Inhal. Toxicol.* 24, 645–51. doi:10.3109/08958378.2012.708065
- Kreyling, W.G., Semmler-Behnke, M., Seitz, J., Scymczak, W., Wenk, A., Mayer, P.,

- Takenaka, S., Oberdörster, G., 2009. Size dependence of the translocation of inhaled iridium and carbon nanoparticle aggregates from the lung of rats to the blood and secondary target organs. *Inhal. Toxicol.* 21 Suppl 1, 55–60.
doi:10.1080/08958370902942517
- Krishnan, R.M., Sullivan, J.H., Carlsten, C., Wilkerson, H.-W., Beyer, R.P., Bammler, T., Farin, F., Peretz, A., Kaufman, J.D., 2013. A randomized cross-over study of inhalation of diesel exhaust, hematological indices, and endothelial markers in humans. *Part. Fibre Toxicol.* 10, 7. doi:10.1186/1743-8977-10-7
- Lee, B.-J., Kim, B., Lee, K., 2014. Air pollution exposure and cardiovascular disease. *Toxicol. Res.* 30, 71–5. doi:10.5487/TR.2014.30.2.071
- Lewtas, J., 2007. Air pollution combustion emissions: characterization of causative agents and mechanisms associated with cancer, reproductive, and cardiovascular effects. *Mutat. Res.* 636, 95–133. doi:10.1016/j.mrrev.2007.08.003
- Li, R., Ning, Z., Majumdar, R., Cui, J., Takabe, W., Jen, N., Sioutas, C., Hsiai, T., 2010. Ultrafine particles from diesel vehicle emissions at different driving cycles induce differential vascular pro-inflammatory responses: implication of chemical components and NF-kappaB signaling. *Part. Fibre Toxicol.* 7, 6. doi:10.1186/1743-8977-7-6
- Líbalová, H., Krcková, S., Uhlířová, K., Kléma, J., Ciganek, M., Rössner, P., Srám, R.J., Vondráček, J., Machala, M., Topinka, J., 2014. Analysis of gene expression changes in A549 cells induced by organic compounds from respirable air particles. *Mutat. Res. - Fundam. Mol. Mech. Mutagen.* 770, 94–105. doi:10.1016/j.mrfmmm.2014.10.002
- Ljungman, P., Bellander, T., Schneider, A., Breitner, S., Forastiere, F., Hampel, R., Illig, T., Jacquemin, B., Katsouyanni, K., von Klot, S., Koenig, W., Lanki, T., Nyberg, F., Pekkanen, J., Pistelli, R., Pitsavos, C., Rosenqvist, M., Sunyer, J., Peters, A., 2009. Modification of the interleukin-6 response to air pollution by interleukin-6 and fibrinogen polymorphisms. *Environ. Health Perspect.* 117, 1373–9.
doi:10.1289/ehp.0800370
- Longhin, E., Gualtieri, M., Capasso, L., Bengalli, R., Mollerup, S., Holme, J., Øvrevik, J., Casadei, S., Di Benedetto, C., Parenti, P., Camatini, M., 2016. Physico-chemical properties and biological effects of diesel and biomass particles. *Env. Pollut.* 215, 366–375. doi:10.1016/j.envpol.2016.05.015
- Maitland, M.L., Lou, X.J., Ramirez, J., Desai, A.A., Berlin, D.S., McLeod, H.L., Weichselbaum, R.R., Ratain, M.J., Altman, R.B., Klein, T.E., 2010. Vascular endothelial growth factor pathway. *Pharmacogenet. Genomics* 20, 346–9.
doi:10.1097/FPC.0b013e3283364ed7
- Malanga, D., De Marco, C., Guerriero, I., Colelli, F., Rinaldo, N., Scrima, M., Mirante, T., De Vitis, C., Zoppoli, P., Ceccarelli, M., Riccardi, M., Ravo, M., Weisz, A., Federico, A., Franco, R., Rocco, G., Mancini, R., Rizzuto, A., Gulletta, E., Ciliberto, G., Viglietto, G., 2015. The Akt1/IL-6/STAT3 pathway regulates growth of lung tumor initiating cells. *Oncotarget* 6, 42667–86. doi:10.18632/oncotarget.5626
- Mestas, J., Ley, K., 2008. Monocyte-endothelial cell interactions in the development of atherosclerosis. *Trends Cardiovasc. Med.* 18, 228–32.
doi:10.1016/j.tcm.2008.11.004

- Mills, N.L., Donaldson, K., Hadoke, P.W., Boon, N.A., MacNee, W., Cassee, F.R., Sandström, T., Blomberg, A., Newby, D.E., 2009. Adverse cardiovascular effects of air pollution. *Nat. Clin. Pract. Cardiovasc. Med.* 6, 36–44. doi:10.1038/ncpcardio1399
- Nemmar, A., Holme, J.A., Rosas, I., Schwarze, P.E., Alfaro-Moreno, E., 2013. Recent advances in particulate matter and nanoparticle toxicology: a review of the in vivo and in vitro studies. *Biomed Res. Int.* 2013, 279371. doi:10.1155/2013/279371
- Noël, A., Xiao, R., Perveen, Z., Zaman, H.M., Rouse, R.L., Paulsen, D.B., Penn, A.L., 2016. Incomplete lung recovery following sub-acute inhalation of combustion-derived ultrafine particles in mice. *Part. Fibre Toxicol.* 13, 10. doi:10.1186/s12989-016-0122-z
- Pálková, L., Vondráček, J., Trilecová, L., Ciganek, M., Pěňčíková, K., Neča, J., Milcová, A., Topinka, J., Machala, M., 2015. The aryl hydrocarbon receptor-mediated and genotoxic effects of fractionated extract of standard reference diesel exhaust particle material in pulmonary, liver and prostate cells. *Toxicol Vitro.* 29, 438–48. doi:10.1016/j.tiv.2014.12.002.
- Radisavljevic, Z., Avraham, H., Avraham, S., 2000. Vascular endothelial growth factor up-regulates ICAM-1 expression via the phosphatidylinositol 3 OH-kinase/AKT/Nitric oxide pathway and modulates migration of brain microvascular endothelial cells. *J. Biol. Chem.* 275, 20770–4. doi:10.1074/jbc.M002448200
- Rose-John, S., 2012. IL-6 trans-signaling via the soluble IL-6 receptor: importance for the pro-inflammatory activities of IL-6. *Int. J. Biol. Sci.* 8, 1237–47.
- Salvi, S., Blomberg, A., Rudell, B., Kelly, F., Sandström, T., Holgate, S.T., Frew, A., 1999. Acute Inflammatory Responses in the Airways and Peripheral Blood After Short-Term Exposure to Diesel Exhaust in Healthy Human Volunteers. *Am. J. Respir. Crit. Care Med.* 159, 702–709. doi:10.1164/ajrccm.159.3.9709083
- Schisler, J.C., Ronnebaum, S.M., Madden, M., Channell, M.M., Campen, M.J., Willis, M.S., 2015. Endothelial Inflammatory Transcriptional Responses Induced by Plasma Following Inhalation of Diesel Emissions. *Inhal Toxicol.* 27, 272–80. doi:10.3109/08958378.2015.1030481
- Schwarze, P.E., Totlandsdal, A.I., Låg, M., Refsnes, M., Holme, J.A., Øvrevik, J., Schwarze, P.E., Totlandsdal, A.I., M. Refsnes, M.L., Holme, J.A., Øvrevik, J., Låg, M., Refsnes, M., Holme, J.A., Øvrevik, J., 2013. Inflammation-Related Effects of Diesel Engine Exhaust Particles: Studies on Lung Cells In Vitro. *Hindawi Publ. Corp. BioMed Res. Int.* 2013, 685142. doi:10.1155/2013/685142
- Stenfors, N., Nordenhäll, C., Salvi, S.S., Mudway, I., Söderberg, M., Blomberg, A., Helleday, R., Levin, J.O., Holgate, S.T., Kelly, F.J., Frew, A.J., Sandström, T., 2004. Different airway inflammatory responses in asthmatic and healthy humans exposed to diesel. *Eur. Respir. J.* 23, 82–6.
- Stone, V., Miller, M.R., Clift, M.J.D., Elder, A., Mills, N.L., Møller, P., Schins, R.P.F., Vogel, U., Kreyling, W.G., Jensen, K.A., Kuhlbusch, T.A.J., Schwarze, P.E., Hoet, P., Pietroiusti, A., De Vizcaya-Ruiz, A., Baeza-Squiban, A., Tran, C.L., Cassee, F.R., 2016. Nanomaterials vs Ambient Ultrafine Particles: an Opportunity to Exchange Toxicology Knowledge. *Environ. Health Perspect.* doi:10.1289/EHP424
- Tedgui, A., Mallat, Z., 2006. Cytokines in atherosclerosis: pathogenic and regulatory

- pathways. *Physiol. Rev.* 86, 515–81. doi:10.1152/physrev.00024.2005
- Törnqvist, H., Mills, N.L., Gonzalez, M., Miller, M.R., Robinson, S.D., Megson, I.L., Macnee, W., Donaldson, K., Söderberg, S., Newby, D.E., Sandström, T., Blomberg, A., 2007. Persistent endothelial dysfunction in humans after diesel exhaust inhalation. *Am. J. Respir. Crit. Care Med.* 176, 395–400. doi:10.1164/rccm.200606-872OC
- Totlandsdal, A.I., Låg, M., Lilleaas, E., Cassee, F., Schwarze, P., 2015. Differential proinflammatory responses induced by diesel exhaust particles with contrasting PAH and metal content. *Environ. Toxicol.* 30, 188–96. doi:10.1002/tox.21884
- Totlandsdal, A.I., Refsnes, M., Skomedal, T., Osnes, J.-B., Schwarze, P.E., Låg, M., 2008. Particle-induced cytokine responses in cardiac cell cultures--the effect of particles versus soluble mediators released by particle-exposed lung cells. *Toxicol. Sci.* 106, 233–41. doi:10.1093/toxsci/kfn162
- Tsai, M.-J., Wang, T.-N., Lin, Y.-S., Kuo, P.-L., Hsu, Y.-L., Huang, M.-S., 2015. Aryl hydrocarbon receptor agonists upregulate VEGF secretion from bronchial epithelial cells. *J. Mol. Med.* 93, 1257–1269. doi:10.1007/s00109-015-1304-0
- Tseng, C.-Y., Chang, J.-F., Wang, J.-S., Chang, Y.-J., Gordon, M.K., Chao, M.-W., 2015. Protective Effects of N-Acetyl Cysteine against Diesel Exhaust Particles-Induced Intracellular ROS Generates Pro-Inflammatory Cytokines to Mediate the Vascular Permeability of Capillary-Like Endothelial Tubes. *PLoS One* 10, e0131911. doi:10.1371/journal.pone.0131911
- Tseng, C.Y., Wang, J.S., Chao, M.W., 2016. Causation by Diesel Exhaust Particles of Endothelial Dysfunctions in Cytotoxicity, Pro-inflammation, Permeability, and Apoptosis Induced by ROS Generation. *Cardiovasc. Toxicol.* 1–9. doi:10.1007/s12012-016-9364-0
- Weldy, C.S., Wilkerson, H.-W., Larson, T. V., Stewart, J.A., Kavanagh, T.J., 2011. DIESEL particulate exposed macrophages alter endothelial cell expression of eNOS, iNOS, MCP1, and glutathione synthesis genes. *Toxicol. Vitr.* 25, 2064–2073. doi:10.1016/j.tiv.2011.08.008
- Xu, Y., Barregard, L., Nielsen, J., Gudmundsson, A., Wierzbicka, A., Axmon, A., Jönsson, B.A.G., Kåredal, M., Albin, M., 2013. Effects of diesel exposure on lung function and inflammation biomarkers from airway and peripheral blood of healthy volunteers in a chamber study. *Part. Fibre Toxicol.* 10, 60. doi:10.1186/1743-8977-10-60
- Zhang, J., Wang, X., Vikash, V., Ye, Q., Wu, D., Liu, Y., Dong, W., 2016. ROS and ROS-Mediated Cellular Signaling. *Oxid. Med. Cell. Longev.* 2016, 4350965. doi:10.1155/2016/4350965

Conclusions and future perspectives

In recent years, air quality regulations have been approved by many countries around the world to preserve health of the exposed population from the negative effects of air pollution (Nemmar et al., 2013). Although new combustion technologies have been developed and particulate emissions have been generally reduced, it is not clearly understood if these changes have resulted in an analogous reduction in the toxic properties of the emitted particles.

Despite numerous efforts have been performed to investigate the health impact of particulate matter (PM), the mechanisms linking size, shape and chemical composition of particles with the biological outcomes have not yet been fully clarified. Furthermore, the relationship between the different emission sources and the biological effects of the emitted particles is still unclear.

Diesel and Biomass combustion-derived particles (CDPs) largely contribute to air pollution and likely to the adverse health effects. In recent years, great attention has been committed to CDPs, since numerous studies have described their involvement in the onset of several pulmonary and cardiovascular diseases. Considering that, acquire importance to fulfill the knowledge regarding CDPs adverse effects on humans in order to develop harmless combustion technologies and to define requisite for selection of a safer type of fuel.

The present work provides a focus on the biological responses induced by CDPs on lung cells cultured *in vitro*. Low doses were chosen to mimic as much as possible a realistic exposure scenario to the selected CDP sources. The doses selected for experiments indeed represents an exposure scenario similar to that of large urban centers, where winter daily PM concentrations can exceed $70 \mu\text{g}/\text{m}^3$ (Li et al., 2003). Particular attention was given to biomass particles obtained from combustion of different fuels in the same stove and its mechanisms of action.

The comparison of the different sources and effects with the particle physico-chemical properties allowed to assess some important mechanisms that are crucial in the toxicity outcomes. The particle properties are known to change in relation with different parameters. With regards to biomass type of fuel, combustion condition and combustion appliances are the main factors that establish the physical and chemical characteristics of particles.

In the first part of the research, the effects of fuel type on the biological outcomes was explored and the results evidenced different toxic potential for PMs emitted from diverse source. The main distinctions can be done between particles derived from pellet combustion and the ones obtained from charcoal and wood. Results showed that pellet PM was the most cytotoxic and genotoxic. Particles from charcoal and wood presented a different behavior, eliciting effects on oxidative stress, xenobiotic metabolism and EMT. These results can be described by the particle chemical composition, which was peculiar for pellet, while charcoal and wood samples had quite similar composition, characterized by a consistent amount

of PAHs. In particular, pellet PM resulted to have a higher content of metals with respect to the others sources (Marchetti et al., 2019).

In the present work, the evaluations of the biomass particles were performed mainly on the A549 cell line, widely used in the research as it proved to be a valid model for testing the cytotoxic effects of PM (Chirino et al., 2017; Choi et al., 2016; Gualtieri et al., 2012; Kasurinen et al., 2017; Rossner et al., 2016; Danielsen et al., 2009; Marabini et al., 2017; Sánchez-Pérez et al., 2009).

Considering that the research is aimed at comparatively investigating the biological effects of PM₁₀s emitted indoor from the burning of different biomasses and that can be considered pioneer in this field, we retained to start the experimentation by using the most diffuse – routinely used – cell line. We are conscious that for additional mechanistic studies, regarding early-carcinogenesis and genotoxicity, more relevant cell lines (such as BEAS-2B or HBEC) should be recommended. Besides, it has been taken into account that previous studies demonstrated that A549 cell line retains several characteristics of human lung epithelial cells, i.e. in CYP expression modulation (Hukkanen et al., 2000). Moreover, A549 cell line has been recognized in literature as a valid model for EMT investigations. Buckley et al. (2010), indeed explored the ability of different epithelial cells to undergo EMT when exposed to the transforming growth factor- β 1 (TGF- β 1) and other pro-inflammatory mediators. The study reported that only A549 cells exhibited enhanced morphological and phenotypical changes recognized as typical EMT markers, compared to the other cell lines investigated. On the same way, numerous other studies have explored the process activation on A549 cells, validating their use also for carcinogenesis investigations (Kasai et al., 2005; Yang et al., 2017; Morales-Bárceñas et al., 2015)

For all the reasons above, A549 cells were chosen as main *in vitro* pulmonary model in this study.

In Chapter 1 we reported that after acute exposure (24 hours) the main toxicological effects were triggered by pellet, that is responsible of early cytotoxic and genotoxic effects. In particular, we correlated the genotoxic effects observed to the zinc content (Marchetti et al., 2019). Zn-enriched biomass particles indeed, have been reported in literature to induce with high cytotoxicity (Uski et al., 2015) and cell death (Zhang et al., 2012). Moreover, our experiments with a Zinc chelator suggest that it might responsible for the cell cycle alterations reported.

At later time points (72 hours, Chapter 2) main results were observed instead after exposure to charcoal and wood, that revealed pro-carcinogenic properties. Long-term exposure revealed that particles differentially affect cell viability and inflammatory response. Moreover, charcoal and wood promote EMT activation, inducing alterations in cell migration ability and invasion capacity.

Considering results on early and long-term exposure, we might also assume that charcoal and wood being more complex particles (as size, density and surface area)

compared to pellet, need more time to release in the culture media chemical compounds and possibly produce adverse effects on cells.

Lung carcinogenesis studies are widely performed in literature on tumorigenic lung cell lines (such as A549) or epithelial cells immortalized with viral oncogenes (BEAS-2B). Nevertheless, these cell lines with mutated TP53 and/or impaired TP53 signaling are less suitable for studying early steps of lung carcinogenesis. For these reasons, we decided to further explore biomass particles properties on a different cell line, the HBEC3-KT. HBEC3-KT are human bronchial epithelial cells immortalized in absence of viral oncoproteins. This cell line indeed represents a well-suited model for genotoxic and pro-carcinogenic effects investigations (Bersaas et al., 2016; Rynning et al., 2018). Thus, to further elucidate the contribution of the coated-organic compounds in the primary response of lung epithelial cells, biomass-derived organic and washed fractions were also tested.

In Chapter 3 several processes linked to *in vitro* lung carcinogenesis were investigated on HBEC-3KT cells. Our data revealed that the effects induced by the particles and by the adsorbed chemicals depended on the PM source. Exposure to washed particles in general gave less response than whole particles and organic extracts. However, results on organic fractions should be further explored for a better understanding of the contribution of the organic compounds on the observed effects, especially for charcoal and wood.

Despite the slight differences that may be likely addressed to the different experimental model, we can find some common results that suggest critical aspects in the particle interactions with the biological system. With regard to pellet, cytotoxicity and genotoxic properties here reported are suggested to be linked to the high metal content, in accordance with literature. Metals indeed, are known inducer of cytotoxicity (Torvela et al., 2014; Perrone et al., 2010; Van Den Heuvel et al., 2016), different cell death pathways (Zhang et al., 2012) and genotoxic damage (Pati et al., 2016; Perrone et al., 2010; Steenhof et al., 2011).

Our findings on charcoal and wood instead are consistent with other studies in which organic compounds, mostly polycyclic aromatic hydrocarbons (PAHs), are proposed as primarily inducer of cellular inflammatory and oxidative effects (Líbalová et al., 2014; Totlandsdal et al., 2015), xenobiotic metabolism (Dilger et al., 2016; Rossner et al., 2016) response and oxidative DNA damage (Gualtieri et al., 2011; Longhin et al., 2013; Marabini et al., 2017). Additionally, particles with a high PAHs content have been reported to stimulate lung cancer, promoting cell migration and invasion (Longhin et al., 2016; Yue et al., 2015).

Furthermore, our results presenting biomass-particles with high PAH and metal content agree with other studies performed using traditional appliances. Particles emitted from old type appliances indeed, are characterized by high content of PAHs and metals and thus, exert relevant biological effects (Vicente and Alves, 2018). On

the contrary, particles emitted from modern stoves showed low biological effects (Longhin et al., 2016).

It is also important to highlight that our studies focusing for the first time on the potential carcinogenic risk of biomass particles through EMT activation suggest that biomass combustion may be a significant contributor in lung cancer progression. Thus, the study evidence the importance of select biomass fuels as energy source taking into account the chemical composition and the biological behavior of the emitted particles, in order to reduce harmful effects on human health.

The last part of the research (Chapter 4) was focused on the biological effects produced by a different emission source, the diesel exhaust particles (DEP), which results from the incomplete combustion of diesel engine. Attention was given to the events linking exposure to pollution with oxidative stress, inflammatory events and particle translocation leading to vascular damage. Pulmonary oxidative stress and inflammation indeed trigger the release of cytokines, promoting atherosclerosis, and increasing blood coagulation (Møller et al., 2016). However, the pathways linking lung exposure to DEP with cardiovascular effects remain controversial. In the study, the release of mediators and signaling factors from the epithelium in response to particles exposure was studied, as possible mechanism inducing endothelial activation. To this purpose, a conditioned media *in vitro* system involving both epithelial and endothelial cells was used. The epithelial cells were exposed to DEP enriched in PAHs and the supernatants used to treat endothelial cells. In order to individuate mediators possibly responsible for the reported endothelial responses, inhibitory studies were also performed. Results showed that the endothelial activation is linked to the action of IL-6 and its receptor, released following exposure to DEP (Bengalli et al., 2017).

In conclusion, the research presented underlines the important role of particle chemical composition in triggering significant biological effects. We evidenced that CDPs from different emission sources and fuels may affect at different extent the respiratory health and activate numerous toxicological pathways, according to their composition. Thus, it is important to improve the knowledge on the hazardous effects produced from such compounds.

The role of CDPs on human health is still under investigation and further studies are necessary to assess the CDPs-induced molecular mechanisms responsible for the toxic effects observed at the lung and cardiovascular levels. Future studies should be focused also on the investigation of other systems, increasing the complexity of the model, in order to obtain more realistic and informative data about the how the cross-talk among several cells might influence lung and cardiovascular responses to CDPs exposure.

Moreover, the research highlights the importance to develop new strategies focused on lowering the health hazard coming from the emission of diesel vehicles

and biomass-propelled heating systems possibly by eliminating the sources of the most toxic chemical compounds.

References

- Bengalli, R., Longhin, E., Marchetti, S., Proverbio, M.C., Battaglia, C., Camatini, M., 2017. The role of IL-6 released from pulmonary epithelial cells in diesel UFP-induced endothelial activation. *Environ. Pollut.* 231, 1314–1321. <https://doi.org/10.1016/j.envpol.2017.08.104>
- Bersaas, A., Arnoldussen, Y.J., Sjøberg, M., Haugen, A., Møllerup, S., 2016. Epithelial-mesenchymal transition and FOXA genes during tobacco smoke carcinogen induced transformation of human bronchial epithelial cells. *Toxicol. Vitro.* 35, 55–65. <https://doi.org/10.1016/j.tiv.2016.04.012>
- Billet, S., Abbas, I., Goff, J. Le, Verdin, A., André, V., Lafargue, P.E., Hachimi, A., Cazier, F., Sichel, F., Shirali, P., Garçon, G., 2008. Genotoxic potential of Polycyclic Aromatic Hydrocarbons-coated onto airborne Particulate Matter (PM_{2.5}) in human lung epithelial A549 cells. *Cancer Lett.* 270, 144–155. <https://doi.org/10.1016/j.canlet.2008.04.044>
- Buckley, S.T., Medina, C., Ehrhardt, C., 2010. Differential susceptibility to epithelial-mesenchymal transition (EMT) of alveolar, bronchial and intestinal epithelial cells in vitro and the effect of angiotensin II receptor inhibition. *Cell Tissue Res.* <https://doi.org/10.1007/s00441-010-1029-x>
- Chirino, Y.I., García-Cuellar, C.M., García-García, C., Soto-Reyes, E., Osornio-Vargas, Á.R., Herrera, L.A., López-Saavedra, A., Miranda, J., Quintana-Belmares, R., Pérez, I.R., Sánchez-Pérez, Y., 2017. Airborne particulate matter in vitro exposure induces cytoskeleton remodeling through activation of the ROCK-MYPT1-MLC pathway in A549 epithelial lung cells. *Toxicol. Lett.* 272, 29–37. <https://doi.org/10.1016/j.toxlet.2017.03.002>
- Choi, Y., Park, K., Kim, I., Kim, S.D., 2016. Combined toxic effect of airborne heavy metals on human lung cell line A549. *Environ. Geochem. Health.* <https://doi.org/10.1007/s10653-016-9901-6>
- Crobeddu, B., Aragao-Santiago, L., Bui, L.C., Boland, S., Baeza Squiban, A., 2017. Oxidative potential of particulate matter 2.5 as predictive indicator of cellular stress. *Environ. Pollut.* 230, 125–133. <https://doi.org/10.1016/j.envpol.2017.06.051>
- Danielsen, P.H., Loft, S., Kocbach, A., Schwarze, P.E., Møller, P., 2009. Oxidative damage to DNA and repair induced by Norwegian wood smoke particles in human A549 and THP-1 cell lines. *Mutat. Res. - Genet. Toxicol. Environ. Mutagen.* 674, 116–122. <https://doi.org/10.1016/j.mrgentox.2008.10.014>
- Dilger, M., Orasche, J., Zimmermann, R., Paur, H.R., Diabaté, S., Weiss, C., 2016. Toxicity of wood smoke particles in human A549 lung epithelial cells: the role of PAHs, soot and zinc. *Arch. Toxicol.* 90, 3029–3044. <https://doi.org/10.1007/s00204-016-1659-1>

- Gualtieri, M., Longhin, E., Mattioli, M., Mantecca, P., Tinaglia, V., Mangano, E., Carla, M., Bestetti, G., Camatini, M., Battaglia, C., 2012. Gene expression profiling of A549 cells exposed to Milan PM_{2.5}. *Toxicol. Lett.* 209, 136–145. <https://doi.org/10.1016/j.toxlet.2011.11.015>
- Gualtieri, M., Øvrevik, J., Mollerup, S., Asare, N., Longhin, E., Dahlman, H.J., Camatini, M., Holme, J.A., 2011. Airborne urban particles (Milan winter-PM_{2.5}) cause mitotic arrest and cell death: Effects on DNA, mitochondria, AhR binding and spindle organization. *Mutat. Res. - Fundam. Mol. Mech. Mutagen.* 713, 18–31. <https://doi.org/10.1016/j.mrfmmm.2011.05.011>
- Hukkanen, J., Lassila, A., Päiväranta, K., Valanne, S., Sarpo, S., Hakkola, J., Pelkonen, O., Raunio, H., 2000. Induction and regulation of xenobiotic-metabolizing cytochrome P450s in the human A549 lung adenocarcinoma cell line. *Am. J. Respir. Cell Mol. Biol.* 22, 360–366. <https://doi.org/10.1165/ajrcmb.22.3.3845>
- Kasai, H., Allen, J.T., Mason, R.M., Kamimura, T., Zhang, Z., 2005. TGF- β 1 induces human alveolar epithelial to mesenchymal cell transition (EMT). *Respir. Res.* <https://doi.org/10.1186/1465-9921-6-56>
- Kasurinen, S., Jalava, P.I., Happonen, M.S., Sippula, O., Uski, O., Koponen, H., Orasche, J., Zimmermann, R., Jokiniemi, J., Hirvonen, M.R., 2017. Particulate emissions from the combustion of birch, beech, and spruce logs cause different cytotoxic responses in A549 cells. *Environ. Toxicol.* <https://doi.org/10.1002/tox.22369>
- Li, N., Hao, M., Phalen, R.F., Hinds, W.C., Nel, A.E., 2003. Particulate air pollutants and asthma: A paradigm for the role of oxidative stress in PM-induced adverse health effects. *Clin. Immunol.* 109, 250–265. <https://doi.org/10.1016/j.clim.2003.08.006>
- Líbalová, H., Krčková, S., Uhlířová, K., Kléma, J., Cigánek, M., Rössner, P., Šrám, R.J., Vondráček, J., Machala, M., Topinka, J., 2014. Analysis of gene expression changes in A549 cells induced by organic compounds from respirable air particles. *Mutat. Res. - Fundam. Mol. Mech. Mutagen.* 770, 94–105. <https://doi.org/10.1016/j.mrfmmm.2014.10.002>
- Longhin, E., Gualtieri, M., Capasso, L., Bengalli, R., Mollerup, S., Holme, J.A., Øvrevik, J., Casadei, S., Di Benedetto, C., Parenti, P., Camatini, M., 2016. Physico-chemical properties and biological effects of diesel and biomass particles. *Environ. Pollut.* 215, 366–375. <https://doi.org/10.1016/j.envpol.2016.05.015>
- Longhin, E., Pezzolato, E., Mantecca, P., Holme, J.A., Franzetti, A., Camatini, M., Gualtieri, M., 2013. Season linked responses to fine and quasi-ultrafine Milan PM in cultured cells. *Toxicol. Vitro.* 27, 551–559. <https://doi.org/10.1016/j.tiv.2012.10.018>
- Marabini, L., Ozgen, S., Turacchi, S., Aminti, S., Arnaboldi, F., Lonati, G., Fermo, P., Corbella, L., Valli, G., Bernardoni, V., Dell'Acqua, M., Vecchi, R., Becagli, S., Caruso, D., Corrado, L.G., Marinovich, M., 2017. Ultrafine particles (UFPs) from domestic wood stoves: genotoxicity in human lung carcinoma A549 cells.

- Mutat. Res. - Genet. Toxicol. Environ. Mutagen. 820, 39–46.
<https://doi.org/10.1016/j.mrgentox.2017.06.001>
- Marchetti, S., Longhin, E., Bengalli, R., Avino, P., Stabile, L., Buonanno, G., Colombo, A., Camatini, M., Mantecca, P., 2019. In vitro lung toxicity of indoor PM10 from a stove fueled with different biomasses. *Sci. Total Environ.* 649, 1422–1433.
<https://doi.org/10.1016/j.scitotenv.2018.08.249>
- Møller, P., Christophersen, D.V., Jacobsen, N.R., Skovmand, A., Gouveia, A.C.D., Andersen, M.H.G., Kermanizadeh, A., Jensen, D.M., Danielsen, P.H., Roursgaard, M., Jantzen, K., Loft, S., 2016. Atherosclerosis and vasomotor dysfunction in arteries of animals after exposure to combustion-derived particulate matter or nanomaterials. *Crit. Rev. Toxicol.*
<https://doi.org/10.3109/10408444.2016.1149451>
- Morales-Bárceñas, R., Chirino, Y.I., Sánchez-Pérez, Y., Osornio-Vargas, Á.R., Melendez-Zajgla, J., Rosas, I., García-Cuellar, C.M., 2015. Particulate matter (PM10) induces metalloprotease activity and invasion in airway epithelial cells. *Toxicol. Lett.* <https://doi.org/10.1016/j.toxlet.2015.06.001>
- Nemmar, A., Holme, J.A., Rosas, I., Schwarze, P.E., Alfaro-Moreno, E., 2013. Recent advances in particulate matter and nanoparticle toxicology: A review of the in vivo and in vitro studies. *Biomed Res. Int.*
<https://doi.org/10.1155/2013/279371>
- Pati, R., Das, I., Mehta, R.K., Sahu, R., Sonawane, A., 2016. Zinc-oxide nanoparticles exhibit genotoxic, clastogenic, cytotoxic and actin depolymerization effects by inducing oxidative stress responses in macrophages and adult mice. *Toxicol. Sci.* 150, 454–472. <https://doi.org/10.1093/toxsci/kfw010>
- Rossner, P., Strapacova, S., Stolcpartova, J., Schmuczerova, J., Milcova, A., Neca, J., Vlkova, V., Brzicova, T., Machala, M., Topinka, J., 2016. Toxic effects of the major components of diesel exhaust in human alveolar basal epithelial cells (A549). *Int. J. Mol. Sci.* 17. <https://doi.org/10.3390/ijms17091393>
- Rudolf, E., Cervinka, M., 2011. Stress responses of human dermal fibroblasts exposed to zinc pyrithione. *Toxicol. Lett.* 204, 164–173.
<https://doi.org/10.1016/j.toxlet.2011.04.028>
- Rynning, I., Neca, J., Vrbova, K., Libalova, H., Rossner, P., Holme, J.A., Gützkow, K.B., Afanou, A.K.J., Arnoldussen, Y.J., Hrubá, E., Skare, Ø., Haugen, A., Topinka, J., Machala, M., Møllerup, S., 2018. In Vitro Transformation of Human Bronchial Epithelial Cells by Diesel Exhaust Particles: Gene Expression Profiling and Early Toxic Responses. *Toxicol. Sci.* 166, 51–64.
<https://doi.org/10.1093/toxsci/kfy183>
- Sánchez-Pérez, Y., Chirino, Y.I., Osornio-Vargas, Á.R., Morales-Bárceñas, R., Gutiérrez-Ruiz, C., Vázquez-López, I., García-Cuellar, C.M., 2009. DNA damage response of A549 cells treated with particulate matter (PM10) of urban air pollutants. *Cancer Lett.* 278, 192–200.

- <https://doi.org/10.1016/j.canlet.2009.01.010>
- Torvela, T., Uski, O., Karhunen, T., Jalava, P., Sippula, O., Tissari, J., Hirvonen, M., Jokiniemi, J., 2014. Reference Particles for Toxicological Studies of Wood Combustion: Formation, Characteristics, and Toxicity Compared to Those of Real Wood Combustion Particulate Mass.
- Totlandsdal, A.I., Låg, M., Lilleaas, E., Cassee, F., Schwarze, P., 2015. Differential proinflammatory responses induced by diesel exhaust particles with contrasting PAH and metal content. *Environ. Toxicol.* <https://doi.org/10.1002/tox.21884>
- Uski, O., Jalava, P.I., Happonen, M.S., Torvela, T., Leskinen, J., Mäki-Paakkanen, J., Tissari, J., Sippula, O., Lamberg, H., Jokiniemi, J., Hirvonen, M.-R., 2015. Effect of fuel zinc content on toxicological responses of particulate matter from pellet combustion in vitro. *Sci. Total Environ.* 511, 331–40.
- Vicente, E.D., Alves, C.A., 2018. An overview of particulate emissions from residential biomass combustion. *Atmos. Res.* 199, 159–185. <https://doi.org/10.1016/j.atmosres.2017.08.027>
- Yang, D., Ma, M., Zhou, W., Yang, B., Xiao, C., 2017. Inhibition of miR-32 activity promoted EMT induced by PM2.5 exposure through the modulation of the Smad1-mediated signaling pathways in lung cancer cells. *Chemosphere* 184, 289–298. <https://doi.org/10.1016/j.chemosphere.2017.05.152>
- Yang, L., Liu, G., Lin, Z., Wang, Y., He, H., Liu, T., Kamp, D.W., 2016. Pro-inflammatory response and oxidative stress induced by specific components in ambient particulate matter in human bronchial epithelial cells. *Environ. Toxicol.* 31, 923–936. <https://doi.org/10.1002/tox.22102>
- Zhang, J., Chang, L., Jin, H., Xia, Y., Wang, L., He, W., Li, W., Chen, H., 2016. Benzopyrene promotes lung cancer A549 cell migration and invasion through up-regulating cytokine IL8 and chemokines CCL2 and CCL3 expression. *Exp. Biol. Med.* <https://doi.org/10.1177/1535370216644530>
- Zhang, Jinyang, Song, W., Guo, J., Zhang, Jinhua, Sun, Z., Ding, F., Gao, M., 2012. Toxic effect of different ZnO particles on mouse alveolar macrophages. *J. Hazard. Mater.* 219–220, 148–155. <https://doi.org/10.1016/j.jhazmat.2012.03.069>

Appendix



ELSEVIER

Contents lists available at ScienceDirect

Environmental Pollution

journal homepage: www.elsevier.com/locate/envpol

The role of IL-6 released from pulmonary epithelial cells in diesel UFP-induced endothelial activation[☆]



Rossella Bengalli^{a,*}, Eleonora Longhin^a, Sara Marchetti^a, Maria C. Proverbio^b,
Cristina Battaglia^c, Marina Camatini^a

^a Polaris Research Centre, Dept. of Earth and Environmental Sciences, University of Milano-Bicocca, Piazza della Scienza, 1, 20126, Milan, Italy

^b Department of Physiopathology and Transplantation, University of Milan, Via Fratelli Cervi 93, 20090, Segrate, Italy

^c Department of Medical Biotechnology and Translational Medicine (BIOMETRA), University of Milan, Via Flli Cervi 93, 20090, Segrate, Italy

ARTICLE INFO

Article history:

Received 15 February 2017

Received in revised form

24 August 2017

Accepted 24 August 2017

Available online 12 September 2017

Keywords:

Conditioned media

Diesel ultrafine particles

Endothelial activation

IL-6

Inflammation

ABSTRACT

Diesel exhaust particles (DEP) and their ultrafine fraction (UFP) are known to induce cardiovascular effects in exposed subjects. The mechanisms leading to these outcomes are still under investigation, but the activation of respiratory endothelium is likely to be involved. Particles translocation through the air-blood barrier and the release of mediators from the exposed epithelium have been suggested to participate in the process. Here we used a conditioned media *in vitro* model to investigate the role of epithelial-released mediators in the endothelial cells activation.

Diesel UFP were sampled from a Euro 4 vehicle run over a chassis dyno and lung epithelial BEAS-2B cells were exposed for 20 h (dose 5 $\mu\text{g}/\text{cm}^2$). The exposure media were collected and used for endothelial HPMEC-ST1.6R cells treatment for 24 h. The processes related to oxidative stress and inflammation were investigated in the epithelial cells, accordingly to the present knowledge on DEP toxicity. The release of IL-6 and VEGF was significantly augmented in diesel exposed cells. In endothelial cells, VCAM-1 and ICAM-1 adhesion molecules levels were increased after exposure to the conditioned media. By interfering with IL-6 binding to its endothelial receptor, we demonstrate the role of this interleukin in inducing the endothelial response.

© 2017 Elsevier Ltd. All rights reserved.

1. Introduction

Diesel exhaust particles (DEP) exposure has been associated to both severe respiratory health effects, such as chronic inflammation and lung cancer (Lewtas, 2007), and cardiovascular diseases such as hypertension and atherosclerosis (BéruBé et al., 2007; Lee et al., 2014). Ultrafine particles (UFP, <100 nm) represent in number the largest fraction of particles emitted by diesel combustion (Nemmar et al., 2013), and arise particular interest for their peculiar properties. UFP have a greater surface area compared to larger particles, providing greater possibilities of interaction with biological systems, and adhesion for harmful chemicals produced by combustion. Furthermore small particles have been shown to evade the pulmonary clearance, reaching the distal parts of the respiratory system and gaining access to the systemic circulation

(Nemmar et al., 2013).

Studies on humans have evidenced that after 24 h exposure to DEP there is a persistent impairment of the respiratory endothelium, which occurs in the presence of mild systemic inflammation, and may cause adverse vascular effects (Törnqvist et al., 2007).

The translocation across the air-blood barrier is one of the proposed mechanisms by which diesel and PM_{0.1} (particulate matter ≤ 100 nm) might lead to cardiovascular diseases. This hypothesis suggests that, once in the circulation, UFP directly interact with the cells of vascular endothelium inducing oxidative stress and inflammation, which determine the activation of response pathways related to endothelial dysfunction (Mills et al., 2009). However the evidences on particles translocation are still conflicting (Stone et al., 2016) and some studies show that only a low percentage of carbonaceous UFP reaches the circulation in exposed animals and humans (Klepczyńska-Nyström et al., 2012; Kreyling et al., 2009). Thus, other processes are likely to concur to the vascular response observed.

The release of mediators and signalling factors from the

[☆] This paper has been recommended for acceptance by David Carpenter.

* Corresponding author. Tel.: +390264482928.

E-mail address: rossella.bengalli@unimib.it (R. Bengalli).

epithelium in response to particles exposure has been suggested as an alternative mechanism inducing endothelial activation (Kelly and Fussell, 2015). Mediators released by *in vitro* and *in vivo* systems in response to diesel exposure include IL-6, IL-8, IL-13, CXCL1/Gro- α , IL-1 β , TNF- α (Kelly and Fussell, 2015; Schwarze et al., 2013).

Endothelial activation is characterized by the increase of the adhesion molecules ICAM-1, VCAM-1 and E-selectin, which enable the adhesion of monocytes to the vascular endothelium, an early step in the formation of atherosclerotic plaques (Galkina and Ley, 2007; Mestas and Ley, 2008). Several studies have addressed the effects of diesel exposure on endothelial cells, and the relation with possible cardiovascular effects. In the HUVEC tube cells, diesel particles have been shown to induce the release of vascular endothelial growth factor VEGF-A and the redistribution of the adherens junction molecule VE-cadherin from the cell membrane to the cytoplasm, thus increasing vascular permeability (Tseng et al., 2016). In another study (Li et al., 2010), diesel particles activated the expression of VCAM-1 adhesion molecule through NF- κ B signalling pathway in HAEC endothelial cells, and consequently stimulated the monocyte binding to the endothelial cells monolayer. However these papers and most of the *in vitro* studies are focused on the direct effects of particles on cardiac and endothelial cells (Tseng et al., 2015), using particles concentrations that might not be reflect real conditions (1–100 μ g/ml, equal to 0.1–10 μ g/cm² in our exposure model). Only few works investigate the indirect vascular effects caused by the respiratory epithelium exposed to particles (Gorr et al., 2015; Totlandsdal et al., 2008; Weldy et al., 2011).

Here we set up a conditioned media *in vitro* system, where lung epithelial cells are exposed to diesel UFP and the supernatants used to treat endothelial cells. The biological effects in both the cell lines have been investigated and inhibitory studies have been performed to individuate the possible mediators responsible for endothelial responses.

2. Materials and methods

Preparation of diesel particles. UFP sampling and preparation for biological investigations have been previously described (Longhin et al., 2016). Briefly, DEP were sampled on Teflon filters (Whatman, Maidstone, UK), from a Euro 4 light duty vehicle without DPF run over a chassis dyno. A Dekati gravimetric impactor (DGI-1570, Finland) was used to remove the bigger aggregates. After sampling filters were preserved at -20°C , until particles extraction was performed by sonication in an ice-cold water-bath (SONICA Soltec, Milan, Italy). Particle suspensions were dried into a desiccator, weighed and stored at -20°C . Samples were re-suspended in sterile water (final concentration 2 mg/ml) just before use. UFP physico-chemical characterization has been previously reported (Longhin et al., 2016).

Cells culture and exposure. BEAS-2B cells were maintained in LHC-9 medium (Gibco, Life Technologies, Monza, Italy) at 37°C with 5% of CO₂. Cells for experiments (passages 13 to 27) were seeded at a concentration of 2.7×10^5 cells/well in 6-well plates and treated the day after with 5 μ g/cm² of diesel UFP. The concentration of 5 μ g/cm² of diesel UFP has been chosen because it was the lower tested dose that induced a significant effect in the *in vitro* system here used after a single acute exposure. After 20 h of exposure, the media were collected and the cellular responses analysed.

HPMEC-ST1.6R cells were received from Dr. Ronald E. Unger (Institute of Pathology, Medical University of Mainz, Johannes Gutenberg University, Mainz, Germany) and maintained in M199 medium (Euroclone, Italy), supplemented with 15% inactivated fetal bovine serum (FBS; Gibco, Life Technologies), 2 mM L-

Glutamine (Sigma Aldrich, Milan, Italy), 20 μ g/ml ECGS (Endothelial Cell Growth Supplement) (Sigma Aldrich), 20 μ g/ml Na Heparin (Sigma Aldrich), 25 mM Hepes (Sigma Aldrich) and 100 U/100 μ g/ml Penicillin/Streptomycin (Euroclone) and were grown at 37°C with 5% of CO₂. Cells for experiments (passages 26 to 37) were seeded at a concentration of 1.5×10^5 cells/well in 6-well plates, and treated the day after with 40% of media collected from epithelial cells diluted in M199 medium. The ratio between BEAS-2B medium (LHC-9) and HPMEC medium (M199) for HPMEC exposure has been preliminary selected in the set-up of the *in vitro* system here used. HPMEC-ST1.6R cells exposure lasted for 24 h.

ROS formation. The oxidative potential of diesel UFP was determined after 1 h of exposure using the 5-(and-6)-Carboxy-2',7'-Dichlorofluorescein Diacetate (carboxy-DCF-DA, Molecular Probes, Life Technologies) probe, that becomes fluorescent when is oxidized by intracellular reactive oxygen species (ROS). Before exposure, BEAS-2B cells were incubated at 37°C with DCFH-DA 5 μ M in PBS for 20 min. After incubation, cells were washed twice with PBS and exposed to 5 μ g/cm² of diesel UFP in fresh media for 1 h. The samples were then washed with PBS and the fluorescent signal, proportional to ROS formation in the cells, was measured with a multiplate spectrophotometer reader (Tecan, Männedorf, Switzerland, excitation/emission wavelengths: 492/525 nm). As positive control, cells were exposed to 10 μ M H₂O₂ (data not shown). Data were expressed as fold increase (FI) of exposed sample over control (untreated cells).

RNA extraction and QPCR. BEAS-2B cells were collected after 20 h of exposure to 5 μ g/cm² of diesel UFP, lysed, and stored in QIAzol Lysis reagent (Qiagen, Hilden, Germany) until RNA extraction. Total RNA was extracted using the miRNeasy extraction kit (Qiagen) and eluted in RNase free-water, according to the manufacturer's guidelines. Quality and quantity of the total RNA samples were evaluated with 2100 Bioanalyzer (Agilent, Santa Clara, CA) and Nanodrop 1000 (Thermo Fisher Scientific, Wilmington, DE), respectively. According to previous investigations, we focused the gene expression analysis on 11 selected genes involved in inflammation (*IL1A*), oxidative stress (aldehyde dehydrogenase 3A1, *ALDH3A1*; heme oxygenase 1, *HMOX1*; thioredoxin reductase 1, *TXNRD1*) and mitogen-activated protein kinase (MAPK) signaling (*IGFBP1*, *EPGN*, *GREM1*, *LIF*, *DAPPI*, *FOSL1*). A customized RT² PCR profiler system (Qiagen, Hilden, Germany) with Sybr green as reporter dye has been used. The expression of each gene within each sample was normalized using the average expression levels of three housekeeping genes (*ACTB*, *B2M*, *GAPDH*). The fold change was calculated for each conditions using the $2^{-\Delta\Delta\text{Ct}}$ method comparing ΔCt of UFP treated cells to ΔCt of control untreated cells. Data of two independent experiments are reported.

Western blotting. After 24 h of exposure to conditioned media, HPMEC-ST1.6R cells were scraped and lysed on ice in RIPA buffer (150 mM NaCl, 1% TritonX-100, 0.5% sodium deoxycholate, 0.1% SDS, 50 mM Tris pH 8.0 and 0.1% of protease inhibitors, added just before use). The total protein content was evaluated by the bicinchoninic acid assay (Sigma Aldrich) according to the manufacturer's instruction. Equal amounts of proteins were loaded onto 10% SDS-PAGE (Sodium Dodecyl Sulphate - PolyAcrylamide Gel Electrophoresis) gels, separated and transferred on nitrocellulose membranes. Equal loading was assessed by Ponceau red staining of membranes. The membranes were then blocked for 1 h (Tris-buffered saline, TBS, 0.1% Tween20, 5% (w/v) Bovine Serum Albumin, BSA) and incubated at 4°C overnight with specific primary antibody diluted according to datasheets (CD54/ICAM-1, VCAM-1 and β -actin for loading control, 1:1000, Cell Signalling Technology, Danvers, USA). The day after, membranes were washed in TBS, 0.1% Tween20 and incubated with specific HRP-linked secondary antibodies for 1 h at RT (anti-rabbit IgG, 1:2000, Cell Signalling).

After detection with Chemiluminescent Peroxidase Substrate (Euroclone), digital images were taken by a luminescence reader (Biospectrum-UVP, Upland, USA) and densitometry analysis performed with dedicated software (VisionWorks LS).

Protein arrays. A panel of protein involved in the MAPK and angiogenesis pathways were investigated by antibody arrays (Proteome Profiler Human Phospho-MAPK Array Kit cod. ARY002B, Proteome Profiler Human Angiogenesis Array Kit cod. ARY007; R&D Systems, Minneapolis, USA). This method allows to detect simultaneously the relative phosphorylation of 24 different kinases or the expression of 55 angiogenesis related proteins which are captured by relative different antibodies spotted in duplicate on a nitrocellulose membrane. Levels of proteins are then assessed using phospho-specific antibodies and chemiluminescent detection.

After exposure well plates with cells were stored overnight at -80°C . Cells were then scraped on ice in provided lysis buffer, homogenized using a syringe with needle, rocked at $2-8^{\circ}\text{C}$ for 30 min and centrifuged (5 min, $14000 \times g$ at 4°C). Total amount of proteins was assessed by bicinchoninic acid assay (Sigma Aldrich) and membrane arrays were processed according to the manufacturer's instructions. Briefly, during incubation of membranes with provided blocking buffer for 1 h at room temperature (RT). 300 μg of total proteins of each sample were incubated with Detection antibody for the same time. Subsequently, the mixtures sample/detection antibody were pipetted onto different membranes and incubated overnight at 4°C on a platform shaker. The day after, membranes were washed 3 times with wash buffer and incubated with Streptavidin-HRP for 30 min at RT. The signal intensities for each antigen-specific antibody spots, proportional to the relative concentration of the antigen in the sample, were detected by chemiluminescence and recorded by a luminescence reader (Biospectrum-UVP). Densitometry analysis was performed with dedicated software (VisionWorks LS-UVP). Data were expressed as signal intensity corrected by the signals of positive and negative controls following manufacturer's guidelines, and fold increase (FI) of diesel exposed samples over unexposed (control) are reported in false colour scale.

ELISA. After exposure, the supernatants of BEAS-2B and HPMEC-ST1.6R cells were collected and protein levels were determined by sandwich ELISA according to the manufacturer's guidelines (IL-6, IL-6R, VEGF, IL-8, MCP-1, TNF- α , Life Technologies). The absorbance of each sample was measured by Multiplate Reader Ascent (Thermo Scientific, USA) at 450 nm and 630 nm, and the amount of proteins in pg/ml calculated on the basis of a standard curve.

Inhibitory studies. IL-6 antibody (aIL-6) has been used to specifically prevent the binding of this molecule with its receptors on endothelial cells. aIL-6 (1 $\mu\text{g/ml}$) was added to BEAS-2B supernatants for 2 h at room temperature, and then the supernatants were used for HPMEC-ST1.6R cells exposure for further 24 h. Endothelial cells responses were thus assessed.

Statistical analyses. Mean and standard error of mean (SEM) of at least three independent experiments are reported. Statistical analyses were performed using Sigma Stat 3.1 software, using *t*-test. Values of $p < 0.05$ were considered statistically significant.

3. Results

Effects on epithelial cells. Diesel UFP exposure ($5 \mu\text{g/cm}^2$) activated oxidative stress response and MAPK signalling in epithelial cells. ROS formation in BEAS-2B cells was observed 1 h after exposure to diesel UFP, with a fold increase of 1.6 over control (Fig. 1).

The analysis of gene expression by qPCR evidenced the up-regulation of oxidative stress responsive genes *HMOX1* and *TXNRD1*, and a strong over-expression of *ALDH3A1*, involved in the

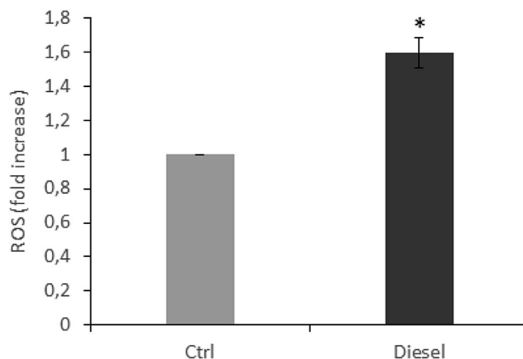


Fig. 1. ROS formation in BEAS-2B cells after 1 h exposure to diesel UFP ($5 \mu\text{g/cm}^2$), measured by carboxy-DCF-DA fluorescence. *Statistically significant according to unpaired *t*-test $p < 0.05$.

metabolism of peroxidised lipids (Table 1). Additionally we observed over-expressed levels of several genes related to the MAPK pathway (Table 1).

To further confirm the activation of MAPK pathway, we measured the level of 24 proteins involved. By mean of protein array (Fig. 2), we observed slightly increased levels of the phosphorylated form of almost all the proteins in the pathway. Remarkable increases were reported for Akt proteins (FI was 4.1 and 3.2 for Akt1 and Akt2 respectively, 3.2 for Akt pan = all Akts) and for ERK2 (FI was 2.6).

To assess the modulation of factors renowned to be relevant for inflammation and vascular signalling, we measured the release of cytokines and proteins in the BEAS-2B cells media by ELISA. The secretion of IL-6 and VEGF proteins was found to be significantly increased in cells exposed to diesel UFP (Fig. 3) while the levels of IL-8, MCP-1 and TNF- α were not significantly modified respect to control (data not shown).

Effects on endothelial cells. HPMEC-ST1.6R cells were treated for 24 h with the media collected from epithelial cultures. The analysis of MAPK (Fig. 4a) and angiogenesis (Fig. 4b) pathways activation in HPMEC cells by protein arrays showed a very weak modulation, involving only few proteins with a fold change between 0.6 and 1.4.

ICAM-1 and VCAM-1 protein expression was investigated as typical markers of endothelial activation, and found significantly

Table 1

Gene expression in epithelial cells exposed to diesel UFP. FC: fold change.

Gene Symbol (assay ID) ^a	FC	FC (min-max)	Biological relevance
<i>ALDH3A1</i> (PPH07009A)	9.25	7.53–10.96	oxidative stress
<i>CXCL2</i> (PPH00552F)	1.43	1.26–1.60	MAPK
<i>DAPP1</i> (PPH00006A)	3.02	1.82–4.22	MAPK
<i>EPCN</i> (PPH19098A)	4.99	3.60–6.38	MAPK
<i>FOSL1</i> (PPH00145C)	2.82	2.76–2.87	MAPK
<i>GREM1</i> (PPH01941B)	4.64	3.87–5.40	MAPK
<i>HMOX1</i> (PPH00161F)	2.53	1.63–3.44	oxidative stress
<i>IER3</i> (PPH10008F)	2.16	1.51–2.81	MAPK, oxidative stress
<i>IGFBP1</i> (PPH02046E)	18.11	17.38–18.84	MAPK
<i>IL1A</i> (PPH00690A)	2.58	2.21–2.95	MAPK, inflammation
<i>LIF</i> (PPH00813F)	3.21	2.80–3.63	MAPK
<i>NFE2L2</i> (PPH06070A)	1.88	1.66–2.11	MAPK
<i>TNFAIP3</i> (PPH00063A)	2.28	1.93–2.63	inflammation
<i>TXNRD1</i> (PPH02104F)	2.47	1.48–3.45	oxidative stress
<i>VEGFA</i> (PPH00251C)	1.14	0.90–1.39	MAPK, angiogenesis

^a ID for RT² qPCR primer assays (Qiagen).

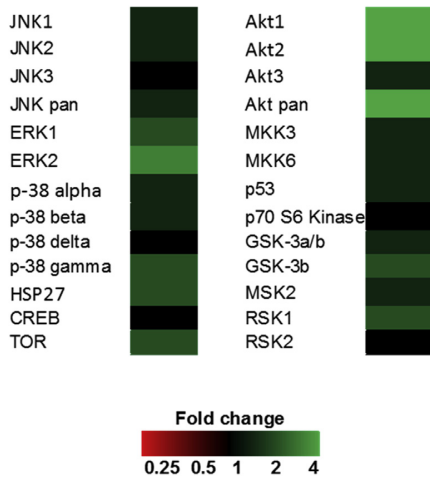


Fig. 2. MAPK proteins phosphorylation in BEAS-2B cells after 20 h exposure to diesel UFP (5 µg/cm²), measured by chemiluminescent detection of proper phospho-MAPK protein array. "pan" indicates all the forms of that protein. Fold changes of protein expression, increased (green), decreased (red) or equal (black) compared to untreated cells are reported. (For interpretation of the references to colour in this figure legend, the reader is referred to the web version of this article.)

augmented in HPMEC-ST1.6R cells indirectly exposed to diesel particles (Fig. 5).

Mechanisms of endothelial activation. Both VEGF and IL-6 signalling can activate ICAM-1 and VCAM-1 transcription in endothelial cells. VEGF-dependent modulation goes through MAPK cascade signalling (Maitland et al., 2010; Radisavljevic et al., 2000). Since we found that this pathway is weakly modulated in our samples, we focused on IL-6 as a possible mediator responsible for endothelial activation. IL-6 interacts with endothelial cells through the so called *trans*-signalling pathway: IL-6 circulating in the serum forms a complex with the soluble form of interleukin-6 receptor (IL-6R), and then binds to the gp130 receptor on endothelial cells membrane (Barnes et al., 2011; Rose-John, 2012). Thus, in order to verify the role of IL-6 signalling in the modulation of adhesion molecules in our model, we first measured IL-6R levels in BEAS-2B supernatants and then we interfered with the binding of IL-6 to gp130 receptor by adding IL-6 antibody to supernatants. The results showed that IL-6R was significantly increased in diesel UFP

exposed cells compared to control (Fig. 6).

When IL-6 antibody was added to the media, a not significant increase of ICAM-1 and VCAM-1 levels was observed in control cells, suggesting that the antibody may present some affinity for IL-6R and/or gp130, and thus may partly work as an agonist to gp130 receptor (Fig. 7). Anyway, in samples exposed to diesel-conditioned media, the addition of IL-6 antibody reduced ICAM-1 and VCAM-1 over-expression, indicating the role of IL-6 in their modulation (Fig. 7).

4. Discussion

In this research we have used an *in vitro* model based on conditioned media to investigate the mechanisms of diesel particles-induced vascular effects. A possible mechanism based on our results is proposed below (Fig. 8).

BEAS-2B lung epithelial cells directly exposed to particles exhibited higher levels of ROS and the activation of oxidative stress-responsive genes. The strongest modulated gene was *ALDH3A1*, an AhR-responsive gene participating in xenobiotic metabolism and involved in the detoxification of aldehydes generated by lipid peroxidation. The modulation of this gene has been previously reported in animals and cells exposed to different types of combustion particles, and indicates the role of organic compounds, mostly polycyclic aromatic hydrocarbons (PAHs), in driving cellular oxidative effects (Líbalová et al., 2014; Noël et al., 2016).

Other oxidative stress-responsive genes here modulated are *NFE2L2* transcription factor and its targets HMOX1 and TXNRD1, enzymes with a protective role against oxidative stress. Among genes with altered expression, several were related to MAPK pathway, e.g. *IGFBP1*, *EPGN*, *GREM1*, *LIF*, *DAPP1*, *FOSL1*, *IL1A* and *CXCL2*. MAPK pathway activation was then validated at protein level by the increased expression of phosphorylated active forms, in particular of Akt1/2 and ERK2. These proteins, known to respond mainly to growth factors signal, were also shown to be directly activated by ROS (Zhang et al., 2016). They are involved in the regulation of many processes including metabolism, proliferation, cell survival, growth, angiogenesis and cytokine production (Zhang et al., 2016). Akt has been reported to activate NF-κB, a renowned factor inducing cytokines transcription (Dan et al., 2008), and interestingly it has been shown to directly modulate IL-6 levels, through NF-κB and STAT3 regulation (Malanga et al., 2015).

IL-6 secretion by lung epithelial cells exposed to diesel particles was previously reported (Nemmar et al., 2013) and here confirmed. Mediators found in other studies e.g. IL-8 and MCP-1, were not

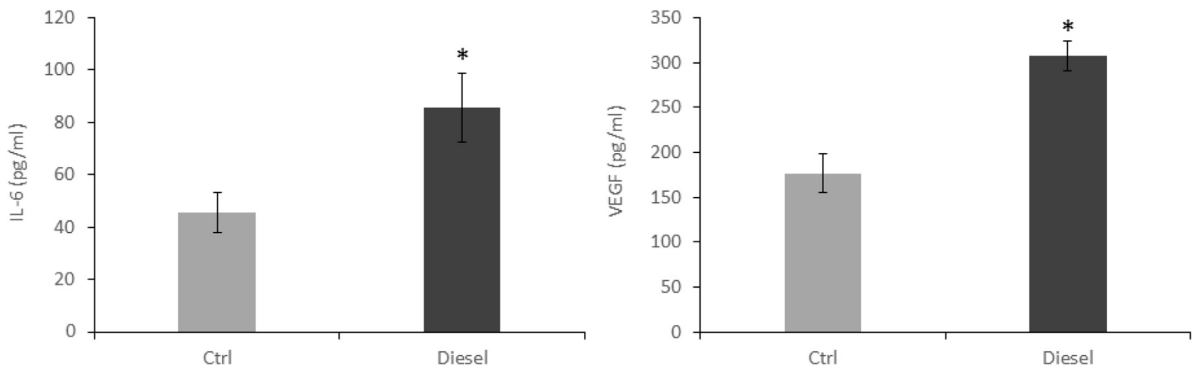


Fig. 3. Proteins secretion (IL-6 and VEGF) from BEAS-2B cells after 20 h exposure to diesel UFP (5 µg/cm²), measured by ELISA. *Statistically significant according to unpaired t-test p < 0.05.

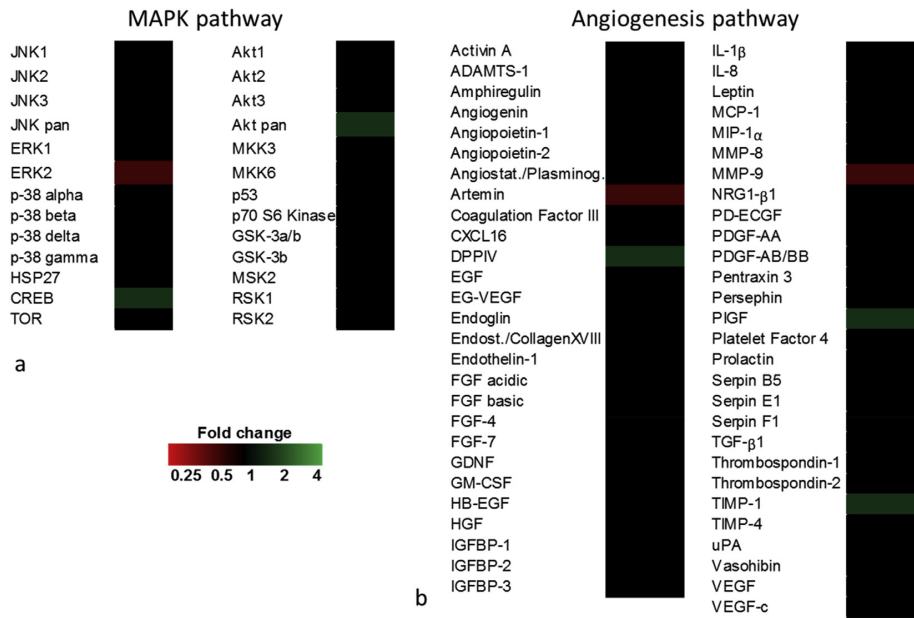


Fig. 4. MAPK (a) and angiogenesis (b) pathways activation in HPMEC cells after 24 h exposure to conditioned media, measured by chemiluminescent detection of protein arrays. Fold changes of protein expression, increased (green), decreased (red) or equal (black) compared to untreated cells are reported. (For interpretation of the references to colour in this figure legend, the reader is referred to the web version of this article.)

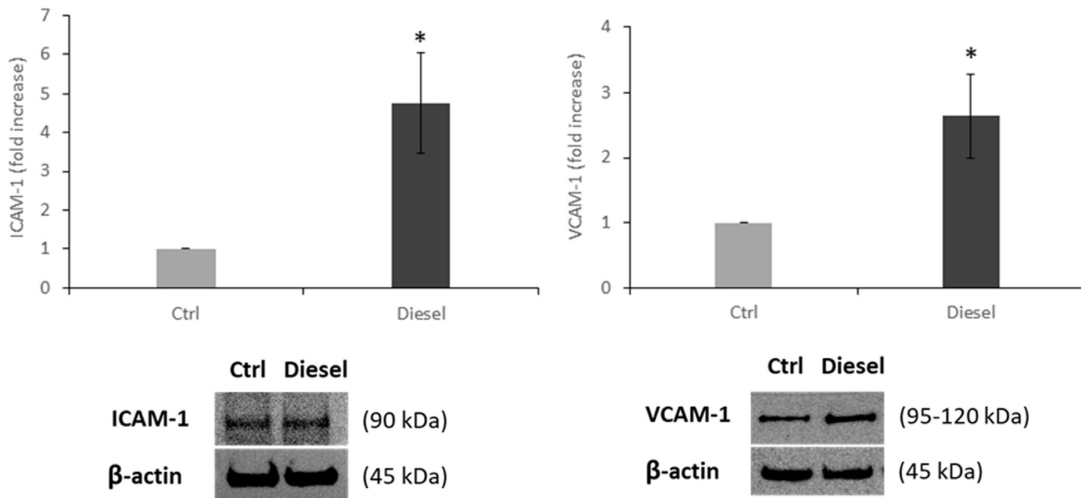


Fig. 5. ICAM-1 and VCAM-1 protein expression in HPMEC-ST1.6R cells after 24 h exposure to conditioned media, measured by western blotting. The protein expression is normalized over the housekeeping protein β-actin and data are presented as fold increase over the control. *Statistically significant according to unpaired t-test $p < 0.05$.

modulated. Increased levels of VEGF were instead measured. Interestingly, aryl hydrocarbon receptor (AhR) agonists were reported to upregulate VEGF secretion from bronchial epithelial cells (Tsai et al., 2015). This mechanism might be of great importance for cardiovascular diseases induced by diesel particles, as AhR is largely recognized to be a main receptor of diesel-adsorbed organic compounds (Pálková et al., 2015). VEGF is a potent inducer of angiogenesis, through the interaction with FLT1, KDR, or NRP1 receptors on endothelial cells membrane, and the subsequent activation of

RAS and MAPK kinases signalling cascades (Maitland et al., 2010). In our case, we found a very weak modulation of MAPK pathway and angiogenesis-related proteins in endothelial cells exposed to conditioned media. We assumed that the levels of VEGF released (around 300 pg/ml) were too low to induce a significant response, since much higher concentrations of VEGF (10–100 ng/ml) are normally used to investigate its effects on endothelial cells (Chang et al., 2000; Tseng et al., 2015).

In our model, the levels of adhesion molecules ICAM-1 and

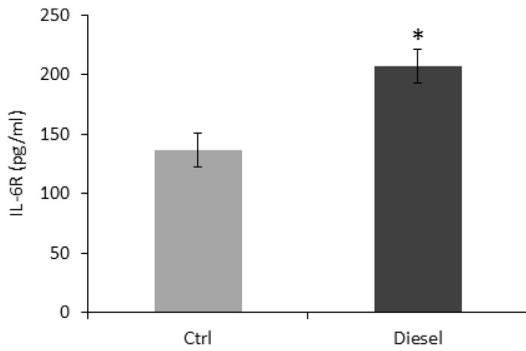


Fig. 6. IL-6R levels in BEAS-2B cells supernatants after 20 h exposure to diesel UFP (5 µg/cm²), measured by ELISA. *Statistically significant according to unpaired *t*-test *p* < 0.05.

VCAM-1 were significantly increased in endothelial cells exposed to conditioned media. ICAM-1/VCAM-1 over-expression is a marker of endothelial activation and leads to monocyte/lymphocyte recruitment and infiltration into the sub-endothelium (Tedgui and Mallat, 2006). It occurs in response of several stimuli and has been reported in cells, animals and humans exposed to diesel or ambient particles (Araujo and Nel, 2009; Hemmingsen et al., 2011; Krishnan et al., 2013; Salvi et al., 1999). The increased expression of these molecules in endothelial cells can be induced by IL-6 *trans*-signaling (Barnes et al., 2011). This pathway occurs in cells that do not express the interleukin-6 receptor IL-6R, like endothelial cells. In humans, soluble IL-6R exists in the serum, released by several cell types, and bind to IL-6 forming an IL-6/sIL-6R complex. This complex can bind to gp130 receptor on endothelial cells membrane and activate STAT3 and its target genes, including ICAM-1 and VCAM-1 (Rose-John, 2012). Thus, here we first assessed the availability of IL-6R in BEAS-2B supernatants, and found its overexpression after diesel exposure. Then we successfully inhibited ICAM-1 and VCAM-1 over-expression induced by diesel by interfering with IL-6/gp130 binding by the addition of IL-6 antibody to epithelial cells media.

Our results demonstrate the role of IL-6 released by the epithelial cells in inducing the observed effects on endothelial cells.

Previous *in vitro* studies compared direct and indirect effects of particles on endothelial cells or cardiomyocytes (Gorr et al., 2015; Totlandsdal et al., 2008; Weldy et al., 2011). Although in all these papers both direct and indirect effects were reported, there was general agreement that the particles concentrations used for direct exposure of endothelial cells likely overestimate the *in vivo* concentration found in the vascular system, due to the small fraction of translocated particles. Besides, the pathways of translocation into the bloodstream are still not clear, as well as the modifications that particles may undergo along this process, making the direct exposure experiments poorly representative of the real situation (Gorr et al., 2015). On the other hand, indirect effects involving the release of inflammatory factors from the exposed lung look highly relevant for the vascular outcomes, and it is possible that the small fraction of translocated particles contributes to this complex mechanism.

Previous investigations to individuate the mediators responsible for indirect effects to the vascular system gave divergent results, further highlighting the complexity of this issue. In a model involving bronchial cells directly exposed to diesel particles and cardiomyocytes exposed to conditioned media, MCP-1 was individuated as the main contributor to the cardiomyocyte dysfunction observed (Gorr et al., 2015), while in another model the role of IL-1 was demonstrated by the use of an IL-1 receptor antagonist (Totlandsdal et al., 2008). With an interesting but slightly different approach, plasma from healthy human volunteers exposed to DEP was used to treat endothelial cells, and significant increase of VCAM-1 mRNA was observed (Channell et al., 2012). In a follow-up study, the same authors measured IL-6 and TNF-α in plasma as possible mediators of endothelial effects, but these markers were not increased (Schisler et al., 2015). These proteins were however found to be augmented in plasma of exposed humans in other studies (Hilt et al., 2002; Törnqvist et al., 2007; Xu et al., 2013). It is likely that the mediators released might differ according to several factors such as particles properties (Li et al., 2010; Totlandsdal et al., 2015), exposure dose and, in particular with regard to human exposure, genetic polymorphism and health status of the subjects

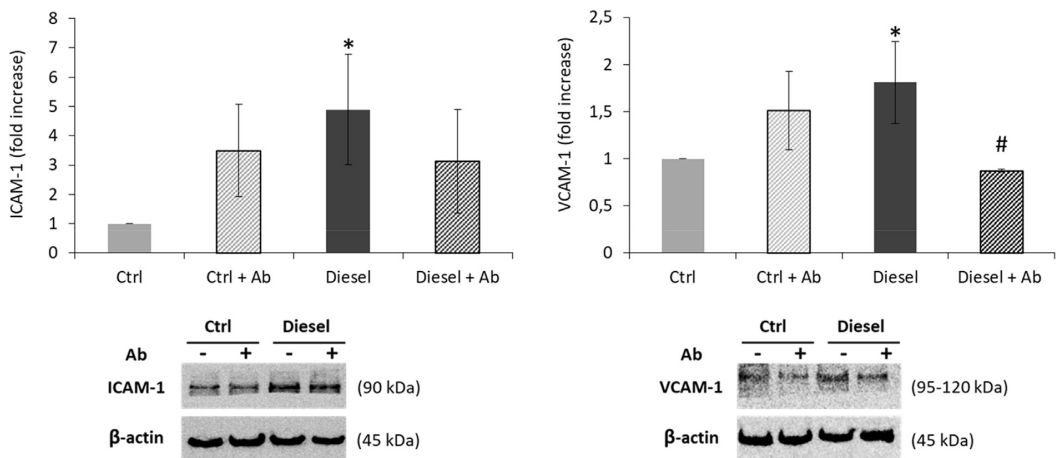


Fig. 7. ICAM-1 and VCAM-1 protein expression in HPMEC cells after 24 h exposure to conditioned media, with (+Ab) and without IL-6 antibody interference, measured by western blotting. The protein expression is normalized over the housekeeping protein β-actin and data are presented as fold increase over the control. *Statistically significant respect to untreated cells (Ctrl) according to unpaired *t*-test *p* < 0.05. # Statistically significant respect to cells exposed to diesel-conditioned media (Diesel) according to unpaired *t*-test *p* < 0.05.

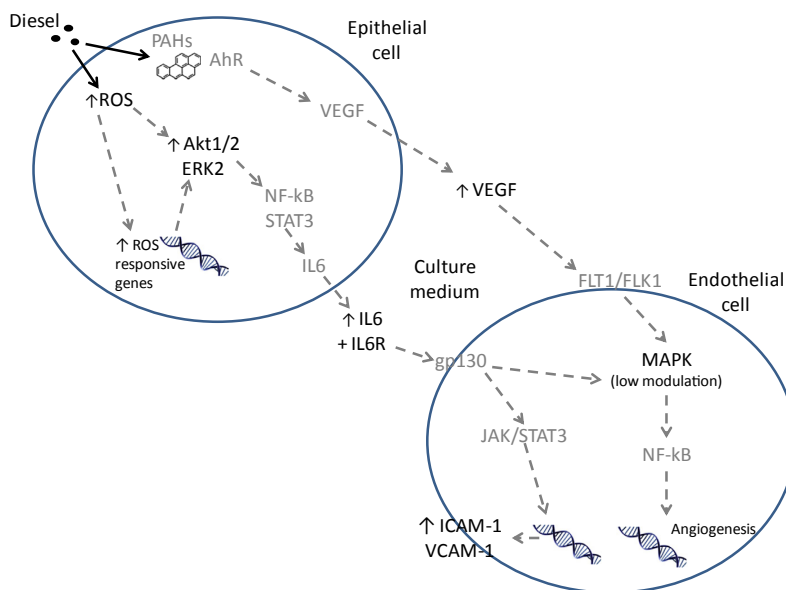


Fig. 8. Summary of the events measured in BEAS-2B and HPMEC-ST1.6R cells, and possible correlations among them. In black: measured events. Possibly involved factors (in grey) and signalling/correlations (broken arrows) are suggested according to the literature. PAH: polycyclic aromatic hydrocarbons.

investigated (Ljungman et al., 2009; Stenfors et al., 2004). As a last consideration, the mediators found in peripheral blood might not be the same factors released by the lung and acting at local level on the pulmonary vessels, which might respond by releasing other mediators.

In conclusion, here we show that a conditioned media model is capable to induce a response in endothelial cells indirectly exposed to diesel UFP, consisting in the modulation of the adhesion molecules ICAM-1 and VCAM-1. We demonstrate that IL-6 released by epithelial cells after diesel UFP exposure is responsible for the effects observed in endothelial cells. Our approach might be useful to investigate local mediators involved in initial endothelial activation, which may have further consequences. The relatively low dose and the exposure time here used caused limited responses both in epithelial and endothelial cells. Further investigations, involving a similar model undergoing repeated exposures, might provide interesting results also regarding the role of VEGF.

Acknowledgments

This study has been supported by Cariplo Foundation (Grant no. 2013-1038).

References

- Araujo, J.A., Nel, A.E., 2009. Particulate matter and atherosclerosis: role of particle size, composition and oxidative stress. *Part. Fibre Toxicol.* 6, 24. <http://dx.doi.org/10.1186/1743-8977-6-24>.
- Barnes, T.C., Anderson, M.E., Moots, R.J., 2011. The many faces of interleukin-6: the role of IL-6 in inflammation, vasculopathy, and fibrosis in systemic sclerosis. *Int. J. Rheumatol.* 2011, 721608. <http://dx.doi.org/10.1155/2011/721608>.
- BéruBé, K., Balharry, D., Sexton, K., Koshy, L., Jones, T., 2007. Combustion-derived nanoparticles: mechanisms of pulmonary toxicity. *Clin. Exp. Pharmacol. Physiol.* 34, 1044–1050. <http://dx.doi.org/10.1111/j.1440-1681.2007.04733.x>.
- Chang, Y.S., Munn, L.L., Hillsley, M.V., Dull, R.O., Yuan, J., Lakshminarayanan, S., Gardner, T.W., Jain, R.K., Tarbell, J.M., 2000. Effect of vascular endothelial growth factor on cultured endothelial cell monolayer transport properties. *Microvasc. Res.* 59, 265–277. <http://dx.doi.org/10.1006/mvres.1999.2225>.
- Channell, M.M., Paffett, M.L., Devlin, R.B., Madden, M.C., Campen, M.J., 2012. Circulating factors induce coronary endothelial cell activation following exposure to inhaled diesel exhaust and nitrogen dioxide in humans: evidence from a novel translational in vitro model. *Toxicol. Sci.* 127, 179–186. <http://dx.doi.org/10.1093/toxsci/kfs084>.
- Dan, H.C., Cooper, M.J., Cogswell, P.C., Duncan, J.A., Ting, J.P.-Y., Baldwin, A.S., 2008. Akt-dependent regulation of NF-(kappa)B is controlled by mTOR and Raptor in association with IKK. *Genes Dev.* 22, 1490–1500. <http://dx.doi.org/10.1101/gad.1662308>.
- Galkina, E., Ley, K., 2007. Vascular adhesion molecules in atherosclerosis. *Arterioscler. Thromb. Vasc. Biol.* 27, 2292–2301. <http://dx.doi.org/10.1161/ATVBAHA.107.149179>.
- Gorr, M.W., Youtz, D.J., Eichenseer, C.M., Smith, K.E., Nelin, T.D., Cormet-Boyaka, E., Wold, L.E., 2015. In vitro particulate matter exposure causes direct and lung-mediated indirect effects on cardiomyocyte function. *Am. J. Physiol. - Hear. Circ. Physiol.* 309, H53–H62. <http://dx.doi.org/10.1152/ajpheart.00162.2015>.
- Hemmingsen, J.G., Møller, P., Nøjgaard, J.K., Roursgaard, M., Loft, S., 2011. Oxidative stress, genotoxicity, and vascular cell adhesion molecule expression in cells exposed to particulate matter from combustion of conventional diesel and methyl ester biodiesel blends. *Environ. Sci. Technol.* 45, 8545–8551. <http://dx.doi.org/10.1021/es200956p>.
- Hilt, B., Qvenild, T., Holme, J., Svendsen, K., Ulvestad, B., 2002. Increase in interleukin-6 and fibrinogen after exposure to dust in tunnel construction workers. *Occup. Environ. Med.* 59, 9–12. <http://dx.doi.org/10.1136/oem.59.1.9>.
- Kelly, F.J., Fussell, J.C., 2015. Linking ambient particulate matter pollution effects with oxidative biology and immune responses. *Ann. N. Y. Acad. Sci.* 1340, 84–94. <http://dx.doi.org/10.1111/nyas.12720>.
- Klepczynska-Nyström, A., Sanchez-Crespo, A., Andersson, M., Falk, R., Lundin, A., Larsson, B.-M., Svartengren, M., 2012. The pulmonary deposition and retention of indium-111 labeled ultrafine carbon particles in healthy individuals. *Inhal. Toxicol.* 24, 645–651. <http://dx.doi.org/10.3109/08958378.2012.708065>.
- Kreyling, W.G., Semmler-Behnke, M., Seitz, J., Scymczak, W., Wenk, A., Mayer, P., Takenaka, S., Oberdörster, G., 2009. Size dependence of the translocation of inhaled iridium and carbon nanoparticle aggregates from the lung of rats to the blood and secondary target organs. *Inhal. Toxicol.* 21 (Suppl. 1), 55–60. <http://dx.doi.org/10.1080/08958370902942517>.
- Krishnan, R.M., Sullivan, J.H., Carlsten, C., Willkerson, H.-W., Beyer, R.P., Bammler, T., Farin, F., Peretz, A., Kaufman, J.D., 2013. A randomized cross-over study of inhalation of diesel exhaust, hematological indices, and endothelial markers in humans. *Part. Fibre Toxicol.* 10, 7. <http://dx.doi.org/10.1186/1743-8977-10-7>.
- Lee, B.-J., Kim, B., Lee, K., 2014. Air pollution exposure and cardiovascular disease. *Toxicol. Res.* 30, 71–75. <http://dx.doi.org/10.5487/TR.2014.30.2.071>.
- Lewtas, J., 2007. Air pollution combustion emissions: characterization of causative agents and mechanisms associated with cancer, reproductive, and cardiovascular effects. *Mutat. Res.* 636, 95–133. <http://dx.doi.org/10.1016/j.mrv.2007.08.003>.

- Li, R., Ning, Z., Majumdar, R., Cui, J., Takabe, W., Jen, N., Sioutas, C., Hsiai, T., 2010. Ultrafine particles from diesel vehicle emissions at different driving cycles induce differential vascular pro-inflammatory responses: implication of chemical components and NF-kappaB signaling. *Part. Fibre Toxicol.* 7, 6. <http://dx.doi.org/10.1186/1743-8977-7-6>.
- Libalová, H., Krcková, S., Uhlířová, K., Kléma, J., Ciganek, M., Rössner, P., Srám, R.J., Vondráček, J., Machala, M., Topinka, J., 2014. Analysis of gene expression changes in A549 cells induced by organic compounds from respirable air particles. *Mutat. Res. - Fundam. Mol. Mech. Mutagen* 770, 94–105. <http://dx.doi.org/10.1016/j.mrfmmm.2014.10.002>.
- Ljungman, P., Bellander, T., Schneider, A., Breitter, S., Forastiere, F., Hampel, R., Illig, T., Jacquemin, B., Katsouyanni, K., von Klot, S., Koenig, W., Lanki, T., Nyberg, F., Pekkanen, J., Pistelli, R., Pitsavos, C., Rosenqvist, M., Sunyer, J., Peters, A., 2009. Modification of the interleukin-6 response to air pollution by interleukin-6 and fibrinogen polymorphisms. *Environ. Health Perspect.* 117, 1373–1379. <http://dx.doi.org/10.1289/ehp.0800370>.
- Longhin, E., Gualtieri, M., Capasso, L., Bengalli, R., Møllerup, S., Holme, J., Øvrevik, J., Casadei, S., Di Benedetto, C., Parenti, P., Camatini, M., 2016. Physico-chemical properties and biological effects of diesel and biomass particles. *Environ. Pollut.* 215, 366–375. <http://dx.doi.org/10.1016/j.envpol.2016.05.015>.
- Maitland, M.L., Lou, X.J., Ramirez, J., Desai, A.A., Berlin, D.S., McLeod, H.L., Weichselbaum, R.R., Ratain, M.J., Altman, R.B., Klein, T.E., 2010. Vascular endothelial growth factor pathway. *Pharmacogenet. Genomics* 20, 346–349. <http://dx.doi.org/10.1097/FPC.0b013e3283364ed7>.
- Malanga, D., De Marco, C., Guerriero, L., Colelli, F., Rinaldo, N., Scrima, M., Mirante, T., De Vitis, C., Zoppi, P., Ceccarelli, M., Riccardi, M., Ravo, M., Weisz, A., Federico, A., Franco, R., Rocco, G., Mancini, R., Rizzuto, A., Gulletta, E., Ciliberto, G., Vigiiletto, G., 2015. The Akt1/IL-6/STAT3 pathway regulates growth of lung tumor initiating cells. *Oncotarget* 6, 42667–42686. <http://dx.doi.org/10.18632/oncotarget.5626>.
- Mestas, J., Ley, K., 2008. Monocyte-endothelial cell interactions in the development of atherosclerosis. *Trends Cardiovasc. Med.* 18, 228–232. <http://dx.doi.org/10.1016/j.tcm.2008.11.004>.
- Mills, N.L., Donaldson, K., Hadoke, P.W., Boon, N.A., MacNee, W., Cassee, F.R., Sandström, T., Blomberg, A., Newby, D.E., 2009. Adverse cardiovascular effects of air pollution. *Nat. Clin. Pract. Cardiovasc. Med.* 6, 36–44. <http://dx.doi.org/10.1038/npcardio1399>.
- Nemmar, A., Holme, J.A., Rosas, I., Schwarze, P.E., Alfaro-Moreno, E., 2013. Recent advances in particulate matter and nanoparticle toxicology: a review of the in vivo and in vitro studies. *Biomed. Res. Int.* 2013, 279371. <http://dx.doi.org/10.1155/2013/279371>.
- Noël, A., Xiao, R., Perveen, Z., Zaman, H.M., Rouse, R.L., Paulsen, D.B., Penn, A.L., 2016. Incomplete lung recovery following sub-acute inhalation of combustion-derived ultrafine particles in mice. *Part. Fibre Toxicol.* 13, 10. <http://dx.doi.org/10.1186/s12989-016-0122-z>.
- Pálková, L., Vondráček, J., Trilecová, L., Ciganek, M., Pěncíková, K., Neča, J., Milcová, A., Topinka, J., Machala, M., 2015. The aryl hydrocarbon receptor-mediated and genotoxic effects of fractionated extract of standard reference diesel exhaust particle material in pulmonary, liver and prostate cells. *Toxicol. Vitr.* 29, 438–448. <http://dx.doi.org/10.1016/j.tiv.2014.12.002>.
- Radisavljevic, Z., Avraham, H., Avraham, S., 2000. Vascular endothelial growth factor up-regulates ICAM-1 expression via the phosphatidylinositol 3 OH-kinase/AKT/Nitric oxide pathway and modulates migration of brain microvascular endothelial cells. *J. Biol. Chem.* 275, 20770–20774. <http://dx.doi.org/10.1074/jbc.M002448200>.
- Rose-John, S., 2012. IL-6 trans-signaling via the soluble IL-6 receptor: importance for the pro-inflammatory activities of IL-6. *Int. J. Biol. Sci.* 8, 1237–1247.
- Salvi, S., Blomberg, A., Rudell, B., Kelly, F., Sandström, T., Holgate, S.T., Frew, A., 1999. Acute inflammatory responses in the airways and peripheral blood after short-term exposure to diesel exhaust in healthy human volunteers. *Am. J. Respir. Crit. Care Med.* 159, 702–709. <http://dx.doi.org/10.1164/ajrccm.159.3.9709083>.
- Schisler, J.C., Ronnebaum, S.M., Madden, M., Channell, M.M., Campen, M.J., Willis, M.S., 2015. Endothelial inflammatory transcriptional responses induced by plasma following inhalation of diesel emissions. *Inhal. Toxicol.* 27, 272–280. <http://dx.doi.org/10.3109/08958378.2015.1030481>.
- Schwarze, P.E., Totlandsdal, A.L., Låg, M., Refsnes, M., Holme, J.A., Øvrevik, J., Schwarze, P.E., Totlandsdal, A.L., Refsnes, M., L. M., Holme, J.A., Øvrevik, J., Låg, M., Refsnes, M., Holme, J.A., Øvrevik, J., 2013. Inflammation-related effects of diesel engine exhaust particles: studies on lung cells in vitro. *Hindawi Publ. Corp Biomed. Res. Int.* 2013, 685142. <http://dx.doi.org/10.1155/2013/685142>.
- Stenfors, N., Nordenhäll, C., Salvi, S.S., Mudway, I., Söderberg, M., Blomberg, A., Helleday, R., Levin, J.O., Holgate, S.T., Kelly, F.J., Frew, A.J., Sandström, T., 2004. Different airway inflammatory responses in asthmatic and healthy humans exposed to diesel. *Eur. Respir. J.* 23, 82–86.
- Stone, V., Miller, M.R., Clift, M.J.D., Elder, A., Mills, N.L., Møller, P., Schins, R.P.F., Vogel, U., Kreyling, W.G., Jensen, K.A., Kuhlbusch, T.A.J., Schwarze, P.E., Hoet, P., Pietrousti, A., De Vizcaya-Ruiz, A., Baeza-Squiban, A., Tran, C.L., Cassee, F.R., 2016. Nanomaterials vs ambient ultrafine particles: an opportunity to exchange toxicology knowledge. *Environ. Health Perspect.* <http://dx.doi.org/10.1289/EHP424>.
- Tedgui, A., Mallat, Z., 2006. Cytokines in atherosclerosis: pathogenic and regulatory pathways. *Physiol. Rev.* 86, 515–581. <http://dx.doi.org/10.1152/physrev.00024.2005>.
- Törnqvist, H., Mills, N.L., Gonzalez, M., Miller, M.R., Robinson, S.D., Megson, I.L., Macnee, W., Donaldson, K., Söderberg, S., Newby, D.E., Sandström, T., Blomberg, A., 2007. Persistent endothelial dysfunction in humans after diesel exhaust inhalation. *Am. J. Respir. Crit. Care Med.* 176, 395–400. <http://dx.doi.org/10.1164/rccm.200606-872OC>.
- Totlandsdal, A.L., Låg, M., Lilleaas, E., Cassee, F., Schwarze, P., 2015. Differential proinflammatory responses induced by diesel exhaust particles with contrasting PAH and metal content. *Environ. Toxicol.* 30, 188–196. <http://dx.doi.org/10.1002/tox.21884>.
- Totlandsdal, A.L., Refsnes, M., Skomedal, T., Osnes, J.-B., Schwarze, P.E., Låg, M., 2008. Particle-induced cytokine responses in cardiac cell cultures—the effect of particles versus soluble mediators released by particle-exposed lung cells. *Toxicol. Sci.* 106, 233–241. <http://dx.doi.org/10.1093/toxsci/kfn162>.
- Tsai, M.-J., Wang, T.-N., Lin, Y.-S., Kuo, P.-L., Hsu, Y.-L., Huang, M.-S., 2015. Aryl hydrocarbon receptor agonists upregulate VEGF secretion from bronchial epithelial cells. *J. Mol. Med.* 93, 1257–1269. <http://dx.doi.org/10.1007/s00109-015-1304-0>.
- Tseng, C.-Y., Chang, J.-F., Wang, J.-S., Chang, Y.-J., Gordon, M.K., Chao, M.-W., 2015. Protective effects of N-Acetyl cysteine against diesel exhaust particles-induced intracellular ROS generates pro-inflammatory cytokines to mediate the vascular permeability of capillary-like endothelial tubes. *PLoS One* 10. <http://dx.doi.org/10.1371/journal.pone.0131911> e0131911.
- Tseng, C.Y., Wang, J.S., Chao, M.W., 2016. Causation by diesel exhaust particles of endothelial dysfunctions in cytotoxicity, pro-inflammation, permeability, and apoptosis induced by ROS generation. *Cardiovasc. Toxicol.* 1–9. <http://dx.doi.org/10.1007/s12012-016-9364-0>.
- Weldy, C.S., Wilkerson, H.-W., Larson, T.V., Stewart, J.A., Kavanagh, T.J., 2011. DIESEL particulate exposed macrophages alter endothelial cell expression of eNOS, iNOS, MCP1, and glutathione synthesis genes. *Toxicol. Vitr.* 25, 2064–2073. <http://dx.doi.org/10.1016/j.tiv.2011.08.008>.
- Xu, Y., Barregard, L., Nielsen, J., Gudmundsson, A., Wierzbicka, A., Axmon, A., Jönsson, B.A.G., Kåredal, M., Albin, M., 2013. Effects of diesel exposure on lung function and inflammation biomarkers from airway and peripheral blood of healthy volunteers in a chamber study. *Part. Fibre Toxicol.* 10, 60. <http://dx.doi.org/10.1186/1743-8977-10-60>.
- Zhang, J., Wang, X., Vikash, V., Ye, Q., Wu, D., Liu, Y., Dong, W., 2016. ROS and ros-mediated cellular signaling. *Oxid. Med. Cell. Longev.* 2016, 4350965. <http://dx.doi.org/10.1155/2016/4350965>.

Combustion-Derived Particles from Different Fuels Induce Different Cytotoxic Effects on A549 cells

Sara Marchetti^{a*}, Rossella Bengalli^a, Eleonora Longhin^a, Giorgio Buonanno^b, Anita Colombo^a, Paride Mantecca^a, Marina Camatini^a

^aPOLARIS Research Centre, Department of Earth and Environmental Sciences, University of Milano-Bicocca, Piazza della Scienza 1, 20126 Milano, Italy;

^bUniversity of Naples "Parthenope", Via Ammiraglio Ferdinando Acton, 38, 80133 Napoli, Italy
s.marchetti16@campus.unimib.it

The biological effects induced in human alveolar cells by biomass combustion-derived particles (PM₁₀), collected from the emission of heating systems operating with different fuels, have been analysed. Particles emitted from pellet, charcoal and wood combustion, were chemically characterized and used for the exposure of monocultures of human A549 alveolar cell line. Cell viability, pro-inflammatory cytokine expressions, oxidative stress and DNA damage were analysed. Pellet-derived particles seem to have higher toxic properties in comparison with charcoal and wood ones, suggesting a correlation between their chemical properties and toxicological profile. These data demonstrate that biomass combustion-derived particles may activate different toxicological pathways, suggesting that the type of fuel and its quality may have an important role in the strategies to prevent respiratory diseases.

1. Introduction

Airborne pollution, which has been classified by the International Agency for Research on Cancer (IARC), as carcinogenic to humans (Group 1), is generally recognized as a significant environmental and health hazard. Several epidemiological studies have associated particulate exposure with adverse health effects including respiratory and cardiovascular diseases and with increased morbidity and mortality (Anderson *et al.*, 2012). Generally, the adverse effects of PM on human health are determined by its size, surface area and chemical composition. PM dimensional class is an important parameter, depending on which particles can be classified as PM₁₀ (particles with an aerodynamic diameter less than 10 μm), PM_{2.5} ($\varnothing < 2.5 \mu\text{m}$) and PM₁ ($\varnothing < 1 \mu\text{m}$) (Camatini *et al.*, 2010). The size and the surface area determine how deeper the particles can deposit within the respiratory system and induce cytotoxic effects, like inflammatory injury or oxidative damage (Longhin *et al.*, 2013). Furthermore, PM is a mixture of chemical and biological elements, including metals, elemental and organic carbon, polycyclic aromatic hydrocarbons (PAHs), and endotoxins, whose physico-chemical characteristics depend on the emission sources (Billet *et al.*, 2007). Regarding the sources, PM can be classified as natural or anthropogenic. The first one includes volcanoes, fires and dust storms; the other, includes particles emitted from mechanical and industrial combustion processes, vehicle emissions and tobacco smoke. Most of the studies related to air quality and their health effects have been performed in urban area, where air pollution is dominated by anthropogenic sources such as diesel engines exhaust and biomass combustion-derived particles (Anderson *et al.*, 2012).

Although air pollutant emissions are dominated by outdoor sources, PM human exposure is strictly related also to the indoor pollution. Biomass combustion for cooking and heating is the main source of indoor pollution, especially in developing country, where it is burned in rudimentary stoves or open fires and represents the primary source of energy (IARC 2010). IARC in 2010 has classified household biomass fuel combustion as Category 2A, probably carcinogenic to humans. Different kind of fuels can be classified under the name of biomass, such as wood, animal dung, agricultural residues, coals or logs (Capistrano *et al.*, 2016).

The adverse health effects induced by biomass-combustion change according to their composition, strongly influenced by the specific fuel (Sussan *et al.*, 2014), the combustion conditions and technology used (Jalava *et al.*, 2012) and the time of exposure (Akunne *et al.*, 2006). Moreover, particles toxicity is strongly influenced by the compounds of the core or their surface area. PAHs and some heavy metals are the principal elements (Buonanno *et al.*, 2015).

Recently, several studies performed to evaluate the biological effect of combustion-derived particles emitted by different fuels, have shown a high variability of results.

For instance, Jalava and coworkers have evaluated the toxicological effects of particulate emissions from seven different residential wood combusting furnaces, evidencing that combustion technology largely affects the particulate emissions and their toxic potential (Jalava *et al.*, 2012). Furthermore, other authors have found that pellet stoves generated less active particles, in terms of pro-inflammatory activity, compared to the ones generate from wood stoves. However, even if pellet stoves have shown reduced *in vitro* effects when compared to wood stoves, they still can occasionally generate biologically active particulate (Corsini *et al.*, 2017).

The different toxic responses are supposed to be linked to the biomass properties. In this work, the toxicity of biomass combustion-derived particles from different fuels (pellet, charcoal and wood) was investigated with the intent to outline possible differences in the cytotoxicity able to provide further information on the effects produced. Biomass particles were chemical characterized and then tested on A549 cell line to evaluate their effects. The mechanisms activated by the interaction between particles and cells are still unclear and PM-induction of oxidative damage has been evaluated.

2. Methods

2.1 PM sampling and processing

PM10 samples were collected in an indoor environment equipped with an open fireplace and processed for cell culture experiments. Particles were obtained by extraction in pure sterile water with an ultrasound bath, dried in a desiccator, weighted and stored at -20 °C until use. For biological investigations, PM were suspended in pure sterile water (R=18.2 MΩcm; TOC=3 ppb) to obtain aliquots at a final concentration of 2 µg/µL and sonicated for 30 seconds with a sonicator equipped with a probe (SONOPULS Bandelin, 0,105 kJ, A 10%, 001.0 s) just prior to cell exposure.

2.2 Chemical characterization

PM samples were chemically characterized for elements (ng/µgPM) and PAHs (ng/mg_{PM}) with a gas chromatograph coupled with a TSQ mass spectrometer (Thermo Fischer Scientific, St Peters, MO, USA) to perform gas chromatography-mass spectrometry (GC/MS). For the separation was used the column Meta-XLB (60 m length, 0.25 mm internal diameter, 0.25 µm film thickness; Teknokroma, Barcelona, Spain), while He (99.9995% purity) was used as carrier gas. The set temperatures were 260 °C, 280 °C and 250 °C for the injector, transfer line and ion source respectively. The extraction and purification recovery was assessed by adding 5 ng of recovery standard (L429-RS Recovery Standard D-IPA Stock Solution, Wellington Laboratories) before injection into the GC/MS. The calculation of the recovery was obtained as the percentage ratio between the internal standard (added before the extraction) and the recovery standard (added before the injection in GC/MS).

2.3 Cell culture and treatment

A549 cells (ATCC CCL-185, American Type Culture Collection, Manassas, USA) were routinely maintained in OptiMEM medium (Gibco, Life Technologies, Monza, Italy) supplemented with 10% inactivated fetal bovine serum (FBS, Gibco) and 1% penicillin/streptomycin (100 X, Euroclone, Pero, Italy). For *in vitro* experiments, cells were cultured in OptiMEM medium with 1% FBS. The concentration of 5 µg/cm² was selected as the lowest tested dose able to induce significant effects in the *in vitro* system here described after a single acute exposure. Cells were exposed after 24 h from seeding to 5 µg/cm² of pellet, charcoal and wood particles, respectively.

2.4 Cell viability, inflammatory response, oxidative stress and DNA damage

At the end of the exposure, the media were collected and the cellular responses analyzed. Cell viability was determined by lactate dehydrogenase (LDH) detection. The assay, that provides information on cell membrane integrity, was performed according to manufacturer's guidelines (Pierce, Thermo Fischer Scientific). The cytokine release as marker of pro-inflammatory response in cells was evaluated. The levels of TNFα were determined in culture medium by ELISA assay following the manufacturers' instructions and the absorbance measured by a multiplate spectrophotometer reader (Tecan, Männedorf, Switzerland) at 450 nm

and 630 nm. Standard curves were used to determine the concentration of proteins in pg/mL. Oxidative stress response was assessed by flow cytometry using the Carboxy-DCFDA probe, which detects the reactive oxygen species (ROS) production. A549 cells were incubated with the Carboxy-DCFDA probe for 20 minutes in Hank's Balanced Salt Solution (Thermo Fisher Scientific; Monza, Italy) and successively, exposed to biomass for 2 h. At the end of the incubation, cells were detached, re-suspended in PBS and analysed at the flow cytometer (CytoFLEX 13/3, Beckman Coulter, USA). Fluorescence of 10,000 events was detected using 525 nm band pass filter (FITC). Data were analysed as mean percentage of positive cells for staining. The activated form of Ataxia-Telangiectasia mutated ATM (p-ATM) and histone H2AX phosphorylation (γ H2AX) were used as markers of DNA damage and analysed with immunocytochemical technique. Cells were grown on cover-slips, exposed for 24 h to PM and etoposide (1,65 μ M), used as positive control, and finally, fixed with 4% paraformaldehyde. Later, cells were incubated for 1 h with blocking-permeabilizing solution (0,1% Tween20, 0,1% Triton X-100 and 1% BSA in PBS) and stained O/N with p-ATM (1:100, Santa Cruz Biotechnology, Dallas, Texas, USA) and γ H2AX Alexafluor-488 conjugated antibody (1:100, Cell Signaling). The day after, cells were incubated with the secondary antibody Alexa Fluor 594 goat anti-mouse IgG. Finally, cell DNA was counterstained with DAPI. Images were taken under a fluorescence microscope (AxioObserver, Zeiss, Germany) equipped with a digital camera. Digital images were taken with the dedicated software (AxioVision4, Carl Zeiss Vision).

2.5 Statistical analysis

The data are reported as mean values of independent experiments \pm SEM. Statistical differences between samples were tested with unpaired t-test or two-way ANOVA and post hoc comparisons performed with Dunnett's method, by GraphPad Prism 6 software. Statistical differences were considered significant at the 95% level ($p < 0.05$).

3. Results

3.1 Biomass characterization

Chemical characterization revealed specific differences between biomasses. PM composition indeed, seems to be strongly affected by the specific type of fuels used. PAHs were the major chemical fraction with a concentration of 8 and 11 times higher in charcoal and wood particles in comparison with pellet. Phenanthrene and Pyrene were the most abundant PAHs in all the particles collected. Pellet-derived PM was enriched in metals, with the higher concentration of Zinc in pellet increased 1.5 and 3 times respect to wood and charcoal particles (data not shown).

3.2 Biological investigations

In vitro experiments were performed on A549. Cell viability, measured with LDH assay, was the first outcome analysed to define the biomass hazardous effect. Cell viability at 24 h of exposure to PM 5 μ g/cm² presented a significant decrease (Figure 1 A). As shown, pellet and wood-derived PM had the major response.

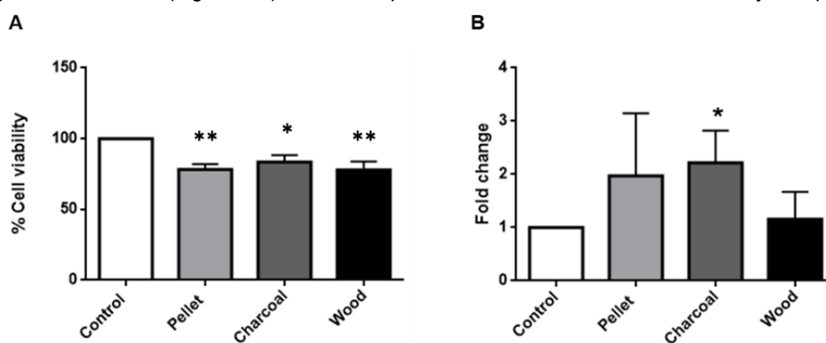


Figure 1: A) Cell viability measured with LDH release. Data are expressed as percentage of viable cells with respect to control. Statistical analysis was performed by Two-way ANOVA with Dunnett's multiple comparison test. B) Intracellular ROS production. Statistical analysis was performed by unpaired t test. ** $p < 0.01$ and * $p < 0.05$ vs control cells.

The reduction in cell viability was not accompanied by a higher inflammatory effect. The levels of the pro-inflammatory cytokine TNF α , were not affected by biomass exposure (data not shown).

The oxidative stress response after exposure to biomasses was also investigated. The cytometric analysis confirms the statistically significant ROS production only after A549 exposure to charcoal (Figure 1B). A slight, but not significant increase in the response was observed also after pellet exposure.

The oxidative DNA damage was assessed by evaluating the phosphorylation of two DNA markers: the histone 2AX (γ H2AX), marker of DNA double-strand breaks (DSBs) and DNA repair, and ATM, involved in the genotoxic stress response. Fluorescence microscopy evidenced the presence of characteristic distinct foci of p-ATM and γ H2AX in chromatin of cells treated with pellet-derived PM (Figure 2).

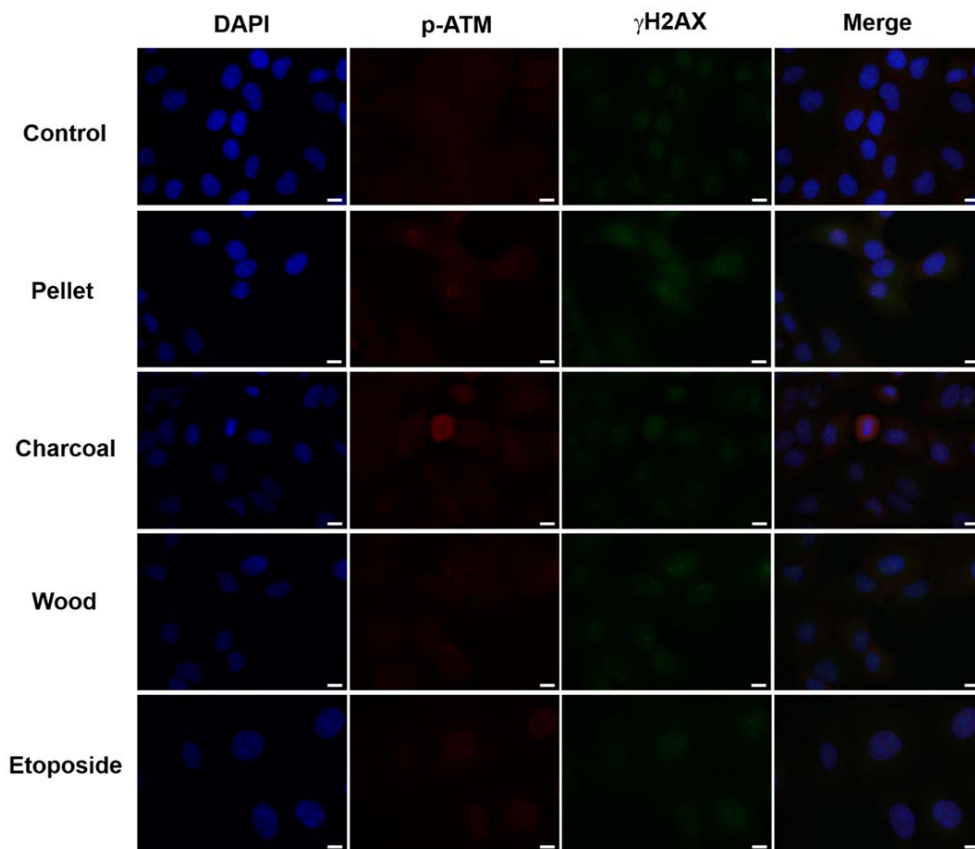


Figure 2: Fluorescence microscopy images showing DNA damage. Scale bar= 10 μ m.

4. Discussion

Biomass particles showed a deep difference in chemical composition. These findings can explain the different toxic effects observed. Pellet-derived PM revealed a higher capacity of triggering cytotoxic and genotoxic effects on A549 cells, since it induces cell death, ROS production and DNA damage. In order to investigate the biological effect of biomasses derived from different emission sources on human A549 cells, the ability of particles to affect cellular metabolic activity and viability at 24 h of exposure was examined at first. As expected from literature data (Marabini *et al.*, 2017), biomasses were able to damage the cell plasma membranes, suggesting the activation of mechanisms of cell death.

Important mechanisms related to PM toxicity and involved in health effects from biomass exposure, are oxidative stress and inflammation (Longhin *et al.*, 2013). The modulation of the inflammatory response after PM exposure was investigated by measuring the release of the cytokine TNF α . Not surprisingly, A549 cells

showed a low inflammatory response, in agreement with previous observations reporting that wood smoke particles are not able to induce a high cytokines release respect to other PM sources in the *in vitro* systems (Longhin *et al.*, 2016). The oxidative stress in response to biomass was also investigated and the cytometric analysis confirms the statistically significant ROS production only after A549 exposure to charcoal. PM-induced ROS formation has been widely reported and linked to metals and PAHs (Yang *et al.*, 2016). Despite a higher presence of metals in pellet-derived PM, this fraction resulted to be less effective on ROS formation in comparison with particles collected from charcoal and wood. The exposure to biomass can also lead to genotoxic effects, such as alterations of DNA integrity and function, analyzed with DSBs.

The ROS increase could be related to the soluble metals as well as to the presence of PAHs and quinones. One of the most severe consequence of ROS damage is its interaction with DNA. DNA damage, if not repaired, can lead to genetic instability and can play an important role in lung cancer development. There are evidences indicating that the exposure to traffic-related air pollution is linked to DNA oxidative damage and this might be associated with an increased risk of cancer (Møller *et al.*, 2014).

In order to evaluate PM-induced genotoxic effect, the presence of DNA lesions by the expression of p-ATM and γ H2AX was investigated. ATM is a protein involved in genotoxic stress and when activated it triggers a cascade of events leading to the phosphorylation of different substrates, including H2AX, which are able to mediate the effects of ATM on DNA repair. These findings indicate an increased expression of p-ATM and γ H2AX only after pellet exposure, suggesting the induction of DNA damage and the subsequent activation of the DNA repair machine. This effect has been previously linked to the presence of PAHs (Longhin *et al.*, 2013). However, a PM10 high content of metals too may be one of the main factors producing the biological responses, including DNA oxidative damage (Van De Huevel *et al.*, 2016).

5. Conclusions

In the last years, great attention has been devoted to the indoor PM fraction, since several studies have reported its involvement in the onset of pulmonary and cardiovascular diseases. The results of this study evidence that pellet-derived PM, which has the higher concentration of metals, activates death mechanisms and oxidative responses in alveolar cells, with consequent oxidative lesions at DNA level. Wood-derived PM is unable to affect the biological endpoints in this research, except for cell viability. The lower toxic properties observed after wood exposure could be explained by the activation of different molecular pathways, still unknown. Charcoal combustion particles induced oxidative stress on A549 cells but not genotoxic damage, suggesting a role of another pathway, probably related to the xenobiotics metabolism. From the obtained results it may be deduced that diverse biomasses may activate lung different toxicological pathways which may depend to their chemical composition. The role of combustion-derived particles on human health is still under investigation and further studies are needed to understand the molecular mechanisms responsible for the lung toxic effects.

Acknowledgments

This research has a financial support from Cariplo Foundation (proj. ID 2013-1038 and the Italian Ministry of Foreign Affairs and International Cooperation (proj. ID PGR00786).

Reference

- Akunne, A.F., Louis, V.R., Sanon, M., Sauerborn, R., 2006, Biomass solid fuel and acute respiratory infections: The ventilation factor. *International Journal of Hygiene and Environmental Health*, 209, 445-450, DOI: 10.1016/j.ijheh.2006.04.009
- Anderson, J.O., Thundiyil, J.G., Stolbach, A., 2012, Clearing the Air: A Review of the Effects of Particulate Matter Air Pollution on Human Health. *Journal of Medical Toxicology*, 8, 166-175, DOI: 10.1007/s13181-011-0203-1
- Billet, S., Garçon, G., Dagher, Z., Verdin, A., Ledoux, F., Cazier, F., Courcot, D., Aboukais, A., Shirali, P., 2007, Ambient particulate matter (PM2.5): Physicochemical characterization and metabolic activation of the organic fraction in human lung epithelial cells (A549), *Environmental Research*, 105, 212-223, DOI: 10.1016/j.envres.2007.03.001
- Buonanno, G., Giovinco, G., Morawska, L., Stabile, L., 2015, Lung cancer risk of airborne particles for Italian population, *Environmental Research*, 142, 443-451. DOI:10.1016/j.envres.2015.07.019
- Camatini M., Gualtieri M. and Mantecca P., 2010, Particles and health: state of the research, *Chemical Engineering Transactions*, 22, 1-14, DOI: 10.3303/CET1022001
- Capistrano, S.J., Zakarya, R., Chen, H., Oliver, B.G., 2016, Biomass smoke exposure enhances rhinovirus-induced inflammation in primary lung fibroblasts, *International Journal of Molecular Sciences*, 17, DOI: 10.3390/ijms17091403

- Corsini, E., Ozgen, S., Papale, A., Galbiati, V., Lonati, G., Fermo, P., Corbella, L., Valli, G., Bernardoni, V., Dell'Acqua M., Becaglie, S., Caruso, D., Vecchi, R., Galli, C.L., Marinovich, M., 2017, Insights on wood combustion generated proinflammatory ultrafine particles (UFP), *Toxicology Letters*, 266, 74-84, DOI: 10.1016/j.toxlet.2016.12.005
- IARC 2010. Monographs on the Evaluation of Carcinogenic Risks to Humans, 2010, 95
- Jalava, P.I., Happonen, M.S., Kelz, J., Brunner, T., Hakulinen, P., Mäki-Paakkanen, J., Hukkanen, A., Jokiniemi, J., Obernberger, I., Hirvonen, M.R., 2012, In vitro toxicological characterization of particulate emissions from residential biomass heating systems based on old and new technologies, *Atmospheric Environment*, 50, 24-35, DOI: 10.1016/j.atmosenv.2012.01.009
- Longhin, E., Gualtieri, M., Capasso, L., Bengalli, R., Mollerup, S., Holme, J.A., Øvrevik, J., Casadei, S., Di Benedetto, C., Parenti, P., Camatini, M., 2016, Physico-chemical properties and biological effects of diesel and biomass particles, *Environmental Pollution*, 215, 366-375, DOI: 10.1016/j.envpol.2016.05.015
- Longhin, E., Pezzolato, E., Mantecca, P., Holme, J.A., Franzetti, A., Camatini, M., Gualtieri, M., 2013, Season linked responses to fine and quasi-ultrafine Milan PM in cultured cells, *Toxicology in Vitro*, 27, 551-559, DOI: 10.1016/j.tiv.2012.10.018
- Marabini, L., Ozgen, S., Turacchi, S., Aminti, S., Arnaboldi, F., Lonati, G., Fermo, P., Corbella, L., Valli, G., Bernardoni, V., Dell'Acqua, M., Vecchi, R., Becaglie, S., Caruso, D., Corrado, L.G., Marinovich, M., 2017, Ultrafine particles (UFPs) from domestic wood stoves: genotoxicity in human lung carcinoma A549 cells, *Mutation Research - Genetic Toxicology and Environmental Mutagenesis*, 820, 39-46, DOI: 10.1016/j.mrgentox.2017.06.001
- Møller, P., Danielsen, P.H., Karottki, D.G., Jantzen, K., Roursgaard, M., Klingberg, H., Jensen, D.M., Christophersen, D.V., Hemmingsen, J.G., Cao, Y., Loft, S., 2014, Oxidative stress and inflammation generated DNA damage by exposure to air pollution particles, *Mutation Research - Reviews in Mutation Research*, 762, 133-166, DOI: 10.1016/j.mrrev.2014.09.001
- Sussan, T.E., Ingole, V., Kim, J.H., McCormick, S., Negherbon, J., Fallica, J., Akulian, J., Yarmus, L., Feller-Kopman, D., Wills-Karp, M., Horton, M.R., Breyse, P.N., Agrawal, A., Juvekar, S., Salvi, S., Biswal, S., 2014, Source of biomass cooking fuel determines pulmonary response to household air pollution, *American Journal of Respiratory Cell and Molecular Biology*, 50, 538-548, DOI: 10.1165/rcmb.2013-0201OC
- Van Den Heuvel, R., Den Hond, E., Govarts, E., Colles, A., Koppen, G., Staelens, J., Mampaey, M., Janssen, N., Schoeters, G., 2016, Identification of PM10 characteristics involved in cellular responses in human bronchial epithelial cells (Beas-2B), *Environmental Research*, 149, 48-56, DOI: 10.1016/j.envres.2016.04.029
- Yang, L., Liu, G., Lin, Z., Wang, Y., He, H., Liu, T., Kamp, D.W., 2016, Pro-Inflammatory Response and Oxidative Stress Induced by Specific Components in Ambient Particulate Matter in Human Bronchial Epithelial Cells, *Environmental toxicology*, 31, 923-936, DOI:10.1002/tox



In vitro lung toxicity of indoor PM₁₀ from a stove fueled with different biomasses

Sara Marchetti ^{a,*}, Eleonora Longhin ^a, Rossella Bengalli ^a, Pasquale Avino ^b, Luca Stabile ^c, Giorgio Buonanno ^{c,d,e}, Anita Colombo ^a, Marina Camatini ^a, Paride Mantecca ^a

^a POLARIS Research Centre, Department of Earth and Environmental Sciences, University of Milano-Bicocca, Piazza della Scienza 1, 20126 Milano, Italy

^b DiAAA, University of Molise, via De Sanctis, 86100 Campobasso, Italy

^c Department of Civil and Mechanical Engineering, University of Cassino and Southern Lazio, Via Di Biasio 43, 03043 Cassino, FR, Italy

^d University of Naples "Parthenope", Via Ammiraglio Ferdinando Acton, 38, 80133 Napoli, Italy

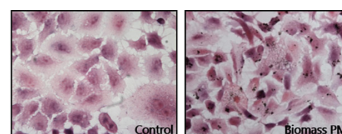
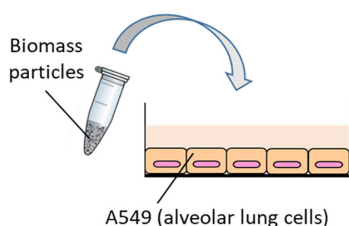
^e Queensland University of Technology, GPO Box 2434, Brisbane, Qld 4001, Australia



HIGHLIGHTS

- Biomass particles with diverse properties induce different biological responses.
- Pellet PM with high metal content induces DNA damage and cell cycle alteration.
- Elevated Zinc concentration causes cytotoxic and genotoxic effects.

GRAPHICAL ABSTRACT



- Cytotoxicity
- Genotoxicity
- Cell cycle alterations

ARTICLE INFO

Article history:

Received 11 June 2018

Received in revised form 3 August 2018

Accepted 19 August 2018

Available online 20 August 2018

Editor: P. Kassomenos

Keywords:

Biomass
PM₁₀
Air pollution
Indoor
Lung cells
Cytotoxicity

ABSTRACT

Biomass combustion significantly contributes to indoor and outdoor air pollution and to the adverse health effects observed in the exposed populations. Besides, the contribution to toxicity of the particles derived from combustion of different biomass sources (pellet, wood, charcoal), as well as their biological mode of action, are still poorly understood. In the present study, we investigate the toxicological properties of PM₁₀ particles emitted indoor from a stove fueled with different biomasses.

PM₁₀ was sampled by gravimetric methods and particles were chemically analyzed for Polycyclic Aromatic Hydrocarbons (PAHs) and elemental content. Human lung A549 cells were exposed for 24 h to 1–10 μg/cm² PM and different biological endpoints were evaluated to comparatively estimate the cytotoxic, genotoxic and pro-inflammatory effects of the different PMs.

Pellet PM decreased cell viability, inducing necrosis, while charcoal and wood ones mainly induced apoptosis. Oxidative stress-related response and cytochrome P450 enzymes activation were observed after exposure to all the biomasses tested. Furthermore, after pellet exposure, DNA lesions and cell cycle arrest were also observed. The severe genotoxic and pro-necrotic effects observed after pellet exposure were likely the consequence of the high metal content. By administering the chelating agent TPEN, the genotoxic effects were indeed rescued. The

Abbreviations: PM, Particulate matter; ROS, Reactive oxygen species; PAHs, polycyclic aromatic hydrocarbons; UFP, ultrafine particles; HO-1, hemeoxygenase 1; TPEN, N,N,N',N'-tetrakis(2 pyridylmethyl)ethylenediamine; CDPs, combustion-derived particles; Zn, Zinc; Pb, lead; CYP1A1, Cytochrome P450, family 1, subfamily A, polypeptide 1; CYP1B1, Cytochrome P450 Family 1 Subfamily B Member 1; B[a]P, Benzo[a]pyrene; p-ATM, phosphorylated form of Ataxia Telangiectasia Mutated; γH2AX, Phosphorylated histone H2AX; GC/MS, gas chromatography–mass spectrometry; SIM, single ion monitoring; INAA, Instrumental Neutron Activation Analysis; TEM, transmission electron microscopy; SEM, scanning electron microscopy; RT, room temperature; PBS, Phosphate Buffered Saline; PI, Propidium Iodide; IL, Interleukin; O/N, overnight; TBS, Tris-Buffered Saline; TBS-T, TBS with 0.1% Tween20; SE, standard error of mean; OM, optical microscopy.

* Corresponding author.

E-mail addresses: s.marchetti16@campus.unimib.it (S. Marchetti), rossella.bengalli@unimib.it (R. Bengalli), p.avino@inail.it (P. Avino), l.stabile@unicas.it (L. Stabile), buonanno@unicas.it (G. Buonanno), anita.colombo@unimib.it (A. Colombo), marina.camatini@unimib.it (M. Camatini), paride.mantecca@unimib.it (P. Mantecca).

higher content in PAHs measured in wood and charcoal PMs was likely the reason of the enhanced expression of metabolizing and oxidative stress-related enzymes, like CYP1B1 and HO-1, and the consequent increase in apoptotic cell death.

These data suggest that combustion particles from different biomass sources may impact on lung cells according to different pathways, finally producing different toxicities. This is strictly related to the PM chemical composition, which reflects the quality of the combustion and the fuel in particular. Further studies are needed to clarify the role of particle dimension and the molecular mechanisms behind the harmful effects observed.

© 2018 Elsevier B.V. All rights reserved.

1. Introduction

The burning of biomass fuels for domestic heating is one of the most significant sources of particulate air pollutants during winter in the developed countries (Li et al., 2017; Secrest et al., 2016). Its role has increased in the last years as consequence of a general effort in improving the use of renewable energy sources and lower costs. Emissions from biomass combustion significantly contribute to the air pollution events and could cause severe health effects in adult and children (Samburova et al., 2016). Indoor air quality can differ with type of housing ventilation, energy technology (type of oven or stove used), environmental pollutant concentration and exposure time. Airborne and combustion particle exposure has been associated with increased lung cancer risk, exacerbation of respiratory diseases and cardiovascular impairment (Jalava et al., 2012; Sussan et al., 2014; Swiston et al., 2008). Furthermore, the International Agency for Research on Cancer (IARC), has classified biomass fuel combustion as probably carcinogenic to humans (Category 2A) (“IARC Monographs on the Evaluation of Carcinogenic Risks to Humans,” 2010).

Previous studies have investigated the toxicological effects of particles derived from biomass combustion in *in vitro* and *in vivo* systems, reporting ROS formation, activation of the response to polycyclic aromatic hydrocarbons (PAHs), DNA damage and cell death (Dilger et al., 2016; Happonen et al., 2013; Muala et al., 2015). The results on inflammatory responses are controversial, since some papers report only minor activation (Kasurinen et al., 2017; Muala et al., 2015), while others highlight release of interleukins and activation of MAPK (Corsini et al., 2017; Uski et al., 2012). One reason of such differences might be related to the use of particles derived from different biomasses and combustion processes. In fact, particles collected from combustion of wood, animal dung, crop residues (Muala et al., 2015), coals (Capistrano et al., 2016), logs (Kasurinen et al., 2017), spring sandstorms or resuspension of local soil (Jin et al., 2016) are all referred as biomass. Therefore, the particle composition can be different depending on fuel type (Muala et al., 2015) and its properties, including content of ash and moisture (Jin et al., 2016), chemical composition, combustion conditions (Lamberg et al., 2013) and combustion appliances used (Kocbach Bølling et al., 2009).

Recently, we reported low biological effects for biomass ultrafine particles (UFPs) produced by a modern boiler propelled with high quality certified pellet. Particle chemical characterization showed that this effect was associated to a low content of harmful compounds such as PAHs and metals (Longhin et al., 2016).

To date, the comprehension of the toxic effects induced by biomass particles emitted from different fuels is still poor. However, it is known that the physicochemical properties related to the content of transition metals and PAHs are associated to different cytotoxic properties, that could be responsible for the several adverse health effects caused by PM exposure (Jin et al., 2016; Yang et al., 2016).

This study intends to investigate how different fuels (*i.e.* pellet, charcoal and wood) used to propel the same stove (commonly used) may affect the properties of the emitted particles and their toxic potential.

Particulate matter (PM10) was sampled on filters by gravimetric technique and PAHs, metals content and particles morphology were investigated. The cytotoxic effect of PM10 was analyzed on the human

alveolar A549 cells, that represent an extensively used model for inhalation toxicology purposes, and in particular for the PM cytotoxic effect (Chirino et al., 2017; Choi et al., 2016; Gualtieri et al., 2012; Kasurinen et al., 2017; Rossner et al., 2016). Cell viability, inflammatory response, antioxidant activity, xenobiotic metabolism activation, cell cycle alterations and DNA damage were evaluated.

Our data demonstrate that combustion particles deriving from different biomasses can activate different toxicological pathways, pointing out the role of the particle physico-chemical properties on the cytotoxic effects produced and the molecular mechanisms involved.

2. Materials and methods

2.1. Particles sampling

PMs were collected on filters through a gravimetric technique. The measurements were performed in a 20 m³ room (with doors and windows closed) equipped with an open fireplace for 4 h. The fuel (pellet, charcoal or wood) was burnt in the open fireplace and continuously fed during the experiment. Three combustion tests were carried out for each fuel. Thus, PMs for biological investigation were sampled on Teflon filter, while particles for the chemical analysis were collected on laden quartz filters. PM10 concentrations were obtained after proper filter conditioning before and after particle samplings (Buonanno et al., 2011, 2009).

The gravimetric sampler used was made up of a volumetric rotating pump Zambelli 6000 Plus (equipped with temperature and atmospheric pressure sensors to measure normalized sampling volume) and a Zambelli PM10 impactor (working at a nominal fixed flow rate of 2.3 m³ h⁻¹ according to the EN 12341) to collect particles on low porosity filters for post-hoc analysis and PM10 mass concentration evaluation.

2.2. Particles characterization

2.2.1. Polycyclic aromatic hydrocarbons (PAHs)

The following PAHs were determined: acenaphthene, acenaphthylene, fluorene, phenanthrene, anthracene, fluoranthene, pyrene, benzo(a)anthracene, chrysene, benzo(b)fluoranthene, benzo(j)fluoranthene, benzo(k)fluoranthene, benzo(e)pyrene, benzo(a)pyrene, perylene, indeno(1,2,3,c,d)pyrene, dibenzo(a,h)anthracene and benzo(g,h,i)perylene. PAHs were quantified by gas chromatography–mass spectrometry (GC/MS) with an isotopic dilution method (Stabile et al., 2018). In particular, filters were spiked before the extraction with 5 ng of perdeuterated PAHs (L429-IS Internal Standard D-IPA Stock Solution, Wellington Laboratories, Guelph, Canada); then the PAHs were Soxhlet-extracted in hexane for 24 h and the samples obtained were concentrated on a rotary evaporator (40 °C, 3.00 × 10⁴ Pa) to 3–5 mL. Finally, the samples were automatically purified, by means of gel permeation chromatography, and concentrated, using an AccuPrep MPS & AccuVap Inline (J2 Scientific, Columbia, MO, USA).

GC/MS analysis was performed by an Ultra Trace gas chromatograph coupled with a TSQ mass spectrometer (Thermo Fischer Scientific, St Peters, MO, USA) used in single ion monitoring (SIM) mode. The column Meta-XLB (60 m length, 0.25 mm internal diameter, 0.25 μm film

thickness; Teknokroma, Barcelona, Spain) was used for the separation, and He (99.9995% purity) was used as carrier gas. The temperatures for the injector, transfer line and ion source were set as 260 °C, 280 °C and 250 °C, respectively. The following oven temperature program was adopted: isothermal oven temperature of 60 °C for 1 min; thermal gradient of 20 °C min⁻¹ up to 250 °C; isothermal oven temperature of 250 °C for 10 min; thermal gradient of 15 °C min⁻¹ up to 300 °C; isothermal oven temperature of 300 °C for 15 min; thermal gradient of 5 °C min⁻¹ up to 325 °C; isothermal oven temperature of 325 °C for 10 min. Each native PAH was quantified using its perdeuterated isotopologues as internal standard, except for acenaphthene (quantified using perdeuterated acenaphthylene), fluorene, anthracene (quantified using perdeuterated phenanthrene), pyrene (quantified using perdeuterated fluoranthene) and benzo(e)pyrene (quantified using perdeuterated benzo(a)pyrene). To calculate the extraction and purification recovery, 5 ng of recovery standard (L429-RS Recovery Standard D-IPA Stock Solution, Wellington Laboratories) were added before injection into the GC/MS. Recovery was calculated as the percentage ratio between the internal standard (added before the extraction) and the recovery standard (added before the injection in GC/MS). Perdeuterated acenaphthene was used to calculate the recovery of acenaphthylene and phenanthrene; perdeuterated pyrene was used to calculate the recovery of fluoranthene, benzo(a)anthracene and chrysene; perdeuterated benzo(e)pyrene was used to calculate the recovery of benzo(b)fluoranthene, benzo(k)fluoranthene, benzo(a)pyrene, perylene, indeno(1,2,3,c,d)pyrene, dibenzo(a,h)anthracene and benzo(g,h,i)perylene.

2.2.2. Elements

The inorganic composition was investigated by a nuclear non-destructive technique: the Instrumental Neutron Activation Analysis (INAA). In particular, PMs (placed into the polyethylene tubes; Kartell, Milan, Italy) were irradiated by a Triga Mark II nuclear reactor of the ENEA-Casaccia Laboratories (1 MW power) (Capannesi et al., 2009). The irradiation was performed in the rotating rack, called Lazy Susan, which can give uniform neutron irradiation to the sample due to the continuous rotation. After neutron irradiation, the radionuclides begin to decay emitting γ -rays. The half-life time ($t_{1/2}$), which is characteristic of nuclides produced, was adopted as criterion for element detection (Avino et al., 2000). Basically, the γ -ray emission of nuclides with long $t_{1/2}$ is negligible after short irradiation (Rabbit) (Avino et al., 2011). However, nuclides with short $t_{1/2}$ were not detected because the sample was very active after the end of irradiation and the cooling time (3–5 days) is greater than the nuclide half-life; moreover, the nuclide activities with long half-lives hide the contribution (Avino et al., 2013, 2011). An 8 h long irradiation in the Lazy Susan was performed at a neutron flux of $2.6 \times 10^{12} \text{ n s}^{-1} \text{ cm}^{-2}$. At the end of irradiation, the samples were highly active and, according to the half-life of each element, only few elements, such as As, Cd, Cr, Cu, Hg, Ni, Se and Zn could be analyzed, whereas Pb was separately analyzed by Inductively Coupled Plasma Atomic Emission Spectroscopy (ICP-AES). For the analysis, primary and secondary standards were used: primary standards (Carlo Erba, Milano, Italy) were Al, As, Br, Cl, Cu, I, Mg, Mn, Na, and V, whereas, as secondary standards, three reference materials (SRMs) such as SRM 2709 (S. Joaquim Soil) and SRM 98a (Plastic Clay) from the National Institute of Standards and Technology (NIST), and a SRM GRX-4 (Soil) from the US Geochemical Survey (USGS) were involved in this study. To guarantee the quality assurance and quality control (QA/QC) of the measurements performed, three SRMs along with the 8 primary standards were adopted: SRM 2709, SRM 98a, and SRM GRX-4. After irradiation, γ -ray spectrometry measurements of different durations were carried out using a Ge (HP) Canberra detector (Meriden, CT, USA) (full width at half maximum 1.68 keV at 1.332 keV) connected to a multichannel analyzer equipped with software packages (Canberra Genie 2k) for a γ -spectra analysis.

2.3. Particles extraction for biological investigations

Particles for *in vitro* exposures were obtained by extraction from Teflon filters according to a standardized procedure previously reported (Longhin et al., 2013). Briefly, filters from the same fuel were pooled in a glass vial and PM was extracted by an ultrasound bath (SONICA Soltec, Milan, Italy) by replicating four 20 min cycles using 2 mL of pure sterile water for each cycle. PM10 water suspensions were then collected in sterile tubes previously weighed, dried into a desiccator and the resulting pellet weighed to determine the mass of particles extracted. Finally, samples were stored at -20 °C until use. For biological investigations, particles were suspended in sterilized water to obtain aliquots at a final concentration of 2 $\mu\text{g}/\mu\text{L}$ just before use. PM suspensions were sonicated for 30 s just prior to cells exposure.

2.4. Morphological characterization of extracted particles

After extraction from the Teflon filters, a morphological characterization of the particles was performed by transmission electron microscopy (TEM) and scanning electron microscopy (SEM). Briefly, aliquots of 8 μL of sonicated particle suspensions at 25 $\mu\text{g}/\text{mL}$ in pure water and 1% Isopropyl alcohol were respectively, pipetted on 200-mesh formvar-coated copper grids and aluminum stubs and dried at room temperature (RT). Samples were observed by a Jeol JEM 1220 TEM, operating at 80 kV, and a Tescan VEGA 5136XM, operating at 20 kV. Images were digitally acquired and elaborated through dedicated softwares.

2.5. Cell culture and exposure

A549 cells, a human lung adenocarcinoma epithelial cell line, were obtained from the American Type Culture Collection (ATCC® CCL-185, American Type Culture Collection, Manassas, USA). Cells were cultured in OptiMEM 1 Reduced Serum Medium (Gibco, Life Technologies, Monza, Italy) supplemented with 10% heat-inactivated fetal bovine serum (FBS, Gibco) and Penicillin/Streptomycin (100 \times , Euroclone, Pero, Italy) in a 5% CO₂ atmosphere at 37 °C.

For particle exposure, cells (passages 39 to 55) were seeded at a concentration of 2×10^4 cells/cm² (12-well plates) or 1.6×10^4 cells/cm² (6-well plates), and grown up to 80% confluence for 24 h. At the optimal confluence, the culture medium was replaced with 1% FBS supplemented OptiMEM medium and cells exposed for 24 h at 37 °C to different doses (1, 2.5, 5, 7.5 and 10 $\mu\text{g}/\text{cm}^2$) for cellular metabolic activity evaluation and to 5 $\mu\text{g}/\text{cm}^2$ (50 $\mu\text{g}/\text{mL}$) PM10 for the following experiments. The same treatment was repeated for all the particles. Unexposed cells were used as control. Cells were exposed also to 14 μM benzo(a)pyrene (B[a]P, Sigma Aldrich, Saint Louis, MO, USA) for xenobiotic metabolism activation studies or 1.65 μM Etoposide (Sigma Aldrich) for DNA damage studies, as positive control (data not showed).

2.6. Cell viability

A549 cell viability was evaluated after 24 h of exposure to increasing PM10 concentrations (1–10 $\mu\text{g}/\text{cm}^2$) for each biomass particles by means of Alamar Blue assay. After exposure, the medium was removed, cells were rinsed twice with Phosphate Buffered Saline (PBS) and incubated for 3 h in 10% Alamar Blue (Invitrogen, Burlington, ON, Canada) supplemented OptiMEM complete medium. The absorbance, proportional to cell metabolic activity, was assessed with a multiplate spectrophotometer reader (Tecan, Männedorf, Switzerland) at excitation and emission wavelengths of 570 and 630 nm respectively.

To provide additional data on biomass cytotoxicity, cell viability was evaluated also by fluorescence microscopy following cells staining with Hoechst 33342 (1 mg/mL) and Propidium iodide (PI, 1 mg/mL). Briefly, after cells exposure to 5 $\mu\text{g}/\text{cm}^2$ PM, supernatants were harvested to recover floating cells, whereas attached cells were collected after trypsinization. Trypsinized and floating cells were then centrifuged at

1200 rpm, pooled, re-suspended in complete medium and stained 1:1 with Hoechst and PI for 20 min at RT in the dark. Cells were finally, centrifuged, re-suspended in FBS and smeared on a glass slide to quickly dry. Cell morphology was evaluated using a fluorescence microscope (Zeiss Axioplan). Cells were scored and classified on the different nuclear morphology as: viable (Hoechst positive and PI negative, with intact plasma membrane and without nuclear anomalies), necrotic (PI positive), apoptotic (bright Hoechst-stained with condensed and/or fragmented nuclei) and mitotic (Hoechst positive with chromosome condensation). At least 300 cells for each sample were scored. Additional cytofluorimetric analyses were performed on cells stained with Annexin V/PI to assess the cell death modality (see Additional file 2).

2.7. Pro-inflammatory cytokines release

Intracellular and released protein levels of the pro-inflammatory cytokine Interleukin 6 (IL-6) and the chemokine IL-8 were measured by commercial enzyme-linked immunosorbent assay (ELISA) kits (IL-6, IL-8, Life Technologies). At the end of the exposure, cell supernatants were collected and centrifuged at 12000 rpm for 6 min at 4 °C to remove debris. The exposed cells were scraped and lysed on ice in RIPA buffer (150 mM NaCl, 1% TritonX-100, 0.5% sodium deoxycholate, 0.1% SDS, 50 mM Tris pH 8.0) and 0.1% of proteases inhibitor, added just before use. The supernatants and cell lysates were stored at –80 °C until measurement. Cytokine analysis was performed according to the manufacturer's instructions. The absorbance of each sample was measured at 450 nm and the amount of proteins in pg/mL quantified by a plate reader (Multiplate Reader Ascent, Thermo Scientific, USA), based on a standard curve.

2.8. Protein extraction and immunoblotting

After exposure, cells for immunoblotting were rinsed twice, scraped and lysed on ice in RIPA buffer and 0.1% of proteases inhibitor, added just before use. Total cellular lysates were centrifuged at 12000 rpm for 15 min and the protein content evaluated by the bicinchoninic acid assay (Sigma Aldrich) according to the manufacturer's instructions. Equal amounts of proteins (30 µg) were loaded onto 12% SDS-PAGE gels, separated and transferred on nitrocellulose membranes. Equal loading was assessed by Ponceau S red staining of protein bands on nitrocellulose. Membranes were rinsed three times with water and Tris-Buffered Saline (TBS) with 0.1% Tween20 (TBS-T) and then, incubated for 1 h with Blocking buffer, TBS-T supplemented with 5% w/v bovine serum albumin (BSA; Sigma) or milk (Skim milk powder, Fluka, Sigma). Membranes were incubated overnight (O/N) at 4 °C with the specific primary antibody (HO-1 P249 Antibody, 1:1000, Cell Signaling Technology, Danvers, USA; Cytochrome P450 1A1 1:500 and CYP1B1, 1:500, Novus Biologicals, Littleton, CO, United States). The day after, membranes were rinsed three times with TBS-T and incubated with specific HRP-linked secondary antibodies in Blocking buffer for 1 h at RT (anti-rabbit IgG, 1:2000, Cell Signaling). Finally, membranes were rinsed as previously described, and exposed to Chemiluminescent Substrate (Euroclone). Monoclonal anti-β-Actin antibody (Cell Signaling, 1:1000) was used as loading control. Digital images were taken by a luminescence reader (Biospectrum-UVP, LLC, Upland, CA, United States) and densitometry analysis performed with dedicated software (Vision Works LS).

2.9. DNA damage analysis

Phosphorylated histone H2AX (γH2AX) and phosphorylated form of Ataxia Telangiectasia Mutated (p-ATM) were used as marker of DNA damage and analysis was performed by flow cytometry. After exposure, cells were trypsinized, washed and fixed with 1% paraformaldehyde in PBS at 4 °C for 15 min. Cells were gently re-suspended in 90% cold

methanol and stored O/N at –80 °C prior to analysis. The samples were centrifuged at 1600 rpm for 6 min to discharge the methanol, washed once in PBS supplemented with 0.5% BSA and then, incubated with the specific antibody in PBS supplemented with 0.5% BSA and 0.2% Triton X-100. Alexa Fluor 488 conjugated γH2AX antibody (1:100, Cell Signaling) and a p-ATM mouse monoclonal antibody (1:100, Santa Cruz Biotechnology, Dallas, Texas, USA) were used. Cells stained for γH2AX were incubated for 4 h at RT, washed once in PBS 0.5% BSA, re-suspended in PBS and analyzed by the CytoFLEX 13/3. Cells stained for p-ATM were incubated with the primary antibody O/N at 4 °C. The day after, cells were washed once in PBS 0.5% BSA and incubated with the secondary antibody (Alexa Fluor 594 goat anti-mouse IgG, 1:500 dilution, Invitrogen/Molecular Probes, Eugene, Oregon, USA) in PBS 0.5% BSA, 0.2% Triton X-100 for 90 min at RT in the dark. Finally, cells were washed once, re-suspended in PBS and analyzed at the flow cytometer. The fluorescence of 10,000 events was detected using 525 (γH2AX) or 617 (p-ATM) nm band pass filter. The same cytometer setting was maintained for staining on independent experiment. Data were analyzed as mean percentage of positive cells for the staining.

Immunofluorescence analyses of p-ATM and γH2AX nuclear foci were also performed to confirm the cytofluorimetric analysis (see Additional file 3).

2.10. Cell cycle analysis

The cell cycle progression of PM-treated cells was investigated after 24 h of exposure by DNA-staining. At the end of the exposure, cells were trypsinized, collected and pooled with the harvested medium. They were then, centrifuged at 1200 rpm for 6 min, fixed in 90% ethanol and stored at –20 °C until analysis. The cell cycle of unexposed control cells was analyzed too.

For the analysis, cells were centrifuged at 1600 rpm for 6 min to discharge the ethanol and resuspended in PBS and RNase DNase-free (1 mg/mL, Sigma-Aldrich, Italy) was added for 30 min at 37 °C. Finally, the fluorescent dye PI was added to stain DNA of cells for 7 min in the dark. Fluorescence was measured by flow cytometer (CytoFLEX 13/3) using 617 nm band pass filters and the analysis performed with the dedicated software (CytExpert software). A total of 10,000 events per sample were analyzed. We maintained the same cytometer setting for all the independent experiments performed. For the analysis, cells in different cell cycle phases were selected and analyzed as mean percentage of cells in each phase.

2.11. Treatment with metal chelator

The metal chelator TPEN (N,N,N',N'-tetrakis(2-pyridylmethyl) ethylenediamine, Sigma) was used, since its high affinity for Zn²⁺. TPEN was firstly dissolved in EtOH and used for incubating cells at the final concentration of 3 µM. This concentration has been selected after preliminary set up experiments. Particles were pre-incubated with TPEN for 1 h before the cells treatment and then added to cell medium. After 24 h exposure, cell cycle analysis was performed, as previously described (see par. 2.10).

2.12. Statistical analysis

Mean and standard error of mean (SE) of at least three independent experiments, carried out following the same experimental conditions, are reported. Statistical analyses were performed using GraphPad Prism 6 software, using One-way or Two-way ANOVA with Dunn's or Dunnett's *post hoc* multiple comparisons tests. Values of $p < 0.05$ were considered statistically significant.

3. Results

3.1. Biomass PM10 chemico-physical characterization

The average mass fraction of PAHs emitted by pellet, charcoal and wood PMs are summarized in Table 1. A high PAH concentration was measured in PM10 emitted by charcoal and wood combustion processes with respect to pellet. BaP, recognized as the most cancerogenic PAH, was measured and its concentration resulted to be 4.03 ng_{BaP}/mg_{PM10}, 27.8 ng_{BaP}/mg_{PM10}, 62 ng_{BaP}/mg_{PM10} for pellet, charcoal and wood, respectively.

Higher metal amounts were detected in PM10 emitted by pellet combustion compared to charcoal and wood, including As, Cd and Ni, which belong to Group 1 carcinogenic compounds ("IARC: *Outdoor Air Pollution a Leading Environmental Cause of Cancer Deaths*," 2013), as summarized in Table 2. A negligible (lower than the detection limit) As amount was measured in charcoal and wood samples, whereas its concentration in PM10 emitted by pellet combustion was equal to 0.09 ng_{As}/μg_{PM10}. Ni and Cd concentration was 12.4 ng_{Ni}/μg_{PM10} and 0.43 ng_{Cd}/μg_{PM10}, 5.7 ng_{Ni}/μg_{PM10} and 0.17 ng_{Cd}/μg_{PM10} and 7.2 ng_{Ni}/μg_{PM10} and 0.24 ng_{Cd}/μg_{PM10}, for pellet, charcoal and wood combustion, respectively.

The particle morphology examined after filters extraction is reported in more detail in the additional Fig. 1 [see Additional file 1]. It is evident that the particles deriving from the combustion of the different biomasses significantly differ in size and shape, with pellet PM samples showing more particles with dimension in the ultrafine range. The PMs derived from charcoal and wood combustion appeared larger and with very irregular shapes (Fig. 1).

3.2. Biomass PM10 biological effects

3.2.1. Cell viability

The cytotoxic effects were investigated by Alamar Blue assay (Fig. 2) and Hoechst/PI staining (Fig. 3) after 24 h exposure to PM10 from 1 μg/cm² to 10 μg/cm². A dose-dependent decrease in cell viability was observed (Fig. 2), with significant differences in comparison to control starting from 5 μg/cm² for pellet PM and from 7.5 μg/cm² for wood (Two-way ANOVA; *p* < 0.05). Cell viability was not affected after exposure to all the charcoal PM doses tested.

The dose of 5 μg/cm², showing low or no effects in the metabolic assay, was selected for the further experiments.

The differential cell count of the Hoechst/PI stained A549 cells, after exposure to 5 μg/cm² PMs for 24 h, suggested a significant decrease in the number of viable cells. In parallel a significant increase in necrotic cells (>14%) was induced by pellet, while charcoal and wood PMs significantly increased the number of apoptotic cells (>13% and 11% respectively) (Fig. 3).

Table 1

Average mass fractions of PAH on PM10 (ng/mg_{PM10}) emitted by pellet, charcoal and wood combustion processes.

Polycyclic aromatic hydrocarbons (PAHs)	Pellet	Charcoal	Wood
Fluoranthene	22.7	173	124
Pyrene	25.3	197	219
Benzo[a]anthracene	5.1	38.8	54.4
Crysene	8.05	61.1	100
Benzo[b]fluoranthene	3.93	29.9	106
Benzo[k]fluoranthene	1.24	15	33.2
Benzo[e]pyrene	1.43	11.5	24.6
Benzo[a]pyrene	4.03	27.8	62
Perylene	0.76	7.44	13.3
Indeno[1.2.3.c.d]pyrene	1.74	12.4	49.1
Dibenzo[a,h]anthracene	0.69	4.55	1.94
Benzo[ghi]perylene	1.88	13.1	45.3
Total	76.85	591.6	832.8

Table 2

Average mass fractions of inorganic elements on PM10 (ng/μg_{PM10}) emitted by pellet, charcoal and wood combustion processes.

Metals	Pellet	Charcoal	Wood
As	0.09	<LOD	<LOD
Cd	0.43	0.17	0.24
Cr	6.2	5.5	5.1
Cu	3.5	2.8	4.1
Hg	7.9	2.3	3.1
Ni	12.4	5.7	7.2
Pb	19.3	2.9	0
Se	4.2	5.9	5.2
Zn	42.8	14.7	28.2
Total	96.82	39.97	53.14

A more sensitive method was used to better discriminate the type of death mechanisms induced by biomass PMs [see Additional file 2]. Thanks to the cytofluorimetric analysis of the Annexin V/PI staining, we were able to discriminate between necrosis and early or late apoptosis. The results confirmed necrosis as the main mechanism of cell death activated by pellet PM. As shown in the Additional Fig. 2, charcoal and wood PMs, activated also the apoptotic process, with a slight increased number of cells in early and late apoptosis compared to control and pellet exposed cells.

3.2.2. Synthesis and release of pro-inflammatory cytokines

To investigate the inflammatory response, the release of two key pro-inflammatory mediators, IL-6 and IL-8, was measured after A549 cells exposure to 5 μg/cm² PM10 for 24 h. No significant increase in IL-6 and IL-8 secretion was obtained after exposure to all the biomass PMs (Fig. 4A and C). Only a slight increase of IL-6 was observed in pellet-exposed cells (Fig. 4A). The intracellular levels of the proteins were also analyzed (Fig. 4B and D). IL-8 expression significantly increased in pellet-exposed cells (One-way ANOVA; *p* < 0.05), while charcoal and wood did not affect IL-8 levels. IL-6 intracellular concentration is higher in the cells exposed to all PMs. Anyway, such increase was not statistically significant (Fig. 4B).

3.2.3. Antioxidant response

The activation of the anti-oxidant response was also evaluated. The expression of hemoxygenase 1 protein (HO-1) was assessed by Western Blot. As showed in Fig. 5, a statistically significant increase in HO-1 expression was observed after exposure to all the three PMs, with wood particles inducing the highest effect.

3.2.4. Xenobiotic metabolism activation

The expression of the enzymes CYP1A1 and CYP1B1, involved in PAHs metabolism, was analyzed. As shown in Fig. 6A, CYP1A1 protein level was not significantly increased by biomass PMs exposure at the dose and time point investigated. On the contrary, positive results were obtained for CYP1B1, with a mild increase of the protein level in cells exposed to pellet, a strong, although not statistically significant, increase in cells exposed to charcoal, and a definite statistically significant increment in cells exposed to wood PM (Fig. 6B).

3.2.5. DNA damage

DNA strand breaks were evaluated by the quantification of the activated form of ATM (p-ATM). To determine if p-ATM activation is followed by H2AX phosphorylation, which reflects the activation of DNA repair mechanisms, cells were also stained and scored for γH2AX. As shown in Fig. 7, only the exposure to pellet PM led to a significant augmented expression of p-ATM compared to the control cells, but it is associated only to a slight activation of γH2AX. It is noteworthy that A549 cells showed high background levels of γH2AX, possibly masking eventual increases induced by PM exposure (Fig. 7B). A representative immunofluorescence image showing the foci of DNA

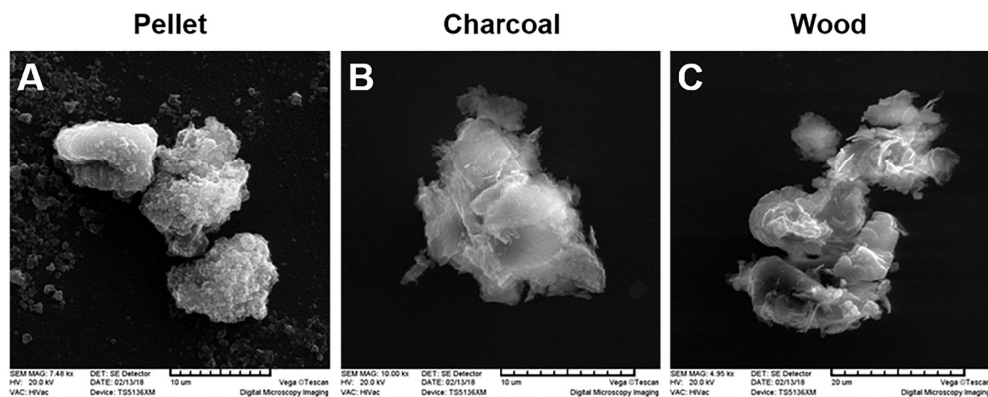


Fig. 1. Morphological characterization of biomass PM10. Scanning Electron Microscopy (SEM) analysis on particles extracted from the sampling filters and suspended in sterile water: pellet (A), charcoal (B), and wood (C).

damage (p-ATM) after the exposure to Pellet PM is reported in the additional Fig. 3 [see Additional file 3].

3.2.6. Cell cycle analysis

A549 cells exposed to $5 \mu\text{g}/\text{cm}^2$ of charcoal and wood PMs did not show cell cycle alterations, while those exposed to pellet PM did (Fig. 8A). Pellet-exposed cells presented a significant increase in G0-G1 phase (from 62.27% of control cells to 76.47%), with a parallel decrease in S and G2-M phases. These results confirm the genotoxic effect, already evidenced by DNA repair system activation, specifically produced by pellet PM.

The metal chelator TPEN (N,N,N',N'-tetrakis(2-pyridylmethyl) ethylenediamine) was used to investigate the role of Zinc in the pellet-induced cell cycle alterations. TPEN *per se* had a slight but not significant effect on the cell cycle, but it was able to completely rescue the alterations induced by pellet PM (Fig. 8B).

4. Discussion

There is today a general awareness that the atmospheric PM-induced biological effects could depend on the particle physico-chemical composition and on the sources of emissions, but still much remains to be explained about the role of specific combustion processes and fuels in determining the toxicity of the emitted particles. In this perspective, more research is needed to understand the toxicological properties of combustion-derived particles (CDPs), the specific biological

mechanism of action and their role in the adverse health effects observed in the exposed populations.

In the present work, we compared the chemical composition and the biological effects of three different biomass CDPs, sampled indoor as PM10 during combustion of pellet, charcoal and wood, using the same stove. PM10s were analyzed for PAHs and metals content and their cytotoxic, pro-inflammatory and genotoxic effects were evaluated *in vitro* on human lung A549 cells.

Charcoal and wood PMs, mainly induced the xenobiotic response enzymes activation and cell apoptosis. Interestingly, pellet particles displayed a different toxicological mechanism, inducing a mild inflammatory response, DNA damage and cell cycle arrest in G1 phase and the consequent cell death by necrosis. Such a difference in the toxicological profiles was likely dependent on the different relative abundances of PAHs and heavy and transition metals observed in the PMs. Indeed, pellet PM contained higher amounts of metals compared to charcoal and wood that, on the contrary, resulted enriched in PAHs.

Among metals, Zinc (Zn) was the most abundant in all samples, but with a concentration in pellet particles 1.5- and 3-fold higher than in wood and charcoal, respectively. Also lead (Pb) concentration presented great differences among the particles, being 6-fold higher in pellet than in charcoal, while it was not detected in wood particles. A higher cytotoxicity of Zn-enriched biomass particles, compared to particles with lower Zn content, was already suggested (Uski et al., 2015), and ZnO particles were shown to induce cell apoptosis or necrosis, according to the cell exposure to lower or higher doses respectively (Zhang et al., 2012). A correlation between cytotoxicity and Pb content in airborne PM was also reported, so as for other metals, such as Cd, As, Cr, and Cu (Michael et al., 2013; Perrone et al., 2010; Van Den Heuvel et al., 2016), and a definitely higher concentration of this metal in pellet PM in respect to wood and charcoal ones.

On the contrary, charcoal and wood particles displayed a PAH content approximately 10-fold higher than pellet ones. Such lower metal content, together with the relatively high PAH content may be responsible of the reduced cytotoxicity and the slightly increased apoptotic event in charcoal and wood exposed cells. This is also in agreement with previous studies, showing that high concentrations of PAHs in urban PM are strongly associated with apoptosis (Uski et al., 2014; Yang et al., 2016), and that PAH-coated carbon particles are able to induce apoptosis in tracheal epithelial cells, while pristine particles are not (Lindner et al., 2017). All together, these observations suggest that the particle-adsorbed chemicals might activate different cell death mechanisms.

The activation of the inflammatory pathway was also investigated as important cell response to biomass PM, possibly involved in necrotic and/or apoptotic processes (Nemmar et al., 2013; Wallach et al.,

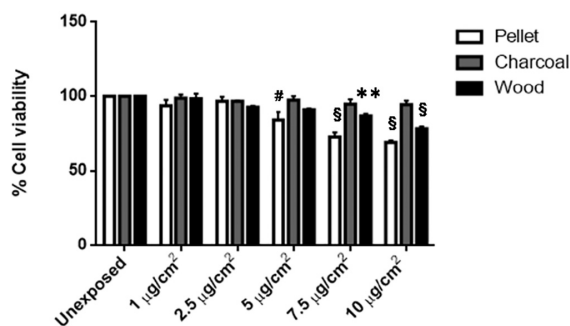


Fig. 2. Cell viability assessed by Alamar Blue assay after 24 h exposure to increasing biomass PM concentrations: 0 (unexposed), 1, 2.5, 5, 7.5 and $10 \mu\text{g}/\text{cm}^2$. Histograms represent the mean \pm SE of at least three independent experiments. Statistical analysis was performed by Two-way ANOVA with Dunnett's multiple comparison test. [§] $p < 0.0001$, [#] $p < 0.001$ and ^{*} $p < 0.01$ vs control cells.

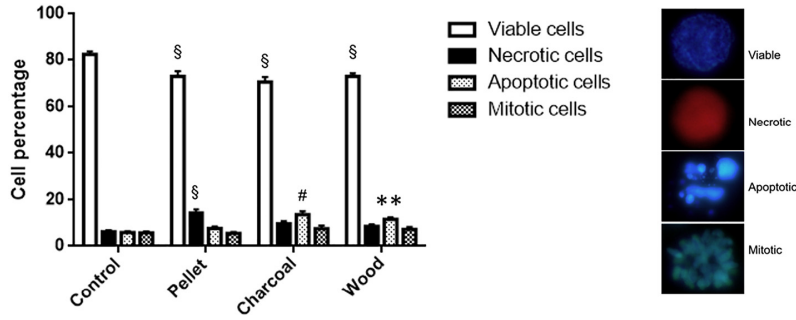


Fig. 3. Cell viability assessed by Hoechst/PI staining after 24 h exposure to 5 µg/cm² biomass PMs. The differential cell count (viable, necrotic, apoptotic and mitotic cells) was based on the nuclei staining and morphology (see the right side of the panel). The data represent mean ± SE of three independent experiments. Statistical analysis was performed by Two-way ANOVA with Dunnett’s multiple comparison test. [§]*p* < 0.0001, [#]*p* < 0.001 and ^{**}*p* < 0.01 vs control cells.

2013). The levels of IL-6 and IL-8, two main pro-inflammatory mediators, were measured in both the intracellular and the extracellular compartments. At the subtoxic dose tested, no significant responses were observed, except for a slight increase in the intracellular level of IL-6 after exposure to all PMs and a statistically significant increase in the intracellular IL-8 in pellet PM-exposed cells (Fig. 4). In literature, the results concerning the biomass particles inflammatory potential are controversial. In A549 cells exposed to diverse wood/biomass particles, low pro-inflammatory cytokines release has been generally reported (Corsini et al., 2017; Danielsen et al., 2011; Dilger et al., 2016). Also in RAW264.7 macrophages wood smoke particles were found to induce cell death with only minor inflammatory response (Muala et al., 2015). In a previous study on ambient PM, we observed that IL-8 response was induced by the fine PM fraction (PM1), mainly as a consequence of the metal content - As and Zn in particular - as demonstrated by PCA analysis (Perrone et al., 2010). Metals in general are known to induce inflammatory responses, thus the increased IL-8 expression in cells exposed to pellet PM may be related to the higher metal content

displayed. The differences between IL-8 intracellular and extracellular expression could be due to an inhibitory effect of the PM on the secretion of IL-8 soluble form. A mismatch between IL-8 gene expression and lack of augmented extracellular release has previously been reported following exposure to urban PM2.5 (Alfaro-Moreno et al., 2009; Kocbach et al., 2008). This IL-8 suppression could be due to PAHs or other chemicals present in the PM, as reported also by previous studies (Fuentes-Mattei et al., 2010; Totlandsdal et al., 2014).

Since the biomass PMs, especially charcoal and wood ones, are enriched in PAHs, we evaluated the activation of two main enzymes of the cytochrome P450 superfamily, CYP1A1 and CYP1B1, that are involved in the xenobiotic metabolism response (Dilger et al., 2016; Rossner et al., 2016). We found a significant induction of CYP1B1 in wood CDPs-exposed cells, in agreement with the highest PAH content. Pellet CDPs did not induce a significant activation of CYP enzymes, accordingly to the lower PAH levels. Although it may seem unexpected, the overall lower induction of CYP1A1 is in agreement with previous studies, in which CYP1B1 resulted more responsiveness than CYP1A1

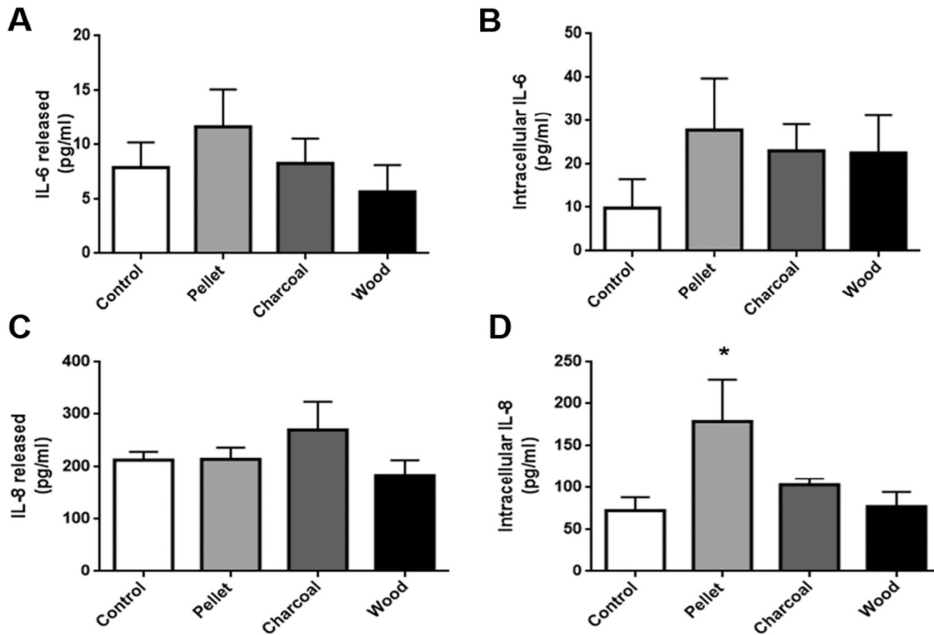


Fig. 4. Pro-inflammatory effects induced by biomass PMs after exposure to 5 µg/cm². **A)** IL-6 secretion. **B)** Intracellular level of IL-6. **C)** IL-8 secretion. **D)** Intracellular level of IL-8. Results are expressed as mean ± SE of five independent experiments. Statistical analysis was performed by One-way ANOVA with Dunnett’s multiple comparison test. ^{*}*p* < 0.05 vs control cells.

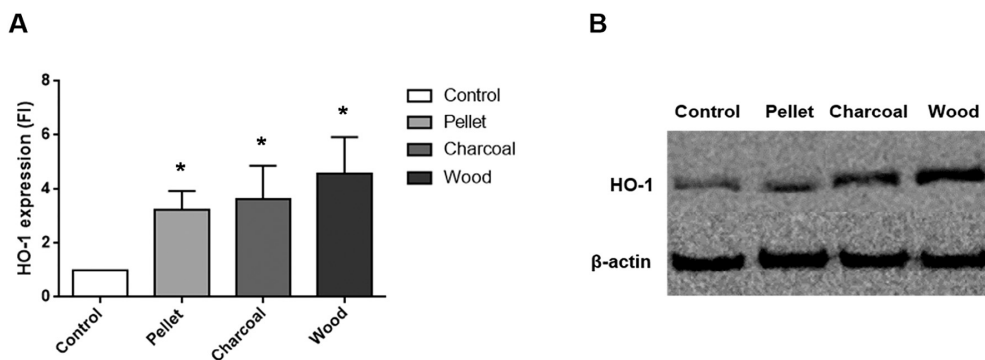


Fig. 5. Expression of the oxidative stress marker HO-1. **A)** Protein analysis after exposure to biomass PMs. Data are presented as mean \pm SE of five independent experiments. Statistical analysis was performed by One-way ANOVA with Dunn's multiple comparison test. * $p < 0.05$ vs control cells. **B)** Representative immunoblotting images displaying HO-1 expressed from A549 cells exposed for 24 h to 5 $\mu\text{g}/\text{cm}^2$. β -Actin was used as control.

in A549 cells exposed to urban PM_{2.5} and Benzo[a]pyrene (B[a]P) (Genies et al., 2013; Gualtieri et al., 2012). Furthermore, according to Genies et al. (2016), A549 response to PAHs could be influenced by their behavior in a mixture of compounds. Individual PAHs indeed, up-regulate in different ways the two enzymes, but their toxic properties could be inhibited or enhanced when they are combined. Since PM is a complex mixture of PAHs, the differences in the concentration of individual PAHs could be therefore responsible for the different responses observed after exposure to biomass PMs. Interestingly, in previous papers the induction of CYP1B1, and not of CYP1A1, was observed after exposure to urban PM_{2.5} and PM₁₀ in both *in vitro* (A549 cells) and *in vivo* systems (Gualtieri et al., 2012; Farina et al., 2013). It may be supposed that specific PAHs and/or the presence of other molecules (e.g. TCDD) may contribute in the expression of such enzyme. Moreover, according to Hukkanen et al. (2000) the expression of CYP1B1 by TCDD (2,3,7,8-tetrachlorodibenzo-p-dioxin) is less dependent on AHR. Interestingly

it has also been reported that CYP1B1 mRNA is the most sensitive target across different cell models compared to CYP1A1 and other three less frequently used AhR target genes (TIPARP, AHRR, ALDH3A1), while CYP1A1 mRNA induction is strictly AhR-dependent (Strapáčová et al., 2018).

Oxidative stress is a main mechanism of PM-mediated cytotoxicity, able to induce cellular damage by targeting several cellular components, including proteins, lipids and nucleic acids. Both PAHs and metals are able to induce ROS production (Crobbeddu et al., 2017; Yang et al., 2016), and in response to oxidative stress cells might react modulating the expression of heme oxygenase 1 (HO-1), one of the key enzyme involved in the anti-oxidant activity (Dilger et al., 2016). Not surprisingly, our results showed that all biomass PMs were able to activate the anti-oxidant response, inducing a statistical significant increase of the HO-1 expression, independently from their chemical compositions.

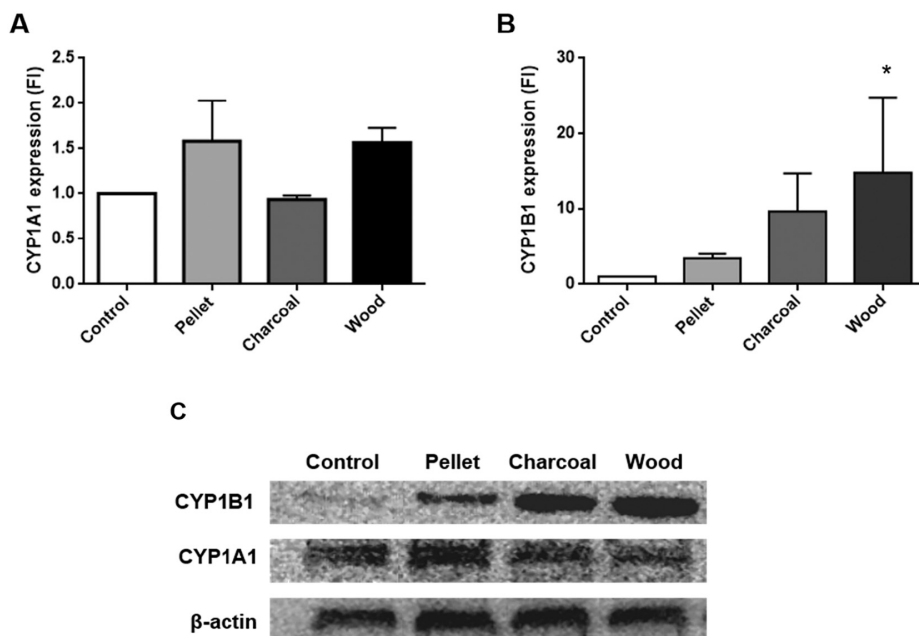


Fig. 6. Activation of PAH-metabolizing enzymes cytochromes P450 (CYPs). **A, B)** Histograms represent CYP1A1 and CYP1B1 expression respectively. Data are presented as mean \pm SE of three independent experiments. Statistical analysis was performed by One-way ANOVA with Dunn's multiple comparison test. * $p < 0.05$ vs control cells. **C)** Representative immunoblotting images displaying CYP1A1 and CYP1B1 expressed from A549 cells exposed for 24 h to 5 $\mu\text{g}/\text{cm}^2$. All the data were normalized to β -actin.

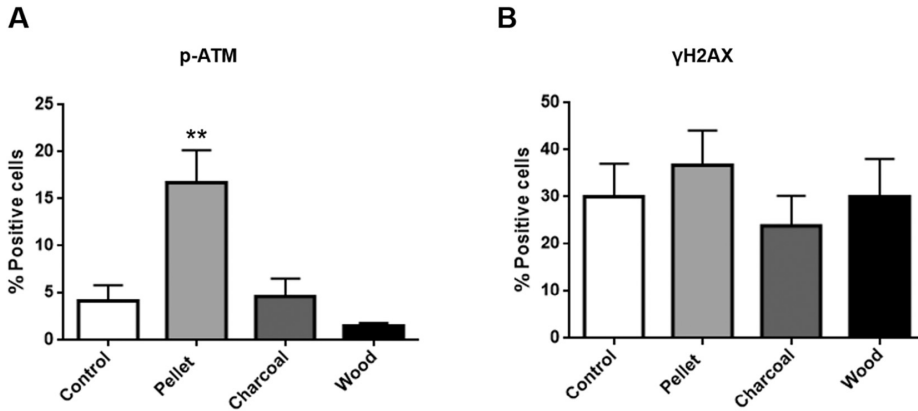


Fig. 7. Induction of ATM and H2AX phosphorylation in A549 cells following exposure to biomass PMs. The histograms show the percentage of positive cells for p-ATM expression (A) and for γH2AX expression (B). Data are presented as mean ± SE of three independent experiments. Statistical analysis was performed by One-way ANOVA with Dunnett’s multiple comparison test. ***p* < 0.01 vs control cells.

Since the PM-induced oxidative stress may result in genotoxic effects, the presence of DNA lesions was then evaluated by quantifying the expression of p-ATM and γH2AX. One of the main signaling pathways that help cells to respond to DNA insults involves the ataxia-telangiectasia mutated (ATM) kinase, which is activated by double strand breaks (DSBs) induced by radiations, oxidative stress and genotoxins (Maréchal and Zou, 2013; Smith et al., 2010). ATM activation triggers a cascade of events that lead to the phosphorylation of different substrates, including H2AX, BRCA1, Chk1/2 and p53, involved in DNA repair, cell-cycle arrest or apoptosis processes. The key event deriving from ATM activation is the phosphorylation of the histone H2AX (γH2AX), that is required for the activation of DNA repair proteins to the damage site (Maréchal and Zou, 2013; Sánchez-Pérez et al., 2009).

Although DNA primary lesions generally occur after 6 h of exposure, our results indicate that also after 24 h it is possible to observe genotoxic lesions. Similar evidences have been observed also in other previous works, even at reduced concentrations compared to the one selected for our research (Gualtieri et al., 2011; Longhin et al., 2013; Marabini et al., 2017). Such differences in the timing of the response to DNA damage may be due to the delayed bioavailability of PAHs carried out by the CDPs. Since PAHs are adsorbed onto the carbonaceous particles, their effects on the cell metabolic response can take place only after the endocytosis and the consequent availability of the xenobiotics at the level of

the smooth endoplasmic reticulum (SER), where the metabolism enzymatic systems are located.

Our results indicate an increased expression of p-ATM and a slight modulation of γH2AX only after pellet exposure, suggestive of DNA lesions, followed by the tentative to activate the DNA repairing machinery. This partial activation might be responsible of the significant cell cycle arrest in G1 phase and cell death by necrosis induced by pellet CDPs.

The reason why no DNA damages were revealed after wood and charcoal exposure may reside in the fact that ROS generation by PAHs involves their conversion into quinones, which are able to generate bulky DNA adducts, not recognized by ATM. On the contrary, metals, generating hydroxyl radicals, could trigger the accumulation of DNA strand breaks that finally activate ATM (Henkler et al., 2010; Rudolf and Cervinka, 2011).

The cell-signaling pathway activated in presence of oxidative DNA damage has been suggested as one of the mechanisms behind cell cycle arrest. DNA damage indeed, activates different checkpoints, finally inhibiting cell cycle progression. Besides, the activated checkpoint may depend on the type of damage (Cuadrado et al., 2006; Gualtieri et al., 2011; Liang et al., 2009). In the present study, only the samples exposed to pellet CDPs showed a significant cell cycle modification, with many cells blocked in G1 phase. This is in accordance with previous data, in which the arrest in G0 checkpoint is reported to be associated to DNA

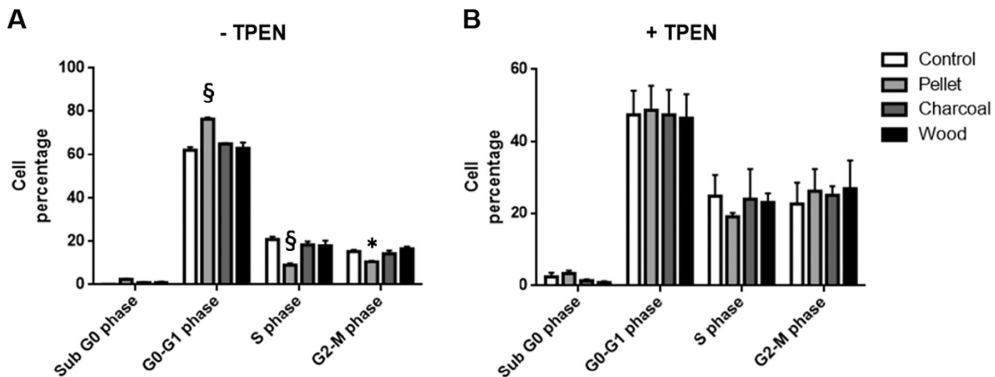


Fig. 8. Cell percentage in each phase of the cycle (SubG0, G1, S, G2/M) after exposure to 5 μg/cm² biomass PMs pre-incubated (B) or not (A) with TPEN. A) Cells exposed to PMs. B) Cells exposed to PMs pre-incubated with TPEN. Data are presented as mean ± SE of four independent experiments. Statistical analysis was performed by Two-Way ANOVA with Dunnett’s multiple comparison test. §*p* < 0.0001 and **p* < 0.05 vs control cells.

damage and increased cellular levels of p53 (Liang et al., 2009; Kastan et al., 1991). Other studies demonstrated the PM-induced arrest of cell cycle in G1 (Reyes-Zárate et al., 2016; Zhang et al., 2007) and in G2/M phase (Longhin et al., 2013), as a function of the variable chemical composition. The amount and type of PAHs was probably the main responsible of the mitotic arrest, while the higher amount of metals in pellet CDPs could be responsible for the arrest in G1 phase, as already suggested (Steenhof et al., 2011). It was reasonable to suspect that Zinc, present in a very high concentration in pellet PM, contributes significantly to the cytotoxic and genotoxic effects of this PM type, even considering the significant cell cycle rescue achieved after incubation with the Zinc chelator probe, TPEN (Fig. 8B). Zinc, and in general transition metals, are known to significantly induce oxidative DNA damage through Fenton reaction-generated ROS, with the consequent accumulation of DNA lesions preventing cells to enter S phase. From the literature, it is known that PM samples containing high Zn concentrations display elevated toxic properties (Torvela et al., 2014; Uski et al., 2015) and that Zn ions and Zn nanoparticles produce significant DNA damage (Pati et al., 2016; Rudolf and Cervinka, 2011). Of course, the very high content of other heavy metals, e.g. Pb and Mercury (Hg), does not allow us to exclude an involvement also of these elements in the enhanced toxicity observed after treatment with pellet CDPs.

In a recent publication we reported that UFPs obtained from the combustion of high-quality certified pellet in a modern automatic 25 kW boiler did not induce significant toxicity in human bronchial cells at concentrations similar to those used in the present study, contrary to diesel exhaust particles, which displayed cytotoxic and genotoxic effects (Longhin et al., 2016). These results clearly point out that the quality of the biomass used and the combustion technology may drastically influence the quality of the emitted particles, with the size and the relative abundance of metals and PAHs as the main physico-chemical variables affected.

5. Conclusions

According to the main evidences of the present study, the physico-chemical properties of the biomass CDPs, reflecting the efficiency of the combustion systems and the biomass fuel quality, do not only influence the acute toxicity, but even the cellular mechanism of action, pointing out the need of further exploring the adverse outcome pathways. In this regard, recently the Air Liquid Interface (ALI) exposure systems received attention as an alternative method to the submerged system in studying the biological effects of ultrafine particles (Loxham et al., 2015) and nanoparticles (Kim et al., 2013). Nevertheless, the widespread adoption of ALI systems is still limited for PM by the minimal efficiency of particles deposition and by the complex strategy needed to characterize the composition of the particles delivered to the cells (Kim et al., 2013). Besides, studies on the comparative biological effects of the UFPs deriving from controlled combustion processes, using 3D lung *in vitro* systems exposed at the ALI, will be of high relevance to depict the hazardous behavior of the different biomass CDPs.

In conclusion, different adverse biological outcomes can result from the exposure to biomass CDPs and the present data confirm that the amount of metals is crucial in inducing acute effects related to cytotoxicity and genotoxicity, while PAHs are responsible for the induction of the xenobiotic metabolizing systems and the oxidative stress cell responses. Since these variable effects induced by solid biomass CDPs, the chemical composition of particles and their toxicological profiles should be known in order to suggest efficient strategies for the prevention of the adverse health effects in indoor exposure, but also for the management of outdoor air quality at local level.

Further investigations are of course needed to better define the molecular mechanisms of action but, at the same time, more stringent regulations are required to guarantee high quality biomass fuels and safer combustion technologies.

Acknowledgments

SM performed the experiments and manuscript writing. EL performed the particles extraction, supervised the flow cytometry analysis, interpreted the results and contributed to writing the manuscript. RB performed the TPEN analysis, interpreted the results and helped with the writing of the manuscript. PA conducted the chemical analysis. LS conducted the PM sampling and helped with the writing of the manuscript. GB defined the experimental plan, conducted the PM sampling and helped with the writing of the manuscript. AC helped with the particle morphological characterization, supervised all the experiments and contributed to writing the manuscript. MC defined the experimental plan, supervised all the experiments and contributed to writing the manuscript. PM performed the morphological analysis, supervised all the experiments and contributed to writing the manuscript. All authors read and approved the final manuscript.

Funding

This study has been supported by the grants of the Cariplo Foundation to MC (proj. ID 2013-1038) and the Italian Ministry of Foreign Affairs and International Cooperation to PM (proj. ID PGR00786).

Conflicts of interest

The authors declare no conflicts of interest.

Appendix A. Supplementary data

Supplementary data to this article can be found online at <https://doi.org/10.1016/j.scitotenv.2018.08.249>.

References

- Alfaro-Moreno, E., Torres, V., Miranda, J., Martínez, L., García-Cuellar, C., Nawrot, T.S., Vanaudenaerde, B., Hoet, P., Ramírez-López, P., Rosas, L., Nemery, B., Osornio-Vargas, A.R., 2009. Induction of IL-6 and inhibition of IL-8 secretion in the human airway cell line Calu-3 by urban particulate matter collected with a modified method of PM sampling. *Environ. Res.* 109, 528–535. <https://doi.org/10.1016/j.envres.2009.02.010>.
- Avino, P., Carconi, P.L., Lepore, L., Moauro, A., 2000. Nutritional and environmental properties of algal products used in healthy diet by INAA and ICP-AES. *J. Radioanal. Nucl. Chem.* <https://doi.org/10.1023/A:1006721811478>.
- Avino, P., Capannesi, G., Rosada, A., 2011. Ultra-trace nutritional and toxicological elements in Rome and Florence drinking waters determined by Instrumental Neutron Activation Analysis. *Microchem. J.* 97, 144–153. <https://doi.org/10.1016/j.microc.2010.08.007>.
- Avino, P., Capannesi, G., Renzi, L., Rosada, A., 2013. Instrumental neutron activation analysis and statistical approach for determining baseline values of essential and toxic elements in hairs of high school students. *Ecotoxicol. Environ. Saf.* 92, 206–214. <https://doi.org/10.1016/j.ecoenv.2013.01.029>.
- Buonanno, G., Dell'Isola, M., Stabile, L., Viola, A., 2009. Uncertainty budget of the SMPS-APS system in the measurement of PM₁, PM_{2.5}, and PM₁₀. *Aerosol Sci. Technol.* 43, 1130–1141. <https://doi.org/10.1080/02786820903204078>.
- Buonanno, G., Dell'Isola, M., Stabile, L., Viola, A., 2011. Critical aspects of the uncertainty budget in the gravimetric PM measurements. *Measurement* 44, 139–147. <https://doi.org/10.1016/j.measurement.2010.09.037>.
- Capannesi, G., Rosada, A., Avino, P., 2009. Elemental characterization of impurities at trace and ultra-trace levels in metallurgical lead samples by INAA. *Microchem. J.* 93, 188–194. <https://doi.org/10.1016/j.microc.2009.07.004>.
- Capistrano, S.J., Zakarya, R., Chen, H., Oliver, B.G., 2016. Biomass smoke exposure enhances rhinovirus-induced inflammation in primary lung fibroblasts. *Int. J. Mol. Sci.* 17. <https://doi.org/10.3390/ijms17091403>.
- Chirino, Y.I., García-Cuellar, C.M., García-García, C., Soto-Reyes, E., Osornio-Vargas, Á.R., Herrera, L.A., López-Saavedra, A., Miranda, J., Quintana-Belmares, R., Pérez, I.R., Sánchez-Pérez, Y., 2017. Airborne particulate matter *in vitro* exposure induces cytoskeleton remodeling through activation of the ROCK-MYPT1-MLC pathway in A549 epithelial lung cells. *Toxicol. Lett.* 272, 29–37. <https://doi.org/10.1016/j.toxlet.2017.03.002>.
- Choi, Y., Park, K., Kim, I., Kim, S.D., 2016. Combined toxic effect of airborne heavy metals on human lung cell line A549. *Environ. Geochem. Health* <https://doi.org/10.1007/s10653-016-9901-6>.
- Corsini, E., Ozgen, S., Papale, A., Galbiati, V., Lonati, G., Fermo, P., Corbella, L., Valli, G., Bernardoni, V., Dell'Acqua, M., Becagli, S., Caruso, D., Vecchi, R., Galli, C.L., Marinovich, M., 2017. Insights on wood combustion generated proinflammatory ultrafine particles (UFP). *Toxicol. Lett.* 266, 74–84. <https://doi.org/10.1016/j.toxlet.2016.12.005>.
- Crobeddu, B., Aragao-Santiago, L., Bui, L.C., Boland, S., Baeza-Squiban, A., 2017. Oxidative potential of particulate matter 2.5 as predictive indicator of cellular stress. *Environ. Pollut.* 230, 125–133. <https://doi.org/10.1016/j.envpol.2017.06.051>.

- Cuadrado, M., Martínez-Pastor, B., Murga, M., Toledo, L.L., Gutiérrez-Martínez, P., López, E., Fernández-Capetillo, O., 2006. ATM regulates ATR chromatin loading in response to DNA double-strand breaks. *J. Exp. Med.* 203, 297–303. <https://doi.org/10.1084/jem.20051923>.
- Danielsen, P.H., Möller, P., Jensen, K.A., Sharma, A.K., Wallin, H., Bossi, R., Autrup, H., Mølhave, L., Ravanat, J.-L., Briedé, J.J., de Kok, T.M., Loft, S., 2011. Oxidative stress, DNA damage, and inflammation induced by ambient air and wood smoke particulate matter in human A549 and THP-1 cell lines. *Chem. Res. Toxicol.* 24, 168–184.
- Dilger, M., Orasche, J., Zimmermann, R., Paur, H.-R., Diabaté, S., Weiss, C., 2016. Toxicity of wood smoke particles in human A549 lung epithelial cells: the role of PAHs, soot and zinc. *Arch. Toxicol.* 90, 3029–3044. <https://doi.org/10.1007/s00204-016-1659-1>.
- Farina, F., Sancini, G., Battaglia, C., Tinaglia, V., Mantecca, P., Camatini, M., Palestini, P., 2013. Milano summer particulate matter (PM10) triggers lung inflammation and extra pulmonary adverse events in mice. *PLoS ONE* 8. <https://doi.org/10.1371/journal.pone.0056636>.
- Fuentes-Mattei, E., Rivera, E., Gioda, A., Sanchez-Rivera, D., Roman-Velazquez, F.R., Jimenez-Velez, B.D., 2010. Use of human bronchial epithelial cells (BEAS-2B) to study immunological markers resulting from exposure to PM2.5 organic extract from Puerto Rico. *Toxicol. Appl. Pharmacol.* 243, 381–389. <https://doi.org/10.1016/j.taap.2009.12.009>.
- Genies, C., Maître, A., Lefebvre, E., Julien, A., Chopard-Lallier, M., Douki, T., 2013. The extreme variety of genotoxic response to benzo[a]pyrene in three different human cell lines from three different organs. *PLoS ONE* 8, 1–11. <https://doi.org/10.1371/journal.pone.0078356>.
- Genies, C., Julien, A., Lefebvre, E., Revol, M., Maître, A., Douki, T., 2016. Inhibition of the formation of benzo[a]pyrene adducts to DNA in A549 lung cells exposed to mixtures of polycyclic aromatic hydrocarbons. *Toxicol. In Vitro* 35, 1–10. <https://doi.org/10.1016/j.tiv.2016.05.006>.
- Gualtieri, M., Øvrevik, J., Møllerup, S., Asare, N., Longhin, E., Dahlman, H.J., Camatini, M., Holme, J.A., 2011. Airborne urban particles (Milan winter-PM2.5) cause mitotic arrest and cell death: effects on DNA, mitochondria, ATR binding and spindle organization. *Mutat. Res. Fundam. Mol. Mech. Mutagen.* 713, 18–31. <https://doi.org/10.1016/j.mrfmmm.2011.05.011>.
- Gualtieri, M., Longhin, E., Mattioli, M., Mantecca, P., Tinaglia, V., Mangano, E., Carla, M., Bestetti, G., Camatini, M., Battaglia, C., 2012. Gene expression profiling of A549 cells exposed to Milan PM2.5. *Toxicol. Lett.* 209, 136–145. <https://doi.org/10.1016/j.toxlet.2011.11.015>.
- Happo, M.S., Uski, O., Jalava, P.I., Kelz, J., Brunner, T., Hakulinen, P., Mäki-Paakkanen, J., Kosma, V.M., Jokiniemi, J., Obernberger, I., Hirvonen, M.R., 2013. Pulmonary inflammation and tissue damage in the mouse lung after exposure to PM samples from biomass heating appliances of old and modern technologies. *Sci. Total Environ.* 443, 256–266. <https://doi.org/10.1016/j.scitotenv.2012.11.004>.
- Henkler, F., Brinkmann, J., Luch, A., 2010. The role of oxidative stress in carcinogenesis induced by metals and xenobiotics. *Cancers* 2, 376–396. <https://doi.org/10.3390/cancers2020376>.
- Hukkanen, J., Lassila, A., Päiväranta, K., Valanne, S., Sarpo, S., Hakkola, J., Pelkonen, O., Raunio, H., 2000. Induction and regulation of xenobiotic-metabolizing cytochrome P450s in the human A549 lung adenocarcinoma cell line. *Am. J. Respir. Cell Mol. Biol.* 22, 360–366. <https://doi.org/10.1165/ajrcmb.22.3.3845>.
- IARC Monographs on the Evaluation of Carcinogenic Risks to Humans 95. IARC: Outdoor Air Pollution a Leading Environmental Cause of Cancer Deaths 51 pp. 229–235.
- Jalava, P.I., Happo, M.S., Kelz, J., Brunner, T., Hakulinen, P., Mäki-Paakkanen, J., Hukkanen, A., Jokiniemi, J., Obernberger, I., Hirvonen, M.R., 2012. In vitro toxicological characterization of particulate emissions from residential biomass heating systems based on old and new technologies. *Atmos. Environ.* 50, 24–35. <https://doi.org/10.1016/j.atmosenv.2012.01.009>.
- Jin, W., Su, S., Wang, B., Zhu, X., Chen, Y., Shen, G., Liu, J., Cheng, H., Wang, X., Wu, S., Zeng, E., Xing, B., Tao, S., 2016. Properties and cellular effects of particulate matter from direct emissions and ambient sources. *J. Environ. Sci. Health A Tox. Hazard. Subst. Environ. Eng.* 51, 1075–1083. <https://doi.org/10.1080/10934529.2016.1198632>.
- Kastan, M.B., Onyekwere, O., Sidransky, D., Vogelstein, B., Craig, R.W., 1991. Participation of p53 protein in the cellular response to DNA damage. *Cancer Res.* 5, 6304–6311.
- Kasurinen, S., Jalava, P.I., Happo, M.S., Sippula, O., Uski, O., Koponen, H., Orasche, J., Zimmermann, R., Jokiniemi, J., Hirvonen, M.R., 2017. Particulate emissions from the combustion of birch, beech, and spruce logs cause different cytotoxic responses in A549 cells. *Environ. Toxicol.* <https://doi.org/10.1002/tox.22369>.
- Kim, J.S., Peters, T.M., O'Shaughnessy, P.T., Adamcakova-Dodd, A., Thorne, P.S., 2013. Validation of an in vitro exposure system for toxicity assessment of air-delivered nanobiomaterials. *Toxicol. In Vitro* <https://doi.org/10.1016/j.tiv.2012.08.030>.
- Kocbach Bølling, A., Pagels, J., Yttri, K.E., Barregård, L., Sallsten, G., Schwarze, P.E., Boman, C., 2009. Health effects of residential wood smoke particles: the importance of combustion conditions and physicochemical particle properties. *Part. Fibre Toxicol.* 6, 29.
- Kocbach, A., Totlandsdal, A.L., Låg, M., Refsnes, M., Schwarze, P.E., 2008. Differential binding of cytokines to environmentally relevant particles: a possible source for misinterpretation of in vitro results? *Toxicol. Lett.* 176, 131–137. <https://doi.org/10.1016/j.toxlet.2007.10.014>.
- Lamberg, H., Tissari, J., Jokiniemi, J., Sippula, O., 2013. Fine particle and gaseous emissions from a small-scale boiler fueled by pellets of various raw materials. *Energy Fuel* 27, 7044–7053. <https://doi.org/10.1021/ef401267k>.
- Li, Q., Jiang, J., Wang, S., Rumchev, K., Mead-Hunter, R., Morawska, L., Hao, J., 2017. Impacts of household coal and biomass combustion on indoor and ambient air quality in China: current status and implication. *Sci. Total Environ.* 576, 347–361. <https://doi.org/10.1016/j.scitotenv.2016.10.080>.
- Liang, Y., Lin, S.-Y., Brunicaudi, F.C., Goss, J., Li, K., 2009. DNA damage response pathways in tumor suppression and cancer treatment. *World J. Surg.* 33, 661–666. <https://doi.org/10.1007/s00268-008-9840-1>.
- Lindner, K., Ströbele, M., Schlick, S., Webering, S., Jenckel, A., Kopf, J., Danov, O., Sewald, K., Buj, C., Creutzenberg, O., Tillmann, T., Pohlmann, G., Ernst, H., Ziemann, C., Hüttmann, G., Heine, H., Bockhorn, H., Hansen, T., König, P., Fehrenbach, H., 2017. Biological effects of carbon black nanoparticles are changed by surface coating with polycyclic aromatic hydrocarbons. *Part. Fibre Toxicol.* 14, 8. <https://doi.org/10.1186/s12989-017-0189-1>.
- Longhin, E., Pezzolato, E., Mantecca, P., Holme, J.A., Franzetti, A., Camatini, M., Gualtieri, M., 2013. Season linked responses to fine and quasi-ultrafine Milan PM in cultured cells. *Toxicol. In Vitro* 27, 551–559. <https://doi.org/10.1016/j.tiv.2012.10.018>.
- Longhin, E., Gualtieri, M., Capasso, L., Bengalli, R., Møllerup, S., Holme, J.A., Øvrevik, J., Casadei, S., Di Benedetto, C., Parenti, P., Camatini, M., 2016. Physico-chemical properties and biological effects of diesel and biomass particles. *Environ. Pollut.* 215, 366–375. <https://doi.org/10.1016/j.envpol.2016.05.015>.
- Loxham, M., Morgan-Walsh, R.J., Cooper, M.J., Blume, C., Swindle, E.J., Dennison, P.W., Howarth, P.H., Cassee, F.R., Teagle, D.A.H., Palmer, M.R., Davies, D.E., 2015. The effects on bronchial epithelial mucociliary cultures of coarse, fine, and ultrafine particulate matter from an underground railway station. *Toxicol. Sci.* 145, 98–107. <https://doi.org/10.1093/toxsci/kfv034>.
- Marabini, L., Ozgen, S., Turacchi, S., Aminti, S., Arnaboldi, F., Lonati, G., Fermo, P., Corbella, L., Valli, G., Bernardoni, V., Dell'Acqua, M., Vecchi, R., Becagli, S., Caruso, D., Corrado, L.G., Marinovich, M., 2017. Ultrafine particles (UFPs) from domestic wood stoves: genotoxicity in human lung carcinoma A549 cells. *Mutat. Res. Genet. Toxicol. Environ. Mutagen.* 820, 39–46. <https://doi.org/10.1016/j.mrgentox.2017.06.001>.
- Maréchal, A., Zou, L., 2013. DNA damage sensing by the ATM and ATR kinases. *Cold Spring Harb. Perspect. Biol.* 5, 1–17. <https://doi.org/10.1101/cshperspect.a012716>.
- Michael, S., Montag, M., Dott, W., 2013. Pro-inflammatory effects and oxidative stress in lung macrophages and epithelial cells induced by ambient particulate matter. *Environ. Pollut.* 183, 19–29. <https://doi.org/10.1016/j.envpol.2013.01.026>.
- Muala, A., Rankin, G., Sehlstedt, M., Unosson, J., Bosson, J.A., Behndig, A., Pourazar, J., Nyström, R., Pettersson, E., Bergvall, C., Westerholm, B., Jalava, P.I., Happo, M.S., Uski, O., Hirvonen, M.-R., Kelly, F.J., Mudway, I.S., Blomberg, A., Boman, C., Sandström, T., 2015. Acute exposure to wood smoke from incomplete combustion - indications of cytotoxicity. *Part. Fibre Toxicol.* 12, 33. <https://doi.org/10.1186/s12989-015-0111-7>.
- Nemmar, A., Holme, J.A., Rosas, I., Schwarze, P.E., Alfaro-Moreno, E., 2013. Recent advances in particulate matter and nanoparticle toxicology: a review of the in vivo and in vitro studies. *Biomed. Res. Int.* 2013, 279371. <https://doi.org/10.1155/2013/279371>.
- Pati, R., Das, I., Mehta, R.K., Sahu, R., Sonawane, A., 2016. Zinc-oxide nanoparticles exhibit genotoxic, clastogenic, cytotoxic and actin depolymerization effects by inducing oxidative stress responses in macrophages and adult mice. *Toxicol. Sci.* 150, 454–472. <https://doi.org/10.1093/toxsci/kfv010>.
- Perrone, M.G., Gualtieri, M., Ferrero, L., Porto, C. Lo, Udristi, R., Bolzacchini, E., Camatini, M., 2010. Seasonal variations in chemical composition and in vitro biological effects of fine PM from Milan. *Chemosphere* 78, 1368–1377. <https://doi.org/10.1016/j.chemosphere.2009.12.071>.
- Reyes-Zárate, E., Sánchez-Pérez, Y., Gutiérrez-Ruiz, M.C., Chirino, Y.I., Osorio-Vargas, Á.R., Morales-Bárceñas, R., Souza-Arroyo, V., García-Cuellar, C.M., 2016. Atmospheric particulate matter (PM10) exposure-induced cell cycle arrest and apoptosis evasion through STAT3 activation via PKC ζ and Src kinases in lung cells. *Environ. Pollut.* 214, 646–656. <https://doi.org/10.1016/j.envpol.2016.04.072>.
- Rössner, P., Strapacova, S., Stolcpartova, J., Schmutzerova, J., Milcova, A., Neca, J., Vlkova, V., Brzicova, T., Machala, M., Topinka, J., 2016. Toxic effects of the major components of diesel exhaust in human alveolar basal epithelial cells (A549). *Int. J. Mol. Sci.* 17. <https://doi.org/10.3390/ijms17091393>.
- Rudolf, E., Cervinka, M., 2011. Stress responses of human dermal fibroblasts exposed to zinc pyrrhione. *Toxicol. Lett.* 204, 164–173. <https://doi.org/10.1016/j.toxlet.2011.04.028>.
- Samburova, V., Connolly, J., Gyawali, M., Yatavelli, R.L.N., Watts, A.C., Chakrabarty, R.K., Zielinska, B., Moosmüller, H., Khlystov, A., 2016. Polycyclic aromatic hydrocarbons in biomass-burning emissions and their contribution to light absorption and aerosol toxicity. *Sci. Total Environ.* 568, 391–401. <https://doi.org/10.1016/j.scitotenv.2016.06.026>.
- Sánchez-Pérez, Y., Chirino, Y.I., Osorio-Vargas, Á.R., Morales-Bárceñas, R., Gutiérrez-Ruiz, C., Vázquez-López, I., García-Cuellar, C.M., 2009. DNA damage response of A549 cells treated with particulate matter (PM10) of urban air pollutants. *Cancer Lett.* 278, 192–200. <https://doi.org/10.1016/j.canlet.2009.01.010>.
- Secrest, M.H., Schauer, J.J., Carter, E.M., Lai, A.M., Wang, Y., Shan, M., Yang, X., Zhang, Y., Baumgartner, J., 2016. The oxidative potential of PM2.5 exposures from indoor and outdoor sources in rural China. *Sci. Total Environ.* 571, 1477–1489. <https://doi.org/10.1016/j.scitotenv.2016.06.231>.
- Smith, J., Mun Tho, L., Xu, N., Gillespie, D.A., 2010. The ATM-Chk2 and ATR-Chk1 pathways in DNA damage signaling and cancer. *Adv. Cancer Res.* 108, 73–112. <https://doi.org/10.1016/B978-0-12-380888-2.00003-0>.
- Stabile, L., Buonanno, G., Avino, P., Frattolillo, A., Guerriero, E., 2018. Indoor exposure to particles emitted by biomass-burning heating systems and evaluation of dose and lung cancer risk received by population. *Environ. Pollut.* 235, 65–73. <https://doi.org/10.1016/j.envpol.2017.12.055>.
- Steenhof, M., Gosens, I., Strak, M., Godri, K.J., Hoek, G., Cassee, F.R., Mudway, I.S., Kelly, F.J., Harrison, R.M., Lebrecht, E., Brunekreef, B., Janssen, N.A., Pieters, R.H., 2011. In vitro toxicity of particulate matter (PM) collected at different sites in the Netherlands is associated with PM composition, size fraction and oxidative potential - the RAPTES project. *Part. Fibre Toxicol.* 8, 26. <https://doi.org/10.1186/1743-8977-8-26>.

- Strapáčová, S., Brenerová, P., Krčmář, P., Andersson, P., van Ede, K.I., van Duursen, M.B.M., van den Berg, M., Vondráček, J., Machala, M., 2018. Relative effective potencies of dioxin-like compounds in rodent and human lung cell models. *Toxicology* 404–405, 33–41. <https://doi.org/10.1016/j.tox.2018.05.004>.
- Sussan, T.E., Ingole, V., Kim, J.H., McCormick, S., Negherbon, J., Fallica, J., Akulian, J., Yarmus, L., Feller-Kopman, D., Wills-Karp, M., Horton, M.R., Breyse, P.N., Agrawal, A., Juvekar, S., Salvi, S., Biswal, S., 2014. Source of biomass cooking fuel determines pulmonary response to household air pollution. *Am. J. Respir. Cell Mol. Biol.* 50, 538–548. <https://doi.org/10.1165/rcmb.2013-02010C>.
- Swiston, J.R., Davidson, W., Attridge, S., Li, G.T., Brauer, M., Van Eeden, S.F., 2008. Wood smoke exposure induces a pulmonary and systemic inflammatory response in firefighters. *Eur. Respir. J.* 32, 129–138. <https://doi.org/10.1183/09031936.00097707>.
- Torvela, T., Uski, O., Karhunen, T., Jalava, P., Sippula, O., Tissari, J., Hirvonen, M., Jokiniemi, J., 2014. Reference Particles for Toxicological Studies of Wood Combustion: Formation, Characteristics, and Toxicity Compared to Those of Real Wood Combustion Particulate Mass.
- Totlandsdal, A.I., Øvrevik, J., Cochran, R.E., Hersheth, J.L., Bølling, A.K., Låg, M., Schwarze, P., Lilleaas, E., Holme, J.A., Kubátová, A., 2014. The occurrence of polycyclic aromatic hydrocarbons and their derivatives and the proinflammatory potential of fractionated extracts of diesel exhaust and wood smoke particles. *J. Environ. Sci. Health A Tox. Hazard. Subst. Environ. Eng.* <https://doi.org/10.1080/10934529.2014.854586>.
- Uski, O.J., Happo, M.S., Jalava, P.I., Brunner, T., Kelz, J., Obernberger, I., Jokiniemi, J., Hirvonen, M.-R., 2012. Acute systemic and lung inflammation in C57Bl/6j mice after intratracheal aspiration of particulate matter from small-scale biomass combustion appliances based on old and modern technologies. *Inhal. Toxicol.* 24, 952–965. <https://doi.org/10.3109/08958378.2012.742172>.
- Uski, O., Jalava, P.I., Happo, M.S., Leskinen, J., Sippula, O., Tissari, J., Mäki-Paakkanen, J., Jokiniemi, J., Hirvonen, M.R., 2014. Different toxic mechanisms are activated by emission PM depending on combustion efficiency. *Atmos. Environ.* 89, 623–632. <https://doi.org/10.1016/j.atmosenv.2014.02.036>.
- Uski, O., Jalava, P.I., Happo, M.S., Torvela, T., Leskinen, J., Mäki-Paakkanen, J., Tissari, J., Sippula, O., Lamberg, H., Jokiniemi, J., Hirvonen, M.-R., 2015. Effect of fuel zinc content on toxicological responses of particulate matter from pellet combustion in vitro. *Sci. Total Environ.* 511, 331–340.
- Van Den Heuvel, R., Den Hond, E., Govarts, E., Colles, A., Koppen, G., Staelens, J., Mampaey, M., Janssen, N., Schoeters, G., 2016. Identification of PM10 characteristics involved in cellular responses in human bronchial epithelial cells (Beas-2B). *Environ. Res.* 149, 48–56. <https://doi.org/10.1016/j.envres.2016.04.029>.
- Wallach, D., Kang, T.-B., Kovalenko, A., 2013. Concepts of tissue injury and cell death in inflammation: a historical perspective. *Nat. Rev. Immunol.* 14, 51–59. <https://doi.org/10.1038/nri3561>.
- Yang, L., Liu, G., Lin, Z., Wang, Y., He, H., Liu, T., Kamp, D.W., 2016. Pro-inflammatory response and oxidative stress induced by specific components in ambient particulate matter in human bronchial epithelial cells. *Environ. Toxicol.* 31, 923–936. <https://doi.org/10.1002/tox.22102>.
- Zhang, J., Ghio, A.J., Gao, M., Wei, K., Rosen, G.D., Upadhyay, D., 2007. Ambient particulate matter induces alveolar epithelial cell cycle arrest: role of G1 cyclins. *FEBS Lett.* 581, 5315–5320.
- Zhang, J., Song, W., Guo, J., Zhang, J., Sun, Z., Ding, F., Gao, M., 2012. Toxic effect of different ZnO particles on mouse alveolar macrophages. *J. Hazard. Mater.* 219–220, 148–155. <https://doi.org/10.1016/j.jhazmat.2012.03.069>.



In vitro pulmonary and vascular effects induced by different diesel exhaust particles

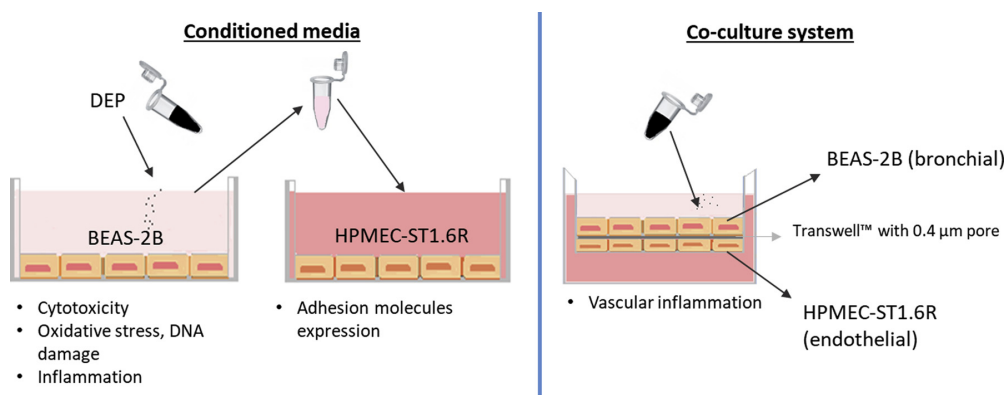


Rossella Bengalli^{a,*}, Alessandra Zerboni^{a,1}, Sara Marchetti^a, Eleonora Longhin^a, Marco Priola^b, Marina Camatini^a, Paride Mantecca^a

^a POLARIS Research Center, Dept. of Earth and Environmental Sciences, University of Milano Bicocca, Piazza della Scienza 1, 20126, Milano, Italy

^b Innovhub-SSI Fuels Division, Via Galileo Galilei, 1, 20097, San Donato Milanese, Milan, Italy

GRAPHICAL ABSTRACT



ARTICLE INFO

Keywords:

Diesel exhaust particles
Inflammatory mediators
Endothelial activation
In vitro toxicity

ABSTRACT

Diesel exhaust particles (DEP) are responsible for both respiratory and cardiovascular effects. However many questions are still unravelled and the mechanisms behind the health effects induced by the exposure to ultrafine particles (UFP) need further investigations. Furthermore, different emission sources can lead to diverse biological responses. In this perspective, here we have compared the effects of three DEPs, two standard reference materials (SRM 1650b and 2975) and one DEP directly sampled from a EuroIV vehicle without Diesel Particulate Filter (DPF). For the biological investigations, different *in vitro* lung models involving both epithelial and

Abbreviations: BSA, bovine serum albumin; CVD, cardiovascular diseases; DEP, diesel exhaust particles; FBS, fetal bovine serum; HO-1, heme-oxygenase-1; ICAM-1, intercellular adhesion molecule-1; IL-6, interleukin-6; IL-8, interleukin-8; NIST, National Institute of Standard and Technologies; PAHs, polycyclic aromatic hydrocarbons; PBS, phosphate buffered saline; PM, particulate matter; TEM, transmission electron microscope; ROS, reactive oxygen species; SRMs, Standard Reference Materials; UFP, ultrafine particles; VCAM-1, vascular cellular adhesion molecule-1; VEGF, vascular endothelial growth factor; ZO-1, zonula occludens-1

* Corresponding author at: Department of Earth and Environmental Sciences, University of Milano Bicocca, Piazza della Scienza 1, Milan, 20126, Italy.

E-mail addresses: rossella.bengalli@unimib.it (R. Bengalli), a.zerboni2@campus.unimib.it (A. Zerboni), s.marchetti16@campus.unimib.it (S. Marchetti), eleonora.m.longhin@gmail.com (E. Longhin), marco.priola@mi.camcom.it (M. Priola), marina.camatini@unimib.it (M. Camatini), paride.mantecca@unimib.it (P. Mantecca).

¹ Equal contributors: Rossella Bengalli, Alessandra Zerboni.

<https://doi.org/10.1016/j.toxlet.2019.01.017>

Received 28 June 2018; Received in revised form 16 January 2019; Accepted 30 January 2019

Available online 01 February 2019

0378-4274/ © 2019 Elsevier B.V. All rights reserved.

vascular endothelial cells, were used. Cell viability, oxidative stress, inflammation, DNA damage and endothelial activation markers were investigated at sub-cytotoxic DEP doses.

The data obtained have shown that only DEP EuroIV, which had the major content of polycyclic aromatic hydrocarbons (PAHs) and metals, was able to induce oxidative stress, inflammation and consequent endothelial activation, as demonstrated by the expression of adhesion molecules (ICAM-1 and VCAM-1) and the release of inflammatory markers (IL-8) from endothelial cells. Standard reference materials were not effective under our experimental conditions. These data suggest that oxidative stress, endothelial activation and systemic inflammatory cytokines release are crucial events after DEP exposure and that the source of DEP emission, responsible of the particle chemical fingerprint, may have a key role in the resulting adverse biological outcomes.

1. Introduction

Air pollution is a growing public health concern, estimated to cause over 3 million premature deaths worldwide, especially attributable to cardiovascular diseases (CVD) (Lelieveld et al., 2015). Ambient particulate matter (PM) is a mixture of solid and liquid particles suspended in air with different size, chemical composition, physical and biological properties. Air pollution is a complex mixture of different compounds that can cause adverse health effects, however the cardiovascular effects are largely attributed to the particulate components (Brook et al., 2010), comprising road dust, vehicle and exhaust particles. Based on aerodynamic diameter particles are divided into PM₁₀ (< 10 µm), PM_{2.5} (< 2.5 µm) and ultrafine particles (UFP < 100 nm). Furthermore, in urban cities, traffic emissions, together with biomass burning, are the major contributors (approximately 26% and 33% respectively) to the average contribution of PM₁₀ and PM_{2.5} sources, especially during high pollution days (PM₁₀ > 50 µg/m³) (Amato et al., 2016). One of the main source of UFP is incomplete combustion of diesel engine and the consequent emissions of diesel exhaust particles (DEP), which are composed of agglomerate of solid carbonaceous material and ashes, volatile organic compounds (VOCs) and sulphur compounds (Kittelson, 1998). There is a persuasive evidence that living close to highly trafficked roads increases the risk of developing systemic inflammation, with consequent endothelial dysfunction, atherosclerosis and thrombosis (Lanki et al., 2015; Miller et al., 2012). Nevertheless, the biological mechanisms behind the effects of air pollution on CVD remain poorly defined. According to the European automobile manufacturers' association (ACEA), during the last decade there has been a large increase in the percentage of diesel-fuelled vehicles with pre-EURO 5 technologies in Europe as a means to cut CO₂ emission from transport (Schwarze et al., 2013). Therefore, increased level of diesel exhaust particles (DEP) emissions has been observed compared to gasoline-fuelled vehicles. Although the recent efforts in many western countries to reduce or even ban the diesel-fuelled vehicles, DEP emission still remains a great concern for public health and may even worsen in the still growing megalopolis of developing countries.

Oxidative stress, inflammation, cytotoxicity, genotoxicity and cell-to-cell contacts disruption are some of the several pathways involved in the response to PM and ultrafine particles (UFP) exposure. DEP exposure induces both cytotoxic and pro-inflammatory effects on vascular endothelial cells (Klein et al., 2017; Lawal et al., 2016) with consequent endothelial dysfunction and development of CVD such as ischemia, myocardial infarction and atherosclerosis (Miller et al., 2012; Robertson and Miller, 2018; Törnqvist et al., 2007). Furthermore, it has been demonstrated that there is a higher incidence of ischemia in smokers chronically exposed to diesel emissions exposure (Finkelstein et al., 2004) and persons with pre-existing CVD are at highest risk. *In vivo* studies have also shown the increased atherosclerotic plaque size and plasma lipid peroxidation in mice exposed to DEP (Miller et al., 2013).

Three main hypotheses have been proposed by which air pollution can promote endothelial activation: i) particle induced inflammatory responses in the lungs, leading to the release of inflammatory and oxidative mediators from the epithelial lung cells to the alveolar

capillaries and blood circulation; ii) activation of airway sensory nerves by pollutants; iii) translocation of particles across the air-blood barrier (ABB) and direct entry of pollutants into the pulmonary circulation.

In the presence of cardiovascular risk factors, the endothelium is activated from the quiescent state to host defence response state (Lawal et al., 2016). During endothelial activation, also referred as endothelial dysfunction, cells activate a molecular process that stimulate the production of cytokines, chemokines and adhesion molecules, which interact with leukocytes and platelets to promote inflammation and ROS production, events that can lead to the formation of atherosclerotic plaques (Eckers and Haendeler, 2015; Vitiello et al., 2014).

As a consequence of an inflammatory status, characterized by the release of cytokines such as interleukin-6 (IL-6), monocytes chemoattractant protein-1 (MCP-1), vascular endothelial growth factor (VEGF) and tumour necrosis factor-alpha (TNF-α), there is an overexpression of adhesion molecules in endothelial cells, including intercellular and vascular adhesion molecules (ICAM-1 and VCAM-1) and E-selectin (Mudau et al., 2012; Sprague and Khalil, 2009). VCAM-1 and ICAM-1 are members of the immunoglobulin superfamily, able to recruit and bind leukocytes and monocytes and involved in the vascular inflammatory pathway. Their expression contributes to endothelial activation and pro-angiogenic processes, that can be induced by cytokines and vascular endothelial growth factor (VEGF), a molecule that acts on the endothelium activating proliferation, migration and cell differentiation (Joško et al., 2000).

Although in the last year there was a transition to engines and fuels with a lower environmental impact, is still unclear if DEPs generated from new technologies have significant lower adverse effects compared with the old ones. The chemical and physical properties of the emitted DEP, especially the content of metals and polycyclic aromatic hydrocarbons (PAHs), can be in fact greatly influenced by the engine technology, fuel, load, temperature, filtration devices and operating conditions in general, such as the driving regime. The comparison of the toxicological potential of DEPs from different emission sources may be of high relevance, not only for the comprehension of the adverse outcome pathways activated, but also for contributing to more specific mitigation strategies.

In the present work, we preliminary have studied the effects induced by three different DEPs on the bronchial cells BEAS-2B, in order to investigate the primary response of lung epithelial cells, focusing on cytotoxicity, cytoskeletal arrangement, oxidative stress, genotoxicity and release of inflammatory mediators. Afterward, the endothelial activation was investigated. To this purpose, a conditioned media and a co-culture model were set up by using BEAS-2B and the microvascular lung HPMEC cells. These *in vitro* systems allowed to analyse the DEP-induced responses on the epithelial and endothelial cells separately, as well as their interplay in the resulting inflammatory effects. The differences observed in toxicity have been related to the DEP chemical composition and emission sources.

2. Materials and methods

2.1. Diesel particles: preparation and sampling

Two standard reference materials from the NIST were used: DEP SRM 1650b and 2975 (Diesel Particle NIST® SRM®, Sigma Aldrich), which derive from the combustion of a heavy engine and a light duty respectively. DEP particles were weighed with a microbalance (Sartorius, Goettingen, Germany) and re-suspended in sterile milli-Q water to a final concentration of 2 mg/ml. Two different ultrasonic systems were chosen to disperse DEP in the water, bath-type sonicator (SONICA Soltec) and a probe-type sonicator (Bandelin Sonoplus, 3 kJ). The DEP suspension was stored at -20 °C.

DEP EuroIV was sampled on Teflon filters (Whatman, Maidstone, UK) from a EuroIV light duty vehicle without DPF (Diesel Particulate Filter) fuelled by commercial gasoline and run over a chassis dyno, as previously reported (Longhin et al., 2016). After sampling, filters were preserved at -20 °C, until particles extraction that was performed by sonication in the bath-type sonicator. Particle suspensions were then dried into a desiccator, weighed and stored at -20 °C. Samples were re-suspended in sterile water (final concentration 2 µg/µL) before use, following the same procedure used for NIST samples.

2.2. Diesel particles characterization

Particles morphology and size were analysed by transmission electron microscopy (TEM). A drop of 5 µL of DEP suspension (50 µg/mL) was deposited on Formvar® coated 200-mesh copper grids. Excess water was gently blotted, then the grids were left to dry in the air and finally inserted into a Jeol JEM-1220 TEM, operating at a voltage of 80 kV and equipped with a CCD camera.

The hydrodynamic size of DEPs was analyzed through Dynamic Light Scattering (DLS). DEP particulates were prepared using the method as previously described, then suspended in culture medium LHC-9, milliQ water and PBS at a concentration of 50 µg/mL and analyzed at DLS (Malvern Zetasizer), using a scattering angle $\theta = 90^\circ$.

Chemical characterization of PAHs through GC-MS was obtained by NIST data sheets for the two SRMs DEP and from a previous work (Longhin et al., 2016) for DEP EuroIV (Supplementary materials, Table S1). Selected metals were analyzed after mineralization in HNO₃/H₂O₂ (2:1 ratio v/v) of the samples and final dilution with ultrapure water. Metals were quantified by ICP-MS (Perkin Elmer SCIEX mod. ELAN 9000). Data are shown in Supplementary materials, Table S2.

2.3. Cells culture maintenance and treatments

BEAS-2B cells (ATCC® CRL9609™), derived from human bronchial epithelium, and the cell line HPMEC-ST1.6R, derived from the pulmonary microvascular circulation (received from Dr. Ronald E. Unger, Institute of Pathology, Medical University of Mainz, Johannes Gutenberg University, Mainz, Germany) were maintained and treated as previously described (Bengalli et al., 2017). Briefly, BEAS-2B cells (used from passage 13 to 27) were seeded at a concentration of 2.7×10^5 cells/well in 6-well plates and the day after treated with DEP (5 µg/cm²) for 20 h. Particles were directly added in the cellular medium. After 20 h, supernatants were collected and centrifuged at 1200 rpm for 6 min in order to discharge cells debris. The 40% of this conditioned medium was diluted in 60% of HPMEC fresh medium and then added to HPMEC-ST1.6R cells for further 24 h.

All the *in vitro* experiments were performed at least in triplicate, and when parallel tests were performed at least a duplicate of samples were used.

2.4. *In vitro* model of lung barrier: co-culture of BEAS and HPMEC on Transwell inserts

HPMEC-ST1.6R (9×10^4 /cm²) cells were cultured on the lower surface of Transwell® inserts (polyester; 0.4 µm pore size; Costar) coated with 0.2% gelatine and incubated for 2 h at 37 °C and 5% CO₂. The filter membranes were then turned upside down and placed in a 12-well plate filled with 1.5 mL M199 complete medium and let grow for 72 h. After that, BEAS-2B (5×10^4 /cm²) cells were cultured on the top surface of the Transwell® inserts (that was previously collagen-coated) with LHC-9 medium and let grow for 48 h. Before particles exposure, both apical and basal compartment were washed with PBS and filled respectively with 250 µL and 1.5 mL of cellular media. Finally, when BEAS-2B cells reached the confluency (after 2–3 days), 5 µg/cm² DEPs were added in the apical compartment for 24 h.

2.5. Cells viability: Alamar blue and H/PI

The AlamarBlue® (Life Technologies, Monza, Italy) assay was used to check the viability of BEAS-2B cells according to manufacturer's instruction and as previously described (Bengalli et al., 2017). Briefly, following incubation with DEPs for 20 h, BEAS-2B supernatants were collected for conditioned media experiments and a solution containing 1:10 of AlamarBlue® reagent and cell medium was added into each well. After 1–2 h incubation the absorbance of the culture medium was read to the spectrophotometer (TECAN Infinite Pro) at 570 and 630 nm wavelengths. The Alamar Blue reagent was used also to assess the cells viability of both apical and basal compartments of the 3D *in vitro* co-culture model.

Moreover, Hoechst 33342/Propidium Iodide (H/PI) staining was used in order to determine the amount of viable, necrotic and apoptotic cells. Briefly, supernatants of control and treated cells were removed and centrifuged in order to keep floating cells pellets. Cells were washed twice with PBS, trypsinized, mixed to the previous cell suspension and suspended in 500 µL of cell medium and stained with H/PI solution (10 µL of 2:1 solution of H/PI) (Sigma Aldrich). Samples were stored in the dark for 15–30 minutes at room temperature. Cells were centrifuged for 6 min at 1200 rpm, and re-suspended in 20 µL of FBS. 3 drops (about 4 µL) of cell suspension were put on the slide. The slide was observed with a fluorescence microscope (Zeiss-Axioplan) with UV filter (365 nm).

At least 300 cells per sample were scored according to nuclei staining and plasma membrane integrity as viable normal cells (H positive and PI negative, without special nuclear characteristic and an intact plasma membrane), necrotic cells (non-apoptotic and PI positive), apoptotic cells (bright H or PI positive stained with condensed or fragmented nuclei), mitotic cells (H positive with chromosome condensation).

2.6. Cell morphology: haematoxylin/eosin and immunostaining

For morphological analysis, cells were seeded on collagenated (PureColl, Advanced BioMatrix, Inc., San Diego, CA, US) cover slide at a concentration of 2.7×10^5 cells/well, cultured for 24 h and exposed to 5 µg/cm² for 20 h. At the end of the treatment, cells were fixed in formalin 10% for 20 min and then washed with PBS. Cells were stained with Mayer's haematoxylin solution and alcoholic eosin (haematoxylin-eosin staining, HE), dehydrated, clarified in xylene and mounted with Eukitt on a slide. The slides were observed under the optical microscope (Zeiss-Axioplan). The pictures were acquired using an AxioCam MRC5 digital camera and processed using the AxioVision Real 4.8 software.

For immunostaining, BEAS-2B cells were fixed with 4% paraformaldehyde and, after washing with PBS, non-specific sites were blocked by incubating cells with cold PBST (PBS 1X with 0.1% Tween20; Sigma Aldrich) containing BSA 2%. Then coverslips were incubated with the primary antibody Rabbit anti-ZO-1 (1: 200; Cell

signaling) prepared in PBS $1 \times$. After two washes, cells were incubated with the secondary antibody Goat anti-Rabbit Alexa Fluor 488 (1: 500, Life Technologies). In addition, cytoskeleton actin was marked with phalloidin-TRITC (1:150, Cytoskeleton Inc.). Nuclei were counterstained with DAPI (4', 6-diamino-2-phenylindole, 1:100, Molecular Probes, Life Technologies, Monza, Italia). Finally the slides were mounted with Prolong-antifade (Life Technologies). The images were acquired with a Zeiss AxioObserver Z1 Reverse Microscope and processed with the AxioVision Real 4.8 software.

2.7. Flow cytometry

The potential of DEPs to induce oxidative stress was analysed through flow cytometry by measuring ROS formation and the expression of γ H2AX as marker of DNA double-strands breaks (DSBs).

For ROS detection, BEAS-2B cells were pre-incubated for 20 min with the probe Carboxy-2',7'-Dichlorofluorescein Diacetate (carboxy-DCFDA, 5 μ M, Life Technologies) and then treated with DEPs for 90 min. After treatments, cells were detached, centrifuged at 1200 rpm for 6 min and re-suspended in PBS. The intensity of fluorescence, in the FITC channel, was examined by flow cytometry (CytoFLEX, Beckman

Coulter) and analysed by the program CytoExpert.

The autofluorescence of cells and DEPs was evaluated analysing the signal from unloaded samples (cells not stained with carboxy-DCFDA). These values were then subtracted from the values to DCFDA stained samples.

For measuring DNA DSBs, cells were probed with the phosphohistone H2AX (Ser139) rabbit mAb Alexa Fluor 488 Conjugate (Cell Signaling). After 24 h treatment with DEPs, cells were detached, washed once in PBS, fixed in 1% paraformaldehyde in PBS for 15 min on ice and re-suspended in 90% cold methanol and stored overnight at -80 °C prior to analysis. After discharging methanol, cells were washed two times with 0.5% bovine serum albumin (BSA) in PBS and incubated with primary antibody in PBS with 5% BSA, 0.2% Triton X-100 (dilution 1:200) for 4 h at 4 °C in the dark. After washing twice with 5% BSA in PBS cells were resuspended in PBS and analysed at the CytoFLEX (Beckman Coulter) in the FITC channel.

2.8. Western blot

After exposure, BEAS-2B and HPMEC-ST1.6R cells monolayers were scraped and lysed on ice in RIPA buffer (150 mM NaCl, 1% TritonX-

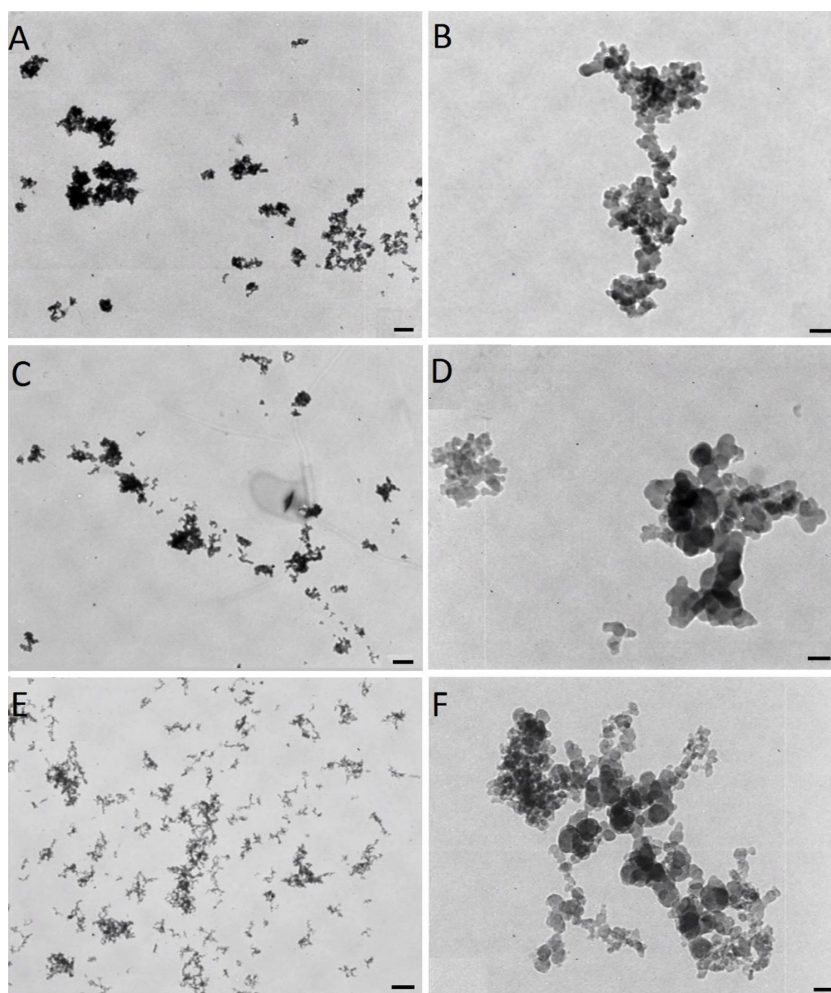


Fig. 1. Morphological characterization of DEPs. TEM images of DEP particles: A, B) DEP 1650b; C, D) DEP 2975; E, F) DEP EuroIV. Scale bars = 500 nm (A, C, E), 100 nm (B), 50 nm (D, F).

100, 0.5% sodium deoxycholate, 0.1% SDS, 50 mM Tris pH 8.0 and 0.1% of protease inhibitors). The total protein content was evaluated by the bicinchoninic acid assay (Sigma Aldrich). The same amounts of proteins were loaded onto 10% SDS-PAGE gels, separated and transferred electrophoretically on nitrocellulose membrane. After blocking for 1 h with blocking buffer TBS-T (TBS, 0.1% Tween20, 5% (w/v) BSA) the membranes were incubated at 4 °C overnight with specific primary antibody: HO-1 and NF- κ B for BEAS-2B and ICAM-1 and VCAM-1 for HPMEC-ST1.6R (antibodies dilution 1:1000, Cell Signaling). Monoclonal anti- β -Actin antibody (Cell Signaling, 1:1000) was used as loading control. The membranes were then rinsed with TBS-T and incubated with anti-rabbit IgG secondary antibody (1:2000 Cell Signaling Technology) for 1 h. After rinsing with TBS-T three times, the proteins-bound were measured with LiteAblot Plus Chemiluminescent Substrate (Euroclone) by using a UVP machine and a dedicated software (VisionWorks LS). Data were normalized to the β -actin content and expressed as fold increase over control.

2.9. ELISA

After exposure, the supernatants from BEAS-2B and HPMEC-ST1.6R cells and the supernatants from the apical and basal compartments of the *in vitro* co-culture model were collected and stored at -20°C until analysis. Protein levels were detected by sandwich ELISA according to the manufacturer's instructions (IL-6, IL-8, sIL-6R, VEGF, Life Technologies). The absorbance of each sample was measured by Multiplate Reader Ascent (Thermo Scientific, USA) at the wavelength of 450 nm and the amount of proteins in pg/mL calculated on the basis of standard curves.

2.10. Statistical analysis

The data represent the mean and standard errors (SE) of at least three independent experiments. Statistical analyses were performed using Sigma Stat 3.2 software, using unpaired *t*-test or One-Way ANOVA and relative post-hoc analysis. Values of $p < 0.05$ were considered statistically significant.

3. Results

3.1. Diesel particles characterization

TEM analysis showed that the three DEPs, when in solution (50 $\mu\text{g}/\text{mL}$ in milliQ water), tend to form aggregates, typical of soot particles. DEP 1650b (Fig. 1A and B) tend to form bigger aggregates with respect to DEP 2975 (Fig. 1C and D) and EuroIV (Fig. 1E and F), as also confirmed by DLS analyses of DEPs suspended in distilled water and in medium (Table 1). The single particles have similar morphology and size lower than 50 nm, in all the three DEP samples. DLS analysis showed that particles have a different behaviour according to the suspension medium, forming less aggregates when in milli-Q water. Nevertheless, even when in cell culture media (LHC-9), particles aggregates relied in the nanometric range, in particular DEP 1650b (471 ± 28 nm) and Euro IV (388 ± 4 nm) showed a mean hydrodynamic diameter higher than DEP 2975 (336 ± 22 nm). Results about the chemical characterization of the three different DEPs are summarized in Supplementary Materials (Table S1).

3.2. DEP effects on BEAS-2B cells

3.2.1. Cell viability

BEAS-2B cells viability was assessed by Alamar Blue metabolic test and H/PI staining and presented in Fig. 2. Data obtained by the enzymatic test show that the three DEPs did not induce significant effects on cell viability (Fig. 2A). On the contrary, an increased viability was observed after exposure to DEP SRM 2975. H/PI staining instead

revealed that there is an increase of necrotic cells of 14% in BEAS-2B cells treated with 5 $\mu\text{g}/\text{cm}^2$ DEP EuroIV, while the other DEPs did not significantly affect cell viability (Fig. 2B).

3.2.2. Cell morphology

Cell morphology and particles deposition was investigated through microscopic analysis after BEAS-2B cells exposure to the three different DEPs (5 $\mu\text{g}/\text{cm}^2$). DEPs interact with cells as well as aggregates and single particles. The HE staining showed that diesel particles came in contact with cells (Fig. 3), especially after DEP 2975 exposure (Fig. 3C), and sometimes they were inside cytoplasmic vacuoles (Supplementary materials S1). Compared to control cells, no evident morphological changes were observed after DEP exposure, except for a slight increase in elongated cell morphologies with emission of longer filopodia (Fig. 3; Supplementary materials S1).

The interference with the expression/organization of cytoskeletal and junctional proteins was qualitatively investigated by *zonula occludens-1* (ZO-1) and actin immunostaining. It has in fact been reported that BEAS-2B cells are able to form apical localised tight junction at the Air-Liquid Interface (ALI) with a Transepithelial resistance (TEER) $> 100 \Omega \cdot \text{cm}^2$ (Stewart et al., 2012). Here we observed the expression of ZO-1 at the cell-to-cell contact points in subconfluent submerged cultures. Under these conditions ZO-1 expression and actin cytoskeleton appeared almost not affected by DEP exposure (Fig. 4).

3.2.3. Oxidative stress and DNA damage

The induction of an oxidative stress response was evaluated with different approaches: 1) ROS detection at early time points, 2) expression of the protein heme oxygenase-1 (HO-1) and nuclear factor- κ B (NF- κ B) as downstream protein of the oxidative pathway and 3) analysis of the expression of the oxidative DNA damage marker γ H2AX. A significant increase of ROS production was observed in BEAS-2B cells after exposure to DEP EuroIV (Fig. 5A) and DEP 1650b, while DEP 2975 did not. These data were also confirmed by Western blot analysis of the anti-oxidant protein HO-1 (Fig. 5C). HO-1 expression was significantly increased after exposure to DEP 1650b and EuroIV with a fold increase of about 5 times compared to unexposed cells. DEP 2975 did not induce a significant increase in HO-1 expression. The expression of NF- κ B was evaluated in order to show the effects of different DEPs on oxidative stress pathways. Data showed that only DEP EuroIV induced a significant higher expression of NF- κ B protein, while DEP 1650b seems to induce a slight, but yet not significant induction of the protein (Fig. 5D).

Since oxidative stress can lead to DNA double strand breaks, as expected γ H2AX was significantly increased after exposure to DEP EuroIV, and only slightly after exposure to DEP 1650 (Fig. 5B). All together these results evidenced that DEP is able to promote cell oxidative stress, but the importance of the oxidative response and damage may depend by the DEP properties.

3.2.4. Release of inflammatory mediators

Since HO-1 is a protective enzyme that activates the secretion of pro-inflammatory proteins, including IL-6 and VEGF, which also

Table 1
DEP characterization: DLS analysis.

	1650b	2975	EuroIV
MilliQ water			
Z-Average (nm)	425.90 \pm 34.15	221.56 \pm 1.23	421.6 \pm 38.63
Pdl	0.461	0.172	0.580
PBS 1X			
Z-Average (nm)	618.76 \pm 106.75	808.73 \pm 298.14	311.16 \pm 43.2
Pdl	0.460	0.338	0.466
LHC-9 medium			
Z-Average (nm)	471.33 \pm 50	336.13 \pm 38.89	388.4 \pm 7.07
Pdl	0.329	0.279	0.358

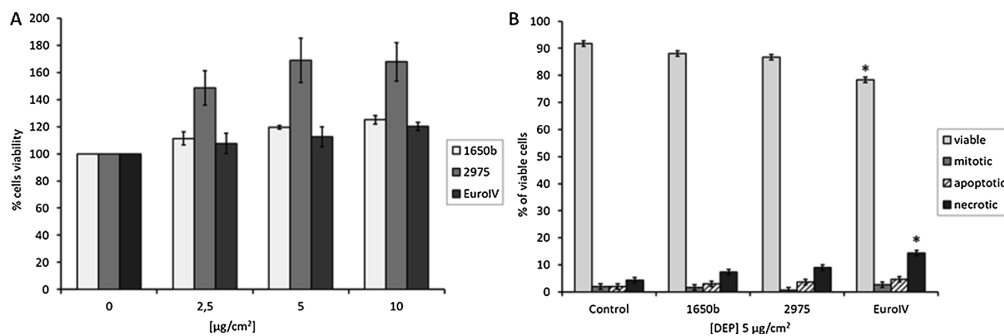


Fig. 2. Cell viability. A) Alamar Blue test: histograms represent the percentage respect to control cells (100%) of viable cells after the exposure to 0, 2,5, 5 and 10 µg/cm² to DEP 1650b (light grey bars), 2975 (grey bars) and EuroIV (black bars). Data show the mean ± SE (n = 4). B) H/P/I staining: the histograms represent the percentage of viable (light grey bars), mitotic (grey bars), apoptotic (dashed bars) and necrotic (black bars) cells after the exposure to DEP (5 µg/cm²) observed by fluorescent microscopy. Data show the mean ± SE of at least three independent experiments. *Statistically significant respect to control according to unpaired *t*-test, *p* < 0.05.

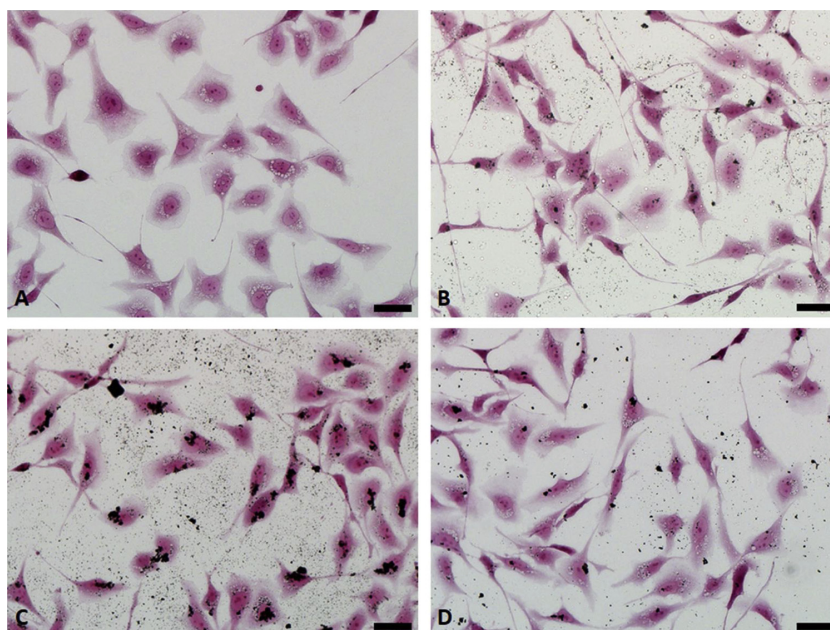


Fig. 3. Morphological analysis. Microscope images of BEAS-2B cells, stained with hematoxylin/eosin, show the slight morphological changes in respect to Control (A) after exposure for 20 h to 5 µg/cm² DEP 1650b (B), 2975 (C) and EuroIV (D). Scale bar = 20 µm.

contribute to the destruction of cell-cell contacts, the release of such proteins was therefore investigated, together with sIL-6R and IL-8.

The quantification was carried out on the supernatant of BEAS cell cultures treated with 5 µg/cm² DEPs for 20 h. Data showed a significant increase in the release of IL-6 and sIL-6R only after exposure to DEP EuroIV (Fig. 6A e B), with a 1.87 and 1.5 fold change than control respectively. No significant results were observed after exposure to the SRM DEPs. The expression of the chemokines IL-8 was not affected by any DEP (Fig. 6C). Moreover, although all DEPs seem to promote the release of VEGF by BEAS-2B exposed cells, only DEP EuroIV determined a statistically significant increase in VEGF secretion compared to untreated cells (Fig. 6D).

3.3. DEP-induced endothelial activation

To investigate the possible mechanism of the lung endothelium

activation, in response to lung epithelial cells stimulation by DEPs, two *in vitro* models, consisting in treatments with conditioned media and 3D co-culture of epithelial and endothelial cells, were used. The results are summarized in the following sections.

3.3.1. Conditioned media experiments

Since endothelial activation is characterized by an increased expression of cellular adhesion molecules, such as ICAM-1 and VCAM-1, the expression of these two proteins was evaluated in endothelial cells after treatment with conditioned media derived from BEAS-2B cells previously exposed to DEPs. As expected, only DEP EuroIV was able to induce ICAM-1 and VCAM-1 expression in HPMEC-ST1.6R (Fig. 7 A and B), since DEP 1650b and 2975 were not able to induce soluble mediators IL-6 complex release.

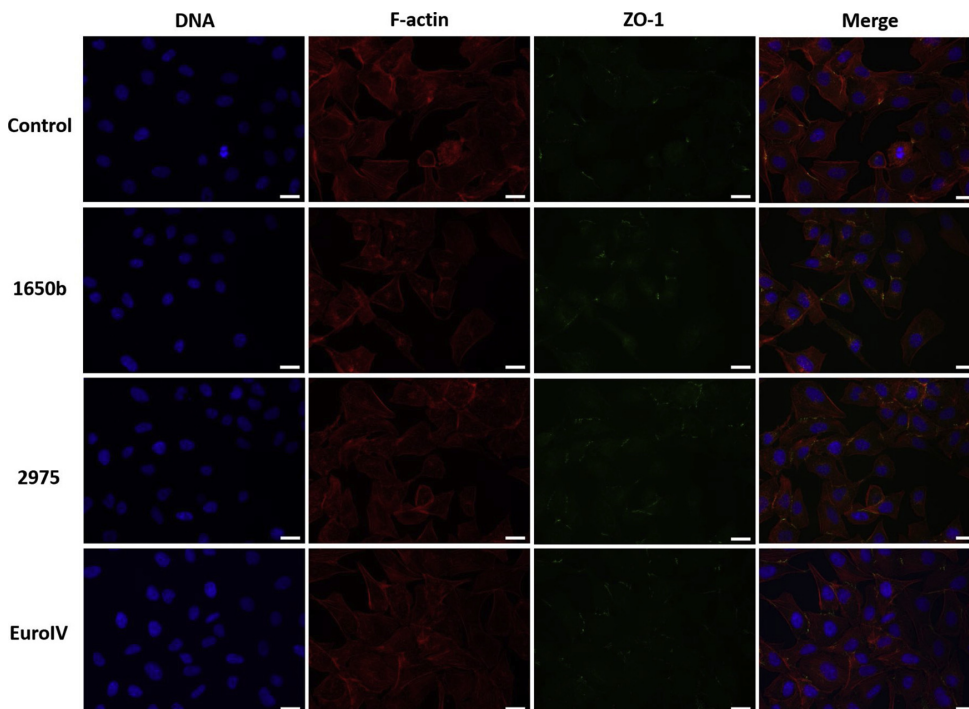


Fig. 4. Fluorescence imaging of BEAS-2B cells exposed to DEPs. The nuclei were stained with DAPI (blue), tight junction proteins with rabbit anti-ZO1 antibody (green) and actin cytoskeleton with rhodamine phalloidin (red). Scale bars = 20 μm .

3.3.2. Co-culture system

In order to confirm the endothelial activation in a model that more closely mimic the *in vivo* situation, we set up an *in vitro* 3D co-culture model of BEAS-2B cells and HPMEC-ST1.6R. No effects on both apical and basal cell viability was observed after the exposure to the three different DEPs (Fig. 8A). With this system we confirmed that the apical exposure to DEP EuroIV was able to induce an endothelial response, consisting in an increased release of IL-6 (Fig. 8B) and IL-8 in the basal (endothelial) compartment (Fig. 8C) of the model. An increase of IL-6 release in the apical compartment after DEP EuroIV was also observed, confirming the data from the conditioned media model. No effects were observed in the endothelial cells after exposure to DEP 1650b and 2975.

4. Discussion

DEP is a complex mixture of compounds, whose physico-chemical characteristics are highly dependent on fuel and engine. Studies on the effects of DEP are frequently conducted using standard reference materials (SRMs). Although a well-characterized material can be very useful for investigating the role of soot particles on the biological effects, not always SRMs are representative of real emissions.

In this research, low doses were used for *in vitro* toxicology screening, and the dose of $5 \mu\text{g}/\text{cm}^2$ was chosen for inflammatory and endothelial activation endpoints, since it may be considered representative of realistic exposure conditions in large urban centres, where during winter the daily PM concentrations may exceed $70 \mu\text{g}/\text{m}^3$ (Li et al., 2003).

Regarding the DEPs tested, the SRMs have been produced under controlled conditions and are representative of the emission of a heavy engine (SRM, 1650b) and a light engine (SRM, 2975). For this reason, also a DEP from a EuroIV light duty engine was tested. It was sampled from a vehicle run according to an urban ARTEMIS driving cycle, representative of real average STOP&GO driving conditions characteristic

of an European city.

According to our results, the three DEPs are constituted of soot ultrafine particles with very similar primary size (c.a. 50 nm) and tendency toward aggregation (Fig. 1). The hydrodynamic behaviour was in fact comparable, with SRM 2975 showing the lowest hydrodynamic diameter in both pure water and cell culture medium (Table 1). According to previous studies (Braun et al., 2007; Longhin et al., 2016), significant differences in the chemical composition among the three DEPs exist. In the two SRMs the most abundant organic compounds are fluoranthene, pyrene, phenanthrene, and 9-fluorenone and both of them show a graphitic structure (Braun et al., 2006). The chemical speciation of the EuroIV DEP showed a typical PAHs composition with high levels of pyrene, phenanthrene, benzo[a]anthracene and dibenzo(a,h)anthracene (Longhin et al., 2016). Furthermore, the content of PAHs was higher in EuroIV DEP, respectively 3 and 7 fold respect to SRM 1650b and 2975 (see Supplementary Table S1).

It is well known that the biological effects of nano-sized particles may depend on their primary size and shape, as well as to their aggregation state (Stone et al., 2017), but according to the results cited above, these properties do not justify the variable toxicity responses we observed in the lung epithelial and endothelial cells when exposed to the three DEPs. It is more likely that the different chemical composition, mainly the differences in PAH species and total content, played a major role.

The main contributors of PM and UFP-induced biological effects are both PAHs and metals adsorbed on the particles carbonaceous core (Sørensen et al., 2003; Totlandsdal et al., 2015), however there are evidences in literature that PAHs themselves can determine inflammatory response (Totlandsdal et al., 2015) and consequent endothelial activation. Furthermore, for what concern metals levels, our data showed that the DEP EuroIV has significantly higher amounts of metals compared to the two SRM DEPs, in particular with respect to Al, Ca, Zn and Fe (see Supplementary Table S2). The amount of metals such

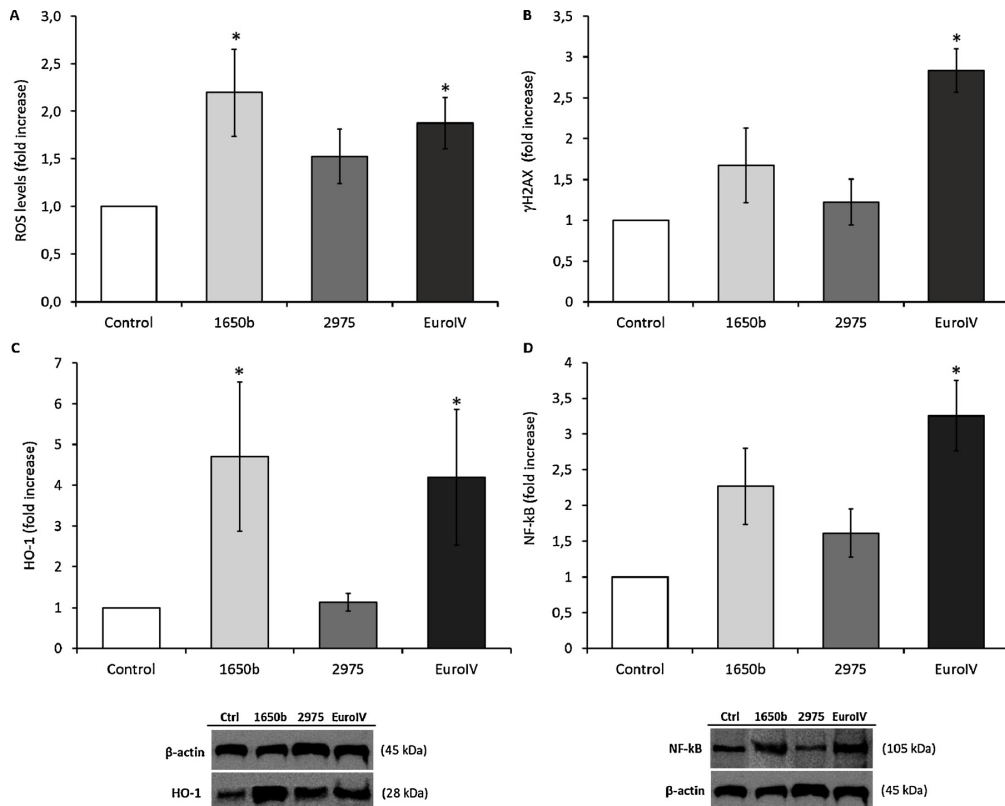


Fig. 5. Oxidative stress and DNA damage. A) ROS levels after 90 min of exposure to $5 \mu\text{g}/\text{cm}^2$ were detected by DCFDA fluorescent probe; B) DNA oxidative damage was investigated after 20 h of exposure to three different DEPs by measuring with cytofluorimetric analysis the expression of γH2AX ; C) The expression of HO-1 was evaluated in BEAS-2B cells after the exposure for 20 h to three different DEPs through Western Blot analysis; D) NF- κB protein expression. Data represent the mean \pm SE of at least three independent experiments. *Statistically significant respect to control according to unpaired *t*-test, $p < 0.05$.

as Fe, Ca and Zn derives from the diesel engine and from diesel oil. The induction of oxidative stress and release of IL-6 has been associated to the higher amount of metals adsorbed in DEP Euro IV, and it has been reported that Fe, Al and Mn levels are crucial for the pro-inflammatory effects on the respiratory system (Shao et al., 2018). Moreover, Van De Heuvel and colleagues have demonstrated that increased Cu, Ni and Zn induce cytokines release in BEAS-2B cells (Van Den Heuvel et al., 2016).

Our results in fact support the thesis that DEPs with higher content of PAHs and metals are more effective and are responsible of the pulmonary and vascular effects observed. A sequence of events, linking UFP exposure to oxidative stress and inflammation with consequent indirect activation of the vascular endothelium has been demonstrated. A statistically significant increase in the expression of ICAM-1 and VCAM-1 was observed only after exposure to DEP EuroIV, the only material able to induce oxidative and inflammatory response in lung epithelial cells. These data agree with the work of Hemmingsen and colleagues in which the effects of different DEPs on endothelial cells activation were investigated. Their results in fact showed that the exposure to DEP generated by a conventional diesel EuroIV engine induced a significantly increased expression of ICAM-1 and VCAM-1 in HUVEC cells, while DEP SRM 2975 did not generate the same response (Hemmingsen et al., 2011).

The existence of a link between endothelial dysfunction and inflammation is supported by diverse clinical and experimental data in which atherosclerosis is associated to the expression of adhesion molecules induced by pro-inflammatory cytokines such as IL-1 β , TNF- α

and C-reactive protein (CRP) produced by the liver in response to IL-6 (Zhang, 2008).

In our research, the correlation between the release of the pro-inflammatory mediators, such as IL-6, and the increased expression of ICAM-1 and VCAM-1 in endothelial cells was confirmed since treatments with DEP SRMs did not induce epithelial release of IL-6 (Fig. 6) and did not even promote an endothelial response.

These data are in contrast with other works in which the same SRM induced inflammation and cytotoxicity in BEAS-2B cells, nevertheless in those works cells were exposed to higher doses of DEP, up to $60 \mu\text{g}/\text{cm}^2$ for DEP 1650b and $10 \mu\text{g}/\text{cm}^2$ for DEP 2975 (Schwarze et al., 2013; Totlandsdal et al., 2015). Here, DEP 1650b was able to induce the formation of ROS and the expression of the anti-oxidant protein HO-1. Nevertheless, this did not activate the downstream oxidative stress pathway (NF- κB expression) and no release of inflammatory mediators, especially IL-6 and its soluble receptor, was detected, with the consequent any activation of the endothelium. These data seem to confirm that this complex has a role in the stimulation of endothelial cells in promoting adhesion molecules expression and a consequent endothelial dysfunction and possible induction of atherosclerotic processes.

Furthermore, we also have observed that DEP EuroIV is able to induce the phosphorylation of 2AX histone (Fig. 5B), suggesting an activation of the mechanism of DNA repair. Several studies show that global histone phosphorylation levels can be indirectly influenced by oxidative stress that leads to the formation of DNA double-strand breaks, which induce the phosphorylation of H2AX to activate DNA repair (Ye et al., 2016).

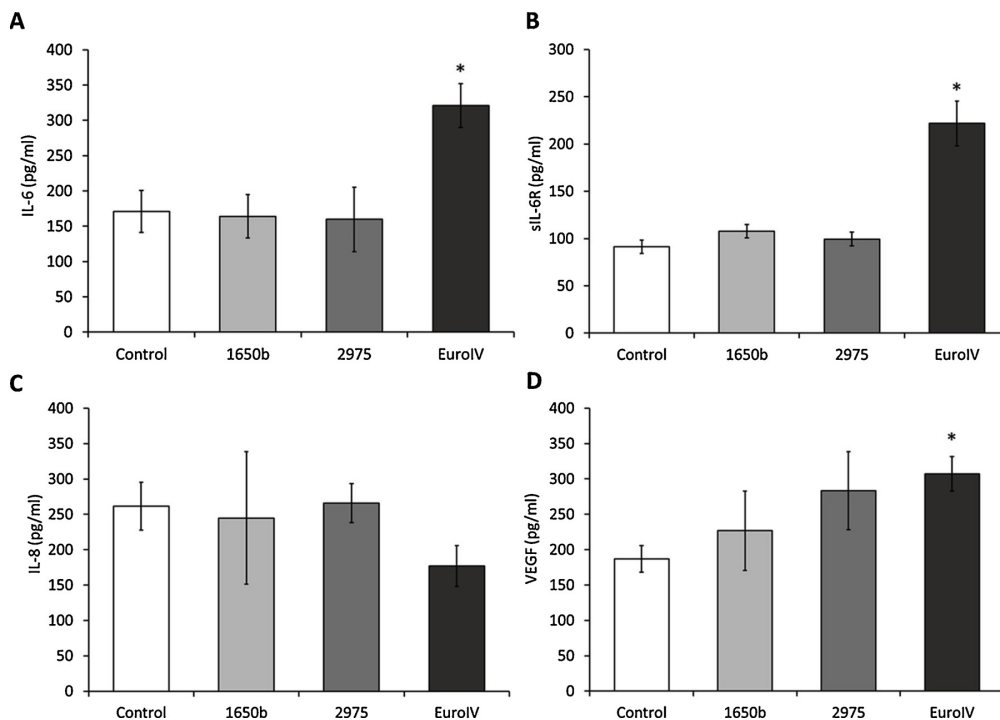


Fig. 6. Release of soluble mediators. The release of IL-6 (A), sIL-6R (B), IL-8 (C) and VEGF (D) was evaluated in BEAS-2B supernatants after the exposure for 20 h to 5 μg/cm² of three different DEPs. Data are presented as pg/ml and they represent the mean ± SE of at least three independent experiments. *Statistically significant respect to control according to unpaired *t*-test, *p* < 0.05.

Previously Li and colleagues have demonstrated that organic DEP extracts, which are enriched in PAHs, induce different biological effects in bronchial cells and macrophages related to the generation of ROS and that HO-1 expression is the most sensitive marker for oxidative stress (Li et al., 2002). In concordance with occurrence of a limited genotoxic stress after DEP exposure, a recent *in vivo* study showed a slight induction of H2AX phosphorylation and formation of bulky adducts (Douki et al., 2018).

The airway epithelium represents the first point of contact in the

respiratory system for particulate matter, and the ways in which it protects against toxic agents include a barrier with tight junctions and early local inflammatory response. The capability of particle to translocate across the epithelial barrier was indirectly investigated through the observation of ZO-1 expression in BEAS-2B cells, as well as actin filaments which are strictly related to cell-to-cell contacts. Tight junctions in BEAS epithelial cells does not appear to be compromised following exposure to the three DEPs, as demonstrated by the unaltered ZO-1 expression and actin cytoskeleton filaments (Fig. 4). We have

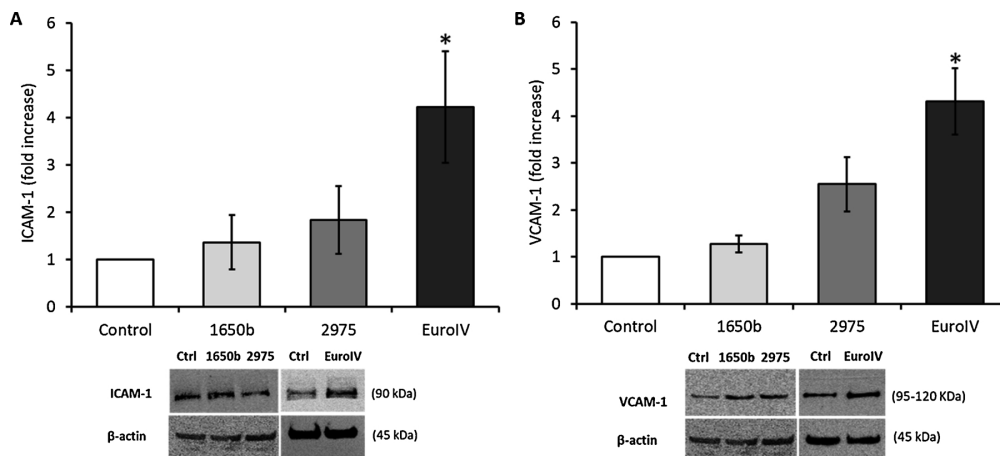


Fig. 7. Endothelial activation. The expression of ICAM-1 (A) and VCAM-1 (B) was evaluated in HPMEC-ST1.6R cells after the exposure for 24 h to conditioned media deriving from BEAS-2B treated with DEPs. Data represent the mean ± SE of at least three independent experiments. *Statistically significant respect to control sample according to ANOVA on Ranks + Dunn's, *p* < 0.05.

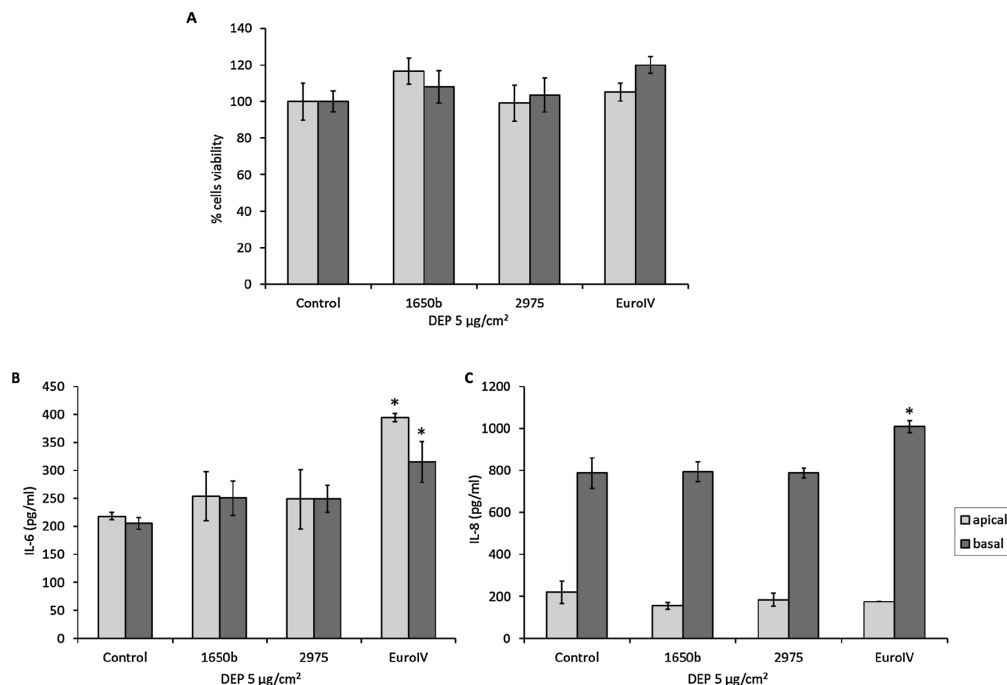


Fig. 8. Effects of DEPs in the co-culture system. Cell viability (A) and IL-6 (B) and IL-8 (C) release were evaluated after apical exposure for 24 h to DEP. Data represents the mean ± SE of at least three independent experiments. *Statistically significant respect to control sample according to unpaired t-test, p < 0.05.

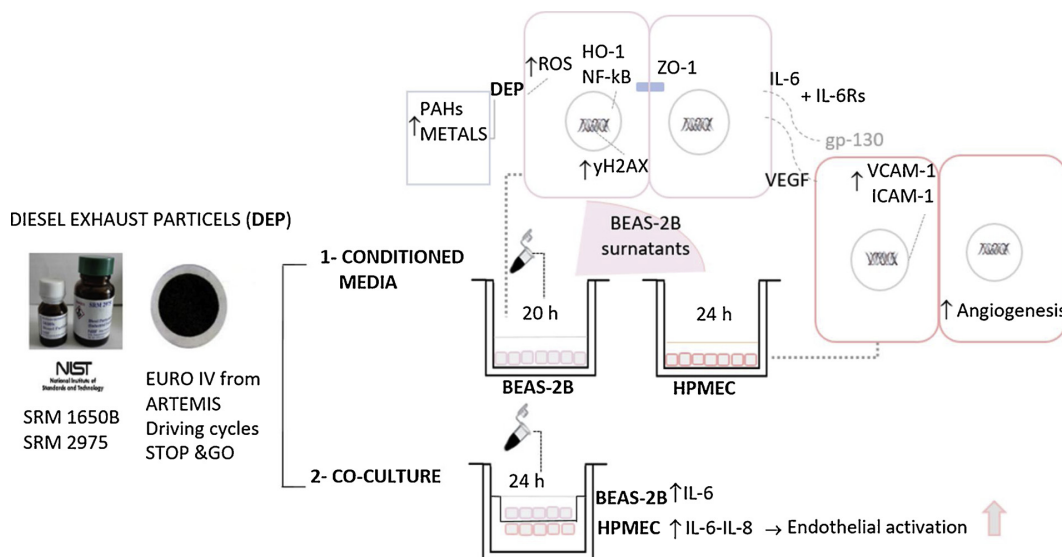


Fig. 9. Graphical scheme of experimental design and of the mechanisms involved in the response to DEP ultrafine particles.

measured also the TEER of co-cultures, but with submerged condition no TEER was developed (data not shown). In fact, with BEAS-2B cells, high values of TEER can be measured only after Air-Liquid interface (ALI) condition and after prolonged days of culturing (28 days) (Stewart et al., 2012). Moreover, with the *in vitro* systems, it is difficult to have particles translocation, especially if no changes in ZO-1 have been observed. In our model we also used Transwell insert with 0.4 µm pore, in order to avoid cells invasion from the apical compartment to

the lower one. Geys and colleagues have shown that with 0.4 µm pores no particles translocation was observed, while on 3 µm pores approximately 6% translocation was observed (Geys et al., 2006). Difficulties in observing translocation of particles in *in vitro* systems is even more evident with environmental particles that do not have defined sizes, unlike commercial metallic nanoparticles that could cross the barrier (with inserts having pores of 3 µm) (George et al., 2015). Even if further investigations on this aspect are needed, our results suggest that the

exposure to DEPs mostly result in the activation of oxidative and inflammatory responses, instead of morphological and structural cellular changes.

Development of an efficient *in vitro* model of the cardiopulmonary system is a fundamental starting point for testing the effects of different particles. In this work, for the first time, we have developed a co-culture model of BEAS-2B and HPMEC cells in which bronchial epithelial cells, while being exposed to DEP, were allowed to communicate with microvascular endothelial cells through a porous membrane. This model was set up in order to understand if the interaction with different cells modulates the response to diesel particles, even compared to the conditioned media system in which cells do not really ‘communicate’ since only endothelial cells receive the soluble mediators coming from bronchial cells.

In this research, the response obtained in monoculture and conditioned media are congruent with the results of the co-culture experiments towards early phase inflammation. The complexity of this *in vitro* system is important for the stimulation of endothelial cells in promoting adhesion molecules, since they more closely mimic realistic and physiological conditions with respect to monocultures.

In the *in vivo* situation cells communicate to each other through direct contact and secreted soluble mediators. The communication between bronchial epithelial cell cytokine products and other cell types in the surrounding tissue environment allows the tissues to orchestrate specific inflammatory and immune responses. Therefore, an exogenous stimulus is not restricted to the epithelium alone but can be transported to other cells *via* soluble mediators. In this perspective, the endothelium of the microvascular circulation plays an important role thanks to its ability to respond to inflammatory mediators and express adhesion molecules involved in the recruitment of inflammatory cells. Such a mechanism stands at the base for the development of several vascular diseases (Mögel et al., 1998).

Furthermore, in the conditioned media system it is quite difficult to understand the role of the different cells in inducing inflammation in response to the particles. In fact, we observed a slight not significant increase of IL-6 release from endothelial cells (Supplementary materials S3). Endothelial activation with this model was instead confirmed by the expression of adhesion molecules ICAM-1 and VCAM-1, as shown in Fig. 7. On the other side, in the co-culture system, we observed a significant release of cytokines from the endothelial (basal) compartment of the model. With this model the release by endothelial cells of IL-6 and IL-8 resulted increased after DEP EuroIV exposure (Fig. 8B and C), suggesting that the cross-talk between cells contributes to the inflammatory response to particles. The cytofluorimetric analysis of VCAM-1 expression in endothelial cells in the co-culture system revealed that the apical (epithelial) exposure to DEP did not induce the expression of this adhesion molecule (see Supplementary materials S4), in contrast to what we have observed in the conditioned media system. This may be due to the high level of released IL-8 from endothelial cells that may reduce VCAM-1 expression. It has been reported that a reduction of VCAM-1 can derive from increased IL-8 levels when endothelial cells are co-cultured with smooth muscle cells (Zhang et al., 2011). In this model, the crosstalk between the two different cell lines was mediated by an augmented secretion of IL-8, which inhibited the expression of VCAM-1 on smooth muscle cells through the ERK signalling pathway.

Nevertheless, the release of IL-8 in the basal compartment is a marker of endothelial activation, as it has crucial roles in chemotaxis, vascular inflammation, arrest of leukocyte and pro-atherogenesis (Sprague and Khalil, 2009; Zhang, 2008). Basing on these findings, the communication between bronchial and endothelial cells should be considered responsible for the amplification of the induced inflammatory effects.

In conclusion, studies on the effects of exposure to different sources of UFP, including DEP, are of crucial importance in order to define new emission reduction strategies based on the properties, number and

sources of UFP, rather than exclusively on atmospheric concentration in terms of mass. The reduction of particles environmental emissions could lead to an increase of air quality with a consequent lower personal exposure and an improvement in living conditions, above all for people genetically predisposed to the onset of CVD or living in urban centres with intense traffic. In this work it was highlighted that using *in vitro* models that involve the use of conditioned media and co-cultures of lung epithelial and endothelial cells, it is possible to investigate the response in endothelial cells indirectly exposed to UFP. In particular, the epithelial secretion of IL-6 and its soluble receptor sIL-6R form a complex that causes the increase in adhesion molecules through receptor gp130 as we have previously reported (Bengalli et al., 2017). Here we have further confirmed that, since SRM DEPs did not induce the release of such soluble complex, the consequent endothelial activation does not occur. This approach can be useful for investigating local mediators involved in endothelial activation. In this experiments the low doses used and the limited exposure times might be responsible of the weak response to the SRM DEPs, with lower PAH and metals content.

The biological mechanisms activated at the endothelial level provide useful information to understand the correlation between the DEP exposure and increase in respiratory and cardiovascular diseases, related to the different physico-chemical characteristics of the UFP and to their source of emission (Fig. 9). Since the exposure to air pollution and living in high trafficked areas is a risk factor for the development of several CVD, the analysis of the different pathways can provide new insights and useful tools for identifying specifically targeted pharmacological treatments, such as those against adhesion molecules (VCAM-1 and ICAM-1) and inflammatory cytokines (IL-6 and IL-8).

Fundings

This work was supported by the grants of the Cariplo Foundation to MC (proj. ID 2013-1038) and the Italian Ministry of Foreign Affairs and International Cooperation to PM (proj. ID PGR00786).

Conflict of interest

We declare no conflict of interest.

Transparency document

The Transparency document associated with this article can be found in the online version.

Acknowledgments

The authors want to thank Dr. Simone Casadei (Innovhub-SSI Fuels Division) for DEP EuroIV sampling and Dr. Maurizio Gualtieri (Italian National Agency for New Technologies, Energy and Sustainable Economic Development - ENEA-SSPT-MET-INAT) for DEP chemical characterization.

Appendix A. Supplementary data

Supplementary material related to this article can be found, in the online version, at doi:<https://doi.org/10.1016/j.toxlet.2019.01.017>.







References

- Amato, F., Alastuey, A., Karanasiou, A., Lucarelli, F., Nava, S., Calzolari, G., Severi, M., Becagli, S., Gianelle, V.L., Colombi, C., Alves, C., Custódio, D., Nunes, T., Cerqueira, M., Pio, C., Eleftheriadis, K., Diapouli, E., Reche, C., Minguillón, M.C., Manousakas, M.-I., Maggos, T., Vratolis, S., Harrison, R.M., Querol, X., 2016. AIRUSE-LIFE + : a harmonized PM speciation and source apportionment in five southern European cities. *Atmos. Chem. Phys.* 16, 3289–3309. <https://doi.org/10.5194/acp-16-3289-2016>.

- Bengalli, R., Longhin, E., Marchetti, S., Proverbio, M.C., Battaglia, C., Camatini, M., 2017. The role of IL-6 released from pulmonary epithelial cells in diesel UFP-induced endothelial activation. *Environ. Pollut.* 231, 1314–1321. <https://doi.org/10.1016/j.envpol.2017.08.104>.
- Braun, A., Mun, B.S., Huggins, F.E., Huffman, G.P., 2007. Carbon speciation of diesel exhaust and urban particulate matter NIST standard reference materials with C(1s) NEXAFS spectroscopy. *Environ. Sci. Technol.* 41, 173–178.
- Brook, R.D., Rajagopalan, S., Pope, C.A., Brook, J.R., Bhatnagar, A., Diez-Roux, A.V., Holguin, F., Hong, Y., Luepker, R.V., Mittleman, M.A., Peters, A., Siscovick, D., Smith, S.C., Whitsel, L., Kaufman, J.D., American Heart Association Council on Epidemiology and Prevention, Council on the Kidney in Cardiovascular Disease, and Council on Nutrition, Physical Activity and Metabolism, 2010. Particulate matter air pollution and cardiovascular disease: an update to the scientific statement from the American heart association. *Circulation* 121, 2331–2378. <https://doi.org/10.1161/CIR.0b013e3181d8bec1>.
- Douki, T., Corbière, C., Preterre, D., Martin, P.J., Lecureur, V., André, V., Landkocz, Y., Pottier, I., Keravec, V., Fardel, O., Moreira-Rebello, S., Pottier, D., Vendeuvre, C., Dionnet, F., Gosset, P., Billet, S., Monteil, C., Sichel, F., 2018. Comparative study of diesel and biodiesel exhausts on lung oxidative stress and genotoxicity in rats. *Environ. Pollut.* 235, 514–524. <https://doi.org/10.1016/j.envpol.2017.12.077>.
- Eckers, A., Haendeler, J., 2015. Endothelial cells in health and disease. *Antioxid. Redox Signal.* 22, 1209–1211. <https://doi.org/10.1089/ars.2015.6323>.
- Finkelstein, M.M., Verma, D.K., Sahai, D., Stefov, E., 2004. Ischemic heart disease mortality among heavy equipment operators. *Am. J. Ind. Med.* 46, 16–22. <https://doi.org/10.1002/ajim.20036>.
- George, I., Naudin, G., Boland, S., Mornet, S., Contremoulins, V., Beugnon, K., Martinon, L., Lambert, O., Baeza-Squiban, A., 2015. Metallic oxide nanoparticle translocation across the human bronchial epithelial barrier. *Nanoscale* 7 (10), 4529–4544. <https://doi.org/10.1039/c4nr07079h>.
- Geys, J., Coenegrachts, L., Vercammen, J., Engelborghs, Y., Nemmar, A., Nemery, B., Hoet, P.H., 2006. In vitro study of the pulmonary translocation of nanoparticles: a preliminary study. *Toxicol. Lett.* 160 (3), 218–226.
- Hemmingsen, J.G., Møller, P., Nejsgaard, J.K., Roursgaard, M., Loft, S., 2011. Oxidative stress, genotoxicity, and vascular cell adhesion molecule expression in cells exposed to particulate matter from combustion of conventional diesel and methyl ester biodiesel blends. *Environ. Sci. Technol.* 45, 8545–8551. <https://doi.org/10.1021/es200956p>.
- Joško, J., Gwóźdź, B., Jedrzejowska-Szypulka, H., Hendryk, S., 2000. Vascular endothelial growth factor (VEGF) and its effect on angiogenesis. *Med. Sci. Monit.* 6, 1047–1052.
- Kittelson, D.B., 1998. Engines and nanoparticles: a review. *J. Aerosol Sci.* 29, 575–588. [https://doi.org/10.1016/S0021-8502\(97\)10037-4](https://doi.org/10.1016/S0021-8502(97)10037-4).
- Klein, S.G., Cambier, S., Hennen, J., Legay, S., Serchi, T., Nelissen, I., Chary, A., Moschini, E., Krein, A., Blömeke, B., Gütleb, A.C., 2017. Endothelial responses of the alveolar barrier in vitro in a dose-controlled exposure to diesel exhaust particulate matter. *Part. Fibre Toxicol.* 14, 7. <https://doi.org/10.1186/s12989-017-0186-4>.
- Lanki, T., Hampel, R., Tiittanen, P., Andrich, S., Beelen, R., Brunekreef, B., Dratva, J., De Faire, U., Fuks, K.B., Hoffman, B., Imboden, M., Jousilahti, P., Koenig, W., Mahabadi, A.A., Künzli, N., Pedersen, N.L., Penell, J., Pershagen, G., Probst-Hensch, N.M., Schaffner, E., Schindler, C., Sugiri, D., Swart, W.J.R., Tsai, M.-Y., Turunen, A.W., Weinmayr, G., Wolf, K., Yli-Tuomi, T., Peters, A., 2015. Air pollution from road traffic and systemic inflammation in adults: a cross-sectional analysis in the European ESCAPE project. *Environ. Health Perspect.* 123, 785–791. <https://doi.org/10.1289/ehp.1408224>.
- Lawal, A.O., Davids, L.M., Marnewick, J.L., 2016. Diesel exhaust particles and endothelial cells dysfunction: an update. *Toxicol. In Vitro* 32, 92–104. <https://doi.org/10.1016/J.TIV.2015.12.015>.
- Lelieveld, J., Evans, J.S., Fnais, M., Giannadaki, D., Pozzer, A., 2015. The contribution of outdoor air pollution sources to premature mortality on a global scale. *Nature* 525, 367–371. <https://doi.org/10.1038/nature15371>.
- Li, N., Wang, M., Oberley, T.D., Sempf, J.M., Nel, A.E., 2002. Comparison of the pro-oxidative and proinflammatory effects of organic diesel exhaust particle chemicals in bronchial epithelial cells and macrophages. *J. Immunol.* 169, 4531–4541.
- Li, N., Hao, M., Phalen, R.F., Hinds, W.C., Nel, A.E., 2003. Particulate air pollutants and asthma. A paradigm for the role of oxidative stress in PM-induced adverse health effects. *Clin. Immunol.* 109, 250–265.
- Longhin, E., Gualtieri, M., Capasso, L., Bengalli, R., Mollerup, S., Holme, J.A., Øvrevik, J., Casadei, S., Di Benedetto, C., Parenti, P., Camatini, M., 2016. Physico-chemical properties and biological effects of diesel and biomass particles. *Environ. Pollut.* 215, 366–375. <https://doi.org/10.1016/j.envpol.2016.05.015>.
- Miller, M.R., Shaw, C.A., Langrish, J.P., 2012. From particles to patients: oxidative stress and the cardiovascular effects of air pollution. *Future Cardiol.* 8, 577–602. <https://doi.org/10.2217/fca.12.43>.
- Miller, M.R., McLean, S.G., Duffin, R., Lawal, A.O., Araujo, J.A., Shaw, C.A., Mills, N.L., Donaldson, K., Newby, D.E., Hadoke, P.W., 2013. Diesel exhaust particulate increases the size and complexity of lesions in atherosclerotic mice. *Part. Fibre Toxicol.* 10, 61. <https://doi.org/10.1186/10.1186/1743-8977-10-61>.
- Mögel, M., Krüger, E., Krug, H.F., Seidel, A., 1998. A new coculture-system of bronchial epithelial and endothelial cells as a model for studying ozone effects on airway tissue. *Toxicol. Lett.* 96–97, 25–32.
- Mudau, M., Genis, A., Lochner, A., Strijdom, H., 2012. Endothelial dysfunction: the early predictor of atherosclerosis. *Cardiovasc. J. Afr.* 23, 222–231. <https://doi.org/10.5830/CVJA-2011-068>.
- Robertson, S., Miller, M.R., 2018. Ambient air pollution and thrombosis. *Part. Fibre Toxicol.* 15, 1. <https://doi.org/10.1186/s12989-017-0237-x>.
- Schwarze, P.E., Totlandsdal, A.I., Låg, M., Refsnes, M., Holme, J.A., Øvrevik, J., 2013. Inflammation-related effects of diesel engine exhaust particles: studies on lung cells in vitro. *Biomed Res. Int.* 2013, 685142. <https://doi.org/10.1155/2013/685142>.
- Shao, J., Wheeler, A.J., Chen, L., Strandberg, B., Hinwood, A., Johnston, F.H., Zosky, G.R., 2018. The pro-inflammatory effects of particulate matter on epithelial cells are associated with elemental composition. *Chemosphere* 202, 530–537. <https://doi.org/10.1016/j.chemosphere.2018.03.052>.
- Sørensen, M., Autrup, H., Møller, P., Hertel, O., Jensen, S.S., Vinzents, P., Knudsen, L.E., Loft, S., 2003. Linking exposure to environmental pollutants with biological effects. *Mutat. Res.* 544, 255–271.
- Sprague, A.H., Khalil, R.A., 2009. Inflammatory cytokines in vascular dysfunction and vascular disease. *Biochem. Pharmacol.* 78, 539–552. <https://doi.org/10.1016/j.bcp.2009.04.029>.
- Stewart, C.E., Torr, E.E., Mohd Jamili, N.H., Bosquillon, C., Sayers, I., 2012. Evaluation of differentiated human bronchial epithelial cell culture systems for asthma research. *J. Allergy* 2012, 1–11. <https://doi.org/10.1155/2012/943982>.
- Stone, V., Miller, M.R., Clift, M.J.D., Elder, A., Mills, N.L., Møller, P., Schins, R.P.F., Vogel, U., Kreyling, W.G., Alstrup Jensen, K., Kuhlbusch, T.A.J., Schwarze, P.E., Hoet, P., Pietrousti, A., De Vizcaya-Ruiz, A., Baeza-Squiban, A., Teixeira, J.P., Tran, C.L., Cassee, F.R., 2017. Nanomaterials versus ambient ultrafine particles: an opportunity to exchange toxicology knowledge. *Environ. Health Perspect.* 125, 106002. <https://doi.org/10.1289/EHP424>.
- Törnqvist, H., Mills, N.L., Gonzalez, M., Miller, M.R., Robinson, S.D., Megson, I.L., MacNee, W., Donaldson, K., Söderberg, S., Newby, D.E., Sandström, T., Blomberg, A., 2007. Persistent endothelial dysfunction in humans after diesel exhaust inhalation. *Am. J. Respir. Crit. Care Med.* 176, 395–400. <https://doi.org/10.1164/rccm.200606-872OC>.
- Totlandsdal, A.I., Låg, M., Lilleaas, E., Cassee, F., Schwarze, P., 2015. Differential proinflammatory responses induced by diesel exhaust particles with contrasting PAH and metal content. *Environ. Toxicol.* 30, 188–196. <https://doi.org/10.1002/tox.21884>.
- Van Den Heuvel, R., Den Hond, E., Govarts, E., Colles, A., Koppen, G., Staelens, J., Mampaey, M., Janssen, N., Schoeters, G., 2016. Identification of PM10 characteristics involved in cellular responses in human bronchial epithelial cells (Beas-2B). *Environ. Res.* 149, 48–56. <https://doi.org/10.1016/j.envres.2016.04.029>.
- Vitiello, L., Spoletini, I., Gorini, S., Pontecorvo, L., Ferrari, D., Ferraro, E., Stabile, E., Caprio, M., la Sala, A., 2014. Microvascular inflammation in atherosclerosis. *IJC Metab. Endocr.* 3, 1–7. <https://doi.org/10.1016/J.IJCME.2014.03.002>.
- Ye, B., Hou, N., Xiao, L., Xu, Y., Xu, H., Li, F., 2016. Dynamic monitoring of oxidative DNA double-strand break and repair in cardiomyocytes. *Cardiovasc. Pathol.* 25, 93–100. <https://doi.org/10.1016/j.carpath.2015.10.010>.
- Zhang, C., 2008. The role of inflammatory cytokines in endothelial dysfunction. *Basic Res. Cardiol.* 103, 398–406. <https://doi.org/10.1007/s00395-008-0733-0>.
- Zhang, Z., Chu, G., Wu, H.X., Zou, N., Sun, B.G., Dai, Q.Y., 2011. IL-8 reduces VCAM-1 secretion of smooth muscle cells by increasing p-ERK expression when 3-D co-cultured with vascular endothelial cells. *Clin. Invest. Med.* 3, E138–E146.

Article

Intracerebral Injection of Extracellular Vesicles from Mesenchymal Stem Cells Exerts Reduced A β Plaque Burden in Early Stages of a Preclinical Model of Alzheimer's Disease

Chiara A. Elia ^{1,2}, Matteo Tamborini ¹, Marco Rasile ^{1,3}, Genni Desiato ^{1,4},
Sara Marchetti ^{1,5,†}, Paolo Swuec ^{6,7}, Sonia Mazzitelli ^{1,‡}, Francesca Clemente ^{5,8,§},
Achille Anselmo ⁸, Michela Matteoli ^{1,3}, Maria Luisa Malosio ^{1,2,*} and Silvia Coco ^{5,*}

¹ Laboratory of Pharmacology and Brain Pathology, Neuro Center, Humanitas Clinical and Research Center -IRCCS- Via Manzoni 56, 20089 Rozzano, Italy

² CNR, Institute of Neuroscience, Via Vanvitelli 32, 20129 Milano, Italy

³ Humanitas University, Department of Biomedical Sciences, Via Rita Levi Montalcini 4, 20090 Pieve Emanuele, Italy

⁴ CNR, Institute of Neuroscience, Via Moruzzi 1, 56125 Pisa, Italy

⁵ School of Medicine and Surgery and Milan Center for Neuroscience (NeuroMI), University of Milano-Bicocca, Via Cadore, 48, 20900 Monza, Italy

⁶ Cryo-Electron Microscopy Lab, Department of Biosciences, University of Milan, Via Celoria 26, 20133 Milano, Italy

⁷ Centro di Ricerca Pediatrica Romeo ed Enrica Invernizzi, University of Milano, Via Celoria 26, 20133 Milano, Italy

⁸ Flow Cytometry Core Facility, Humanitas Clinical and Research Center, Via Manzoni 56, 20089 Rozzano, Italy

* Correspondence: marialuisa.malosio@in.cnr.it (M.L.M.); silvia.coco@unimib.it (S.C.)

† Sara Marchetti's current address: POLARIS Research Center, Dept. of Earth and Environmental Sciences, University of Milano-Bicocca, Piazza della Scienza 1, 20126 Milano, Italy.

‡ Sonia Mazzitelli's current address: Deutsches Zentrum für Neurodegenerative Erkrankungen e.V. (DZNE) Otfried-Müller-Straße 27, 72076 Tübingen, Germany.

§ Francesca Clemente's current address: Tumor Immunology Unit, Division of Immunology, Transplantation and Infectious Diseases, San Raffaele Scientific Institute -IRCCS-, Via Olgettina 32, 20132 Milan, Italy.

Received: 17 June 2019; Accepted: 26 August 2019; Published: 10 September 2019



Abstract: Bone marrow Mesenchymal Stem Cells (BM-MSCs), due to their strong protective and anti-inflammatory abilities, have been widely investigated in the context of several diseases for their possible therapeutic role, based on the release of a highly proactive secretome composed of soluble factors and Extracellular Vesicles (EVs). BM-MSC-EVs, in particular, convey many of the beneficial features of parental cells, including direct and indirect β -amyloid degrading-activities, immunoregulatory and neurotrophic abilities. Therefore, EVs represent an extremely attractive tool for therapeutic purposes in neurodegenerative diseases, including Alzheimer's disease (AD). We examined the therapeutic potential of BM-MSC-EVs injected intracerebrally into the neocortex of APP^{swe}/PS1^{dE9} AD mice at 3 and 5 months of age, a time window in which the cognitive behavioral phenotype is not yet detectable or has just started to appear. We demonstrate that BM-MSC-EVs are effective at reducing the A β plaque burden and the amount of dystrophic neurites in both the cortex and hippocampus. The presence of Neprilysin on BM-MSC-EVs, opens the possibility of a direct β -amyloid degrading action. Our results indicate a potential role for BM-MSC-EVs already in the early stages of AD, suggesting the possibility of intervening before overt clinical manifestations.

Keywords: bone marrow mesenchymal stem cells; extracellular vesicles; Alzheimer's disease; APP^{swe}/PS1^{dE9} AD mice; Neprilysin; dystrophic neuritis; SMI; A β plaques

1. Introduction

Alzheimer's disease (AD), the leading cause of dementia, has recently been attracting a lot of attention from the scientific community, since millions of people are affected by this incurable pathology; furthermore, the number of patients is destined to increase in the coming decades [1]. The limited knowledge of the etiology of Alzheimer's has rendered in vain numerous attempts hitherto pursued to find a resolutive treatment that is not simply limited to the alleviation of symptoms. Therefore, a worldwide effort is underway to discover the mechanisms responsible for the disease onset and progression and to find an efficacious therapy, developing either novel treatments [2–4] or preventive strategies [5].

Cell therapy is becoming a new reality for many diseases. Due to the plasticity and multifaceted features of stem cells, recent studies have also focused on their possible exploitation in AD [6–8]. Multipotent bone marrow mesenchymal stem cells (BM-MSCs) represent a heterogeneous subset of stromal cells. They can be isolated from bone marrow or many other adult tissues, including periosteum, trabecular bone, adipose tissue, synovium, pancreas, placenta and cord blood [9]. They typically give rise to cells of diverse lineages, including adipocytes, chondrocytes and osteocytes. In recent years, BM-MSCs have been shown to be endowed with immunoregulatory abilities [10]. This property makes them suitable as possible therapeutic tools for AD [11], a disease characterized by a large inflammatory component mediated by microglia activation [2]. Interestingly, transplantation of human adipose tissue-derived MSCs (ADSC) into the brain has been shown to reduce A β deposition and to restore microglial function in transgenic APP^{swe}/PS1^{dE9} (APP/PS1) mice, a preclinical model widely used for the study of AD [12]. Moreover, BM-MSCs alleviated memory deficits in AD mice by modulating immune responses [13].

More recently the discovery of Extracellular Vesicles (EVs) originating from MSCs, retaining most of the properties of the cells of origin, is leading scientists to develop cell-free therapies to limit the potential side effects associated with the use of stem cells [14], including induction of vascular obstruction [15], lung retention after transplantation (resulting in a reduction in the population of cells that reach the target site) [16], the production of allo-antibodies was observed following repeated administration of MSCs [17], as well as a controversial protumorigenic effect [18]. In *in vitro* experiments, exosomes from human ADSC significantly decreased both secreted and intracellular A β levels in N2a cells engineered to overexpress human APP, by virtue of the proteolytic activity of neutral endopeptidase neprilysin (NEP), the dominant A β peptide-degrading enzyme in the brain, towards A β ₁₋₄₂ peptide [19]. Human ADSC derived EVs were thus envisaged to represent a therapeutic tool based on their A β -degrading ability [19]. Another therapeutic perspective put forward is a possible role of EVs in A β ₁₋₄₂ scavenging, thanks to the ability of EVs glycosphingolipids to bind to A β and to convey it to the microglia for phagocytosis [20]. In addition, MSC-EVs have been described to exert an antiapoptotic, neuroprotective role [21,22] and to promote neurite outgrowth and axon regeneration of injured neurons [23,24]. Therefore, MSC-EVs, similarly to parental cells, are endowed with anti-inflammatory, amyloid- β degrading and neurotrophic activities that could stimulate neighboring parenchymal cells to start repairing damaged tissues. These properties have been considered very interesting to test in *in vivo* models of AD (for a recent review, see [11]). Altogether, this evidence suggests that MSC-derived EVs might play a therapeutic effect in AD.

Despite the massive investments in AD drugs, the disappointing failure of several clinical trials conducted in recent years is forcing the neuroscience community to orient itself towards initiating the treatments at earlier stages of the pathology. Indeed, the pathophysiological process of AD is known to begin decades before diagnosis, with amyloid buildup occurring when only subtle clinical symptoms, if any at all, are evident [25].

In the present study, we hypothesized that the early therapeutic exploitation of MSC-EVs could be efficacious in addressing some of the disease features of AD, which may possibly slow, or even prevent, manifestation of the pathological signs. For this purpose, bone marrow mouse MSC-EVs were injected into the neocortex of APP/PS1 mice at two different time points: 5 months, when amyloid plaques were

definitely present, and 3 months, when they were instead just starting to appear. Our results indicate that an early intervention with BM-MSC-EVs reduces pathological signatures of AD, thus suggesting that MSC-EVs could be regarded as a potentially effective treatment for the disease.

2. Materials and Methods

2.1. Culture of Purified Murine Bone Marrow Mesenchymal Stem Cells

Primary Bone Marrow Mesenchymal Stem Cells (BM-MSCs) were prepared from 4–12 week-old C57BL/6 mice by flushing femur and tibia bones cavities using plain culture medium, removing red blood cells by lysis with 0.84% (*w/v*) NH₄Cl solution for 5 min at RT, then filtering through a 70 µm filter mesh and seeding them in tissue culture flasks in αMEM supplemented with 20% (*v/v*) FBS (HyClone, Cat.N. SH30070.03, GE Healthcare Bio-Sciences, Pittsburgh, PA, USA) in a 5% CO₂ incubator. Nonadherent cells were removed 48 hours later by changing the medium. Cells were passaged at sub-confluency (~80%) with a split ratio of 1:3, or cryopreserved and stored at –80 °C in 10% DMSO in FBS. BM-MSCs were used from passages 9 to 14 (P9–P14).

2.2. BM-MSC Osteogenic and Adipogenic Lineage Differentiation Assay

Differentiation of murine BM-MSCs towards the osteogenic and adipogenic lineages was performed in 6-well plates (5 × 10³ cells/well) with osteogenic differentiation medium (αMEM with 5% FBS, dexamethasone 10 nM, ascorbic acid 0.3 M, β-glycerophosphate 10 mM), adipogenic differentiation medium (αMEM with 5% FBS, dexamethasone 10 nM and insulin 0.5 µg/mL) or control medium (αMEM with 5% FBS). After 30 days, osteogenic and adipogenic differentiation were revealed by Alizarin Red and Red Oil O staining, respectively.

2.3. Senescence Associated β-Galactosidase (SA-β-Gal) Assay

For SA-β-Galactosidase staining cells were washed in PBS and fixed in 2% (*w/v*) formaldehyde, 0.2% (*w/v*) glutaraldehyde for 5 min at RT and after 1 wash in PBS were incubated O/N in freshly prepared staining solution at pH 6.0 containing 1mg/mL Xgal (5-bromo-4-chloro-3-indolyl-β-galactopyranoside, Sigma-Aldrich®, Merck KGaA, Darmstadt, Germany) in 8 mM citric acid/sodium phosphate buffer, 150 mM NaCl, 2 mM MgCl₂, 5 mM potassium ferrocyanide and 5 mM potassium ferricyanide. Cell nuclei were counterstained with Hoechst 33342 and visualized with a 20× objective on a wide field system (Olympus Cell'R system with an IX81 inverted microscope, Olympus, Hamburg, Germany) equipped with an MT20 illumination device with fluorescent filters (Ex: 361 nm; Em: 486 nm) and Differential Interference Contrast (DIC). For each condition, a minimum of 6 fields (containing on average of 50 cells) were acquired (Olympus Xcellence 1.2 RealTime controller software), and the percentage of β-Gal positive cells on the total number of cells was calculated after manually counting with Fiji ImageJ software the β-Gal positive cells that appeared with a black cytoplasm (DIC channel) and the Hoechst positive nuclei (Hoechst channel). The percentage of β-Gal positive cells on the total number of cells was plotted and subjected to statistical analysis with Graphpad Prism v.7.0 software.

2.4. Flow Cytometry Profiling of BM-MSCs

Cells were stained using the appropriate saturating concentrations of the following conjugated antibodies: FITC-conjugated mouse hematopoietic lineage Cocktail (Lin, eBioscience™, San Diego, CA, USA), rat anti-mouse CD31 Brilliant-Violet™510-conjugated, rat anti-mouse Ly 6A/E (Sca1) phycoerythrin-conjugated, hamster anti-rat/mouse CD49a Alexa-Fluor®647-conjugated (BD Biosciences, San Jose, CA, USA), rat anti-mouse CD9 FITC-conjugated, rat anti-mouse/human CD44 Alexa-Fluor®647-conjugated, Armenian hamster anti-mouse/rat CD29 Pacific Blue™ conjugated, rat anti-mouse CD73 Alexa-Fluor®647-conjugated, rat anti-mouse CD105 PE/Cy7™-conjugated, rat anti-mouse CD117 (c-kit) PerCP™/Cy5.5-conjugated (BioLegend®, San Diego, CA, USA). Following surface staining, cells were fixed using 2% (*w/v*) paraformaldehyde (PFA) in PBS for 20 min on ice.

An LSR Fortessa analyzer (BD Biosciences, San Jose, CA, USA), equipped with 4 lasers and able to discriminate up to 18 fluorophores, was used for sample acquisition. Instrument performance was checked daily using CS&T Beads (BD Biosciences, San Jose, CA, USA) and SPHERO Rainbow beads (Spherotech, Lake Forest, IL, USA). Data acquisition and analysis were performed with FACSDiva v.6.2 (BD Biosciences, San Jose, CA, USA) and Flow-Jo v.9.7 (Tree Star Inc., Ashland, OR, USA), respectively.

2.5. Isolation of BM-MSC-Derived EVs

EVs were obtained from BM-MSC supernatants by a protocol adapted from [26], whereby a monolayer of approx. 3×10^6 murine BM-MSCs, seeded in tissue culture flasks, was washed three times with PBS and incubated in serum-free α MEM for 3 h to induce EV release. The culture medium was then collected and centrifuged at 4 °C, first at 300 g for 10 min to discard dead cells, then at $1000 \times g$ for 20 min to eliminate cellular debris, and finally for 90 min at 110,000 g to pellet EVs composed of Exosomes and Microvesicles. For in vivo studies following removal of the centrifugation supernatant, EVs were rinsed in PBS and ultracentrifuged again before use. EV-enriched pellets were resuspended in PBS. For biochemical studies, EVs were solubilized in lysis buffer (10 mM HEPES-NaOH pH 7.5; 2 mM EDTA pH 8.0; 1% (w/v) SDS; supplemented with protease and phosphatase inhibitors) and protein content was quantified by micro-BCA assay (Thermo Fisher Scientific, Waltham, MA, USA).

2.6. BM-MSC-EV Characterization with Nanoparticle Tracking Analysis (NTA)

NTA measurements were performed with NanoSight NS300 (Malvern Panalytical, Malvern, UK) for determination of the size and concentration of isolated EV samples. Diluted samples (1:6 in 500 μ L of PBS) were injected into the sample chamber with sterile syringes (BD Plastipak Insulin syringe, Franklin Lakes, NJ, USA) until the liquid reached the tip of the nozzle. All measurements were performed in dynamic mode, with syringe pump infusion rate 30, at room temperature and with the same viscosity value. EV samples and the EV-depleted media were analyzed right after isolation with manual shutter and gain adjustments. NTA 3.3 Dev Build 3.3.301 software was used for recordings, measurements and data output collection. Five dynamic measurements of each sample were performed (60 s each). Scripts were run via SOP-type procedures with default options for standard measurements. For each polydisperse sample, the average FTLA (particles/frame against size distribution) was considered. Raw particles size and concentration data were plotted and subjected to statistical analysis with GraphPad Prism 6.0[®] or 7.0[®] software.

2.7. BM-MSC EV Profiling by Flow Cytometry

To limit background noise from dust and salt crystals, 0.22- μ m-filtered sheath fluid was used for sample acquisition. The FSC and SSC gate for identifying EVs was determined by using dimensional beads (size range: 0.1–0.9 μ m, Biocytex, Marseille, France; and 0.79–1.34 μ m, Spherotech Inc. Lake Forest, IL, USA). Only events smaller than 0.9 μ m were included in the analysis gate. Cell membrane fragments stained using phalloidin-TRITC (Sigma-Aldrich[®], Merck KGaA, Darmstadt, Germany) at 4 °C for 30 min, in the dark, were excluded from the analysis gate for detection of MSC-EVs. EVs were stained using the appropriate saturating concentrations of conjugated monoclonal antibodies anti-CD9-FITC and anti-CD49-A647 in filtered PBS for 20 min at 4 °C. Staining specificity was further confirmed by subjecting stained EVs following acquisition to 0.05% (w/v) TX-100 solubilization and reacquiring the sample afterwards. All gated regions were defined using the appropriate fluorescence minus-one (FMO) controls. Fluidic stability, laser alignment, and time delay were checked daily to minimize fluctuations in the fluorescent signal recovered. FACS Canto II analyzer (BD Biosciences, San Jose, CA, USA) equipped with 3 lasers able to discriminate up to 10 fluorophores was used for sample acquisition. Instrument performance was checked daily using CS&T Beads (BD Bioscience, San Jose, CA, USA) and SPHERO Rainbow beads (Spherotech, Lake Forest, IL, USA). Prior to the acquisition of the EV sample, the instrument was cleaned by washing more than 10 times with Clean FACS buffer (BD Biosciences, San Jose, CA, USA) and water in turn, for 10 min each at a high flow rate.

The instrument data acquisition and analysis were performed with FACSDiva v.6.2 (BD Pharmingen) and Flow-Jo v.9.7 (Tree Star Inc., Ashland, OR, USA), respectively.

2.8. Cryo-Electron Microscopy of BM-MSC EVs

Right after preparation of EVs by centrifugation, a 3.5- μ L droplet of EVs freshly resuspended in PBS at a final concentration of 0.2×10^9 particles/ μ L was applied on a copper 300-mesh Quantifoil R2/1 holey carbon grid, previously glow discharged for 30 seconds at 30 mA using a GloQube system (Quorum Technologies, Laughton, UK). After an incubation of 60 seconds, the grid was plunge-frozen in liquid ethane using a Vitrobot Mk IV (Thermo Fisher Scientific, Waltham, MA, USA) operating at 4 °C and 100% RH. Images of the vitrified specimens were acquired using a Talos Arctica transmission electron microscope operating at 200 kV and equipped with a CETA 16M (all from Thermo Fisher Scientific, Waltham, MA, USA) camera. Images with applied defocus values between 3 and 5 μ m were acquired with a total exposure time of 2 seconds and a total accumulated dose of 95 electrons per A2 at nominal magnifications of 22,000 \times or 45,000 \times , corresponding to a pixel size of 4.7 Å/pixel and 2.3 Å/pixel at the specimen level, respectively.

2.9. Western Blotting of BM-MSC Cell and EV Lysates

Western blots of BM-MSC lysates (lysis buffer: 10mM HEPES-NaOH pH 7.5; 2mM EDTA pH8.0; 1% (*w/v*) SDS; supplemented with protease and phosphatase inhibitors) at different passages and of EVs at passage 14 were prepared and after addition of Laemmli loading buffer were denatured (10 min at 65 °C) and loaded onto 4–15% Criterion™ TGX Stain-Free™ (Bio-Rad, Hercules, CA, USA) for SDS-PAGE. The proteins were transferred to nitrocellulose membranes using the Trans Blot® Turbo System™ (Bio-Rad, Hercules, CA, USA).

Membranes were cut according to molecular weight standards in order to maximize incubation with different antibodies and were allowed to react with antibodies directed against the following proteins: Histone H2A.X phospho S139 (1:50000; Abcam, Cambridge, UK), p16^{INK4a} (1:1000; Santa Cruz, Dallas, TX, USA), Nephrilysin (1:1000; Merck-Millipore, Burlington, MA, USA), AGO-2 (1:1000; Sigma-Aldrich®, Merck KGaA, Darmstadt, Germany), Alix (1:1000; Cell Signaling, Danvers MA, USA), CD9 (1:500; Sigma-Aldrich®, Merck KGaA, Darmstadt, Germany), TSG101 (1:1000; Sigma-Aldrich®, Merck KGaA, Darmstadt, Germany), CD63 (1:500; Sigma-Aldrich®, Merck KGaA, Darmstadt, Germany) & Santa Cruz, Dallas, TX, USA) and HSP70 (1:5000; Sigma-Aldrich®, Merck KGaA, Darmstadt, Germany), in 5% (*w/v*) BSA (Sigma-Aldrich®, Merck KGaA, Darmstadt, Germany) or skimmed milk (Régilait, Saint-Martine-Belle-Roche, France) in TBS-T (137 mM NaCl, 20 mM Tris-HCl pH 7.5, 0.1% (*v/v*) Tween-20). Bands of interest were revealed following incubation with goat anti-rabbit, anti-mouse and anti-Armenian hamster secondary antibodies conjugated with HRP and revealed by SuperSignal™ West Pico PLUS or Femto (Thermo Scientific™, Thermo Fisher Scientific, Waltham, MA, USA). Acquisition of chemiluminescence signals was performed with a ChemiDoc MP system (Bio-Rad, Hercules, CA, USA). Normalization of Western blot signals was performed on the total protein loaded on each lane by the Stain-Free™ technology using the Image Lab™ v.6.0 (Bio-Rad, Hercules, CA, USA) software as previously described [27].

2.10. Quantitative RT-PCR

BM-MSC P14 and primary murine Fibroblasts, prepared from the skin of 3-day-old pups according to previously described protocols [28,29], were solubilized in 500 μ L of TRI Reagent® solution (ZYMO RESEARCH, Irvine, CA, USA) for RNA extraction. Total RNA was isolated using the RNA Direct-zol™ MiniPrep Isolation Kit (ZYMO RESEARCH, Irvine, CA, USA) according to the manufacturer's protocol. After elution in 25 μ L DNase/RNase-free water, the total RNA was quantified using NANODrop 2000c spectrophotometer (Thermo Fisher Scientific, Waltham, MA, USA) and its quality checked for by 260/280 nm optical density ratio. 1 μ g of RNA underwent reverse transcription with the High-Capacity cDNA Reverse Transcription kit (Applied Biosystems™, Thermo

Fisher Scientific, Waltham, MA, USA). Quantitative real-time polymerase chain reaction (qRT-PCR) was performed in a final volume of 10 μ L by means of a Sybr Green detection kit (SensiFAST™ SYBR® Lo-ROX, Bioline, Paris, France) in a Viiia7 Real-Time PCR System (Applied Biosystems™, Thermo Fisher Scientific, Waltham, MA, USA). Each transcript was evaluated with at least duplicate measurements and Nprilysin relative expression was calculated following normalization against that of β -actin with the comparative $\Delta\Delta$ CT method using the values obtained from skin fibroblasts mRNA as a reference. The following primers were used: Nprilysin Forward: 5'-CCCAGTGTATGGTATACCAG-3'; Reverse: 5'-TGGCCAATACCTCCATTATCA-3'; β -actin Forward: 5'-GCCATCCTGCGTTCTGGA-3', Reverse: 5'-GCTCTTCTCCAGGGAGGA-3'.

2.11. Animal Studies

Procedures involving animal handling and care were performed in accordance with protocols approved by the Humanitas Clinical and Research Center (Rozzano, Milan, Italy) in compliance with national (4D.L. N.116, G.U., suppl. 40, 18-2-1992) and international law and policies (EEC Council Directive 2010/63/EU, OJ L 276/33, 22-09-2010; National Institutes of Health Guide for the Care and Use of Laboratory Animals, US National Research Council, 2011). All efforts were made to minimize the number of mice used and their suffering. For in vivo experiments, 5–6 animals per experimental condition were used of the double transgenic Alzheimer's Disease mouse model APP/PS1 (APP^{swe}-PS1^{dE9}) purchased from Jackson Laboratory [30] (Bar Harbor, ME, USA). Animals were housed and bred in the SPF animal facility of Humanitas Clinical and Research Center. BM-MS-C-EVs were resuspended in PBS before intracranial injection into male APP/PS1 mice. The head skin of anesthetized animals (100 mg/kg ketamine/10 mg/kg xylazine) was incised with a scalpel and the skull exposed. The skull surface and the bregma served as the stereotaxic zero points. The cranium was perforated at two sites (AP 1 mm, ML 2 mm, DV 2 mm), once in each hemisphere, and using a Hamilton precision syringe (26G needle), 4 μ L of BM-MS-C-derived EV suspension (5.6 μ g/ μ L, corresponding to 22.4 μ g of MS-C-EVs obtained from $\sim 3 \times 10^6$ cells corresponding $\sim 1 \times 10^9$ particles) or 4 μ L of PBS was injected into the neocortex as previously described [31]. Twenty-five days after treatment, animals were sacrificed according to the approved animal protocol guidelines and intracardially perfused with 4% (*w/v*) PFA.

2.12. Immuno-Histochemical and Immunofluorescence Staining

Brains of perfused animals, after further ON fixation in 4% (*w/v*) PFA, were washed with PBS and freshly cut by vibratome (Leica VT1000-S vibroslicer). 30 μ m thick para-sagittal sections were stored in anti-freezing solution (*v/v*: 3% glycerol, 3% Ethylene glycol, 40 mM phosphate buffer, pH 7.4) at -20°C , following cryopreservation in 7% (*w/v*) and 20% (*w/v*) sucrose solutions (in 0.1M Phosphate Buffer, pH: 7.4), until use. For immunohistochemical staining, free-floating slices were permeabilized in PBS solution (PBS, 3% (*v/v*) Methanol, 0.1% (*w/v*) Triton X-100) and treated with 3% (*v/v*) Hydrogen Peroxide. For antigen retrieval, slices were treated with 90% (*v/v*) formic acid in water. Slices were subsequently washed with 0.1% (*w/v*) Triton X-100 in PBS and incubated for 1 h at RT in blocking solution (10% (*v/v*) horse serum, 0.1% (*w/v*) Triton-X100 in PBS). All slices were stained O/N at 4°C with 6E10 antibody (β -amyloid, 1-16 Monoclonal Antibody, Covance®, BioLegend®, San Diego, CA, USA) in blocking solution. The immuno-detection was performed with an anti-mouse secondary antibody followed by MAC1 Mouse Probe and MAC1 Universal HRP-Polymer (Biocare Medical, Pacheco, CA, USA) and DAB (3'DiAminoBenzidine; Biocare Medical, Pacheco, CA, USA) revelation. Slices were mounted on glass slides with FluorSave™ Reagent (Calbiochem®, Merck KGaA, Darmstadt, Germany).

For immunofluorescence staining, brain sections were incubated for 10 min in 0.04% (*w/v*) ThT (Sigma-Aldrich®, Merck KGaA, Darmstadt, Germany) solution, then washed for 1 minute with 80% (*v/v*) methanol in water and stained O/N at 4°C with Iba1 (rabbit anti-mouse, FUJIFILM Wako Chemicals Europe GmbH, Neuss, Germany) and Smi31 and Smi32 monoclonal anti-mouse antibodies (BioLegend®, San Diego, CA, USA). After washing, the secondary antibodies (anti-rabbit secondary

antibody conjugated with Alexa 488 and anti-mouse secondary antibody conjugated with Alexa 633 fluorochromes) were incubated for 1h at RT in blocking solution. Slices were mounted on glass slides and mounted with FluorSave™ Reagent (Calbiochem®, Merck KGaA, Darmstadt, Germany).

2.13. Image Acquisitions and Analysis

Immuno-histochemically stained slices were acquired by Olympus DotSlide microscope with a 10× objective, connected to a computer equipped with OlyVIA® 2.9 viewer software (Olympus, Hamburg, Germany). Quantification of β -amyloid plaques on immuno-histochemically stained brain slices of APP/PS1 mice was performed using ImageJ software. Four parameters were evaluated to describe plaques: Area Mean (μm^2), Plaque Solidity (a.u.), i.e., β -amyloid intensity within immune-revealed plaques and calculated as $[\text{Area}]/[\text{Convex area}]$, and Plaque Density (n plaques/ μm^2 slice area). About 10 slices for each APP/PS1 animal injected with PBS or EVs were analyzed. Within each slice, two areas of interest were manually selected: the cortex and the hippocampus. Within these areas, the total number of plaques was counted. An arbitrary threshold has been fixed and maintained for the whole analysis of slices of the same experimental group. Collected data were averaged and analyzed with Graph Pad Prism6® software. All values were expressed as the mean \pm SEM. Graphs represent the average of plaques area (Area, μm^2), solidity (a.u.) and of plaque density (n/ μm^2) for all analyzed animals (5–6 animals per group).

Confocal images were acquired using a Leica TCS SP5 confocal microscope equipped with a HCX PL APO lambda blue 63x/1.4 OIL objective. ThT signal was revealed by exciting with 405 nm, Iba1 with 488 nm and Smi31-32 with 633 nm lasers. Voxel size was established using Nyquist criteria. Confocal images were analyzed by IMARIS v7.4.2 software (Oxford Instruments, Abingdon-on-Thames, UK). Briefly, 3D image reconstruction of Z-planes of ThT and Smi31-32 signals was performed and spots of Smi31-32 signal were quantified using the IMARIS software function “Spot” with the following parameters: detected spot number/estimated diameter = 0.962 μm ; Background Subtraction Quality between 40 and 200. Spot detection was monitored and corrected manually, setting 90 μm as the minimum spot to be considered as a bona fide Smi31-32 signal. The ThT signal volume was quantified by the “Surface” function, setting Smooth as 0.192, Absolute Intensity, Threshold between 140 and 75. Smi31-32 ROI volume analysis was drawn according to the Iba1 (to detect microglia cells around the plaques) fluorescence around the ThT signal. Smi31-32 spot density was estimated with the following formula: Ratio of [Smi31-32 spots / (Iba1 ROI volume minus ThT volume)].

2.14. Statistical Analysis

Average values obtained from plaques quantifications of EVs treated versus non-treated APP/PS1 animals were compared using the unpaired non-parametric Mann-Whitney test, with Prism6® software. In general, the one tail hypothesis was chosen (reduction of all parameters tested) with Welch’s correction. All data are expressed as means \pm SEM. *p*-Values lower than 0.05 were considered statistically significant. In the graphs, one * corresponds to $p < 0.05$, two ** corresponds to $p < 0.01$.

3. Results

EVs derived from mouse BM-MSCs were investigated for a possible therapeutic effect in APP/PS1 mice. To this end, MSCs were prepared from adult bone marrow and characterized for typical markers, following criteria suggested by the International Society for Cellular Therapy [32], including evaluating their ability to differentiate towards osteogenic and adipogenic lineages.

The flow cytometry characterization shows that BM-MSCs express stemness markers, such as SCA1, along with CD73 and CD105, specific markers for the mesenchymal origin of cells. BM-MSCs were also positive for markers expected to be present on the surface of EVs, such as CD44, CD29, CD49 and CD9 [11]. Lineage Hematopoietic Markers (LIN), CD117 and CD31, were not detected, excluding the contamination of cell cultures by hematopoietic cells or their precursors (Figure 1a). Reliability of BM-MSC preparations was confirmed by the repeatability of the staining for the different

markers in 6 independent preparations (Figure 1b). Differentiation of BM-MSCs towards osteogenic (Alizarin Red staining) and adipogenic (Oil-red O staining) lineages further confirms the identity of our cell cultures (Figure 1c) [33]. Passages from 9 to 14 have been used since mouse BM-MSCs, differently from other species (i.e., human and rat), maintain a high contamination of hematopoietic cells for a longer time in culture [34]. Possible senescence was evaluated by comparing SA- β -Gal activity in BM-MSC at P6 and P14, representative of early and late passages of the cultures used in our experiments (Figure 1d). The percentage of β -Gal positive cells was similar in the two passages (Figure 1e). Furthermore, two other markers of senescence, the phosphorylation of Ser-139 of histone H2A.X (Figure 1f), indicative of oxidative stress, and the protein level of the cell cycle regulator p16^{INK4A} (Figure 1g), were investigated by Western blot. Lysates from BM-MSCs at passages ranging from P5 to P17 were compared with cells treated with H₂O₂ to induce oxidative stress (positive control), showing that no significant difference in senescence processes activation was detected in the passages of BM-MSCs used for our experiments compared to earlier ones.

EVs secreted by BM-MSCs into the cell culture medium were purified by ultracentrifugation following a widely used protocol yielding a pool of microvesicles and exosomes [26]. Nanoparticle tracking analysis (NTA) allowed the determination of the size and the concentration of isolated EVs (Figure 2a). The results of 5 independent preparations show the three most represented vesicle populations, associated with three peak sizes (two >100 nm, one ~400 nm), indicating the successful isolation of a pool of EVs, including both exosomes and microvesicles. The mean concentration of the major vesicle peak (130 nm) was 1.48×10^6 particles/mL (± 88027 SEM) (Figure 2a, left panel). The total concentration measured as the area under the curve (AUC) of the mean values of all preparations tested resulted in 1.4×10^9 particles/mL (Figure 2a, right panel). The analysis of EV-depleted supernatants showed a mean particle concentration of 3.18×10^5 particles/mL (± 26123 SEM) and a major peak at 94.50 nm (Figure 2a, green line), indicating an efficient yield of the procedure for EVs larger than 100 nm. The analysis by cryo-electron microscopy performed on EV preparations just after centrifugation showed the presence of vesicles of different sizes compatible with exosomes and microvesicles, surrounded by a lipid bilayer and with a variably dense content, confirming furthermore the integrity and the identity of the vesicles (Figure 2b). A first characterization of EVs' specific surface markers was performed by flow cytometry. In particular, CD9 and CD49, even though the latter was expressed at a lower extent, were detected on BM-MSC-EVs (Figure 2c). The gating strategy used beads allowing selection of events below 1.34 μ m. Using Phalloidin to label cellular debris, we further gated against contaminating events that could fall within this size. To further ensure that the analyzed events were within the size range of EVs, we also performed a calibration with Megamix beads (Biotec) ranging from 0.1 μ m to 0.9 μ m using the same acquisition parameters used for EV analysis, showing that most of the gated events positive for CD9 and CD49 were in the range between 0.1 and 0.9 μ m (Supplementary Figure S1). To support the vesicular origin of CD9 and CD49 events, antibody-stained EVs, following first flow cytometry acquisition, were treated with 0.05% (*w/v*) Triton-X100 for 30 min and re-acquired afterwards for the same time, showing a massive reduction of (CD9⁺/CD49⁺) events thereafter (Figure 2d). This supports the vesicular nature of these events [35]. In addition, well-established EV markers, such as Alix, CD9, CD63, HSP70, AGO2 and TSG101, were identified by Western blots in P14 EV lysates obtained from approximately 1×10^9 particles and compared to BM-MSC lysates (Figure 2e).

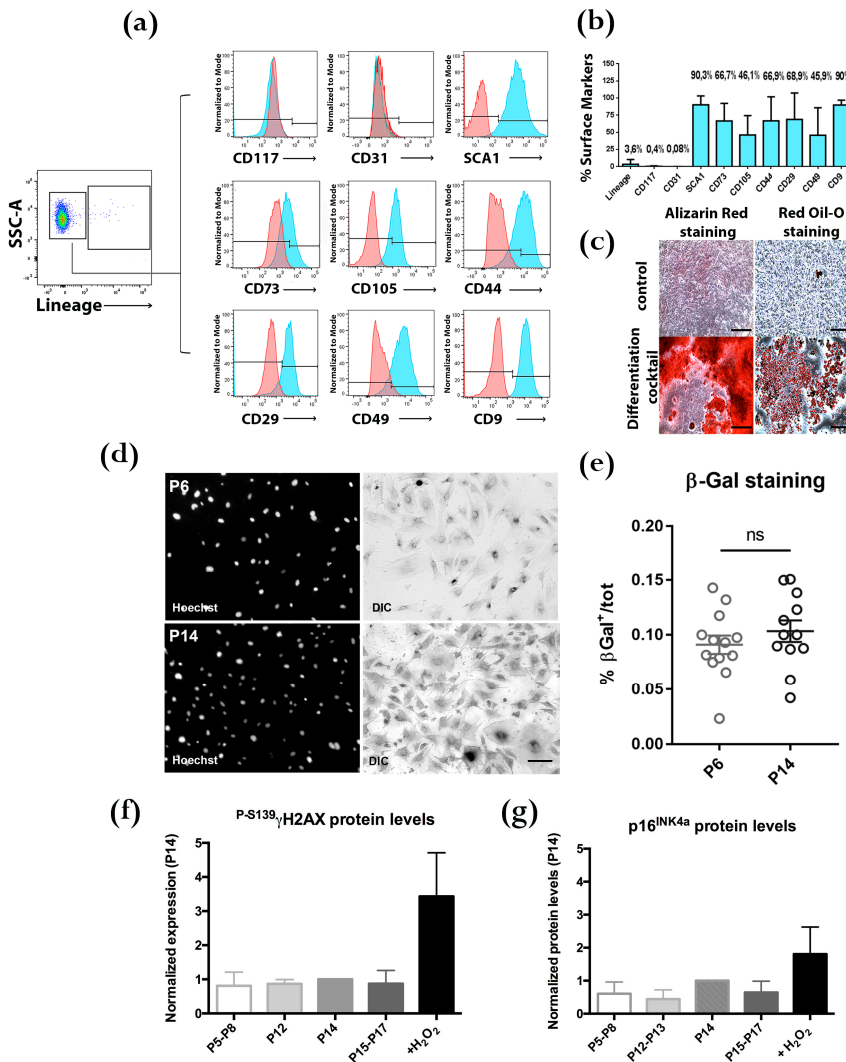


Figure 1. Characterization of murine Bone Marrow Mesenchymal Stem Cells (BM-MSCs). (a) Representative panels of flow cytometry analysis showing surface markers of BM-MSCs between passages 6 and 14. Lineage Hematopoietic Markers (LINEAGE) negative cells ($96.4 \pm 8.4\%$) are also negative for CD117 and CD31, excluding contamination by hematopoietic cells; they are strongly positive for SCA1 (stemness marker) for CD73 and CD105 (mesenchymal markers) and for CD44, CD29, CD49 and CD9 (markers also found on EVs). (b) Percentages of surface marker positive populations (mean ± SEM; flow cytometry experiments of 6 independent BM-MSC cultures). (c) Representative images showing differentiation of BM-MSCs into OSTEOCYTES (Alizarin Red staining) and ADIPOCYTES (Oil-red O staining) lineages. Controls: untreated BM-MSC cultures (upper row). Scale bars: 400 μm. (d) β-Gal assay was performed on BM-MSCs at P6 and P14 to test senescence of cells maintained in culture. Cells positive for X-gal were quantified and compared to the total population; no significant differences between the passages were detected ($p = 0.3462$; statistical analysis was performed by ANOVA test). Scale bar: 100 μm. (e) Representative images for X-Gal of BM-MSCs at P6 and P14. (f,g) Histone H2A.X phospho S139 (f) and p16^{INK4A} (g) Western blot analysis, showing that senescence processes are not differently activated during cell passages in vitro.

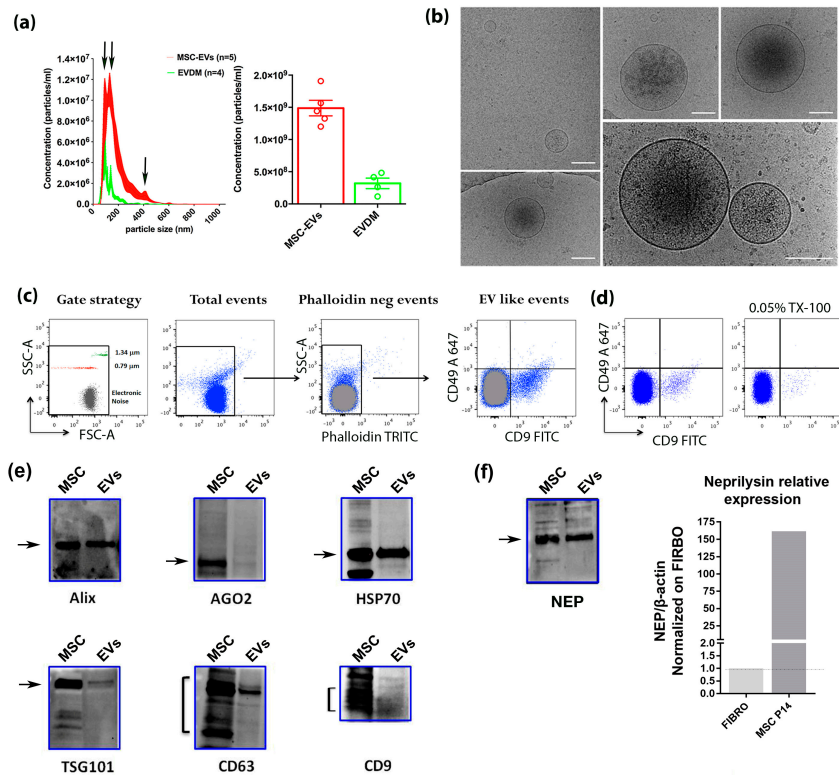


Figure 2. Characterization of BM-MSC-derived EVs. (a) Left panel: Nanoparticle Tracking Analysis (NanoSight NS300) of BM-MSC-EVs isolated by ultracentrifugation (red) compared to EV-depleted medium (EVDM) (green). Particle size distribution (left panel) shows that three populations corresponding to ~100 nm, ~150 nm, ~400 nm are the most represented on the red plot (arrows), indicating isolation of different pools of vesicles (> 100 nm exosomes and microvesicles). The green plot shows that fewer and smaller-sized vesicles (average size = 94.50 nm) remain in the medium after ultracentrifugation. Right panel: total particle concentration of isolated BM-MSC-EVs (red histogram) compared to the EVDM (green histogram). All data represent means and standard error of the mean (SEM) of 5 (BM-MSC-EV) and 4 (EVDM) independent preparations. (b) Visualization of purified BM-MSC-EVs by cryo-EM: a heterogeneous population of EVs surrounded by a lipid bilayer of sizes compatible with exosomes and microvesicles with an electron-dense core was observed. Note the integrity of membrane vesicles. Scale bar = 150 nm. (c) Representative panels showing flow cytometry analysis of EVs from BM-MSCs. Arrows between panels indicate the consecutive gating strategies for the analysis. The “gate strategy” panel shows the forward (FSC-A) and side (SSC-A) scatter density profile of 0.79 μm (red dots) and 1.34 μm (green dots) dimensional beads, which were used to include all events (< 1.34 μm) for specific marker analysis. Smaller events defined as “Electronic Noise”, falling below the limit of resolution of the instrument were also included in the “Total events” gate. BM-MSC-EVs appear in the “Total events” panel. Events falling within the “Electronic Noise”, represented in gray, were subtracted from all analysis gates. Bona fide EVs were Phalloidin negative (“Phalloidin neg events”) and were shown to be mainly CD9-FITC+, CD49-A647+ or double positive (“EV-like events”). (d) Adding 0.05% (*w/v*) TX-100 for 30 min after acquisition (left panel) resulted in a major decrease in the CD49+/CD9+ stained population (right panel). (e) EVs and BM-MSC lysates (5 μg) were analyzed by immunoblotting with antibodies against EV proteins Alix, AGO2, HSP70, TSG101, CD63 and CD9. (f) Left panel: Immunoblotting showing the presence of Nephrilysin on EVs and in BM-MSC lysates (5 μg). Right panel: Real-time PCR analysis of Nep relative expression in P14 BM-MSC RNA normalized to β -actin and to the expression in murine primary fibroblasts.

Since previous work reported the presence of Neprilysin (NEP), an enzyme able to exert A β -degrading activity, on human ADSC and their exosomes, we also tested NEP expression in BM-MSCs and their derived EVs. Interestingly, NEP could be detected in the EVs' lysates and its mRNA was also expressed in P16 BM-MSCs, at a level more than 100 times that of murine fibroblasts (Figure 2f).

The earliest signs of cognitive impairments in APP/PS1 mice have been reported in six-month-old animals [36]. Conversely, amyloid plaque deposition has been shown to start at approximately six weeks of age in the neocortex and at about three to four months of age in the hippocampus [37,38]. To assess the effects of BM-MSC-EVs in the APP/PS1 AD mice at early stages of the disease, before the behavioral manifestations become apparent, we performed intraparenchymal injections of EVs in the cortex of mice at 3 and 5 months of age and evaluated, 25 days later, EV effects on two of the typical early signs of the disease, A β deposition and appearance of dystrophic neurites (Figures 3 and 4). No gross AD-unrelated behavioral alteration was observed in mice treated with EVs compared to PBS-treated ones. Brain sections from hippocampus and cortex of EV-treated APP/PS1 compared to mice injected with vehicle (PBS, referred to as the controls) were immunohistochemically stained with 6E10 antibody, reacting with the N-terminal domain of human A β ₁₋₄₂ peptide. The injection of BM-MSC-EVs in 5-month-old mice (Figure 3) resulted 1 month later (i.e., at 6 months) in a reduction of A β plaque area in both hippocampus and cerebral cortex, depicted by two representative images with their close-up views on plaques (Figure 3a). Moreover, plaque solidity, a parameter that represents A β loading of plaques, was strongly reduced, in particular within the neocortex (Figure 3b), the region in which the injection has been performed. In addition, the plaque density (number of plaques/ μm^2) was significantly affected by EV treatment in the hippocampal region, but not in the cortex (Figure 3b).

We then performed the same analysis in 4-month-old mice (Figure 4) displaying significantly smaller and a lower number of plaques relative to the 6-month-old mice (compare the area and density in the control animals in Figures 3b and 4b). The injection of BM-MSC-EVs was able to decrease the average plaque area, mostly in the hippocampus, and reduced the density (number of plaques/ μm^2) both in the hippocampus and in the cortex when compared to the age-matched controls (Figure 4b). On the basis of these results, we can hypothesize that EVs may operate not only by promoting the disaggregation of A β pre-existing deposits (Figure 3), but also by preventing or slowing down the formation of new plaques (Figure 4).

It is known that, in neurons, microtubule disruption and microtubule-based transport impairment, as well as neurofilament disorganization, lead to dystrophic neurite formation [39,40]. Along with dysfunction associated with axonal swelling and impaired transport, the axonal dystrophy is likely to exacerbate downstream neurodegeneration, leading to cognitive deficits. In an attempt to investigate whether the reduction of A β plaques resulted in amelioration of neurite morphology, we analyzed dystrophic neurites in the cortex and hippocampus of AD mice. Immunostaining of brain sections 25 days following injection of EVs at both ages was performed with Smi31-32 antibodies, which recognize neurofilament H and M [41] (Figure 5). ThT-positive plaques were surrounded by dystrophic neurites (Smi31-32-positive) at both ages analyzed, with the results being significantly higher at 6 months than at 4 months (Figure 5a). Notably, the injection of BM-MSC-EVs reduced the number of Smi31-32 positive dots in the area of the plaques. Although the decrease was evident at both ages, the results were only statistically significant at 6 months (Figure 5b,c).

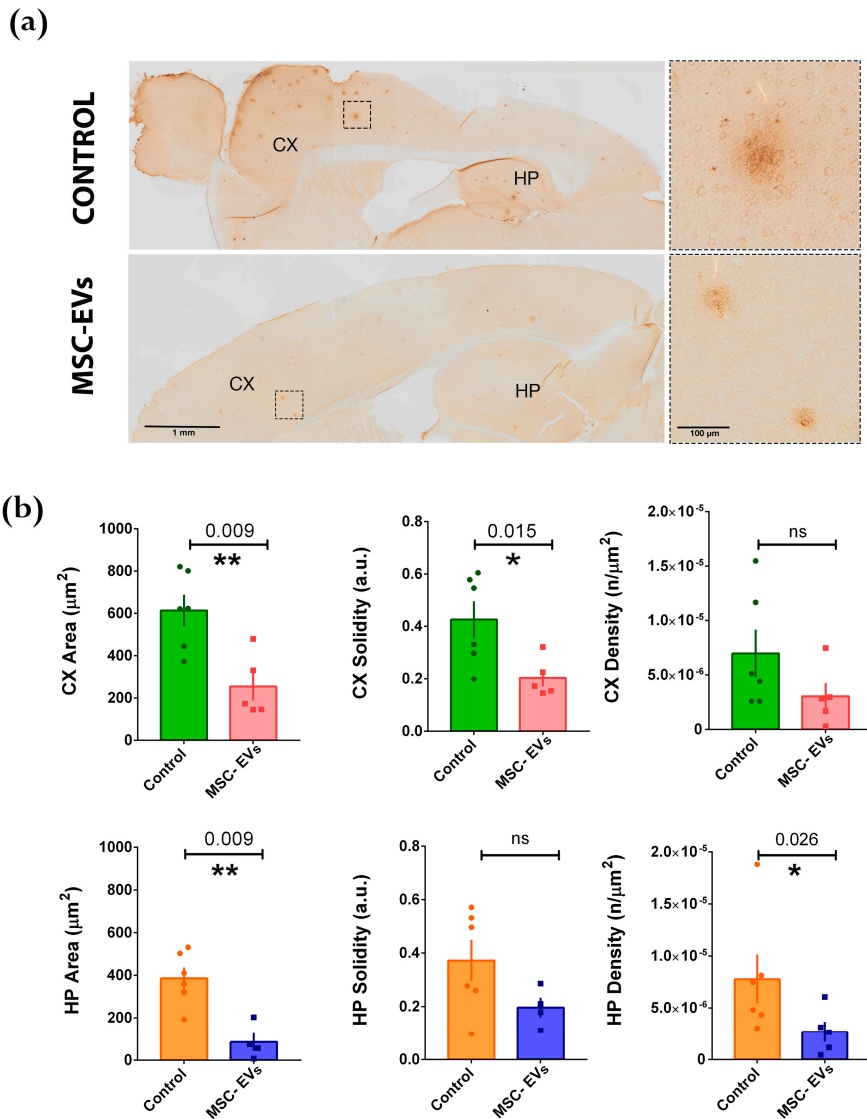
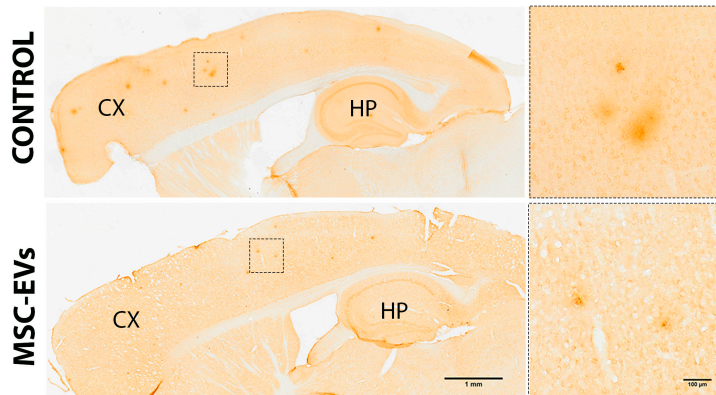


Figure 3. Intracerebral injection of BM-MSC-EVs (MSC-EVs) into 5-month-old APP/PS1 mice reduces amyloid deposition after ~1 month. **(a)** Immunohistochemical staining (DAB) of Aβ₁₋₄₂ plaques in brains of APP/PS1 mice treated with vehicle (CONTROL, top) or MSC-EVs (bottom). Scale bar: 1 mm. Panels on the right show higher magnification of representative plaques, contoured in the inset. Scale bar: 100 μm. Cortex (CX) and Hippocampus (HP) are indicated. **(b)** Quantification of Aβ₁₋₄₂ positive plaques in the Cortex (CX; upper graphs: green and red histograms) and in the Hippocampus (HP; lower graphs: orange and blue histograms). Each dot represents an animal for which 10 slices have been scored. Statistical analysis was performed by non-parametric Mann-Whitney test (* $p < 0.05$; ** $p < 0.01$).

(a)



(b)

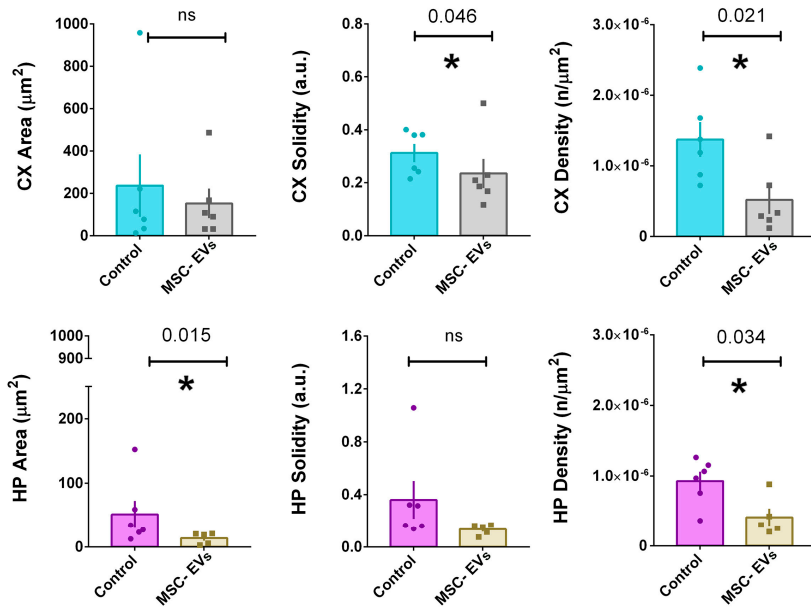


Figure 4. Intracerebral injection of BM-MSC-EVs (MSC-EVs) into 3-month-old APP/PS1 mice reduces amyloid deposition after ~1 month. (a) Immunohistochemical staining (DAB) of A β 1-42 plaques in brains of APP/PS1 mice treated with vehicle (CONTROL, top) or MSC-EVs (bottom). Scale bar: 1 mm. Panels on the right show higher magnification of representative plaques, contoured in the inset. Scale bar: 100 μm . Cortex (CX) and Hippocampus (HP) are indicated. (b) Quantification of A β 1-42 positive plaques in the Cortex (CX; upper graphs: light blue and grey histograms) and in the hippocampus (HP; lower graphs: violet and brown histograms). Each dot represents an animal for which 10 slices have been scored. Statistical analysis was performed by non-parametric Mann-Whitney test (* $p < 0.05$; ** $p < 0.01$).

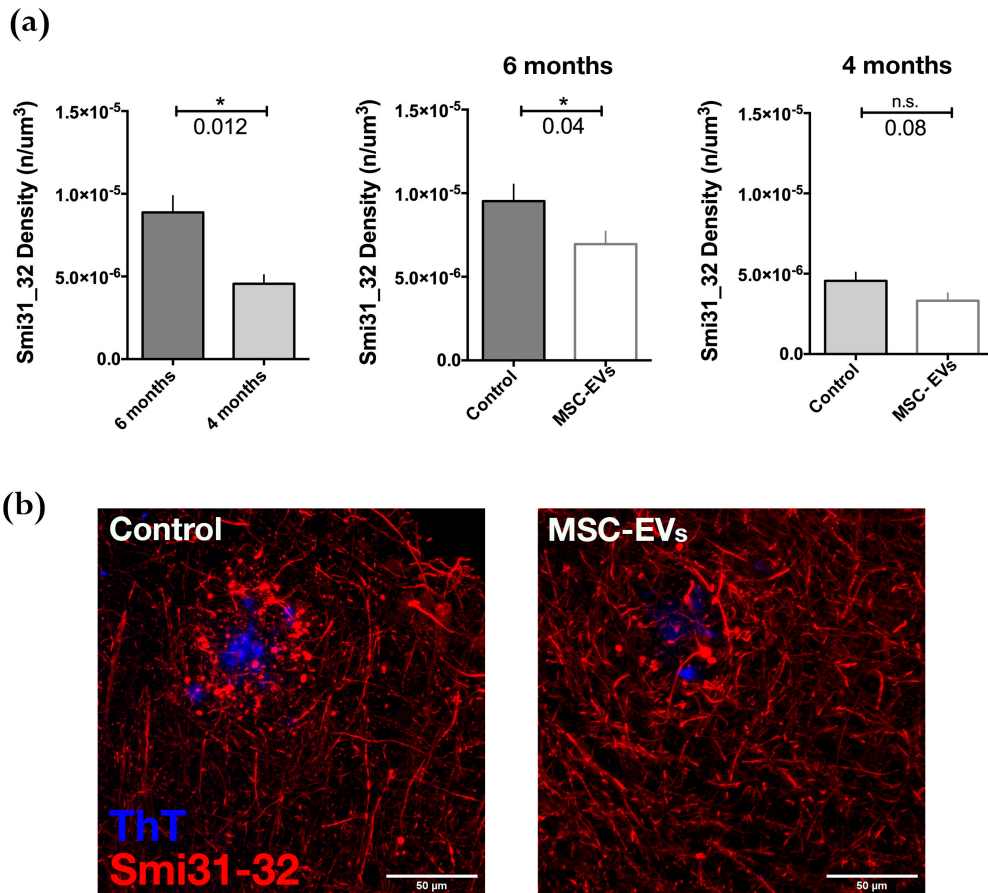


Figure 5. Dysmorphic Neurites around A β plaques in APP/PS1 brain cortex slices are reduced following MSC-EVs treatment. (a) Left panel: Quantification of Smi31-32 spots (density), representing dystrophic neurites, in the 3D reconstructed ROIs acquired around plaques in brain slices of 6- (dark grey histogram) and 4-month-old (light grey histogram) control APP/PS1 mice. Smi31-32 signal density in 6-month-old APP/PS1 brains is significantly reduced (central panel, white histogram), but not at 4 months (right panel). Statistical analysis was performed by non-parametric Mann-Whitney test ($* p < 0.05$). (b) Representative max projections of confocal images of brain slices of 6-month-old APP/PS1 mice 25 days following treatment with EVs (MSC-EVs) or with PBS (Control). Immunostaining with ThT (blue, A β plaques) and Smi31-32 (red, dystrophic neurites) are shown. Scale bars: 50 μ m.

4. Discussion

MSC-derived EVs are increasingly attracting the attention of the scientific community as possible therapeutic tools. By promoting neurogenesis, angiogenesis and remodeling of nervous processes and being endowed with immunomodulatory actions [42–45], MSC-EVs might exert protective roles in the brain.

In the last few years, the possibility of exploiting the therapeutic potential of EVs has been evaluated in AD preclinical models, where encouraging outcomes have been achieved [11,46,47].

The studies reported so far, however, have explored the therapeutic potential of MSC-EVs at a stage in which the pathology is already developed and the cognitive deficits are overt, i.e., a condition that is difficult to revert. In particular, two different labs have investigated the effects of EVs on AD mice when the pathology is clearly manifested: Cui and collaborators have shown that 7-month-old APP/PS1

mice, treated twice a week for 4 months with exosomes extracted from hypoxic MSCs, improved cognitive impairments compared to untreated AD mice [47]; Wang and coworkers conclude from their study that MSC-derived EV treatment of AD mice suppress iNOS expression and ameliorates cognitive behavior by partially rescuing the A β -induced deficits in hippocampal synaptic plasticity [48]. We therefore wondered whether carrying out the intervention earlier could lead to positive outcomes, possibly slowing down AD progression. Even if it is still probably too early to answer this question, our results could represent a perspective in this direction. In the present study, we assessed the effects of BM-MS-C-EVs in AD mice at a young age when the plaques are just beginning to appear and the overt cognitive deficits are not yet manifested.

Following extensive characterization of EVs obtained from murine BM-MS-Cs, we showed that they are a mixed population mostly composed of exosomes and microvesicles, endowed with well-established markers and preserving their integrity following purification, as shown by Cryo-EM. To investigate the actions induced by BM-MS-C-derived EV injection, we compared APP/PS1 mice of 3 and 5 months of age bilaterally injected into the cortex with vehicle (PBS, controls) or MS-C-EVs. Our data suggest that EVs may operate not only by promoting the disaggregation of A β pre-existing deposits (5 months => 6 months), but also preventing or slowing down the formation of new ones (3 months => 4 months). This in turn could account for neuroprotective effects, as suggested by the reduction of dystrophic neurites in treated mice.

What are the mechanisms involved in MS-C-EV effects? We can speculate that on the one hand, EVs might act directly on the plaques, inducing their disaggregation through an interaction between EV lipid membranes and A β plaques. EVs have been shown to also act as amyloid scavengers based on A β ₁₋₄₂ ability to bind to glycosphingolipids that are extremely abundant in exosomes [20]. This would lead to phagocytosis of A β -along with EVs binding to it- by phagocytic cells (i.e., microglial cells), in line with the hypothesis that MS-C-EVs could promote A β clearance by a direct binding. This possibility would be consistent with the decrease in the plaque area, as well as in the amount of A β within plaques (solidity) observed in treated mice.

On the other hand, MS-C-EVs have been described to carry the enzymatically active NEP, a type II membrane-associated metalloendopeptidase involved in the proteolysis of A β [19,49]. When added to N2a line cells, AD-MS-C exosomes reduced both extracellular and intracellular A β ₁₋₄₂ deposits [19]. Along this line, the presence of NEP in the lysates of both mouse BM-MS-C and their derived EVs, together with the detection of mRNA expression in the cells (surprisingly high when compared to fibroblasts) suggests that this could be a possible mechanism explaining EV action on A β -plaques in 3- and 5-month-old APP/PS1 mice. In addition, EVs might also act on microglia cells. In fact, in AD brains microglia clusters around A β ₁₋₄₂ deposit and acquire a polarized phenotype with hypertrophic processes extending towards plaques [50–52]. Microglia are thought to regulate the degree of amyloid deposition by phagocytosis of amyloid aggregates with a potentially protective impact on AD progression [53,54]. Therefore, EVs could act by enhancing microglia functionality and phagocytosis/degradation ability [51].

Furthermore, MS-C-EVs have been reported to induce antioxidant effects. De Godoy and colleagues proposed that MS-C-EVs, thanks to their content including antioxidant enzymes and anti-inflammatory and/or trophic molecules, exert a neuroprotective action. The authors demonstrated that EVs secreted by MS-C contain and carry catalase that endows EVs of reactive oxygen species (ROS) scavenging activity [55].

It is likely that MS-C-EVs operate through pleiotropic mechanisms, involving a combination of the above processes, including the inhibition of inflammatory responses, regulation of the immune system, as well as by carrying biologically active molecules, which in turn may act either directly on amyloid plaques or on microglial cells, which are the main responsible for A β phagocytosis in the brain.

To clarify EV mechanisms of action, a deeper characterization of the content of EVs and of the different types that participate in tissue repair [56,57] is mandatory. To this end, also exploring novel purification protocols able to recover also the smallest fractions of EVs is urgently needed [58].

It has been reported that EVs contain, in addition to the above-mentioned lipids, proteins and nucleic acids (miRNA, mRNA). Among these, miRNAs inside the lumen could be horizontally transferred to target cells, contributing to the gene expression regulation. For instance, miR-21 overexpression through engineered EVs has been shown not only to decrease plaque deposition but also to down-regulate the levels of TNF- α and IL-1 β therefore inducing anti-inflammatory effects [47].

In this study, we focused our attention on EV actions on A β plaques and dystrophic neurites, which represent one of the typical hallmarks of AD. We are aware that the correlation between plaque load and cognitive scores in humans has recently been questioned [59,60], prompting the scientific community to look for additional factors, beyond the “Amyloid Hypothesis”, as the etiological mechanism of AD. However, our results represent a clear indication that plaque formation could be delayed by BM-MS-C-EVs and that this may significantly reduce the extent of dystrophic neurites. Dystrophic neurites forming around plaques have been recently found to evolve toward progressively more degenerated forms [61], and to promote the accumulation of the amyloid precursor protein (APP) cleaving enzyme (BACE1), which is required for A β generation [39]. Given all these processes lead to exacerbation of amyloid pathology in AD, the MSC-EVs-mediated reduction of dystrophic neurite formation may represent an important cue for slowing disease progression.

Moreover, since MSCs have a high immunoregulatory potential and their derived EVs maintain such ability, next studies will be focused on the analysis of the anti-inflammatory action and how it could cooperate with A β degrading action in AD therapy. Indeed, MSC-EVs can induce anti-inflammatory effects through the regulation of cytokine release [47,55,62] or iNOS inhibition or by preventing A β oligomer toxicity [48], given that iNOS is a common target of many inflammatory pathways and an important endpoint for the therapeutic effects of EVs.

Finally, we believe that EVs and their abilities inherited from BM-MS-Cs could represent an applicable, safe and cost-effective approach in cell-free regenerative medicine to improve therapy for preventing the earliest stages of the disease to proceed towards AD. We can venture the hypothesis that our data could support the use of EVs in patients when the first signs of Mild Cognitive Impairment begin to appear. Nonetheless, before translating their use into the clinic, a better understanding of EV actions and their biological functions need to be undertaken, together with the choice of the best route of administration. In this respect, intranasal administration, being less invasive, easy and cheap could represent a valid option.

In conclusion, our results highlight that intracortical delivery of bona fide murine BM-MS-C-EVs to APP/PS1 mice at 3 months, before overt clinical signs, is able to prevent A β plaque formation and in 5-month-old mice can reduce dystrophic neurons occurrence. As far as we know, this study represents the first evidence of a possible preventive effect of BM-MS-C-EVs in an animal model of AD. This result can be relevant if we consider that until now clinical trials and treatments adopted for AD therapy did not produce the desired results, probably because started too late.

Supplementary Materials: The following are available online at <http://www.mdpi.com/2073-4409/8/9/1059/s1>, Figure S1: EV flow cytometry analysis based on Megamix and CS&T beads.

Author Contributions: Conceptualization, C.A.E., S.C., M.M. and M.L.M.; methodology, C.A.E., M.R., M.T., G.D., A.A., P.S. and So.M., software; validation, A.A., M.L.M., M.M. and S.C.; formal analysis C.A.E., M.R., M.T., G.D. and M.L.M.; investigation C.A.E., M.R., M.T., Sa.M., F.C., A.A., G.D.; resources; data curation C.A.E., M.L.M. and S.C.; writing - original draft preparation S.C., M.L.M. and M.M.; writing - reviewing and editing C.A.E., S.C., M.M. and M.L.M.; visualization C.A.E., M.R., G.D., M.T., A.A., P.S., M.L.M. and S.C.; supervision M.M., A.A., M.L.M. and S.C.; project administration M.M., M.L.M. and S.C.; funding acquisition M.M., M.L.M. and S.C.

Funding: This work was supported by grants from Regione Lombardia “NeOn”, POR-FESR 2014-2020, ID 239047, CUP E47F17000000009 and “AMANDA” CUP_B42F16000440005 CNR Research Project on Ageing, Cariplo 2015-0594, and Fondazione Pisa 107/16.

Acknowledgments: We acknowledge Silvia Penati (Institute of Neuroscience-CNR, Milan (IT) and Humanitas Clinical and Research Institute, Rozzano, Milan (IT), Claudio Comunian (Bio-Rad Italia) and Agnese Tognati (Bio-Rad Italia) for their technical support with Stain Free™ protein analysis; the Imaging facility of Humanitas Clinical and Research Institute, in particular Diego Morone (present address: Institute for Research in Biomedicine,

Bellinzona (CH) for personal and technical support in image acquisition and analysis; the flow-cytometry facility of Humanitas Clinical and Research Institute.

Conflicts of Interest: The authors declare no conflict of interest. The funders had no role in the design of the study; in the collection, analyses, or interpretation of data; in the writing of the manuscript, or in the decision to publish the results.

Abbreviations

AD	Alzheimer's disease
EVs	extracellular vesicles
MVs	microvesicles
A β	amyloid beta
MSCs	mesenchymal stem cells
BM-MSCs	bone marrow mesenchymal stem cells
ADSC	adipose tissue-derived MSCs
CNS	central nervous system
PFA	paraformaldehyde
PBS	phosphate buffered saline
NTA	nanoparticle tracking analysis
DAB	DiaminoBenzadine
APP	amyloid precursor protein

References

1. Association, A. Alzheimer's Association Report 2018 Alzheimer's disease facts and figures. *Alzheimer's Dement.* **2018**, *14*, 367–429. [[CrossRef](#)]
2. Wang, S.; Colonna, M. Microglia in Alzheimer's disease: A target for immunotherapy. *J. Leukoc. Biol.* **2019**. [[CrossRef](#)]
3. Martins, Y.A.; Tsuchida, C.J.; Antoniassi, P.; Demarchi, I.G. Efficacy and Safety of the Immunization with DNA for Alzheimer's Disease in Animal Models: A Systematic Review from Literature. *J. Alzheimers Dis. Rep.* **2017**, *1*, 195–217. [[CrossRef](#)]
4. Zanni, R.; Garcia-Domenech, R.; Galvez-Llompant, M.; Galvez, J. Alzheimer: A Decade of Drug Design. Why Molecular Topology can be an Extra Edge? *Curr. Neuropharmacol.* **2018**, *16*, 849–864. [[CrossRef](#)]
5. Train the Brain, C. Randomized trial on the effects of a combined physical/cognitive training in aged MCI subjects: The Train the Brain study. *Sci. Rep.* **2017**, *7*, 39471. [[CrossRef](#)]
6. Ge, M.; Zhang, Y.; Hao, Q.; Zhao, Y.; Dong, B. Effects of mesenchymal stem cells transplantation on cognitive deficits in animal models of Alzheimer's disease: A systematic review and meta-analysis. *Brain Behav.* **2018**, *8*, e00982. [[CrossRef](#)]
7. Izadpanah, M.; Seddigh, A.; Ebrahimi Barough, S.; Fazeli, S.A.S.; Ai, J. Potential of Extracellular Vesicles in Neurodegenerative Diseases: Diagnostic and Therapeutic Indications. *J. Mol. Neurosci.* **2018**, *66*, 172–179. [[CrossRef](#)]
8. Lee, H.J.; Lee, J.K.; Lee, H.; Shin, J.W.; Carter, J.E.; Sakamoto, T.; Jin, H.K.; Bae, J.S. The therapeutic potential of human umbilical cord blood-derived mesenchymal stem cells in Alzheimer's disease. *Neurosci. Lett.* **2010**, *481*, 30–35. [[CrossRef](#)]
9. da Silva Meirelles, L.; Chagastelles, P.C.; Nardi, N.B. Mesenchymal stem cells reside in virtually all post-natal organs and tissues. *J. Cell Sci.* **2006**, *119*, 2204–2213. [[CrossRef](#)]
10. Wei, Y.; Xie, Z.; Bi, J.; Zhu, Z. Anti-inflammatory effects of bone marrow mesenchymal stem cells on mice with Alzheimer's disease. *Exp. Med.* **2018**, *16*, 5015–5020. [[CrossRef](#)]
11. Elia, C.A.; Losurdo, M.; Malosio, M.L.; Coco, S. Extracellular Vesicles from Mesenchymal Stem Cells Exert Pleiotropic Effects on Amyloid-beta, Inflammation, and Regeneration: A Spark of Hope for Alzheimer's Disease from Tiny Structures? *Bioessays* **2019**, *41*, e1800199. [[CrossRef](#)] [[PubMed](#)]
12. Kim, S.; Chang, K.A.; Kim, J.; Park, H.G.; Ra, J.C.; Kim, H.S.; Suh, Y.H. The preventive and therapeutic effects of intravenous human adipose-derived stem cells in Alzheimer's disease mice. *PLoS ONE* **2012**, *7*, e45757. [[CrossRef](#)] [[PubMed](#)]

13. Lee, J.K.; Jin, H.K.; Endo, S.; Schuchman, E.H.; Carter, J.E.; Bae, J.S. Intracerebral transplantation of bone marrow-derived mesenchymal stem cells reduces amyloid-beta deposition and rescues memory deficits in Alzheimer's disease mice by modulation of immune responses. *Stem Cells* **2010**, *28*, 329–343. [[CrossRef](#)] [[PubMed](#)]
14. Liang, X.; Ding, Y.; Zhang, Y.; Tse, H.F.; Lian, Q. Paracrine mechanisms of mesenchymal stem cell-based therapy: Current status and perspectives. *Cell Transpl.* **2014**, *23*, 1045–1059. [[CrossRef](#)] [[PubMed](#)]
15. Musial-Wysocka, A.; Kot, M.; Majka, M. The Pros and Cons of Mesenchymal Stem Cell-Based Therapies. *Cell Transpl.* **2019**. [[CrossRef](#)] [[PubMed](#)]
16. Makela, T.; Takalo, R.; Arvola, O.; Haapanen, H.; Yannopoulos, F.; Blanco, R.; Ahvenjarvi, L.; Kiviluoma, K.; Kerkela, E.; Nystedt, J.; et al. Safety and biodistribution study of bone marrow-derived mesenchymal stromal cells and mononuclear cells and the impact of the administration route in an intact porcine model. *Cytotherapy* **2015**, *17*, 392–402. [[CrossRef](#)] [[PubMed](#)]
17. Cho, P.S.; Messina, D.J.; Hirsh, E.L.; Chi, N.; Goldman, S.N.; Lo, D.P.; Harris, I.R.; Popma, S.H.; Sachs, D.H.; Huang, C.A. Immunogenicity of umbilical cord tissue derived cells. *Blood* **2008**, *111*, 430–438. [[CrossRef](#)]
18. Karnoub, A.E.; Dash, A.B.; Vo, A.P.; Sullivan, A.; Brooks, M.W.; Bell, G.W.; Richardson, A.L.; Polyak, K.; Tubo, R.; Weinberg, R.A. Mesenchymal stem cells within tumour stroma promote breast cancer metastasis. *Nature* **2007**, *449*, 557–563. [[CrossRef](#)]
19. Katsuda, T.; Tsuchiya, R.; Kosaka, N.; Yoshioka, Y.; Takagaki, K.; Oki, K.; Takeshita, F.; Sakai, Y.; Kuroda, M.; Ochiya, T. Human adipose tissue-derived mesenchymal stem cells secrete functional neprilysin-bound exosomes. *Sci. Rep.* **2013**, *3*, 1197. [[CrossRef](#)]
20. Yuyama, K.; Sun, H.; Sakai, S.; Mitsutake, S.; Okada, M.; Tahara, H.; Furukawa, J.; Fujitani, N.; Shinohara, Y.; Igarashi, Y. Decreased amyloid-beta pathologies by intracerebral loading of glycosphingolipid-enriched exosomes in Alzheimer model mice. *J. Biol. Chem.* **2014**, *289*, 24488–24498. [[CrossRef](#)]
21. Cocucci, E.; Racchetti, G.; Meldolesi, J. Shedding microvesicles: Artefacts no more. *Trends Cell Biol.* **2009**, *19*, 43–51. [[CrossRef](#)] [[PubMed](#)]
22. Farinazzo, A.; Turano, E.; Marconi, S.; Bistaffa, E.; Bazzoli, E.; Bonetti, B. Murine adipose-derived mesenchymal stromal cell vesicles: In vitro clues for neuroprotective and neuroregenerative approaches. *Cytotherapy* **2015**, *17*, 571–578. [[CrossRef](#)]
23. Riazifar, M.; Pone, E.J.; Lotvall, J.; Zhao, W. Stem Cell Extracellular Vesicles: Extended Messages of Regeneration. *Annu. Rev. Pharm. Toxicol.* **2017**, *57*, 125–154. [[CrossRef](#)] [[PubMed](#)]
24. Mead, B.; Tomarev, S. Bone Marrow-Derived Mesenchymal Stem Cells-Derived Exosomes Promote Survival of Retinal Ganglion Cells Through miRNA-Dependent Mechanisms. *Stem Cells Transl. Med.* **2017**, *6*, 1273–1285. [[CrossRef](#)] [[PubMed](#)]
25. Jack, C.R., Jr.; Knopman, D.S.; Jagust, W.J.; Petersen, R.C.; Weiner, M.W.; Aisen, P.S.; Shaw, L.M.; Vemuri, P.; Wiste, H.J.; Weigand, S.D.; et al. Tracking pathophysiological processes in Alzheimer's disease: An updated hypothetical model of dynamic biomarkers. *Lancet Neurol.* **2013**, *12*, 207–216. [[CrossRef](#)]
26. Thery, C.; Amigorena, S.; Raposo, G.; Clayton, A. Isolation and characterization of exosomes from cell culture supernatants and biological fluids. *Curr. Protoc. Cell Biol.* **2006**. [[CrossRef](#)] [[PubMed](#)]
27. Gurtler, A.; Kunz, N.; Gomolka, M.; Hornhardt, S.; Friedl, A.A.; McDonald, K.; Kohn, J.E.; Posch, A. Stain-Free technology as a normalization tool in Western blot analysis. *Anal. Biochem.* **2013**, *433*, 105–111. [[CrossRef](#)]
28. Rittie, L.; Fisher, G.J. Isolation and culture of skin fibroblasts. *Methods Mol. Med.* **2005**, *117*, 83–98. [[CrossRef](#)] [[PubMed](#)]
29. Seluanov, A.; Vaidya, A.; Gorbunova, V. Establishing primary adult fibroblast cultures from rodents. *J. Vis. Exp.* **2010**. [[CrossRef](#)] [[PubMed](#)]
30. Jankowsky, J.L.; Zheng, H. Practical considerations for choosing a mouse model of Alzheimer's disease. *Mol. Neurodegener.* **2017**, *12*, 89. [[CrossRef](#)]
31. Mazzitelli, S.; Filipello, F.; Rasile, M.; Lauranzano, E.; Starvaggi-Cucuzza, C.; Tamborini, M.; Pozzi, D.; Barajon, I.; Giorgino, T.; Natalello, A.; et al. Amyloid-beta 1-24 C-terminal truncated fragment promotes amyloid-beta 1-42 aggregate formation in the healthy brain. *Acta Neuropathol. Commun.* **2016**, *4*, 110. [[CrossRef](#)] [[PubMed](#)]

32. Dominici, M.; Le Blanc, K.; Mueller, I.; Slaper-Cortenbach, I.; Marini, F.; Krause, D.; Deans, R.; Keating, A.; Prockop, D.; Horwitz, E. Minimal criteria for defining multipotent mesenchymal stromal cells. The International Society for Cellular Therapy position statement. *Cytotherapy* **2006**, *8*, 315–317. [[CrossRef](#)] [[PubMed](#)]
33. Kundrotas, G.; Gasperskaja, E.; Slapsyte, G.; Gudleviciene, Z.; Krasko, J.; Stumbryte, A.; Liudkeviciene, R. Identity, proliferation capacity, genomic stability and novel senescence markers of mesenchymal stem cells isolated from low volume of human bone marrow. *Oncotarget* **2016**, *7*, 10788–10802. [[CrossRef](#)] [[PubMed](#)]
34. Meirelles Lda, S.; Nardi, N.B. Murine marrow-derived mesenchymal stem cell: Isolation, in vitro expansion, and characterization. *Br. J. Haematol.* **2003**, *123*, 702–711. [[CrossRef](#)] [[PubMed](#)]
35. Mastoridis, S.; Bertolino, G.M.; Whitehouse, G.; Dazzi, F.; Sanchez-Fueyo, A.; Martinez-Llordella, M. Multiparametric Analysis of Circulating Exosomes and Other Small Extracellular Vesicles by Advanced Imaging Flow Cytometry. *Front. Immunol.* **2018**, *9*, 1583. [[CrossRef](#)]
36. Serneels, L.; Van Biervliet, J.; Craessaerts, K.; Dejaegere, T.; Horre, K.; Van Houtvin, T.; Esselmann, H.; Paul, S.; Schafer, M.K.; Berezovska, O.; et al. gamma-Secretase heterogeneity in the Aph1 subunit: Relevance for Alzheimer's disease. *Science* **2009**, *324*, 639–642. [[CrossRef](#)]
37. Howlett, D.R.; Bowler, K.; Soden, P.E.; Riddell, D.; Davis, J.B.; Richardson, J.C.; Burbidge, S.A.; Gonzalez, M.I.; Irving, E.A.; Lawman, A.; et al. Abeta deposition and related pathology in an APP x PS1 transgenic mouse model of Alzheimer's disease. *Histol. Histopathol.* **2008**, *23*, 67–76. [[CrossRef](#)]
38. Zhong, Z.; Yang, L.; Wu, X.; Huang, W.; Yan, J.; Liu, S.; Sun, X.; Liu, K.; Lin, H.; Kuang, S.; et al. Evidences for B6C3-Tg (APP^{swe}/PSEN1dE9) double-transgenic mice between 3 and 10 months as an age-related Alzheimer's disease model. *J. Mol. Neurosci.* **2014**, *53*, 370–376. [[CrossRef](#)]
39. Sadleir, K.R.; Kandalepas, P.C.; Buggia-Prevot, V.; Nicholson, D.A.; Thinakaran, G.; Vassar, R. Presynaptic dystrophic neurites surrounding amyloid plaques are sites of microtubule disruption, BACE1 elevation, and increased Abeta generation in Alzheimer's disease. *Acta Neuropathol.* **2016**, *132*, 235–256. [[CrossRef](#)]
40. Dickson, T.C.; King, C.E.; McCormack, G.H.; Vickers, J.C. Neurochemical diversity of dystrophic neurites in the early and late stages of Alzheimer's disease. *Exp. Neurol* **1999**, *156*, 100–110. [[CrossRef](#)]
41. Vickers, J.C.; Chin, D.; Edwards, A.M.; Sampson, V.; Harper, C.; Morrison, J. Dystrophic neurite formation associated with age-related beta amyloid deposition in the neocortex: Clues to the genesis of neurofibrillary pathology. *Exp. Neurol.* **1996**, *141*, 1–11. [[CrossRef](#)] [[PubMed](#)]
42. Koniusz, S.; Andrzejewska, A.; Muraca, M.; Srivastava, A.K.; Janowski, M.; Lukomska, B. Extracellular Vesicles in Physiology, Pathology, and Therapy of the Immune and Central Nervous System, with Focus on Extracellular Vesicles Derived from Mesenchymal Stem Cells as Therapeutic Tools. *Front. Cell Neurosci.* **2016**, *10*, 109. [[CrossRef](#)] [[PubMed](#)]
43. Xin, H.; Li, Y.; Cui, Y.; Yang, J.J.; Zhang, Z.G.; Chopp, M. Systemic administration of exosomes released from mesenchymal stromal cells promote functional recovery and neurovascular plasticity after stroke in rats. *J. Cereb. Blood Flow Metab.* **2013**, *33*, 1711–1715. [[CrossRef](#)] [[PubMed](#)]
44. Xin, H.; Li, Y.; Liu, Z.; Wang, X.; Shang, X.; Cui, Y.; Zhang, Z.G.; Chopp, M. MiR-133b promotes neural plasticity and functional recovery after treatment of stroke with multipotent mesenchymal stromal cells in rats via transfer of exosome-enriched extracellular particles. *Stem Cells* **2013**, *31*, 2737–2746. [[CrossRef](#)] [[PubMed](#)]
45. Di Trapani, M.; Bassi, G.; Midolo, M.; Gatti, A.; Kamga, P.T.; Cassaro, A.; Carusone, R.; Adamo, A.; Krampera, M. Differential and transferable modulatory effects of mesenchymal stromal cell-derived extracellular vesicles on T, B and NK cell functions. *Sci. Rep.* **2016**, *6*, 24120. [[CrossRef](#)] [[PubMed](#)]
46. Galipeau, J.; Sensebe, L. Mesenchymal Stromal Cells: Clinical Challenges and Therapeutic Opportunities. *Cell Stem Cell* **2018**, *22*, 824–833. [[CrossRef](#)] [[PubMed](#)]
47. Cui, G.H.; Wu, J.; Mou, F.F.; Xie, W.H.; Wang, F.B.; Wang, Q.L.; Fang, J.; Xu, Y.W.; Dong, Y.R.; Liu, J.R.; et al. Exosomes derived from hypoxia-preconditioned mesenchymal stromal cells ameliorate cognitive decline by rescuing synaptic dysfunction and regulating inflammatory responses in APP/PS1 mice. *FASEB J.* **2018**, *32*, 654–668. [[CrossRef](#)] [[PubMed](#)]
48. Wang, S.S.; Jia, J.; Wang, Z. Mesenchymal Stem Cell-Derived Extracellular Vesicles Suppresses iNOS Expression and Ameliorates Neural Impairment in Alzheimer' Disease Mice. *J. Alzheimers Dis.* **2018**, *61*, 1005–1013. [[CrossRef](#)] [[PubMed](#)]

49. Katsuda, T.; Oki, K.; Ochiya, T. Potential application of extracellular vesicles of human adipose tissue-derived mesenchymal stem cells in Alzheimer's disease therapeutics. *Methods Mol. Biol.* **2015**, *1212*, 171–181. [[CrossRef](#)]
50. Wegiel, J.; Wisniewski, H.M. The complex of microglial cells and amyloid star in three-dimensional reconstruction. *Acta Neuropathol.* **1990**, *81*, 116–124. [[CrossRef](#)]
51. Condello, C.; Yuan, P.; Grutzendler, J. Microglia-Mediated Neuroprotection, TREM2, and Alzheimer's Disease: Evidence From Optical Imaging. *Biol. Psychiatry* **2018**, *83*, 377–387. [[CrossRef](#)] [[PubMed](#)]
52. Itagaki, S.; McGeer, P.L.; Akiyama, H.; Zhu, S.; Selkoe, D. Relationship of microglia and astrocytes to amyloid deposits of Alzheimer disease. *J. Neuroimmunol.* **1989**, *24*, 173–182. [[CrossRef](#)]
53. Lee, C.Y.; Landreth, G.E. The role of microglia in amyloid clearance from the AD brain. *J. Neural Transm. (Vienna)* **2010**, *117*, 949–960. [[CrossRef](#)] [[PubMed](#)]
54. Morgan, D. The role of microglia in antibody-mediated clearance of amyloid-beta from the brain. *CNS Neurol. Disord. Drug Targets* **2009**, *8*, 7–15. [[CrossRef](#)] [[PubMed](#)]
55. de Godoy, M.A.; Saraiva, L.M.; de Carvalho, L.R.P.; Vasconcelos-Dos-Santos, A.; Beiral, H.J.V.; Ramos, A.B.; Silva, L.R.P.; Leal, R.B.; Monteiro, V.H.S.; Braga, C.V.; et al. Mesenchymal stem cells and cell-derived extracellular vesicles protect hippocampal neurons from oxidative stress and synapse damage induced by amyloid- β oligomers. *J. Biol. Chem.* **2018**, *293*, 1957–1975. [[CrossRef](#)] [[PubMed](#)]
56. Bruno, S.; Grange, C.; Deregiibus, M.C.; Calogero, R.A.; Saviozzi, S.; Collino, F.; Morando, L.; Busca, A.; Falda, M.; Bussolati, B.; et al. Mesenchymal stem cell-derived microvesicles protect against acute tubular injury. *J. Am. Soc. Nephrol.* **2009**, *20*, 1053–1067. [[CrossRef](#)] [[PubMed](#)]
57. Lopatina, T.; Bruno, S.; Tetta, C.; Kalinina, N.; Porta, M.; Camussi, G. Platelet-derived growth factor regulates the secretion of extracellular vesicles by adipose mesenchymal stem cells and enhances their angiogenic potential. *Cell Commun. Signal.* **2014**, *12*, 26. [[CrossRef](#)] [[PubMed](#)]
58. Gallart-Palau, X.; Serra, A.; Wong, A.S.; Sandin, S.; Lai, M.K.; Chen, C.P.; Kon, O.L.; Sze, S.K. Extracellular vesicles are rapidly purified from human plasma by PProtein Organic Solvent PRecipitation (PROSPR). *Sci. Rep.* **2015**, *5*, 14664. [[CrossRef](#)]
59. Nelson, P.T.; Alafuzoff, I.; Bigio, E.H.; Bouras, C.; Braak, H.; Cairns, N.J.; Castellani, R.J.; Crain, B.J.; Davies, P.; Del Tredici, K.; et al. Correlation of Alzheimer disease neuropathologic changes with cognitive status: A review of the literature. *J. Neuropathol. Exp. Neurol.* **2012**, *71*, 362–381. [[CrossRef](#)]
60. Morris, G.P.; Clark, I.A.; Vissel, B. Inconsistencies and controversies surrounding the amyloid hypothesis of Alzheimer's disease. *Acta Neuropathol. Commun.* **2014**, *2*, 135. [[CrossRef](#)]
61. Sharoar, M.G.; Hu, X.; Ma, X.M.; Zhu, X.; Yan, R. Sequential formation of different layers of dystrophic neurites in Alzheimer's brains. *Mol. Psychiatry* **2019**, *24*, 1369–1382. [[CrossRef](#)] [[PubMed](#)]
62. Losurdo, M.; Pedrazzoli, M.; D'Agostino, C.; Lonati, E.; Rizzi, L.; Molteni, L.; Elia, C.A.; Dander, E.; D'Amico, G.; Torsello, A.; et al. Analysis of the anti-inflammatory effect of preconditioned mesenchymal stem cell-derived extracellular vesicles in a model of Alzheimer's disease. In Proceedings of the NEUROMI Forth International Meeting of the Milan Center For Neuroscience: "Brain Stimulation and Brain Plasticity: From Basic Research to Clinical Practice", Milan, Italy, 21–23 November 2018.





Article

Seasonal Variation in the Biological Effects of PM_{2.5} from Greater Cairo

Sara Marchetti ¹, Salwa K. Hassan ², Waleed H. Shetaya ², Asmaa El-Mekawy ²,
Elham F. Mohamed ², Atef M. F. Mohammed ², Ahmed A. El-Abssawy ², Rossella Bengalli ¹,
Anita Colombo ¹, Maurizio Gualtieri ³ and Paride Mantecca ^{1,*}

¹ Department of Earth and Environmental Sciences, Research Center POLARIS, University of Milano-Bicocca, 20126 Milan, Italy; s.marchetti16@campus.unimib.it (S.M.); rossella.bengalli@unimib.it (R.B.); anita.colombo@unimib.it (A.C.)

² Air Pollution Research Department, Environmental Research Division, National Research Centre, 33 El-Bohouth St., Dokki, Giza 12622, Egypt; salwakamal1999@gmail.com (S.K.H.); wh.shetaya@nrc.sci.eg (W.H.S.); asmaamekawy75@gmail.com (A.E.-M.); elham_farouk0000@yahoo.com (E.F.M.); ateffathy2006@yahoo.com (A.M.F.M.); elabssawysalem@gmail.com (A.A.E.-A.)

³ ENEA SSPT-MET-INAT Bologna Research Centre, Via Martiri di Monte Sole, 4, 40129 Bologna, Italy; maurizio.gualtieri@enea.it

* Correspondence: paride.mantecca@unimib.it; Tel.: +39-02-6448-2916

Received: 11 September 2019; Accepted: 5 October 2019; Published: 9 October 2019



Abstract: Greater Cairo (Egypt) is a megalopolis where the studies of the air pollution events are of extremely high relevance, for the geographical-climatological aspects, the anthropogenic emissions and the health impact. While preliminary studies on the particulate matter (PM) chemical composition in Greater Cairo have been performed, no data are yet available on the PM's toxicity. In this work, the *in vitro* toxicity of the fine PM (PM_{2.5}) sampled in an urban area of Greater Cairo during 2017–2018 was studied. The PM_{2.5} samples collected during spring, summer, autumn and winter were preliminary characterized to determine the concentrations of ionic species, elements and organic PM (Polycyclic Aromatic Hydrocarbons, PAHs). After particle extraction from filters, the cytotoxic and pro-inflammatory effects were evaluated in human lung A549 cells. The results showed that particles collected during the colder seasons mainly induced the xenobiotic metabolizing system and the consequent antioxidant and pro-inflammatory cytokine release responses. Biological events positively correlated to PAHs and metals representative of a combustion-derived pollution. PM_{2.5} from the warmer seasons displayed a direct effect on cell cycle progression, suggesting possible genotoxic effects. In conclusion, a correlation between the biological effects and PM_{2.5} physico-chemical properties in the area of study might be useful for planning future strategies aiming to improve air quality and lower health hazards.

Keywords: air pollution; PM_{2.5}; toxicity; lung; *in vitro* systems

1. Introduction

The World Health Organization (WHO) stated that air pollution is the major environmental and public health risk, due to its effect on global air quality and climate. The WHO reported that, indeed, each year, about 7 million people die because of air pollution, with 4.2 million of these deaths (60%) caused by the exposure to outdoor ambient air pollution [1]. For that reason, greater attention should be paid to environmental pollution and its effects on human health, possibly by planning and implementing national, long-term health policies. Cooperation with non-governmental organizations is also necessary to identify and try to mitigate the several environmental threats and sources of air

pollutants. Planning and control programs to manage air quality should be implemented to reduce air pollution and the associated adverse health effects, and finally, obtain an improvement in public health all over the world [2,3].

In recent years, many developing countries, like Egypt, have experienced rapid urbanization, industrial development, construction activities and an increase in traffic flow, all of which seriously threaten the environment with the huge amounts of pollutants emitted. One of the major air pollutants is particulate matter (PM), which contributes to acidification of precipitation and climatic change, and affects Earth's radiation balance, agriculture, material and cultural heritages and ecosystems [4–6]—but is also one of the most deleterious pollutants for human health.

Acute and long-term exposure to PM has been associated with an increase in mortality and morbidity in the population [2,3]. Several studies in the last decades have associated particulate exposure to premature deaths, allergies [4], ischemic heart disease or strokes, respiratory illness and infections [2], chronic obstructive pulmonary disease (COPD), exacerbation of asthma and increased cancer incidence, especially lung cancer [7]. Nevertheless, the mechanisms of action involved in the pathogenesis of such adverse health effects are still debated and different PM physicochemical properties, such as size, surface area and chemical composition, are suggested to be determinants for their onset [8].

PM is a complex and heterogeneous mixture of natural and anthropogenic origin composed of water-soluble inorganic compounds, organic carbons, and elemental carbon and metals. It is emitted from direct sources, and/or formed from conversion of gases into secondary particles through chemical reactions [9]. The differences in emission sources and the subsequent atmospheric chemical reactions lead to increase in variation in size, shape, surface area, chemical composition, solubility and origin of the aerosol in the atmosphere [10,11].

Studies have been performed in Greater Cairo (Egypt) on urban, residential, suburban and industrial areas reporting the organic PM (Polycyclic Aromatic Hydrocarbons, PAHs) and inorganic (i.e., sulphate and nitrate) PM's chemical compositions, including the volatile organic compounds (VOCs), potentially toxic trace and major elements and gases [12–14]. These studies evidenced high levels of atmospheric pollution, suggesting that low air quality should be considered the most serious environmental concern in Greater Cairo. The general climate of Cairo city is cold, moist and rainy in winter, whereas it is characterized by high temperatures, high solar radiation, a clear sky and being rainless, during summer. Cairo may be also exposed to three types of episodes: dust storms (during spring), haze dust and straw rice combustions (during autumn).

However, the knowledge is limited on the levels of fine PM ($PM_{2.5}$) in Greater Cairo, as is the case in regard to its chemical composition, its biological impact and its possible health effects. Our previous work [15] reported that the average concentrations of $PM_{2.5}$ in the Dokki urban area were higher than the maximum yearly standards in the European Commission's environmental quality standards for ambient air (25 mg/m^3). $PM_{2.5}$ concentrations also exceeded the Egyptian air quality standard for $PM_{2.5}$ value ($80 \text{ }\mu\text{g/m}^3$ for 24 h) during December 2010 [16].

$PM_{2.5}$ pollution in fact greatly varies at the regional scale, depending on the local emission sources and climatic and geographic variables. These parameters have been shown to affect the biological reactivity and thus the final impact on human health [17].

Different toxicological mechanisms have been suggested to be activated by airborne particles. Several studies on in vitro systems reported the release of pro-inflammatory mediators, oxidative stress [18], cell death [19] and genotoxicity [20] as the main effects observed after exposure to PM. Cell cycle alterations are also reported [21]. Furthermore, accumulating evidence demonstrates a strong seasonality of the adverse health effects produced by PM, with differences according to climatic conditions and emission sources [4,22]. In vivo studies also demonstrated a link between PM exposure and lung inflammation, which triggers the onset of cardiovascular adverse events [23,24].

At present, no literature is available on the toxicological profile of PM from Greater Cairo, despite the great importance attributable to the knowledge of the specific toxic outcomes of the particles

sampled in specific local representative sites. To fill this gap of knowledge, the present work aimed at comparatively investigating the chemical composition and in vitro toxic effects of the urban PM_{2.5} collected during different seasons in the urban area of Dokki, Giza (Greater Cairo).

After samplings, PM_{2.5} was analyzed for ionic species, elements and PAHs, while the toxicity was evaluated on the human alveolar epithelial cells, A549. The cytotoxic, inflammatory and genotoxic potentials of the PM_{2.5} samples collected during spring, summer, autumn and winter were investigated.

In addition to the basic knowledge on the toxicity mechanisms associated to the Greater Cairo urban PM_{2.5}, these results will be relevant for implementing future risk mitigation strategies, not only on the basis of PM mass concentration, but also considering the specific PM biological effects.

2. Results

2.1. PM_{2.5} Physico-Chemical Characterization

The average seasonal variations of the concentrations (mg/g) of the water-soluble ionic species in PM_{2.5} during the period of study at the Dokki urban area are shown in Table 1. From that table, it is evident that sulphate and nitrate were the ions with the highest concentrations, whereas the lowest levels were found for Mg²⁺ and K⁺ during the four seasons. The highest concentration of water-soluble ions was detected in summer. Statistical analysis revealed significant differences among seasons, showing a higher content of ionic species in summer compared to spring ($p < 0.0001$), autumn ($p < 0.001$) and winter ($p < 0.0001$). Among all the water-soluble ions determined in the present study, SO₄²⁻ was the most abundant PM_{2.5} chemical component of the different seasons. The total secondary inorganic ions (NO₃⁻, SO₄²⁻ and NH₄⁺) were the dominant water-soluble ions in PM_{2.5} during the four seasons.

Table 1. Contents of water-soluble inorganic ions (WSII) in fine particulate matter (PM_{2.5}) collected during 2017 (mg/g).

Water-Soluble Inorganic Ions Title	Spring	Summer	Autumn	Winter
Cl ⁻	22.66 ± 4.57	33.79 ± 1.54	42.67 ± 25.99	33.71 ± 10.94
NO ₃ ⁻	50.81 ± 11.24	65.42 ± 15.14	55.58 ± 3.64	38.35 ± 14.02
SO ₄ ²⁻	106.74 ± 21.52	204.33 ± 24.44	107.02 ± 8.10	86.13 ± 20.29
Na ⁺	23.94 ± 10.52	19.83 ± 1.88	30.73 ± 19.39	32.93 ± 11.01
NH ₄ ⁺	28.63 ± 1.97	53.33 ± 2.01	37.86 ± 0.79	25.60 ± 10.33
K ⁺	20.67 ± 1.16	18.41 ± 6.09	19.83 ± 2.45	13.02 ± 6.44
Mg ²⁺	19.16 ± 5.48	18.55 ± 2.41	21.40 ± 9.22	13.59 ± 8.49
Ca ²⁺	33.96 ± 3.18	35.75 ± 5.28	37.99 ± 19.59	32.47 ± 10.86
Σ WSIs	306.58 [§] ± 59.65	449.42 ± 58.79	353.08 ^{***} ± 89.17	275.79 ^{§ †} ± 92.37

Seasonal mean concentrations (mg/g) of water-soluble inorganic ions (WSII) in PM_{2.5} sampled by a high-volume sampler in Dokki urban area during the period of study. ± Standard deviation between individual samples of the same season. $n = 24$ for each season. Statistical differences among seasons were analyzed by one-way ANOVA with Tukey's multiple comparisons test. [§] $p < 0.0001$, ^{***} $p < 0.001$ summer compared to other seasons, [†] $p < 0.01$ autumn versus winter.

Table 2 summarizes the seasonal variations in the metal/metalloid contents (mg/g) of the PM_{2.5} samples. It is evident that Al and Fe were the dominant elements during the four seasons, followed by Pb, Cu, Zn and Mn. The minimum concentrations were noted for Co and Hg. The concentrations of the individual measured metals were found to follow the following pattern: Al > Fe > Pb > Cu > Zn > Mn > V > Ni > As > Cd > Co > Hg. The highest mean concentrations of the measured metal were found in spring, whereas the lowest levels were detected in summer. Significant differences were observed between seasons, with an increase in metal content during spring in comparison to summer ($p < 0.001$) and autumn ($p < 0.0001$). Winter was found statistically augmented with respect to autumn ($p < 0.001$). These results indicate that crustal metals (Al and Fe) were the most abundant constituents in PM_{2.5} of the study area.

Table 2. Contents of potentially toxic metals/metalloids in PM_{2.5} collected during 2017 (mg/g).

Metals	Spring	Summer	Autumn	Winter
Al	32.41 ± 8.26	23.11 ± 5.08	20.93 ± 0.15	27.98 ± 7.86
Fe	14.4 ± 7.34	8.58 ± 2.32	9.96 ± 0.13	14.54 ± 4.5
Mn	0.50 ± 0.08	0.44 ± 0.10	0.39 ± 0.02	0.52 ± 0.09
V	0.31 ± 0.11	0.23 ± 0.07	0.20 ± 0.01	0.18 ± 0.04
Zn	0.99 ± 0.61	0.68 ± 0.15	0.69 ± 0.01	0.86 ± 0.17
Ni	0.31 ± 0.10	0.19 ± 0.03	0.20 ± 0.02	0.17 ± 0.02
Co	0.011 ± 0.00	0.010 ± 0.00	0.053 ± 0.01	0.033 ± 0.03
Cd	0.09 ± 0.08	0.02 ± 0.00	0.18 ± 0.01	0.11 ± 0.09
Cu	1.27 ± 0.06	0.99 ± 0.30	0.75 ± 0.01	0.88 ± 0.14
Pb	2.93 ± 0.61	2.08 ± 1.13	2.60 ± 0.23	2.5 ± 0.78
As	0.16 ± 0.03	0.18 ± 0.05	0.15 ± 0.01	0.2 ± 0.06
Hg	0.008 ± 0.00	0.010 ± 0.00	0.008 ± 0.00	0.010 ± 0.00
Σ Ms	53.39 ± 15.68	40.51 ^{***} ± 6.24	36.12 [§] ± 0.41	47.96 [‡] ± 12.40

Seasonal mean concentrations (mg/g) of potentially toxic metals/metalloids (Ms) in PM_{2.5} collected during the period of study. ± Standard deviation between individual samples of the same season. *n* = 24 for each season. Statistical differences among seasons were analyzed by one-way ANOVA with Tukey's multiple comparisons test. [§] *p* < 0.0001 and ^{***} *p* < 0.001 spring versus summer and autumn, [‡] *p* < 0.001 autumn versus winter.

The mean seasonal concentrations (mg/g) of the individual PAH compounds during the period of study are shown in Table 3. It can be noticed that BGP, DBA, IND, BaP, BkF, BbF and CRY were the most abundant PAH compounds during the different seasons. NA and ACY were the lowest concentrations during the period of study. These results also indicate that the concentrations of PAHs were similar in winter and summer. In addition, statistical differences revealed that PAHs' content was increased in summer compared to spring (*p* < 0.001) and autumn (*p* < 0.05). Significant differences were observed also between winter and spring (*p* < 0.0001).

Table 3. Contents of organic PM (Polycyclic Aromatic Hydrocarbons, PAHs) in PM_{2.5} collected during 2017 (mg/g).

PAHs	Spring	Summer	Autumn	Winter
NA	0.17 ± 0.09	0.13 ± 0.03	0.28 ± 0.04	0.33 ± 0.01
ACY	0.25 ± 0.02	0.23 ± 0.06	0.26 ± 0.05	0.31 ± 0.01
ACE	0.32 ± 0.02	0.42 ± 0.10	0.38 ± 0.06	0.53 ± 0.01
FLU	0.29 ± 0.02	0.38 ± 0.09	0.29 ± 0.04	0.47 ± 0.01
PHE	0.46 ± 0.03	0.60 ± 0.14	0.52 ± 0.11	0.61 ± 0.01
ANT	1.84 ± 0.10	2.31 ± 0.38	0.52 ± 0.10	0.63 ± 0.02
FLT	1.69 ± 0.08	1.93 ± 0.38	2.41 ± 0.42	2.55 ± 0.04
PYR	1.85 ± 0.10	2.17 ± 0.48	1.99 ± 0.37	2.05 ± 0.03
BaA	2.10 ± 0.13	2.29 ± 0.50	2.38 ± 0.44	2.49 ± 0.02
CRY	3.42 ± 0.15	4.21 ± 0.89	3.87 ± 0.59	4.10 ± 0.04
BbF	4.27 ± 0.25	4.95 ± 1.01	4.41 ± 0.62	5.06 ± 0.09
BkF	3.71 ± 0.17	5.13 ± 1.04	3.74 ± 0.57	4.48 ± 0.04
BaP	3.21 ± 0.19	4.12 ± 0.71	2.78 ± 0.36	3.31 ± 0.06
IND	2.33 ± 0.13	2.79 ± 0.54	3.49 ± 0.56	3.50 ± 0.05
DBA	3.25 ± 0.23	3.84 ± 0.77	3.94 ± 0.77	4.12 ± 0.06
BGP	3.64 ± 0.20	4.35 ± 0.78	4.78 ± 0.70	4.62 ± 0.06
ΣPAHs	32.82 ± 1.90	39.85 [§] ± 7.20	36.05 [‡] ± 5.78	39.14 [§] ± 0.55

Seasonal mean concentrations (mg/g) of PAHs in PM_{2.5} sampled by a high-volume sampler in the Dokki urban area during the period of study. ± Standard deviation between individual samples of the same season. *n* = 24 for each season. Statistical differences among seasons were analyzed by one-way ANOVA with Tukey's multiple comparisons test. [§] *p* < 0.0001 spring versus summer and winter, [‡] *p* < 0.05 summer versus autumn.

The apportionment of PAHs according to selected, characteristic ratio values (Table S1) shows that the main difference between summer–spring and winter–autumn seasons is related to the contribution

of coal and biomass burning emission. This source can explain also the differences observed in PM atmospheric concentration.

The morphological characterization of PM_{2.5} obtained by scanning electron microscope analysis is shown in Figure 1. According to their respective sampling season, the particles that seems to be well dispersed have a size of less than 10 μm .

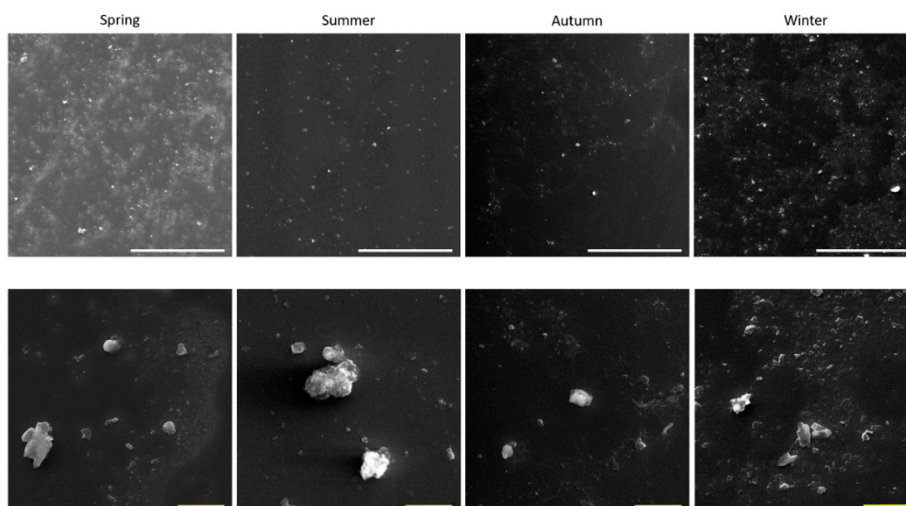


Figure 1. PM_{2.5} morphological characterization. Scanning electron microscope observations on the extracted particles: spring, summer, autumn and winter. Particles were observed to the concentration of 25 $\mu\text{g}/\text{mL}$. White scale bar: 100 μm . Yellow scale bar: 10 μm .

The endotoxin levels in PM-extracted samples are reported in the Supplementary Materials (Figure S1). The results showed that all PM_{2.5} samples contained about 60 EU/mL, with no significant seasonal variations.

2.2. Biological Responses

2.2.1. Cell Viability

The impact of PM_{2.5} samples on cell viability was assessed by Alamar Blue assay after exposure to increasing doses (1–10 $\mu\text{g}/\text{cm}^2$). None of the treatments produced any significant alterations in cellular metabolic activity when compared to the corresponding control (Figure 2).

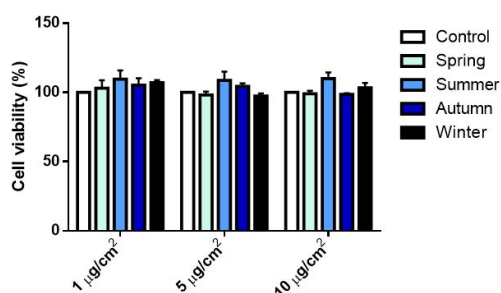


Figure 2. Cellular metabolic activity assessed by Alamar Blue assay after 24 h exposure to increasing doses (1, 5 and 10 $\mu\text{g}/\text{cm}^2$) of PM_{2.5} collected in different seasons. Each bar shows mean \pm SEM of four independent experiments ($n = 4$). Statistical differences among seasons were analyzed by two-way ANOVA with Dunnett's multiple comparisons test.

2.2.2. Release of Inflammatory Mediators

The activation of the inflammatory response was evaluated by measuring the secretions of the cytokines IL-6 and IL-8 after 24 h exposure to all the PM_{2.5} doses tested. IL-6 release significantly increased only after exposure to autumn and winter PMs (Figure 3a). Spring and summer PMs did not affect IL-6 levels. On the other hand, IL-8 secretion was significantly increased after exposure to all the PMs, although to a lesser extent, following treatment with the one collected during summer (Figure 3b). Interestingly, significant differences were observed among seasons: autumn and winter PMs indeed induced an increased release of IL-6 compared to spring and summer PMs. Regarding IL-8 instead, differences among seasons were observed only between summer and autumn, with the latter statistically increased compared to the warmer season.

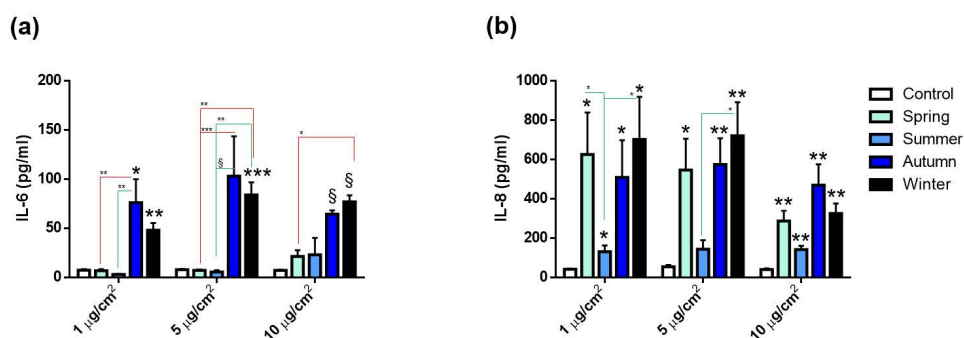


Figure 3. Pro-inflammatory cytokines' releases. IL-6 (a) and IL-8 (b) protein secretion by A549 cells after 24 h of exposure to increasing doses (1, 5 and 10 µg/cm²) of PM_{2.5} collected in different seasons. Each bar shows mean ± SEM of four independent experiments ($n = 4$). PM versus control. Statistical analysis was performed by unpaired *t*-test. Statistical differences among seasons were analyzed by two-way ANOVA with Tukey's multiple comparisons test. § $p < 0.0001$, *** $p < 0.001$, ** $p < 0.01$ and * $p < 0.05$.

2.2.3. Cell Cycle Alterations

The effects on the cell cycle progression after exposure to the PM_{2.5} from the different seasons was also evaluated. Spring and summer PMs seemed to affect DNA replication, since a significant increase in S-phase cell populations and a parallel decrease of those in G2/M phase was observed (Figure 4c). On the contrary, the exposure to autumn and winter PMs did not induce cell cycle alterations at any of the tested doses (Figure 4a–c).

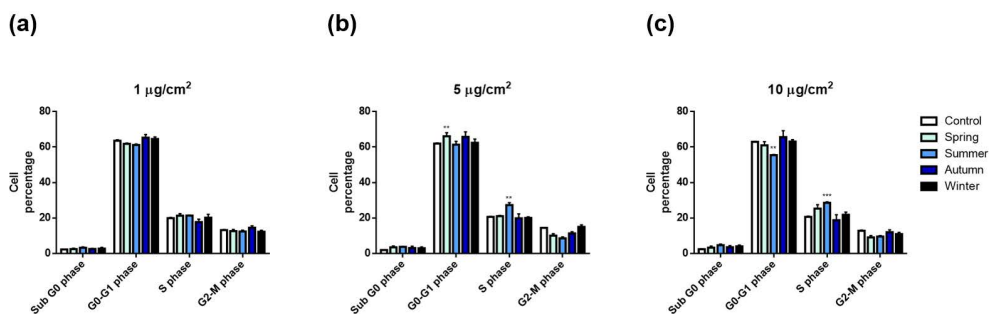


Figure 4. Cell cycle analysis of A549 cells after 24 h exposure to increasing doses (1, 5 and 10 µg/cm²—(a,b,c), respectively) of PM_{2.5} collected in different seasons. Each bar shows mean ± SEM of four independent experiments ($n = 4$). Statistical analysis was performed by two-way ANOVA with Dunnett's multiple comparison test. *** $p < 0.001$ and ** $p < 0.01$ versus control cells.

2.2.4. Oxidative Stress and PAH Metabolizing Enzymes' Activations

Oxidative stress and xenobiotics' metabolism responses were investigated following exposure to $10 \mu\text{g}/\text{cm}^2$ $\text{PM}_{2.5}$ for 24 h. Since it represents an early cell response, the reactive oxygen species (ROS) production was measured after 3 h exposure (Figure 5).

As shown in Figure 5a, PM samples induced a slight increase of intracellular ROS in respect to control, but no significant differences among the sampling seasons existed.

To determine whether the exposure to the different PMs triggered an anti-oxidant response, the expression of the stress-inducible heme-oxygenase 1 protein (HO-1) was also evaluated. As shown in Figure 5b, HO-1 expression was increased after exposure to all PMs, but a significantly higher value was registered only for winter PM.

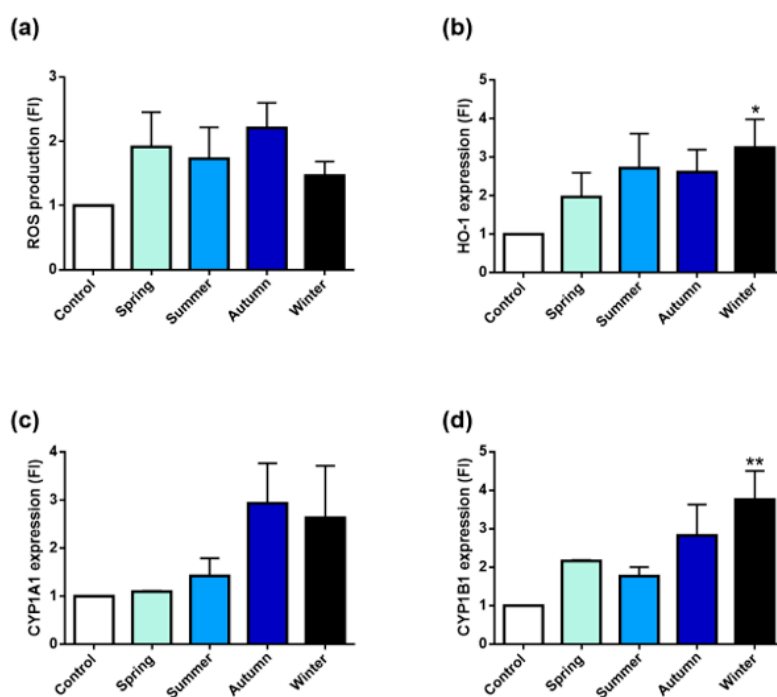


Figure 5. Oxidative stress and xenobiotics' metabolism pathways' activations in A549 cells after exposure to $10 \mu\text{g}/\text{cm}^2$ seasonal $\text{PM}_{2.5}$. (a) Intracellular reactive oxygen species (ROS) generation induced by the different PMs after 3 h of treatment. (b) HO-1 protein expression in A549 upon exposure to $\text{PM}_{2.5}$ for 24 h. CYP1A1 (c) and CYP1B1 (d) protein expression after 24 h of treatment. Bars represent means \pm SEM of three independent experiments ($n = 3$). Statistical analysis was performed by one-way ANOVA with Dunn's (b) and Dunnett's (c,d) multiple comparison test. ** $p < 0.01$ and * $p < 0.05$ versus control cells.

The induction of CYP1A1 and CYP1B1 expression was also measured (Figure 5c,d). As indicated in Figure 5c, $\text{PM}_{2.5}$ collected during spring and summer had a very limited effect on CYP1A1 expression. Instead, autumn and winter induced CYP1A1 more efficiently. A similar trend was observed also for the induction of CYP1B1. The latter protein indeed, was found to be increased by all PMs, with winter PM inducing the highest and most statistically significant effect (Figure 5d).

2.3. Correlations between Chemical Parameters and Biological Effects

Overall correlation showed expectedly high, positive correlations within the compounds belonging to the same chemical class; namely, metals and trace elements, PAHs and soluble ions (Figure 6).

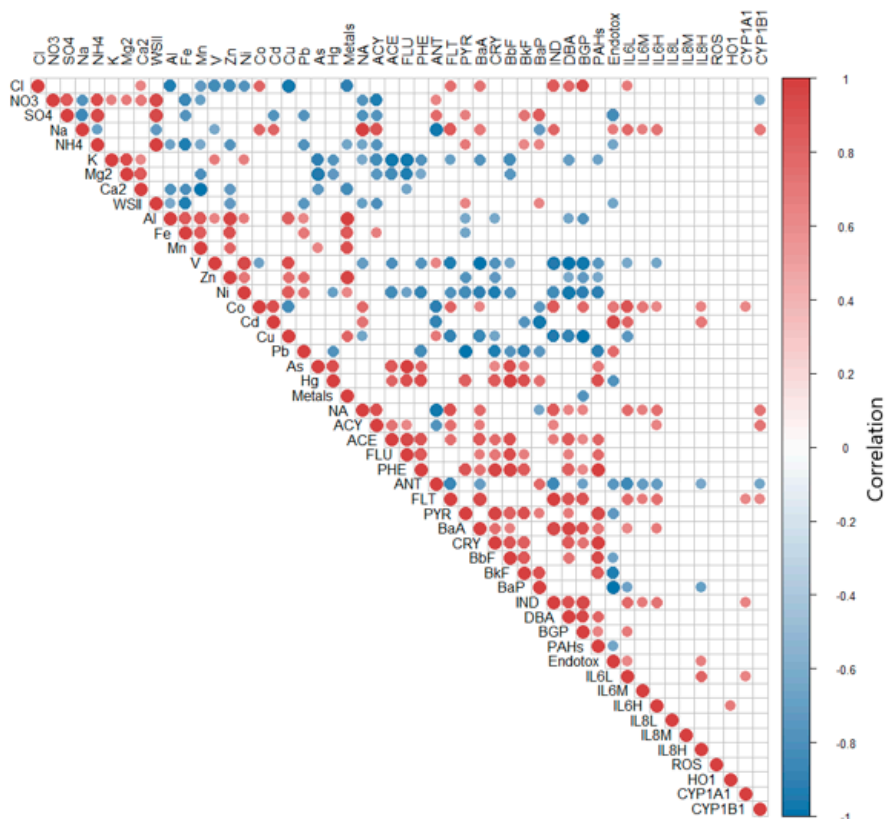


Figure 6. Correlation diagram of chemical species and biological responses analyzed from fine PM extracted from filters sampled during the different seasons. Dark red spots indicate high positive correlation while dark blue ones indicate negative correlation. Only the correlations with statistical significance $p < 0.01$ are reported. Number of variables = 50; number of samples = 16 (the chemical parameters are considered constant during each season according to the pooling of homogeneous filters).

The figure reports only the correlations that showed significant ($p < 0.01$) positive or negative correlations; Fe, Mn, Zn, Al and Ni correlated among themselves and with the total sum of metals and trace elements (Metals); similarly, sulphates (SO_4^{2-}), nitrate (NO_3^-) and ammonia (NH_4^+) correlated among each other and with the sum of the water-soluble inorganic ions (WSIs). Of major interest, the correlation graph showed correlations, mainly positive, between the proteins analyzed and the chemical properties of the sampled PMs. Of interest, Cyp enzymes correlated positively with organic compounds (NA, ACY, FLT and IND), providing evidence of the activation of gene transcription in response to PM-bounded PAHs. Interesting is the correlation with cobalt (Co), whose emission in the atmosphere is related to combustion of coal and other human activities. Accordingly, the source's contribution to the characteristic PAHs ratio (Table S2) supports an increase of coal combustion during autumn and winter.

The correlation plot of CYP1B1 (Figure 7) with the selected compounds (FLT, ACY and NA) showed R^2 equal to 0.50, a slope of 1.36 and a p -value of 0.001. Despite the limited correlation value, which was, however, expected—due the complexity of the biological responses to air pollution and the interplay of different biological pathways within the cells—the plot is statistically significant and clearly shows an increase of the response moving from summer samples to winter ones.

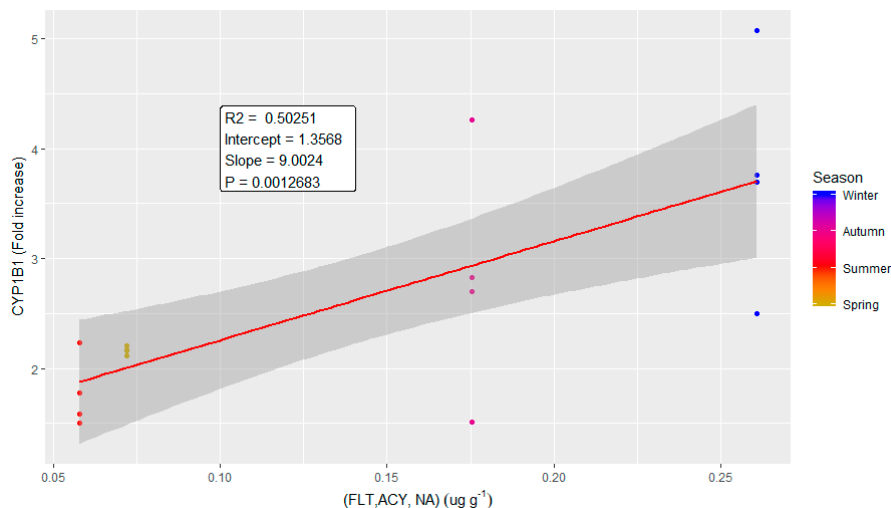


Figure 7. Correlation plot of the modulation of CYP1B1 protein expression and a linear correlation of the chemical variables identified from the correlation diagram reported in Figure 6. NA, FLT and ACY were linearly combined to obtain a single variable describing the variation of these compounds along the sampling campaign. The data are reported in different colours for the different seasons. The linear correlation (in red) is reported with its 95% confidence interval (grey shadow). The parameters describing the correlation curve are also reported in the plot.

A similar correlation plot was obtained for CYP1A1 and a linear combination of organic compounds (FLT and IND) and cobalt. For that protein, the plot values were: $R^2 = 0.39$, slope = 1.5 and p -value = 0.005.

Among the inflammatory proteins, interesting correlations were determined (the respective plots are reported in the supplementary materials: Figures S3, S4 and S5), and in general showed a lower contribution to the biological effects of PM sampled in spring, and a higher contribution to winter samples. IL-6, for the high dose of treatment (IL6H), is correlated to organic (FLT, NA, IND, BaA) and inorganic (Na and Co) compounds (Supplementary Figure S2), while IL-6 at the medium dose of treatment (IL6M) correlates to Na, Co, FLT, NA and IND (Figure S3). Correlations were also found between IL-8 (at the high dose of treatment, IL8H) and Cd and endotoxin (Figure S4). Interestingly, the correlation of IL-8 with endotoxin and Cd contributed differently in the four seasonal samples: summer PM had the weakest association, while autumn PM the strongest. Considering the two variables independently (Figures S4A and S4B), it appears that the correlation of IL-8 with endotoxin was driven mainly by autumn and spring PM samples, rather than from winter and summer ones. This peculiar correlation was likely due to the relationship of airborne bacterial distribution and meteorological parameters, such as temperature and relative humidity.

For HO-1, IL-8 (at low and medium doses of treatment) and IL-6 (at the lower dose of treatment), the correlation plots were not significant (p -value > 0.05) and are not reported.

3. Discussion

Recently, great attention has been devoted to air pollution in developing countries, like Egypt and sub-Saharan countries. In this research effort, seasonal $PM_{2.5}$ was, for the first time for the region, collected to evaluate and correlate its physical, chemical and biological properties. $PM_{2.5}$ samples were collected in the Greater Cairo region, where urbanization and industrialization have rapidly increased in the last few decades, causing an increase in the atmosphere's pollution [25]. The high rate of emission from industrial activities, electric power stations and traffic density, coupled with low wind speeds and the frequent thermal inversions in the area, resulted in high local pollution load. Therefore, Greater Cairo is considered one of the most polluted megacities in the world, as reported

by several works. Boman et al. [15] in 2013, investigated the PM_{2.5} mass concentration in a urban residential area, Dokki, the same as our study. They stated that between September 2010 and May 2011, the PM_{2.5} concentration was 51 µg/m³, well above the EU and WHO quality standards set for health protection. Krzyzanowski instead, in 2014, reported the cities in the world with the highest PM_{2.5} concentrations. Among those, the annual mean reported in Cairo was 80 µg/m³, one of the highest observed [26]. Those data have been confirmed more recently by Shaltout [27].

Previous studies performed in Greater Cairo area were focused only on the seasonal differences in chemical composition, areal distributions and concentrations of airborne particles. Studies performed by Boman [15] and Shaltouth [27] reported higher concentrations of PM_{2.5} during winter months and related that seasonality to the lower height of the boundary layer and lower wind speed in winter, which leads to reducing the dispersion of particulate matter in the air. The relative peak of PM_{2.5} concentrations observed during the spring months, may be an effect of the hot “Khamsin” southerly wind, which occurs in Egypt, predominantly during this season, and which bring air masses loaded with dust and sand [15]. Hassan [12] also reported that during autumn, winter and spring, several types of pollution episodes, including straw rice combustions, haze dust and dust storms, could represent a severe environmental hazard in Egypt.

Nevertheless, the biological effects of such particles collected in Greater Cairo are still unknown. Therefore, the main aim of our study was to define the cytotoxic effects produced on lung epithelial cells by PM_{2.5} collected in Giza during the different seasons and investigate the relationship between the adverse effects observed and the particulate’s chemical composition. In the present study, PM_{2.5} samples were analyzed for PAHs, metals and water-soluble inorganic ions (WSIs). Furthermore, cytotoxic, pro-inflammatory and genotoxic effects were evaluated *in vitro* on human A549 alveolar cells.

Regarding the chemical composition, water soluble ions were the most representative compound, with seasonal differences observed mainly in the SO₄²⁻ concentration. WSIs predominantly were found in the summer PM_{2.5}, due to the high temperatures and photochemical reactions [28,29]. PM_{2.5} was characterized also by a high PAH content, especially in summer and winter, compared to spring and autumn. Among metals, the higher amount was observed in spring and the lowest in autumn, with Al and Fe being the most abundant metals in all the seasons.

Furthermore, morphological characterization showed that, once extracted from the filters, PM_{2.5} samples were mainly constituted by irregularly shaped particles, mostly in the fine range, which tended to form aggregates. The content of endotoxins in Giza PMs was also evaluated. No significant differences according to the sampling season were observed. On the contrary, previous works performed in different regions reported a higher endotoxin content in PM samples collected during summer [22,30]. These results, however, are not surprising, considering that the endotoxin content can vary among the different seasons and cities and is influenced by environmental factors, like humidity and temperature [31,32].

The PM_{2.5}-induced biological effects were analyzed according to the sampling season by evaluating cell viability, inflammatory response and cell cycle progression in human lung A549 cells exposed for 24 h to PM doses representative of a daily particle deposition on a lung. Literature data on highly polluted regions reported that PM_{2.5} concentrations can exceed 100 µg/m³/24 h [33,34]. Those concentrations correspond to 0.06 and 3 µg/cm² deposited in the alveolar and tracheobronchial regions, respectively [33]. The selected doses were, therefore, in accordance with those reported by Li et al. [33], according to which the *in vitro* dose range of 0.2–20 µg/cm² was necessary to observe biological effects. Biomarkers of cell oxidative stress and the xenobiotic metabolizing system were also evaluated.

No effects on cell viability were detected after exposing cells at the selected PM_{2.5} doses (Figure 2). Accordingly, previous data on PM_{2.5} biological responses have shown no significant effects on cell viability [29,35]. Herein, we report a significant release of inflammatory mediators (IL-6 and IL-8) after fine PM exposure. The inflammatory response is, therefore, related to the specific chemical composition of particles [36], as also showed in Figure 6 and in Supplementary Materials.

Nevertheless, considering that endotoxins are known inducers of inflammation, and given their high content in all samples, we would have expected a strong inflammatory response after exposure to all the seasons' samples investigated, and possibly in a dose-response manner. Conversely, not all samples induced cytokine production on a linear dose-response manner. A slight modulation of the cytokines' release was indeed observed at the highest dose, especially for IL-8, suggesting a possible hormetic effect, in which the biological system adapts responses to environmental insults by improving its functionality and tolerance. Another possible explanation for that reduction might be the possible alteration of interleukins' secretion by PM_{2.5} exposure. A recent study indeed showed that PM_{2.5}, at 10 µg/cm², increased mRNA-synthesis and intracellular protein levels of IL-6 and IL-8, but it appeared to impair cytokine release in bronchial cells, in particular that of IL-8, possibly by altering cytoskeletal organization involved in protein secretion [35]. The individual composition of the tested PMs could also lead to different cell inflammatory responses, as already demonstrated in literature [30,37].

The main results point out that the toxicity responses were dependent upon the seasonal PM_{2.5}'s chemical variability. Regarding the release of pro-inflammatory cytokines, only the PM_{2.5} collected in autumn and winter induced an increase in IL-6 secretion, while IL-8 was increased after exposure to all PMs (Figure 3).

At a low concentration exposure, it was not possible to define a significant correlation between PM chemical composition and IL's release. On the contrary, the correlations between IL-6 and the mean and high doses of treatment, and IL-8 with the higher dose of treatment, revealed interesting associations. IL-6 was related at both the mean and high doses of treatment to the presence of naphthalene (NA), anthracene (ANT), indeno(1, 2, 3-cd)pyrene (IND), cobalt (Co) and sodium (Na) suggesting the importance of both combustion and natural sources in determining the increase of inflammatory responses. However, with exposure to the high concentration, other compounds (namely, ACY, BaA and Vanadium) were associated to an increased protein release. This difference seems to suggest that (i) besides the combustion process other anthropogenic sources as well, likely industrial ones, may contribute to the inflammatory potency of PM, and (ii) that when increasing the doses, the complexity of the biological response pathways may cover or uncover the importance of specific chemical species. For IL-8, a significant correlation was found between Cd and endotoxin. Again, this specific correlation may signify that this protein responds more rapidly to the bacterial compounds, well known to induce inflammatory responses, but that the release is highly affected by other compounds, such as Cd, that can modulate the intensity of the response.

Autumn and winter PMs were also able to increase the CYP1A1 and CYP1B1 expressions, and HO-1's expression was also significantly higher after winter PM_{2.5} exposure. The increase in CYP enzymes was positively related to specific organic species, again suggesting the importance of combustion activities emitting those compounds. We reported an interesting association between CYP1A1 with PAHs and Co. Since the combustion of coal and some industrial activities may determine the contemporaneous emission of these compounds, it will be relevant in future studies to evaluate the contribution of these sources to local air quality. However, it is important to remember the differential behavior of individual PAHs when combined in a mixture, in relation to biological responses. Individual PAHs indeed, are able to modulate CYP1A1 and CYP1B1 genes in different ways; however, their effect when combined in a mixture of compounds is uncertain [38,39].

According to these observations, in the human alveolar A549 cells, the PM_{2.5} collected during the colder seasons mainly induced the xenobiotic metabolizing system and the consequent antioxidant and pro-inflammatory cytokine release responses, which can be interpreted as active defense mechanisms. Under the conditions tested, in fact, neither the cell viability nor the cell cycle progression were affected after exposure to autumn and winter PM_{2.5}. In the winter PM_{2.5}, the highest amount of Fe was also measured (Table 2). This transition metal may have had contributed to the increased intracellular red-ox activity, which finally resulted in HO-1 overexpression, although no significant correlations were found.

Our results are consistent with literature data reporting the release of pro-inflammatory cytokines in epithelial cells exposed to PM with a high PAH content [39,40]. Moreover, they are in agreement with previous observations where particles collected in different seasons induced variable biological effects [41–43].

Regarding the effects of the PMs collected during the warmer seasons, only summer PM_{2.5} induced a concentration-dependent arrest in S-phase, with a corresponding decrease in the percentage of G0/G1 cells (Figure 4). This points out that-phase arrest is related to altered DNA replication, suggesting the presence of DNA damage or an alteration of the DNA replication machinery. In the summer PM_{2.5}, the highest concentrations of ionic species, especially sulphates, and a particularly high concentration of the genotoxic PAH, BaP, were measured (Tables 1 and 2). Deng et al. [44] supported our results by showing that inorganic extracts from dust storm and PM_{2.5} can alter cell cycle progression in human lung fibroblasts, inducing accumulations of cells arrested in S-phase. Organic extracts instead, induced alterations in G0–G1 phase [44]. It had already been shown that nitro-PAHs and BaP alter cell cycle progression in different human cell lines, inducing S-phase arrest [45,46]. In particular, Hockley [46] reported S-phase accumulation in human hepatocarcinoma (HepG2) after exposure to BaP. All considered, we can conclude that the summer PM_{2.5}, enriched in sulphates and BaP, may pose a genotoxic risk. It is interesting to note that, in parallel to the genotoxic insult, there was no activation of the defense mechanisms, such as cytokine secretion and CYP-mediated metabolism (Figures 3 and 5).

It is well known that inflammatory response and oxidative stress play a key role in the PM-induced toxic effects [2]. A slight increase in ROS generation was observed for the sampled PMs, with no significant differences among the seasons. The results were confirmed by western blot analysis, in which an increased expression in HO-1 was observed, especially after exposure to winter PM, suggesting the activation of the anti-oxidant response. HO-1 indeed, is a defense protein induced in several cell types, both in vivo and in vitro, in the presence of oxidative stress and inflammatory stimuli [24,47]. Our results are in agreement with literature's data, showing the modulation of the oxidative stress response as a common mechanism triggered by exposure to fine PM [48,49].

4. Materials and Methods

4.1. Site Description and PM_{2.5} Collection

The Greater Cairo region (Cairo, Giza, and Shoubra El-Khiema cities) lies to the south of Delta in the Nile basin. The narrow strip of Giza Governorate runs along the western side of the River Nile, opposite to the city of Cairo (Figure 8). It lies between two big industrial areas, one in the north (Shoubra El-Khiema) and the other in the southeast (Helwan).

Sampling collection was carried out from December 2016 to November 2017. Samples were collected from a point approximately 25 m above the ground level on the roof of the National Research Centre (NRC). The NRC is in the urban area of Giza (Dokki, 30°2'10.148" N, 31°12'0.419" E), situated to the southwest of Cairo's city center (Figure 1), which is characterized by high traffic density. Daily (24 h, two samples per week; 24 samples per season) PM_{2.5} samples were collected using a both high-volume air sampler for analysis of the chemical composition and a low volume Dewell–Higgins type cyclone sampler (Casella CEL, Bedford, UK) for the biological effects.

PM_{2.5} samples for chemical analysis were collected on glass fiber filters (20.3 cm × 25.4 cm) using the high-volume sampler. Glass fiber samples were equilibrated for 24 h, using controlled temperature and relative humidity desiccators, before and after sampling. The collected PM_{2.5} mass was determined by the difference in weight of the filter's mass before and after sampling; then, PM_{2.5} concentration was calculated from the mass and volume of air. After weighting, filters were stored at 4 °C until chemical analysis, to prevent evaporation of volatilized components. For the analysis, each filter was cut into four parts and one piece for each filter was used for ionic species, metals or PAHs' detection respectively. Filters collected during the same season were pooled to obtain data representative of the entire sampling season.

A low volume Dewell–Higgins type cyclone sampler (Casella CEL, Bedford, UK) with a Teflon filter (25 mm, 0.2 μm) was used to collect $\text{PM}_{2.5}$ for biological investigations. Blank control filters were collected from all sampling campaigns and treated similarly to the others.

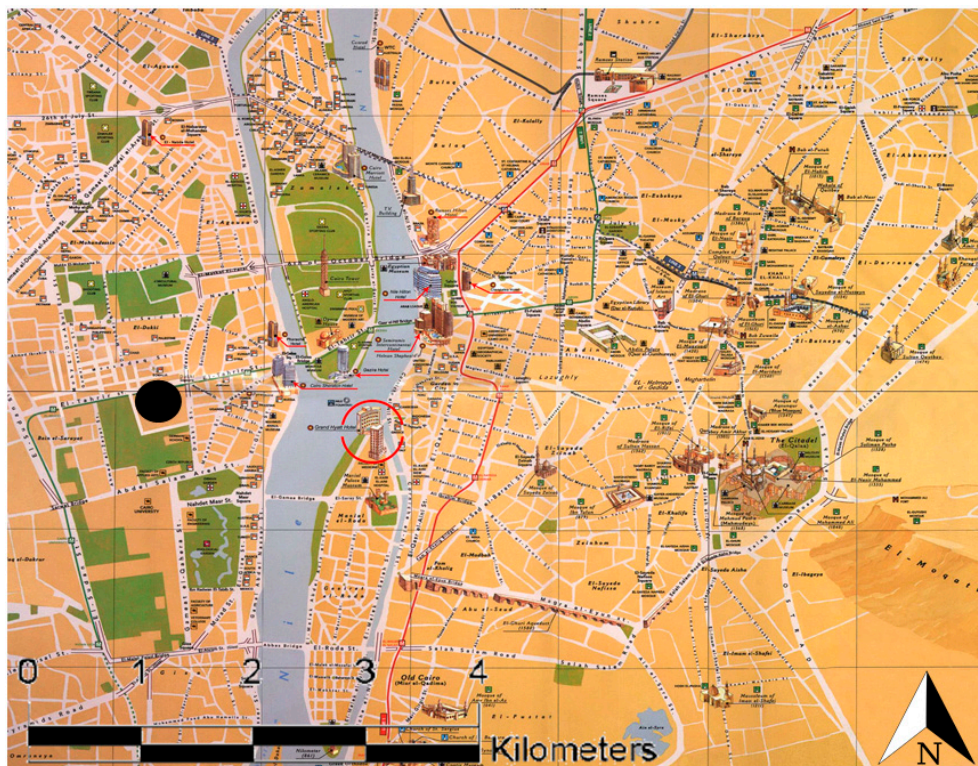


Figure 8. Detailed map of the Greater Cairo area, showing Cairo city with its streets (white lines), the Nile river (blue area) and several parks (green areas). Black dot represents our sampling site in Dokki district.

4.2. $\text{PM}_{2.5}$ Chemical Characterization

4.2.1. Water Soluble Inorganic Ionic Species (WSIs)

One quarter of each filter was cut into pieces and the water-soluble components were extracted into 20 mL of distilled water in 50 mL polypropylene tubes by ultrasonic bath (KQ300DE, Kunshan Ultrasonic Instrument Co., Ltd., China) for 40 min. The water samples were filtered with a 0.45 μm PTFE syringe filter (Pall Co. Ltd., USA) and stored at 4 $^{\circ}\text{C}$ until analysis. An ion chromatography system (Thermo IC-5000) was used to analyze the concentrations of three anions (Cl^- , NO_3^- and SO_4^{2-}) and five cation (Ca^{2+} , Mg^{2+} , NH_4^+ , K^+ and Na^+) species. The anions were detected with an Ion Pac ASRS-4 suppressor and an Ion Pac AS11-HC \times 250 mm analytical column. The eluent for anion analysis was 10 mmol/L Na_2CO_3 . The cations were detected with an Ion Pac CSRS-4 suppressor and an Ion Pac CS12A \times 250 mm analytical column. The eluent for cations analysis was 10 mmol/L $\text{CH}_4\text{O}_3\text{S}$. Injection of the samples was done automatically using a 10 μL loop. External standard solutions were used to generate the standard curve, and the correlation coefficient was higher than 0.999. Replicates and blanks were checked every 10 sample runs for quality control. Blank samples are analyzed in the same way to evaluate analytical bias and precision with ion chromatography. All the blanks were lower than method detection limits (MDLs), and the concentration data for the WSII were corrected by

these filter blanks. The MDLs were calculated as three times the standard deviations of seven replicate blank samples. The MDLs for SO_4^{2-} , NO_3^- , Cl^- , NH_4^+ , K^+ , Na^+ , Ca^{2+} and Mg^{2+} were $0.001 \mu\text{g}/\text{m}^3$.

4.2.2. Elemental Concentration

Filters and blanks were extracted by acid digestion. Filters were cut into small pieces, placed in a conical flask and added with 1 M nitric acid at 70°C for 3 h in ultrasonic bath and analyzed by inductively coupled plasma optical emission spectrometry (ICP MS) to determine the concentrations of toxic metals/metalloids (Al, Zn, Fe, V, Mn, Co, Ni, Cu, As, Pb, Hg and Cd). Multi-element analysis was undertaken using an Agilent 8800 Triple Quadrupole ICP-MS (ICP-QQQ) operated with helium in the collision cell to eliminate isobaric interferences. The ICP-QQQ was equipped with a standard sample introduction system, including a glass concentric nebulizer, quartz spray chamber and torch, and nickel-tipped cones. Samples and calibration standards were introduced from an Agilent ASX-500 Series auto-sampler. Internal standards, including Rh and Ir ($10 \mu\text{g}/\text{L}$) were directly introduced to the sample stream via a T-piece. For Hg measurements, internal standards were $10 \mu\text{g}/\text{L}$ In and Rh prepared in a matrix of ultra-pure 1% $\text{HNO}_3/0.5\%$ HCl. To reduce memory effects and improve the washout of Hg from the ICP system a washing protocol including (a) 1 g/L EDTA, 0.08 g/L Triton X-100 and 6 g/L NH_4OH , (b) technical grade 5% $\text{HNO}_3/5\%$ HCl and (c) ultra-pure 1% $\text{HNO}_3/0.5\%$ HCl, was introduced between samples [50]. Limits of detection (LOD) was calculated from 16 blanks and all analyses were run in triplicate.

4.2.3. Polycyclic Aromatic Hydrocarbons (PAHs)

PAHs were extracted in a Soxhlet apparatus for 24 h using purified normal hexane and dichloromethane (DCM) mixture (50/50, *v/v*) according to Fang et al. [51]. The organic extracts were then concentrated using a rotary evaporator, cleaned by clean silica gel/alumina columns consisting of 5 g anhydrous sodium sulfate, 20 g silica gel (deactivated 5% with distilled water), 10 g alumina (deactivated 1% with distilled water), 5 g sand, and glass wool according to Park et al. [52]. The extracts were concentrated, exchanged to 2 mL hexane, placed on the columns, and eluted with 1:1 pentane–dichloromethane (200 mL). The eluted extracts were concentrated on a rotary evaporator and exchanged to 1 mL hexane and stored in a freezer until analysis. For PAHs analysis, a $1\text{-}\mu\text{L}$ extract was withdrawn from the samples, including the blank samples, and injected into a Hewlett-Packard gas chromatography (GC; model HP6890), fitted with a flame ionization detector. A HP-5 ($30\text{ m} \times 320 \mu\text{m} \times 0.25 \mu\text{m}$) capillary column was used with hydrogen as carrier gas. The concentrations of the target PAH compounds were quantified by an external standard solution of 15 PAH compounds (PAH mixture, Supelco, Inc., Cairo, Egypt). The concentrations of the following PAH compounds in the particulate phase were determined: naphthalene (NA), acenaphthylene (ACY), acenaphthene (ACE), fluorene (FLU), phenanthrene (PHE), anthracene (ANT), fluoranthene (FLT), pyrene (PYR), benzo(a)anthracene (BaA), chrysene (CRY), benzo(b)fluoranthene (BbF), benzo(a)pyrene (BaP), dibenzo(a,h)anthracene (DBA), benzo(ghi)perylene (BGP) and indeno (1, 2, 3,-cd)pyrene (IND).

4.3. Filter Extraction and Particle Characterization

For in vitro toxicity studies, filters from the same season were extracted in water by mechanical detachment, together with the adsorbed compounds. To maximize particle extraction and recovery, we used also an ultrasound bath (Sonica Soltec, Milan, Italy) by replicating five 20-min ultrasonic cycles. Particle suspensions were then collected in sterile tubes previously weighed, and dried into a desiccator [29]. Desiccation process was performed using a dryer put under vacuum at room temperature (RT) in the dark with warm silica gels for about two weeks (until complete water evaporation). Silica gels were substituted, and vacuum restored every two days. Once dried, the sterile tubes were weighted to determine the mass of the extracted particles and stored at -20°C until further use. This procedure assured a good efficiency of extraction, guaranteeing the similarity of the extracted particles to the collected ones [53].

For cell exposure, particles were suspended in sterile water to obtain aliquots at a final concentration of 2 $\mu\text{g}/\mu\text{L}$. PMs were sonicated for 30 secs just prior to cell exposure.

Particles extracted from filters and re-suspended in water were morphologically characterized by scanning electron microscopy. Briefly, aliquots of 8 μL of sonicated particle suspensions at 25 $\mu\text{g}/\text{mL}$ in pure water and 1% Isopropyl alcohol were respectively, pipetted on aluminum stubs and dried at RT. Samples were then graphite-coated and observed by a Tescan VEGA 5136XM, operating at 20 kV. Images were digitally acquired and elaborated through dedicated software.

The presence of endotoxins in the extracted PM_{2.5} was assessed using the Limulus Amebocyte Lysate (LAL) chromogenic quantitative detection kit (GenScript, PiscatawayNJ, USA), according to manufacturer's instructions.

Briefly, PM extracts for cell treatments at the concentration of 2 $\mu\text{g}/\mu\text{L}$ were diluted with endotoxin-free LAL reagent water to the concentration of 10 $\mu\text{g}/\text{mL}$, mixed with the LAL supplied in the kit and incubated at 37 °C for 16 min. A chromogenic substrate solution was then mixed with samples and incubated at 37 °C for additional 6 min. The reaction was stopped with three-color stabilizers. The absorbance of each reaction was read by a multiplate spectrophotometer reader (Tecan, Männedorf, Switzerland) at 545 nm. The endotoxin content of each sample was calculated from a standard curve of *Escherichia coli* and the concentration expressed as endotoxin units per milligram (EU/mg) of tested particles.

4.4. PM_{2.5} In Vitro Toxicity

4.4.1. Cells Culture and Exposure Conditions

PM biological effects were evaluated on A549 cells, a human lung adenocarcinoma epithelial cell line obtained from the American Type Culture Collection (CCL-185, American Type Culture Collection, Manassas, VA, USA). Cells were cultured at 37 °C in a humidified atmosphere containing 5% CO₂ in OptiMEM I Reduced Serum Medium (Gibco, Life Technologies, Monza, Italy) supplemented with 10% heat-inactivated fetal bovine serum (FBS, Gibco) and 1% Penicillin/Streptomycin (100 X, Euroclone, Pero, Italy).

Cells were seeded 24 h before treatment at a concentration of 2×10^4 cells/cm² in 12-well plates or 1.6×10^4 cells/cm² in 6-well plates. Culture medium was removed and replaced by 1% FBS supplemented OptiMEM medium and cells exposed for 24 h at 37 °C to increasing PM_{2.5} concentrations (1, 5 and 10 $\mu\text{g}/\text{cm}^2$) in 12-well plates for cell viability, inflammatory response and cell cycle alteration evaluations. Cells exposed to extracts from blank filters were also used as additional negative control (see Supplementary Materials, Figure S6).

For oxidative stress investigations and protein expression analysis cell were exposed to 10 $\mu\text{g}/\text{cm}^2$ PM in 6-well plates. Unexposed cells (treated with cellular medium only) were used as control.

4.4.2. Cell Viability Assay

Cell viability was measured in A549 cells exposed to PM_{2.5} (1–10 $\mu\text{g}/\text{cm}^2$) for 24 h by means of the Alamar Blue assay (Invitrogen, Burlington, ON, Canada). Briefly, at the end of the exposure, medium was collected and stored for inflammatory response evaluation (more detail in the following paragraph), cells were rinsed with phosphate buffer saline (PBS) and incubated for 3 h in a solution containing 1:10 of Alamar Blue reagent and OptiMEM complete medium. The absorbance of each sample, proportional to cell viability, was measured by a multiplate spectrophotometer reader (Tecan, Männedorf, Switzerland) at excitation and emission wavelengths of 570 and 630 nm, respectively. Cell viability was calculated as a percentage of viable cells with respect to control (unexposed) samples.

4.4.3. Pro-Inflammatory Cytokine Release

At the end of treatments, cell culture supernatants were recovered and centrifuged at 12,000 rpm for 6 min at 4 °C to remove debris and floating cells. The resulting supernatants were collected and

stored at -20°C until the test was performed. IL-6 and IL-8 protein levels were measured by sandwich ELISA, according to the manufacturer guidelines (Life Technologies, Monza, Italy). The absorbance of each sample, whose color intensity is proportional to the amount of cytokine, was measured at 450 nm and 630 nm. The amount of proteins in pg/mL was calculated based on a standard curve.

4.4.4. Flow Cytometry Analysis of the Cell Cycle

Cell cycle distribution after exposure to $\text{PM}_{2.5}$ was assessed by DNA-staining with propidium iodide (PI). Briefly, after 24 h of exposure, cells were trypsinized, harvested, fixed in ice cold 90% EtOH and stored at -20°C until analysis. Then, cell suspensions were centrifuged (1600 rpm for 6 min), the supernatants discarded, and the pellet incubated in PBS and RNase DNase-free (20 $\mu\text{g}/\text{mL}$, Sigma-Aldrich, Saint Louis, MO, USA Italy) for 30 min at 37°C . Finally, DNA was stained with the fluorescent dye PI (10 $\mu\text{g}/\text{mL}$, Sigma Aldrich, Milan, Italy) and 10,000 cells per sample were scanned by flow cytometry, using 617 nm band pass filter (CytoFLEX 13/3, Beckman Coulter, Krefeld, Germany). The different phases of the cell cycle were assessed with CytExpert analysis software (Krefeld, Germany).

4.4.5. ROS Production

The intracellular production of reactive oxygen species (ROS) was analyzed by flow cytometry. A549 cells were plated in 12-well plates at a density of 2×10^4 cells/cm² and allowed to grow for 24 h. A549 cells were incubated with 5 μM Carboxy-2',7'-Dichlorofluorescein Diacetate (carboxy-DCFDA, 2 mM, Life Technologies, Monza, Italy) in PBS for 20 min at 37°C . Cells were then washed in PBS and exposed to 10 $\mu\text{g}/\text{cm}^2$ PM for 3 h. At the end of incubation, cells were trypsinized, harvested and suspended in PBS. The ROS production, detectable by the oxidation of the probe, was quantified by measuring the fluorescence intensity in the FITC channel of 10000 events with the cytometer CytoFLEX (Beckman Coulter, Krefeld, Germany). Data were analyzed using the CytoExpert software.

4.4.6. Western Blot Analysis

After 24 h of exposure to 10 $\mu\text{g}/\text{cm}^2$ PM in 6-well plates, cells were scraped and lysed on ice with RIPA buffer (150 mM NaCl, 1% Triton X-100, 0.5% sodium deoxycholate, 0.1% SDS, 50 mM Tris pH 8.0) and 0.1% of proteases inhibitor, added just before use. Cellular lysates were centrifuged at 12000 rpm for 15 min and collected to determine the protein concentration by bicinchoninic acid assay (Sigma Aldrich, Milan, Italy), performed according to the manufacturer instructions. 30 μg of proteins were loaded onto 12% SDS-PAGE gels, separated and transferred on nitrocellulose membranes. Blocking buffer in Tris-Buffered Saline (TBS) with 0.1% Tween20 (TBS-T) supplemented with 5% w/v bovine serum albumin (BSA; Sigma) or milk (Skim milk powder, Fluka, Sigma, Milan, Italy) was added to incubate the membranes for 1 h. After blocking, membranes were incubated in rabbit polyclonal antibodies HO-1 (1:1000, Cell Signaling Technology, Danvers, CO, US), CYP1A1 and CYP1B1 (1:500, Novus Biologicals, Littleton, CO, United States) O/N at 4°C . The membranes were then washed three times with TBS-T and incubated in Blocking buffer for 1 h at RT with the specific HRP-linked secondary antibodies (anti-rabbit IgG, 1:2000, Cell Signaling). Membranes were finally washed and detected by enhanced chemiluminescence (ECL, Euroclone). Digital images were taken by a luminescence reader (Biospectrum-UVP, LLC, Upland, CA, United States) and densitometry analysis performed with dedicated software (Vision Works LS, Cambridge, UK). Monoclonal anti- β -Actin antibody (Cell Signaling, 1:1000) was used as loading control.

4.5. Statistical Analyses

Data on chemical characterization are expressed as mean \pm standard deviation between individual samples of the same season.

Data on biological responses are expressed as the mean \pm standard error of mean (SEM) of at least three biological replicates carried out following the same experimental conditions. For the chemical and

biological endpoints, the statistical analyses were performed by unpaired *t*-test, one-way or two-way ANOVA with Dunn's, Dunnett's or Tukey's post hoc multiple comparisons tests, using the software Graph Pad, Prism Program version 6. Values of $p < 0.05$ were considered statistically significant.

Correlations among the characterized chemical parameters and the biological effects, obtained on the pooled PM samples, were evaluated by the software environment R Studio (RStudio Team, 2016, Boston, Massachusetts, USA) running on R version 3.5.1 (R Core Team, 2018 University of Auckland, New Zealand). General correlations were determined (Hmisc, package, Frank E Harrell Jr, with contributions from Charles Dupont and many others, 2019, Nashville, Tennessee, USA) among selected biological parameters; namely, IL6, IL8, CYP1B1, CYP1A1 and HO-1, and the chemical variables analysed. Where different concentrations of exposure were performed, the data from each dose were maintained (such as for interleukins) in order to investigate also possible chemistry dose-related effects. The final matrix was composed by 50 columns (40 chemical plus 10 biological variables) and 16 rows (the chemical variables were replicated during each season while the biological responses from each experiment were reported). From the results obtained, specific correlation plots were performed between a single biological output and one or more relevant chemical variables previously identified. If different compounds were selected for the correlation plot, their linear combination were used in order to weight each variable equally. The overall correlation plot reports only the correlations that were significant ($p < 0.01$) while for the single linear correlation plot the R^2 , the line coefficient and the *p*-value of the correlation are reported.

5. Conclusions

Our data demonstrate that the toxic potential of the urban PM_{2.5} from Greater Cairo is linked to the seasonal changes in the chemical composition. The variable content in PAHs, metals and ionic species, indeed determined different biological effects in human lung cells exposed *in vitro*.

The fine PMs from colder seasons promoted cell xenobiotic responses and highly pro-inflammatory effects, while the ones from warmer seasons displayed a direct effect on cell cycle progression. These results were significantly associated to specific organic and inorganic species and are in line with previous studies reporting PM-induced toxic effects on lung cells, associated to season-related changes in composition [29,41,54]. Of course, the seasonal-dependent biological effects are affected by the regional climatological variables and emission sources, which finally determine a great variability in the physico-chemical characteristics of the PM pollution. Considering the developing countries, improvements in the characterizations of the emission sources, by means of source apportionment techniques, in parallel to the studies on the PM biological reactivity and epidemiological evidences, are highly recommended to better characterize the potential health risks and possible future mitigation strategies.

Supplementary Materials: Supplementary materials can be found at <http://www.mdpi.com/1422-0067/20/20/4970/s1>.

Author Contributions: Conceptualization, P.M. and S.K.H.; investigation, S.M., S.K.H., W.H.S., A.E.-M., E.F.M., A.M.F.M. and A.A.E.-A.; data curation, M.G., writing—original draft preparation S.M. and S.K.H.; writing—review and editing, S.M., M.G. and P.M.; supervision, R.B. and A.C.; project administration, P.M.; funding acquisition, S.K.H. and P.M.

Funding: The results were achieved in the framework of the program of Italy–Egypt Joint Science and Technology Cooperation with the project “Managing air quality and health risk: from airborne fine particulate (PM_{2.5}) characterization to the biological mechanism of action,” granted by the Italian Ministry of Foreign Affairs and International Cooperation (MAECI) (PGR00786 to PM) and by the Egyptian Academy of Scientific Research and Technology, Science and Technology Development Fund (STDF) (ID: 26001).

Acknowledgments: This paper is dedicated to the memory of Professor Marina Camatini, President of the Research Center POLARIS, University of Milano-Bicocca. Authors wish to thank M. Saibene and P. Gentile (University of Milano-Bicocca) for the SEM characterizations.

Conflicts of Interest: The authors declare no conflict of interest.

Abbreviations

WHO	World Health Organization
PM	particulate matter
COPD	chronic obstructive pulmonary disease
PAHs	polycyclic aromatic hydrocarbons
VOCs	volatile organic compounds
NA	Naphthalene
ACY	Acenaphthylene
ACE	Acenaphthene
FLU	Fluorene
PHE	Phenanthrene
ANT	Anthracene
FLT	Fluoranthene
PYR	Pyrene
BaA	Benzo(a)anthracene
CRY	Chrysene
BbF	Benzo(b)Flouranthene
BkF	Benzo(k)Flouranthene
BaP	Benzo (a) pyrene
IND	Indeno(1,2,3-cd) pyrene
DBA	Dibenzo(a,h) anthracene
BGP	Benzo(ghi)perylene
WSIs	water-soluble ions
Ms	metals/metalloids
MDLs	method detection limits
ICP MS	Inductively Coupled Plasma Optical Emission Spectrometry
ICP-QQQ	Triple Quadrupole ICP-MS
DCM	dichloromethane
GC	gas chromatography
LAL	Limulus Amebocyte Lysate
PI	Propidium Iodide
ROS	reactive oxygen species
H ₂ O ₂	Hydrogen peroxide
TBS	Tris-Buffered Saline
TBS-T	TBS with 0.1% Tween20
BSA	bovine serum albumin

References

1. WHO World Health Organization Releases 7 million Premature Deaths Annually Linked to Air Pollution. 2014. Available online: <http://www.who.int/mediacentre/news/releases/2014/air-pollution/en/> (accessed on 21 June 2018).
2. Anderson, J.O.; Thundiyil, J.G.; Stolbach, A. Clearing the Air: A Review of the Effects of Particulate Matter Air Pollution on Human Health. *J. Med. Toxicol.* **2012**, *8*, 166–175. [[CrossRef](#)] [[PubMed](#)]
3. Burnett, R.; Chen, H.; Szyszkowicz, M.; Fann, N.; Hubbell, B.; Pope, C.A.; Apte, J.S.; Brauer, M.; Cohen, A.; Weichenthal, S.; et al. Global estimates of mortality associated with long-term exposure to outdoor fine particulate matter. *Proc. Natl. Acad. Sci. USA* **2018**. [[CrossRef](#)] [[PubMed](#)]
4. Cesari, D.; De Benedetto, G.E.; Bonasoni, P.; Busetto, M.; Dinioi, A.; Merico, E.; Chirizzi, D.; Cristofanelli, P.; Donato, A.; Grasso, F.M.; et al. Seasonal variability of PM_{2.5} and PM₁₀ composition and sources in an urban background site in Southern Italy. *Sci. Total Environ.* **2018**, *612*, 202–213. [[CrossRef](#)] [[PubMed](#)]
5. Yanagi, Y.; de Assunção, J.V.; Barrozo, L.V. The impact of atmospheric particulate matter on cancer incidence and mortality in the city of São Paulo, Brazil. *Cad. Saúde Pública* **2012**, *28*, 1737–1748. [[CrossRef](#)] [[PubMed](#)]

6. Zauli-Sajani, S.; Rovelli, S.; Trentini, A.; Bacco, D.; Marchesi, S.; Scotto, F.; Zigola, C.; Lauriola, P.; Cavallo, D.M.; Poluzzi, V.; et al. Higher health effects of ambient particles during the warm season: The role of infiltration factors. *Sci. Total Environ.* **2018**, *627*, 67–77. [[CrossRef](#)] [[PubMed](#)]
7. Karakatsani, A.; Analitis, A.; Perifanou, D.; Ayres, J.G.; Harrison, R.M.; Kotronarou, A.; Kavouras, I.G.; Pekkanen, J.; Hämeri, K.; Kos, G.P.; et al. Particulate matter air pollution and respiratory symptoms in individuals having either asthma or chronic obstructive pulmonary disease: A European multicentre panel study. *Environ. Heal. A Glob. Access Sci. Source* **2012**, *11*, 1–16. [[CrossRef](#)]
8. Valavanidis, A.; Vlachogianni, T.; Fiotakis, K.; Loridas, S. Pulmonary oxidative stress, inflammation and cancer: Respirable particulate matter, fibrous dusts and ozone as major causes of lung carcinogenesis through reactive oxygen species mechanisms. *Int. J. Environ. Res. Public Health* **2013**, *10*, 3886–3907. [[CrossRef](#)]
9. Im, U.; Markakis, K.; Koçak, M.; Gerasopoulos, E.; Daskalakis, N.; Mihalopoulos, N.; Poupkou, A.; Kindap, T.; Unal, A.; Kanakidou, M. Summertime aerosol chemical composition in the Eastern Mediterranean and its sensitivity to temperature. *Atmos. Environ.* **2012**, *50*, 164–173. [[CrossRef](#)]
10. Zhang, Y.; Wen, X.-Y.; Wang, K.; Vijayaraghavan, K.; Jacobson, M.Z. Probing into regional O₃ and particulate matter pollution in the United States: 2. An examination of formation mechanisms through a process analysis technique and sensitivity study. *J. Geophys. Res.* **2009**, *114*, D22305. [[CrossRef](#)]
11. Tai, A.P.K.; Mickley, L.J.; Jacob, D.J. Correlations between fine particulate matter (PM_{2.5}) and meteorological variables in the United States: Implications for the sensitivity of PM_{2.5} to climate change. *Atmos. Environ.* **2010**, *44*, 3976–3984. [[CrossRef](#)]
12. Hassan, S.K.; Khoder, M.I. Chemical characteristics of atmospheric PM_{2.5} loads during air pollution episodes in Giza, Egypt. *Atmos. Environ.* **2017**, *150*, 346–355. [[CrossRef](#)]
13. Khoder, M.I. Diurnal, seasonal and weekdays-weekends variations of ground level ozone concentrations in an urban area in greater Cairo. *Environ. Monit. Assess.* **2009**, *149*, 349–362. [[CrossRef](#)] [[PubMed](#)]
14. Lowenthal, D.H.; Gertler, A.W.; Labib, M.W. Particulate matter source apportionment in Cairo: Recent measurements and comparison with previous studies. *Int. J. Environ. Sci. Technol.* **2014**, *11*, 657–670. [[CrossRef](#)]
15. Boman, J.; Shaltout, A.A.; Abozied, A.M.; Hassan, S.K. On the elemental composition of PM_{2.5} in central Cairo, Egypt. *X-Ray Spectrom.* **2013**, *42*, 276–283. [[CrossRef](#)]
16. EEAA State of the Environment Report in Egypt. *Issued 2014* **2012**. [[CrossRef](#)]
17. Perrone, M.G.; Gualtieri, M.; Consonni, V.; Ferrero, L.; Sangiorgi, G.; Longhin, E.; Ballabio, D.; Bolzacchini, E.; Camatini, M. Particle size, chemical composition, seasons of the year and urban, rural or remote site origins as determinants of biological effects of particulate matter on pulmonary cells. *Environ. Pollut.* **2013**, *176*, 215–227. [[CrossRef](#)]
18. Michael, S.; Montag, M.; Dott, W. Pro-inflammatory effects and oxidative stress in lung macrophages and epithelial cells induced by ambient particulate matter. *Environ. Pollut.* **2013**. [[CrossRef](#)]
19. Gualtieri, M.; Øvrevik, J.; Møllerup, S.; Asare, N.; Longhin, E.; Dahlman, H.J.; Camatini, M.; Holme, J.A. Airborne urban particles (Milan winter-PM_{2.5}) cause mitotic arrest and cell death: Effects on DNA, mitochondria, AhR binding and spindle organization. *Mutat. Res. Fundam. Mol. Mech. Mutagen.* **2011**, *713*, 18–31. [[CrossRef](#)]
20. Líbalová, H.; Krčková, S.; Uhlířová, K.; Milcová, A.; Schmutzerová, J.; Cigánek, M.; Kléma, J.; Machala, M.; Šrám, R.J.; Topinka, J. Genotoxicity but not the AhR-mediated activity of PAHs is inhibited by other components of complex mixtures of ambient air pollutants. *Toxicol. Lett.* **2014**, *225*, 350–357. [[CrossRef](#)]
21. Longhin, E.; Holme, J.A.; Gutzkow, K.B.; Arlt, V.M.; Kucab, J.E.; Camatini, M.; Gualtieri, M. Cell cycle alterations induced by urban PM_{2.5} in bronchial epithelial cells: Characterization of the process and possible mechanisms involved. *Part. Fibre Toxicol.* **2013**, *10*, 63. [[CrossRef](#)]
22. Longhin, E.; Pezzolato, E.; Mantecca, P.; Holme, J.A.; Franzetti, A.; Camatini, M.; Gualtieri, M. Season linked responses to fine and quasi-ultrafine Milan PM in cultured cells. *Toxicol. Vitro.* **2013**, *27*, 551–559. [[CrossRef](#)]
23. Nemmar, A.; Al-Maskari, S.; Ali, B.H.; Al-Amri, I.S. Cardiovascular and lung inflammatory effects induced by systemically administered diesel exhaust particles in rats. *Am. J. Physiol. Cell. Mol. Physiol.* **2007**, *292*, L664–L670. [[CrossRef](#)] [[PubMed](#)]
24. Sancini, G.; Farina, F.; Battaglia, C.; Cifola, I.; Mangano, E.; Mantecca, P.; Camatini, M.; Palestini, P. Health risk assessment for air pollutants: Alterations in lung and cardiac gene expression in mice exposed to milano winter fine particulate matter (PM_{2.5}). *PLoS One* **2014**, *9*. [[CrossRef](#)] [[PubMed](#)]

25. Hu, T.; Cao, J.; Shen, Z.; Wang, G.; Lee, S.; Ho, K. Size Differentiation of individual atmospheric aerosol during winter in Xi'an, China. *Aerosol Air Qual. Res.* **2012**, *12*, 951–960. [[CrossRef](#)]
26. Krzyzanowski, M.; Apte, J.S.; Bonjour, S.P.; Brauer, M.; Cohen, A.J.; Prüss-Ustun, A.M. Air Pollution in the Mega-cities. *Curr. Environ. Heal. Rep.* **2014**, *1*, 185–191. [[CrossRef](#)]
27. Shaltout, A.A.; Hassan, S.K.; Karydas, A.G.; Zaki, Z.I.; Mostafa, N.Y.; Kregsamer, P.; Wobrauschek, P.; Strelci, C. Comparative elemental analysis of fine particulate matter (PM_{2.5}) from industrial and residential areas in Greater Cairo-Egypt by means of a multi-secondary target energy dispersive X-ray fluorescence spectrometer. *Spectrochim. Acta Part B At. Spectrosc.* **2018**, *145*, 29–35. [[CrossRef](#)]
28. Liu, W.J.; Xu, Y.S.; Liu, W.X.; Liu, Q.Y.; Yu, S.Y.; Liu, Y.; Wang, X.; Tao, S. Oxidative potential of ambient PM_{2.5} in the coastal cities of the Bohai Sea, northern China: Seasonal variation and source apportionment. *Environ. Pollut.* **2018**, *236*, 514–528. [[CrossRef](#)] [[PubMed](#)]
29. Gualtieri, M.; Øvreivik, J.; Holme, J.A.; Perrone, M.G.; Bolzacchini, E.; Schwarze, P.E.; Camatini, M. Differences in cytotoxicity versus pro-inflammatory potency of different PM fractions in human epithelial lung cells. *Toxicol. Vitro.* **2010**, *24*, 29–39. [[CrossRef](#)] [[PubMed](#)]
30. Jalava, P.I.; Happo, M.S.; Huttunen, K.; Sillanpää, M.; Hillamo, R.; Salonen, R.O.; Hirvonen, M.R. Chemical and microbial components of urban air PM cause seasonal variation of toxicological activity. *Environ. Toxicol. Pharmacol.* **2016**, *40*, 375–387. [[CrossRef](#)]
31. Guan, T.; Yao, M.; Wang, J.; Fang, Y.; Hu, S.; Wang, Y.; Dutta, A.; Yang, J.; Wu, Y.; Hu, M.; et al. Airborne endotoxin in fine particulate matter in Beijing. *Atmos. Environ.* **2014**, *97*, 35–42. [[CrossRef](#)]
32. Heinrich, J.; Pitz, M.; Bischof, W.; Krug, N.; Borm, P.J.A. Endotoxin in fine (PM_{2.5}) and coarse (PM_{2.5-10}) particle mass of ambient aerosols. A temporo-spatial analysis. *Atmos. Environ.* **2003**, *37*, 3659–3667. [[CrossRef](#)]
33. Li, N.; Hao, M.; Phalen, R.F.; Hinds, W.C.; Nel, A.E. Particulate air pollutants and asthma: A paradigm for the role of oxidative stress in PM-induced adverse health effects. *Clin. Immunol.* **2003**, *109*, 250–265. [[CrossRef](#)] [[PubMed](#)]
34. Xing, Y.F.; Xu, Y.H.; Shi, M.H.; Lian, Y.X. The impact of PM_{2.5} on the human respiratory system. *J. Thorac. Dis.* **2016**, *8*, E69–E74. [[CrossRef](#)] [[PubMed](#)]
35. Longhin, E.; Holme, J.A.; Gualtieri, M.; Camatini, M.; Øvreivik, J. Milan winter fine particulate matter (wPM_{2.5}) induces IL-6 and IL-8 synthesis in human bronchial BEAS-2B cells, but specifically impairs IL-8 release. *Toxicol. Vitro.* **2018**, *52*, 365–373. [[CrossRef](#)] [[PubMed](#)]
36. Hetland, R.B.; Cassee, F.R.; Refsnes, M.; Schwarze, P.E.; Låg, M.; Boere, A.J.F.; Dybing, E. Release of inflammatory cytokines, cell toxicity and apoptosis in epithelial lung cells after exposure to ambient air particles of different size fractions. *Toxicol. Vitro.* **2004**, *18*. [[CrossRef](#)]
37. Steenhof, M.; Gosens, I.; Strak, M.; Godri, K.J.; Hoek, G.; Cassee, F.R.; Mudway, I.S.; Kelly, F.J.; Harrison, R.M.; Lebret, E.; et al. In vitro toxicity of particulate matter (PM) collected at different sites in the Netherlands is associated with PM composition, size fraction and oxidative potential—The RAPTES project. *Part. Fibre Toxicol.* **2011**, *8*, 26. [[CrossRef](#)]
38. Genies, C.; Jullien, A.; Lefebvre, E.; Revol, M.; Maitre, A.; Douki, T. Inhibition of the formation of benzo[a]pyrene adducts to DNA in A549 lung cells exposed to mixtures of polycyclic aromatic hydrocarbons. *Toxicol. Vitro.* **2016**, *35*, 1–10. [[CrossRef](#)]
39. Dergham, M.; Lepers, C.; Verdin, A.; Billet, S.; Cazier, F.; Courcot, D.; Shirali, P.; Garçon, G. Prooxidant and proinflammatory potency of air pollution particulate matter (PM_{2.5-0.3}) produced in rural, urban, or industrial surroundings in human bronchial epithelial cells (BEAS-2B). *Chem. Res. Toxicol.* **2012**, *25*, 904–919. [[CrossRef](#)]
40. Libalová, H.; Krčková, S.; Uhlířová, K.; Kléma, J.; Cigánek, M.; Rössner, P.; Šrám, R.J.; Vondráček, J.; Machala, M.; Topinka, J. Analysis of gene expression changes in A549 cells induced by organic compounds from respirable air particles. *Mutat. Res. Fundam. Mol. Mech. Mutagen.* **2014**, *770*, 94–105. [[CrossRef](#)]
41. Cachon, B.F.; Firmin, S.; Verdin, A.; Ayi-Fanou, L.; Billet, S.; Cazier, F.; Martin, P.J.; Aissi, F.; Courcot, D.; Sanni, A.; et al. Proinflammatory effects and oxidative stress within human bronchial epithelial cells exposed to atmospheric particulate matter (PM_{2.5} and PM_{>2.5}) collected from Cotonou, Benin. *Environ. Pollut.* **2014**, *185*, 340–351. [[CrossRef](#)]
42. Capasso, L.; Longhin, E.; Caloni, F.; Camatini, M.; Gualtieri, M. Synergistic inflammatory effect of PM₁₀ with mycotoxin deoxynivalenol on human lung epithelial cells. *Toxicol.* **2015**, *104*, 65–72. [[CrossRef](#)] [[PubMed](#)]

43. Manzano-León, N.; Serrano-Lomelin, J.; Sánchez, B.N.; Quintana-Belmares, R.; Vega, E.; Vázquez-López, I.; Rojas-Bracho, L.; López-Villegas, M.T.; Vadillo-Ortega, F.; de Vizcaya-Ruiz, A.; et al. TNF α and IL-6 responses to particulate matter in vitro: Variation according to PM size, season, and polycyclic aromatic hydrocarbon and soil content. *Environ. Health Perspect.* **2016**, *124*, 406–412. [[CrossRef](#)] [[PubMed](#)]
44. Deng, F.; Guo, X.; Liu, H.; Fang, X.; Yang, M.; Chen, W. Effects of dust storm PM_{2.5} on cell proliferation and cell cycle in human lung fibroblasts. *Toxicol. Vitro.* **2007**, *21*, 632–638. [[CrossRef](#)] [[PubMed](#)]
45. Øvrevik, J.; Arlt, V.M.; Øya, E.; Nagy, E.; Mollerup, S.; Phillips, D.H.; Låg, M.; Holme, J.A. Differential effects of nitro-PAHs and amino-PAHs on cytokine and chemokine responses in human bronchial epithelial BEAS-2B cells. *Toxicol. Appl. Pharmacol.* **2010**, *242*, 270–280. [[CrossRef](#)] [[PubMed](#)]
46. Hockley, S.L.; Arlt, V.M.; Brewer, D.; Giddings, I.; Phillips, D.H. Time- and concentration-dependent changes in gene expression induced by benzo(a)pyrene in two human cell lines, MCF-7 and HepG2. *BMC Genomics* **2006**, *7*, 1–23. [[CrossRef](#)] [[PubMed](#)]
47. Mantecca, P.; Farina, F.; Moschini, E.; Gallinotti, D.; Gualtieri, M.; Rohr, A.; Sancini, G.; Palestini, P.; Camatini, M. Comparative acute lung inflammation induced by atmospheric PM and size-fractionated tire particles. *Toxicol. Lett.* **2010**, *198*, 244–254. [[CrossRef](#)] [[PubMed](#)]
48. Loxham, M.; Morgan-Walsh, R.J.; Cooper, M.J.; Blume, C.; Swindle, E.J.; Dennison, P.W.; Howarth, P.H.; Cassee, F.R.; Teagle, D.A.H.; Palmer, M.R.; et al. The effects on bronchial epithelial mucociliary cultures of coarse, fine, and ultrafine particulate matter from an underground railway station. *Toxicol. Sci.* **2015**, *145*, 98–107. [[CrossRef](#)] [[PubMed](#)]
49. Gualtieri, M.; Longhin, E.; Mattioli, M.; Mantecca, P.; Tinaglia, V.; Mangano, E.; Carla, M.; Bestetti, G.; Camatini, M.; Battaglia, C. Gene expression profiling of A549 cells exposed to Milan PM_{2.5}. *Toxicol. Lett.* **2012**, *209*, 136–145. [[CrossRef](#)]
50. Shetaya, W.H.; Osterwalder, S.; Bigalke, M.; Mestrot, A.; Huang, J.H.; Alewell, C. An Isotopic Dilution Approach for Quantifying Mercury Lability in Soils. *Environ. Sci. Technol. Lett.* **2017**, *4*, 556–561. [[CrossRef](#)]
51. Fang, G.C.; Chang, C.N.; Wu, Y.S.; Fu, P.P.C.; Yang, I.L.; Chen, M.H. Characterization, identification of ambient air and road dust polycyclic aromatic hydrocarbons in central Taiwan, Taichung. *Sci. Total Environ.* **2004**, *327*, 135–146. [[CrossRef](#)]
52. Park, J.-S.; Wade, T.L.; Sweet, S. Atmospheric distribution of polycyclic aromatic hydrocarbons and deposition to Galveston Bay, Texas, USA. *Atmos. Environ.* **2001**, *35*, 3241–3249. [[CrossRef](#)]
53. Bein, K.J.; Wexler, A.S. Compositional variance in extracted particulate matter using different filter extraction techniques. *Atmos. Environ.* **2015**, *107*, 24–34. [[CrossRef](#)]
54. Robertson, S.; Gray, G.A.; Duffin, R.; McLean, S.G.; Shaw, C.A.; Hadoke, P.W.F.; Newby, D.E.; Miller, M.R. Diesel exhaust particulate induces pulmonary and systemic inflammation in rats without impairing endothelial function ex vivo or in vivo. *Part. Fibre Toxicol.* **2012**, *9*, 9. [[CrossRef](#)] [[PubMed](#)]



© 2019 by the authors. Licensee MDPI, Basel, Switzerland. This article is an open access article distributed under the terms and conditions of the Creative Commons Attribution (CC BY) license (<http://creativecommons.org/licenses/by/4.0/>).

